Electrical Conductivity of Brain Cortex Slices in Seizing and Non-seizing States

A thesis

submitted in fulfilment

of the requirements for the degree

of

Doctor of Philosophy (Physics)

at

The University of Waikato

by

Maher Elbohouty

THE UNIVERSITY OF
WAIKATO
Te Whare Wānanga o Waikato

2013

Dedication

To the soul of my father Mohammed, who continuously supported me with endless generosity and love. I miss you Dad.

To my mother Fardous
To my wife Noha
To my son Ahmed
To my daughter Salma
To my sisters: Mona, Rokaia, Eman and Asmaa
To my brother Anas

Thank you for your support and patience.

Acknowledgements

I may not have been able to complete this thesis without help from many great people. I am grateful for everyone who helped me in this work. I am lucky being surrounded by these helpful professionals.

Special thanks to chief supervisor Dr Marcus Wilson, I am glad being his student. He is always available, is friendly and helps me. I would like to thank Associate Professor Alistair Steyn-Ross for supervising and solving my personal issues.

Dr Logan Voss is the dark horse of this work. He trained me and helped me a lot in the biological section and put considerable efforts into editing it. Thank you to Dr Jonathon Mason, Dr Greg Jacobson for advice, Dr Vladimir Bubanja for introducing me to the van der Pauw method, Dr Hunt for helping in statistics and Ehsan with Matlab.

I am glad to have great technicians here, Ian Honey, Stewart Finlay and Luke van de Pas. They were always happy to help.

Finally, my thanks go to Fisher & Paykel Healthcare for the study award and The University of Waikato for an International Doctoral Scholarship.

Maher Elbohouty

Abstract

The electrical conductivity of thin living slices of mouse cerebral cortex is measured. Two only out of fifteen different attempting ways were effective. I have successfully measured the electrical conductivity of mouse brain cortex in seizing and non-seizing conditions. The first successful approach is called the van der Pauw method, where four silver-silver chloride cylindrical wire electrodes were immersed in full length at the corners of the sample. The second is a one-dimensional technique where two flat electrodes were placed on either face of the 400 μm thick samples.

In both methods the electrodes were connected to an Agilent E4980A impedance monitor. The conductivity at 10 kHz of each sample was calculated based on measurements of injected current and potential difference between electrodes. Both approaches were validated by measuring electrical conductivities of known solutions. There were two main challenges: the small size of the sample and keeping it alive. I overcame these challenges by suitable electrodes and fast measuring equipment (Agilent E4980A *LCR* meter). For the one-dimensional technique I also measured the conductivity across the frequency range 20 Hz to 2 MHz.

The results consistently show the mean conductivity of seizing brain tissue is significantly lower than that of non-seizing tissue at 10 kHz. Also, the conductivity of seizing slices is lower than the conductivity of non-seizing slices over the frequency range 20 Hz to 2 MHz.

These results suggest a link between electrical conductivity and seizure activity. I have not investigated the causes of these differences but explanations consistent with the literature are a change in chemical environment during seizure or a reduction in gap junction connectivity.

Preface

An on-going question in the field of epilepsy research is what causes seizures to start? The theme of my thesis is to investigate whether there is a link between seizure activity and tissue electrical conductivity. In this work I measured the electrical conductivity of seizing and non-seizing mouse brain slices using a range of different methodologies.

Starting with the Introduction (Chapter 1) I present some basic information about brain composition, activities, disorder and how to measure its activities. In Chapter 2, I have compiled a literature review. I started my collection by focusing on measurements on conductivity and seizures. Then I stated the conductivity changes due to death, temperature, age and stimulation frequency. The common principles used in this work, including measurement basics and some statistics, are presented in Chapter 3.

The experimental chapters are 4 to 8. Successful methods are reported in Chapters 5, 7 and 8. A two-dimensional method with coronal slices was used in Chapter 5, while a one-dimensional method with coronal and transverse slices was used in Chapters 7 and 8. Chapters 4 and 6 and Section 5.1 describe unsuccessful methods. The conclusion is presented in Chapter 9. These experimental chapters are my original contribution.

In Appendices, I include parts from work of my supervisor Wilson (Wilson, M. T. 2012, pers. comm.). The preliminary computer code was provided by my supervisor Steyn-Ross (Steyn-Ross, D. A. 2009, pers. comm.) as indicated in initial notes in Appendix B. The solver for the van der Pauw equation using the Newton Raphson method in Section B-2 was provided by my supervisor Wilson (Wilson, M. T. 2012, pers. comm.).

The work in Chapter 5 has been submitted to a journal and is presently under review. I may submit more parts for publication. Data arising from this work have been presented in conferences as a talk and posters as detailed in the list of publications.

List of Publications arising from this work

I. M. Elbohouty, M. T. Wilson, L. J. Voss, D. A. Steyn-Ross, L. Hunt "*In vitro Electrical Conductivity of Seizing and Non-seizing Mouse Brain Slices at 10 kHz*", accepted by the journal Physics in Medicine and Biology, 10 April 2013.

II. M. Elbohouty, M. T. Wilson, L. J. Voss, D. A. Steyn-Ross. "*Methodology to Measure the Electrical Conductivity of Seizing and Non-Seizing Mouse Brain Slices*", presented as a contributed talk and conference proceeding at the 20th Australian Institute of Physics Congress – Sydney – December 2012.

III. M. Elbohouty, M. T. Wilson, L. J. Voss, D. A. Steyn-Ross, L. Hunt. "*The Electrical Conductivity of Mouse Brain Slices in Seizing and Non-Seizing Conditions*", Poster at the 30th International Australasian Winter Conference on Brain Research – Queenstown – New Zealand, August 2012.

IV. M. Elbohouty, M. T. Wilson, L. J. Voss, D. A. Steyn-Ross. "*Measuring Electrical Conductivity of Brain Tissue*", Oral presentation at the New Zealand Institute of Physics (NZIP) Conference – Wellington – October 2011.

V. M. Elbohouty, M. T. Wilson, L. J. Voss, D. A. Steyn-Ross. "*Measuring Electrical Conductivity of Brain Slices*", Oral presentation at the 19th Australian Institute of Physics Congress – Melbourne – Australia. December 2010.

VI. M. Elbohouty, M. T. Wilson, L. J. Voss, D. A. Steyn-Ross. "*Measuring Electrical Conductivity of Mouse Brain Slices*", Poster at the 28th International Australasian Winter Conference on Brain Research – Wanaka – August 2010.

List of Special Terms and Abbreviations

1DC	one-dimensional method in coronal direction
1DT	one-dimensional method in transverse direction
2D	two-dimensional method
ACSF	artificial cerebrospinal fluid
α-dispersion	arises due to counterion polarization
Ag/AgCl	silver-silver chloride electrode
anterioposterior axis	axis connecting between front end (anterior) and back end (posterior)
β-dispersion	due to interface polarization
CM	conductivity meter, RE388Tx, EDT direct ion, Dover UK
coronal direction	Slice planes are perpendicular to the direction from front to back
CPE	constant phase element which means modelling a frequency-dependent element so that the phase of immittance becomes independent of frequency
Cx36	gap junction channels are composed of a family of proteins known as connexins, one of which is Cx36
DUT	device under test
ECG	electrocardiogram
EEG	electroencephalogram
electroporation	structural defects or ‘pores’ on cell membrane created by destroying the bilayer lipid due to electrical current
EMG	electromyogram
γ-dispersion	results from permanent dipole relaxation of small molecules
I_c	conduction current: generated from the free charges
I_d	displacement current: generated from bound charges in the tissue
in vitro	in glass
in vivo	in living tissue

LCR meter	Agilent E4980A, instrument is capable of measuring inductance (*L*), capacitance (*C*) and resistance (*R*) of an electrical circuit
LFP	local field potential
MEA	multielectrode array
MW test	Mann-Whitney test
seizures	hyper-synchronized bursts of activity in cerebral cortex and hippocampus
slice holder	flat Ag/AgCl electrodes that built at fixed separation distance of 400 µm. It sandwiches the brain slices
Syringe V3	a 10 ml syringe which has been modified by inserting a flat stainless steel electrode at its internal cylinder top and its piston top as shown in Figure 6-1
transverse direction	Slice planes are perpendicular to the direction from top (superior) to bottom (inferior)
vdP	van der Pauw method
V_{th}	thermal noise voltage

Contents

1 Introduction

In this Chapter I present some basic facts about neurons, gap junctions, brain electrical activities, electrical conductivity, seizures, current flow and live cells.

1.1 Background on Neuron

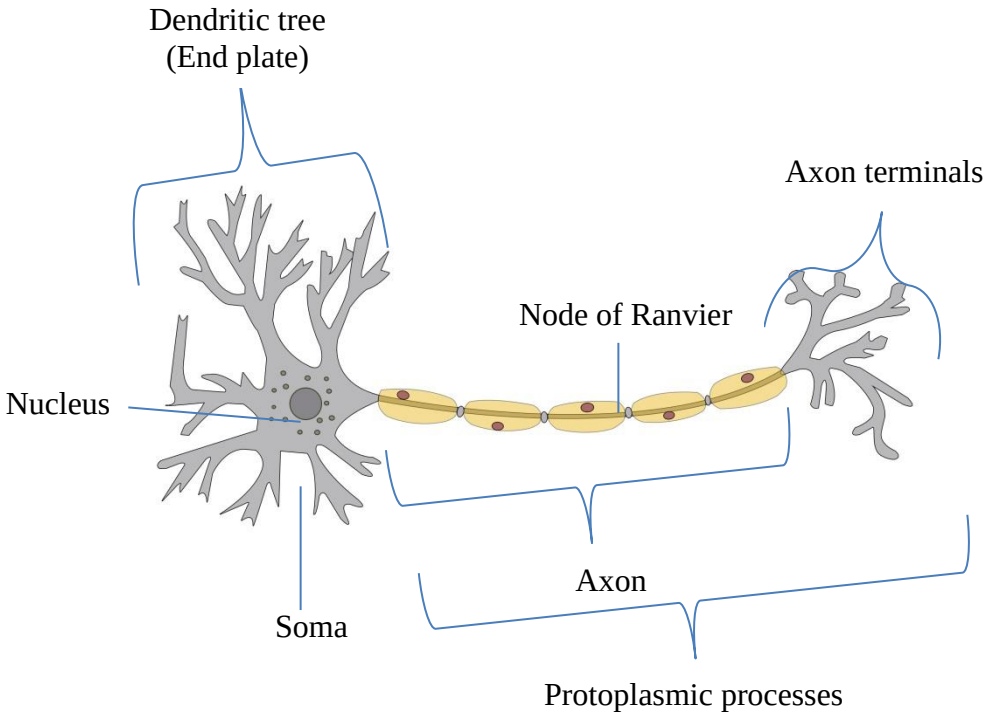

Figure 1-1: A typical structure of nerve cells. Modified from Sheeler & Bianchi (1983)

A neuron is a highly specialized cell for the conduction and transmission of impulses. Important features and specialisations of neurons include: 1. the cell body, containing various organelles; 2. the protoplasmic processes (dendrons); 3. dendrites, which receive and transmit impulse to the cell body, 4. axons, which conduct impulses away from the cell body; these may be one metre or few millimetres long; and 5. the endplate, which is found at the end of the dendrite and is the location of the synapses (Figure 1-2) (Sheeler & Bianchi, 1983). The outer layer of the brain, called the cortex, contains roughly 15 – 33 billion neurons, linked with up to 10,000 synaptic connections each.

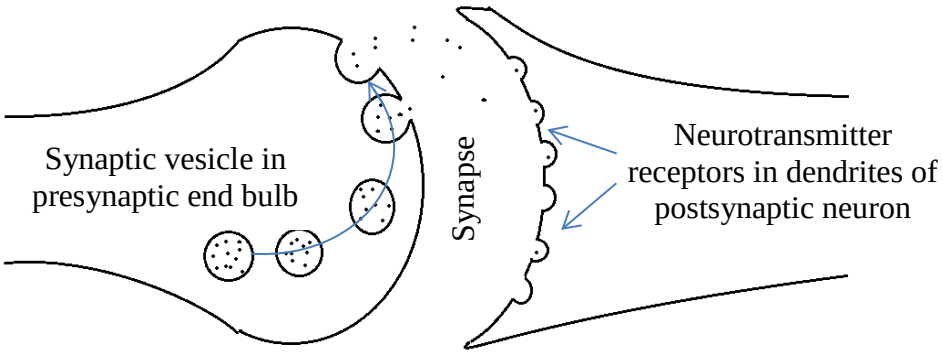

Figure 1-2: Sketch of synapse

1.1.1 Conduction of Nerve Impulses

Physiologically, the main role of a neuron is the transmission of a signal or impulse from one part of the body to another. The impulse normally starts at the axon hillock and travels through the cell to the end of the axon. The impulse is a transitory chemical change in the condition of the plasma membrane causing a change in the potential difference between the inside and outside of the cell. Experimentally, an impulse can typically be stimulated to begin anywhere on the cell surface by applying a variety of stimuli which include electric shock, pressure (pinching), heat, cold, pH change, light, and various chemicals. Once started, the impulse is spread along the membrane with no need of a continuing stimulus. The speed of the impulse travelling through the fibre does not depend on the strength of the stimulus. Two main changes occur when the impulse passes along the plasma membrane. The first is an action potential (i.e., a change in electrical potential across the membrane), and the second is a change in membrane permeability.

The axon is a good electrical conductor because the cytoplasm of the axon and the surrounding extracellular fluid are ionic solutions. The axolemma (the cell membrane surrounding an axon) is a weak insulator with a considerably higher electrical resistance than the axon and its fluid. An electrical potential can be measured when a microelectrode inserted into the axoplasm and the other electrode is placed in the extracellular fluid. A resting potential (–50 to –90 mV) is a constant state in all cells that are not

conducting an impulse. The inside of the cell is negative compared to the outside.

1.1.2 Ion Gradients Across the Membrane

An imbalance between anions and cations in the axoplasm and extracellular fluid causes the resting potential across the cell membrane as in Table 1-1. Ions like sodium and potassium diffuse through the cell membrane according to concentration gradients. A metabolic energy pump maintains the concentration differences of these two cations.

Table 1-1: Ion concentrations for axoplasm and extracellular fluid ($[Ion]_o/[Ion]_i$ = ratio of external to internal ion concentration) (Sheeler & Bianchi, 1983)

	Extracellular (mmol/litre)	Intracellular (mmol/litre)	$[Ion]_o/[Ion]_i$
Na^+	145	12	12.1
K^+	4	155	1/39
Other cations	5	-	-
Cl^-	120	4	30
HCO_3^-	27	8	3.4
Other anions	7	155[a]	
Resting potential	0 mV	–90 mV	

[a]Value for organic anions

The action potential can be recorded when a neuron is stimulated. The internal voltage rapidly changes from –90 mV to about +20 or +30 mV within 0.5 to 1.0 millisecond; the membrane then recovers, and the –90 mV resting potential is restored. The impulse sweeping along the axon represents a transitory change in a potential of 110 to 120 mV. Figure 1-4 (in Section 1.3) is an example of a sequence of action potentials recorded from rat.

1.1.3 Initiation of the Action Potential

Scientists found that any stimulus to the neuron above a certain threshold is followed by a high transport of Na^+ into the axoplasm. The high inward Na^+ transport may be due to a temporary increase in the size of the pores or "Na^+ gates". That causes a reversal of the electrical potential across the membrane which is immediately followed by an opening of potassium gates to restore the former potential. Only a small amount of the Na^+ and K^+ that exists outside and inside the cell respectively need to pass through the membrane in order to cause the reverse polarization followed by the repolarization. Sheeler & Bianchi (1983) assert that the nerve fibre can conduct many times in succession without diminishing the concentration gradients across the membrane. The Na^+/K^+-pump restores the original ion concentrations between successive conductions. In less than 5 milliseconds, the normal distribution of Na^+ and K^+ across the membrane can be restored.

Conduction of the Action Potential: The speed at which the impulse is propagated along the nerve fibre is directly dependent upon the diameter of the axon. But impulse conduction in mammalian nerve fibres is fast because of a change in *capacitance* and not because of an increase in axon diameter. The capacitance is due to the presence of myelin which is a good insulator.

Synaptic Transmission: When the impulse or action potential reaches the end-plate of the axon, *neurotransmitters* are released from vesicles in the axonal endings into the synaptic or myoneural junction. The secretions diffuse across the junction and may initiate an action potential in the next neuron. The neurotransmitter released at a neural junction induces a momentary voltage change in the postsynaptic cell. If the voltage change is strong enough, an action potential in the neural cell membrane will be produced, which similarly causes a wave of depolarization to spread through the membrane.

1.2 Gap Junctions

Gap junctions are proteinaceous channels which bridge the gap between neurons to make direct neuron-neuron contact. In other words, they create pores connecting the cytoplasms of adjacent cells as shown in Figure 1-3. Gap junctions allow ions and small molecules to pass between adjacent cells

(Lodish *et al.*, 2003). They have the alternate names of intercytoplasmic junctions or electrical synapses. Impulse transmission through gap junctions is almost a thousand times faster than at chemical synapses. Gap junction channels are composed of a family of proteins known as connexins. The importance of connexins is emphasized by generation of mutant mice with inactivating mutations in connexin genes. For example, Cx43-deficient mice show numerous abnormalities including defective oocyte maturation when gap junction communication is suppressed in the ovary. Mutations in several connexin genes are related to human diseases, including neurosensory deafness (Cx26 and Cx31), cataract or heart malformations (Cx43, Cx46, and Cx50), and the X-linked form of Charcot-Marie-Tooth disease (Cx32), which is marked by progressive degeneration of peripheral nerves. So, the intercellular communication mediated by gap junction channels plays an important role in the nervous system (Ryerse, 1989).

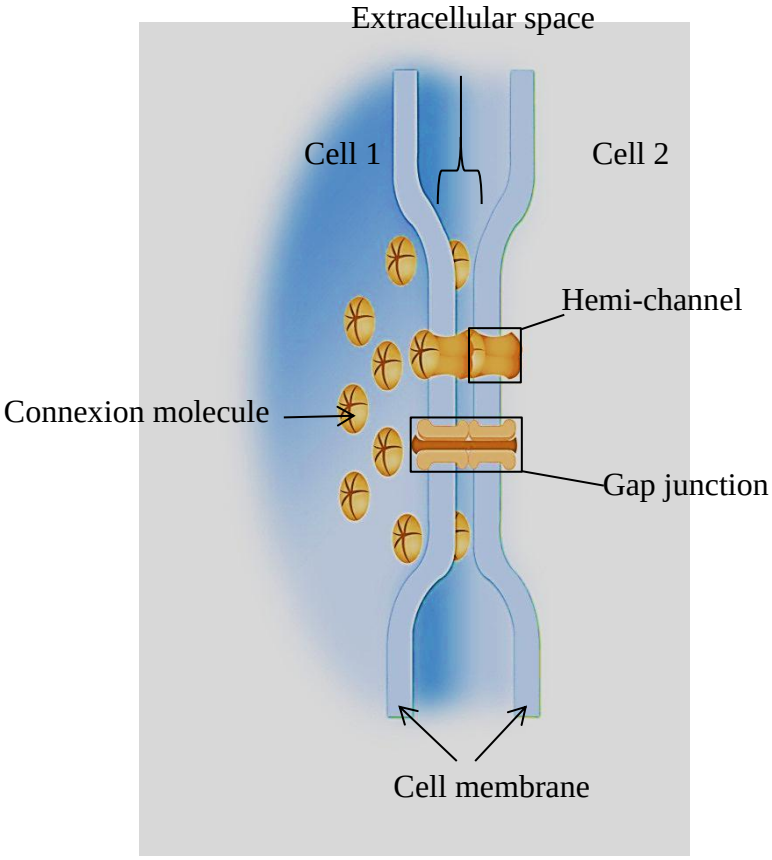

Figure 1-3: Schematic model of a gap junction

1.3 Measurements of Brain Electrical Activity

There are a number of methods for analysing brain electrical activity in single neurons or in groups of such cells (Matthews & Jezzard, 2004; Bédard *et al.*, 2006; Shah *et al.*, 2010). These methods are summarized below.

1.3.1 Intracellular measurements

The behaviour of individual neurons can be studied by activating a single neuron and recording the response; that is done by inserting an electrode inside the cell and recording the voltage difference between the inside and outside of the cell. This is the most direct measure of cellular activity, but it is the most difficult to perform experimentally. In live animals, it is an invasive technique. Action potentials are illustrated in Figure 1-4.

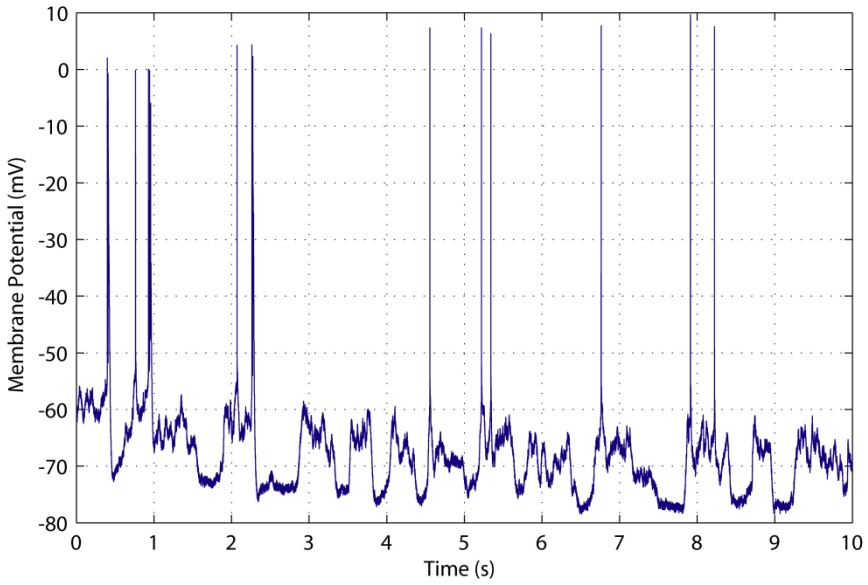

Figure 1-4: Intracellular measurements of rat neuron voltage (John Reynolds, University of Otago, used with permission)

1.3.2 Local Field Potential (LFP)

Electrodes placed on the surface of the brain will record local behaviour due to many neurons. This is a less direct measure of activity, but is easier to carry out. In live animals, it is also invasive.

1.3.3 Electroencephalogram (EEG)

The activity of the brain is recorded by electrodes placed on the skin on the skull or inserted through the skull. This method allows the recording of spontaneous electrical activity in the brain over a short period of time. In humans, EEG is recorded from electrodes placed on the scalp. It is non-invasive, easy to carry out, and is sufficient for discriminating brain activity in local areas. However it has much lower spatial resolution than the LFP measurements.

1.3.4 Functional Magnetic Resonance Imaging (fMRI)

Brain activity is measured by recording blood flow, blood volume or blood-oxygen-level changes that reflect altered activity. This method allows the recording of brain activity. For example it could distinguish reorganisation of patterns of brain activation that are a consequence of disease or injury. It is non-invasive, easy to carry out, and is sufficient for discriminating brain activity in local areas. MRI is unpleasant for the subject, very noisy and the subject has to lie still. MRI is very expensive.

1.3.5 Electrical Impedance Tomography (EIT)

Electrical Impedance Tomography (EIT) is a mapping of the electrical properties of a tissue by using multiple surface electrodes (typically of EEG type). It can determine normal, benign and malignant tissue. In addition, it is inexpensive, portable and sensitive to biological changes that alter electrical properties. EIT has disadvantages such as measurements are contaminated by characteristics of different tissue layers and data may be corrupted by subject movements.

Holder *et al.* (1996) successfully measured the percentage changes of the impedance of rabbit brain due to cerebral activation using EIT. They suggested that their success may enable use of EIT technique to monitor impedance changes of human brain during epilepsy. Yerworth *et al.* (2002) developed an EIT and optimised it for imaging the brain during an epileptic seizures. The first clinical study of epileptic seizure in humans using EIT was done by Fabrizi *et al.* (2006). They did a pre-surgical assessment to localize seizure loci for patients before going to neurosurgery. Recently

Oh *et al.* (2011) succeeded in monitoring fast neural activity in the brain with high resolution (few millimetres) and high precision (in milliseconds).

EIT is under development and measures relative changes in conductivity in an inhomogeneous sample. However van der Pauw method (that used in Section 5.2) measures absolute values of conductivity in an homogenous sample.

1.4 Electrical Conductivity

In this part, I will highlight the mechanisms of how tissue conducts electrical current. The differences between metal and tissue will be explained. Resistive and capacitive components of tissue impedance will be described. The dependence of tissue electrical properties on frequency will be emphasised (Brown *et al.*, 1999; Grimnes & Martinsen, 2008).

Solid materials can be classified by electrical conductance into three categories: conductors, insulators and semiconductors. Conductors conduct electricity by free charge carriers. Metals are characterized by high conductivity which is greater than 10^4 S/m due to conduction by free electrons. Insulators have dielectric properties; applying an electric field causes a movement of bound charges. Dielectrics are characterized by very small conductivity which is less than 10^{-10} S/m. Semiconductors in a simplistic sense could be considered as intermediate stage between conductors and insulators. Conductivities of semiconductors range from 10^{-4} to 1 S/m. Conduction in liquids follows different mechanisms from conduction in solids. Electrolytes are ions dissolved in a solution; conductivity is mainly by movement of a whole ion which is a charge carrier. Electrolyte conductivities are typically in the range 1 to 100 S/m.

Tissues may be considered as electrolytes enclosed in cell membranes. This combination makes tissue have capacitive (Figure 1-5a) and resistive (Figure 1-5b) properties as in Figure 1-6. Tissue components are neither purely resistive nor purely capacitive. For simplicity, consider a slab of insulator (Figure 1-5a) and a slab of conductor (Figure 1-5b) each of thickness x and

surface area A. In what follows, the insulator relative permittivity is denoted by ε_r, and permittivity of vacuum by ε_0; the slab capacitance is C. The conductor resistance is denoted by R and conductivity by σ.

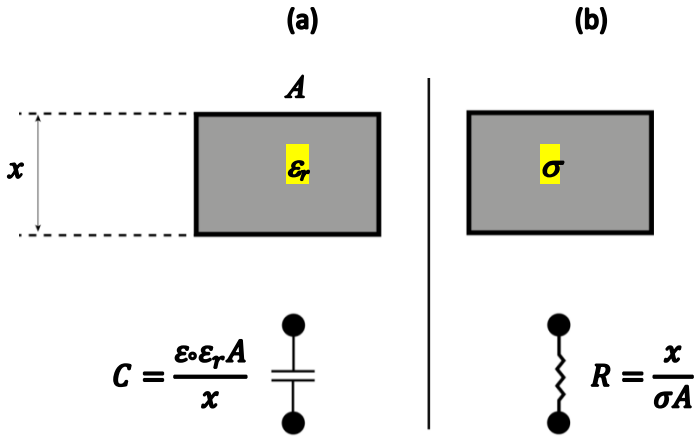

Figure 1-5: Cell membrane in a biological tissue represented as a capacitor (a). Electrolytes in cytoplasm represented as resistor (b)

A typical biological tissue can be modelled simply as a capacitor and a resistor connected in parallel (Figure 1-6). At low frequencies conductivity σ is dominant while permittivity $\varepsilon = \varepsilon_0 \varepsilon_r$ is dominant at high frequencies.

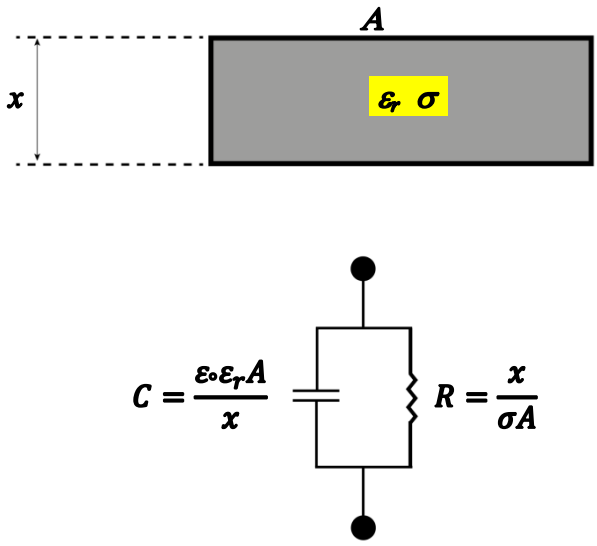

Figure 1-6: Tissue can be modelled as a capacitor and a resistor connected in parallel (Brown et al., 1999)

1.4.1 Relaxation Process

Conductivity σ and permittivity ε are functions of frequency. At any given frequency, their ratio defines an effective time-constant $\varepsilon/\sigma \equiv RC$. There are a number of models used to describe the time-constant with each tissue type having its own appropriate model. The Dilute Particle Suspension model is appropriate for modelling blood, where the conductivity is mainly due to electrolyte outside the cells, while the Multilayer model is suitable for tightly packed tissue as cells will contribute significantly to the conductivity (Kuang & Nelson, 1998).

A two-component circuit is not usually sufficient to represent the actual experimental tissue behaviour. Equivalent circuits containing three ideal components have been used to describe tissue behaviour. Four three-components models can be constructed, two resistors and one capacitor (2*R*-1*C*) in parallel and series as in Figure 1-7, and one resistor and two capacitors (1*R*-2*C*) in parallel and series as in Figure 1-8. I will outline three models that represent biological tissue: Fricke, Debye and Cole.

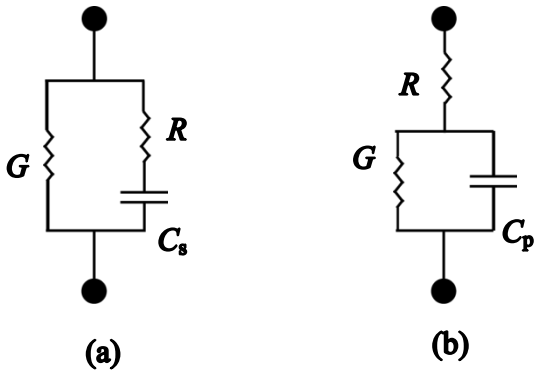

Figure 1-7: Conductor 2R-1C models: (a) parallel and (b) series

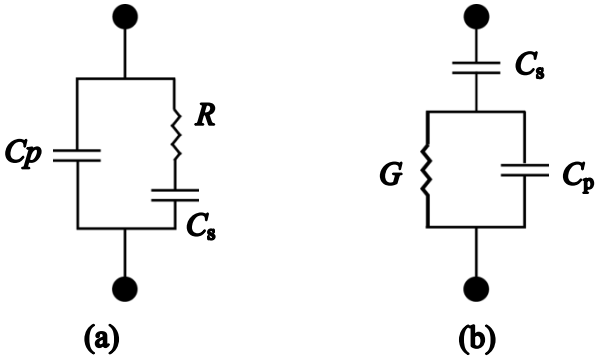

Figure 1-8: Conductor 1R-2C models: (a) parallel and (b) series

I will be using a series combination of Figure 1-6 and Figure 1-7 (a) for my own model in Chapter 8.

1.4.2 Fricke Model

In 1924 Fricke constructed a tissue model. He considered R_p as the resistance of the extracellular fluid, R_s as the resistance of the intracellular fluid connected in series with C_s which represents the membrane capacitance as in Figure 1-9.

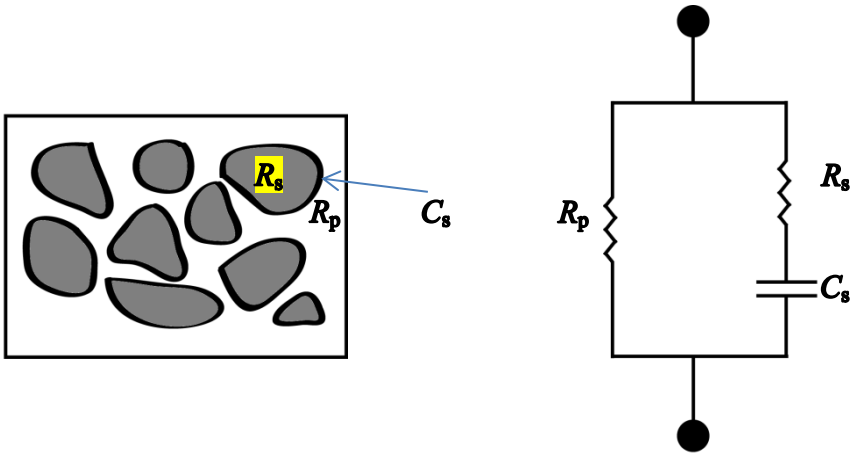

Figure 1-9: Diagram of cells and its Fricke model

By considering the biological tissue as cells suspended in an electrolyte, Fricke (1925) showed that the capacitance factor in a biological tissue arises from polarization of the suspension and the static capacitance of the cell membrane. Later, Fricke (1932) introduced the concept of a Constant Phase Element (CPE) which means modelling a frequency-dependent element so that the phase of immittance (i.e., either impedance or admittance) becomes independent of frequency by assuming a capacitor or resistor whose value is

frequency dependent. For a Fricke constant phase element CPE_F, we denote impedance as Z_{cpeF} and admittance $Y_{cpeF} = 1/Z_{cpeF}$. The Fricke model describes conductivity measurements; Fricke explained that at lower frequencies, the conductivity of the tissue is based mainly on movement of the current around the cells not through them. At higher frequencies the cell membrane loses its insulating properties and becomes conductive; as a result, current also moves through the cells.

1.4.3 Debye Model

Applying an electric field to an electric dipole within a material causes polarization. That is modelled and described by Debye's equations (Debye, 1929). Figure 1-10 shows the equivalent circuit for the Debye equations. In this model C_∞ and $C_\circ$ are capacitance at infinite and zero (static) frequencies respectively and k is a geometric factor.

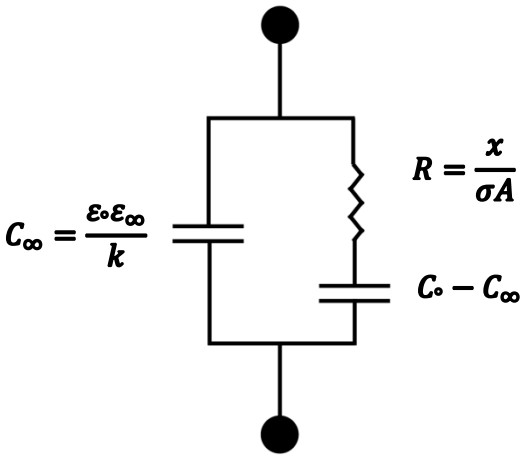

Figure 1-10: Debye model

However, over a wide range of frequencies, experimental results do not agree with predictions from Debye's model (Brown *et al.*, 1999).

1.4.4 Cole Equation

The complete Cole (1940) admittance system is the best model to describe cells and living tissue (Grimnes & Martinsen, 2008). In this model, R_∞ and $R_\circ$ are used for resistance at infinite and zero (static) frequencies respectively and $\Delta R = (R_\infty - R_\circ)$, G_∞ and $G_\circ$ are used for conductance at infinite and zero (static) frequencies respectively and $\Delta G = (G_\infty - G_\circ)$, G_p for

extra cellular liquid conductance, Z_{cpeF} for impedance, Y_{cpeF} for admittance. This version is described by the admittance (Y=1/Z).

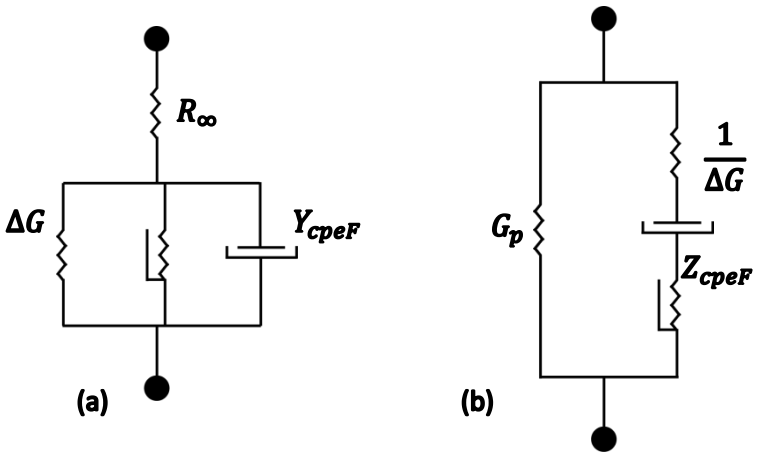

Figure 1-11: The complete Cole model: (a) Cole$_z$ system, (b) Cole$_y$ system, where —∿— is an ideal resistor, while ⊣≈⊢ and ⊣‖⊢ are electrolytic components with frequency-dependent values.

The dependent variable in the Cole equation is immittance. Cole introduced the Cole$_z$ equation to describe tissue impedance

$$Z = R_\infty + \frac{\Delta R}{1 + (j\omega t_z)^\propto} \qquad (1\text{-}1)$$

where t_z refers to a characteristic time constant, α to a dimensionless material constant parameter that is independent of tissue geometry or frequency. It is always positive $0 \leq \alpha \leq 1$. The simplest equivalent circuit for equation (1-1) is shown in Figure 1-11(a). By ignoring the series resistance R_∞, the admittance of the parallel part that remains is

$$Y_{cole} = \Delta G + \Delta G(j\omega t_z)^\propto \qquad (1\text{-}2)$$

But it is difficult to deal with this admittance using the characteristic time-constant t_z. The impedance form is easier

$$Z_{cole} = \frac{1}{\Delta G + \Delta G(j\omega t_z)^\propto} \qquad (1\text{-}3)$$

Equation (1-3) describes an ideal conductor in parallel with a Fricke CPE$_f$. The ideal conductor and the Fricke CPE$_f$ are both in series with resistor R_∞.

Grimnes & Martinsen (2008) find the best suited equation for the 2*R*-1*C* from the four models described at the end of Section 1.4.1. Therefore, they described tissue admittance by Cole$_y$ equation

$$Y = G_{\circ} + \frac{\Delta G}{1 + \left(j\omega t_y\right)^{-\alpha}} \qquad (1\text{-}4)$$

The Cole model is a semi-empirical model based on measured data. It has been successfully applied to wide ranges of materials. However it does not give the underlying mechanisms of measured phenomena. I have not used this model in Chapter 8 because it has too many parameters.

1.5 Current Flow and Electrical Damage to Cells

1.5.1 Frequency-dependent Electrical Conduction of Brain Tissue

Brain tissue contains free charge carriers (ions) so it could be considered as a conductor and described in conductivity terms. But dielectric terms are also partly involved because the tissue contains bound charges. In addition to the free charge carriers and the bound charges, there are pumps that actively transport ions. This is an important factor in neural function. For electric fields of frequencies less than 100 kHz conductivity is dominant.

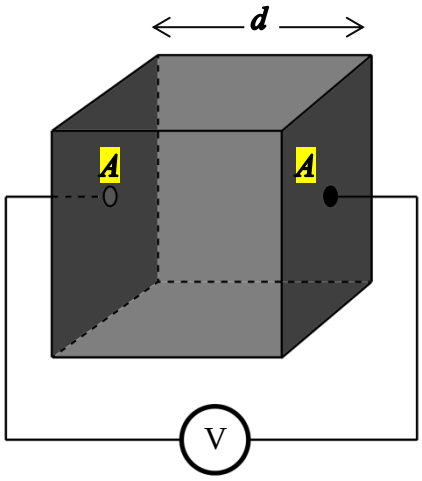

Figure 1-12: Unit cube of tissue

The electric properties of brain tissue can be determined by electrical conductivity. A conduction and displacement current will flow if a sinusoidal varying potential V is applied to a unit cube of tissue as in Figure 1-12. The conduction current I_c obeys $I_c = VG$, where G is the tissue

conductance. The displacement current I_d is 90° out of phase with conduction current, and has a magnitude given by

$$I_d = \frac{dV}{dt}\frac{A}{d}\varepsilon_r\varepsilon_\circ = V_\circ \frac{A}{d}\, 2\pi f \varepsilon_r\varepsilon_\circ \qquad (1\text{-}5)$$

where $\varepsilon_\circ$ is the dielectric permittivity of free space, ε_r is the dielectric relative permittivity of the sample and f is the frequency of the applied sinusoidal potential.

Figure 1-13 shows that at low frequencies ($\lesssim 10^6$ Hz) the displacement current (I_d) that is generated from bound charges in the tissue is negligible compared to the conduction current (I_c) that is generated from the free charges. It is clear that $I_c \approx 200\ I_d$ at 10 kHz.

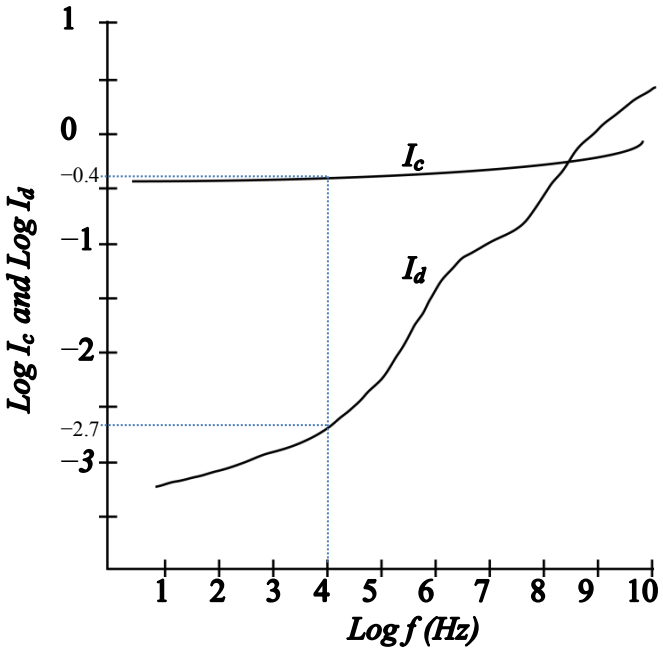

Figure 1-13 : Frequency dependence of conduction and displacement currents in tissue (Brown et al., 1999)

Neurons will be affected by electric current as the frequency increases in three different bands as described by the following:

- Frequencies below 0.1 Hz cause electrolysis at the interface between the electrodes and the tissue
- Frequencies above 10 Hz cause a reversible electrolysis and then cause a neural stimulation. In particular neurons could be stimulated

if their potential difference (80 mV) is reversed for more than 20 μs or using stimuli with frequency less than 50 kHz

- Frequencies above 100 kHz cause heating of the tissue. These high frequencies are used in electro-surgery to cut tissue.

1.5.2 Electrical Damage to Cells

Super-physiological electrical current causes tissue damage; there are two main mechanisms for the current to cause injury to cells:

- Heat effect of the current where the electrical energy dissipates and converts to heat energy. The oscillation of electrical dipole molecules at microwave frequencies causes tissue burning.
- The effect of electric forces on charged components of the cell.

The damaging effect of electric current on the cells depends on (Lee & Astumian, 1996; Lee, 2005):

- Cell size. Larger cells will experience more damage.
- Frequency. If the frequency is less than 10 kHz joule heating will cause damage to the cell membranes, while between 10 kHz and 10 MHz joule heating and dielectric heating of proteins are more likely.

In electroporation, structural defects or 'pores' are created by destroying the bilayer lipid membrane of the cell. Electroporation may be caused by potentials greater than 0.6-0.8 mV across a transmembrane distance (10 nm). Electroporation may also called electropermeabilization if it is used as a technique to form pores in a single cell (Wang *et al*., 2010).

1.6 Dielectric Phenomena and Dispersion of Biological Tissue

The effect of current on biological material arises from the charge displacement response to the current. The bulk properties of tissue are determined from frequency-dependent charge movement.

Three major dispersions of biological tissue were observed by Schwan (1957). These relaxation ranges are labelled α, β and γ (Schwan, 1963) as shown in Figure 1-14.

At low frequency (20 Hz to 1 kHz), α-dispersion arises (Figure 1-14) because current flow across cell surfaces causes a non-permanent dipole (Pethig & Kell, 1987b). Foster & Schwan (1989) proposed that α-dispersion is due to counterion (ion of opposite charge) polarization arising from ionic diffusion in the electrical double-layers beside a charged protein and cell membrane surfaces. Electrical conduction of the tissue is almost totally due to the extracellular electrolytes and the conduction across the cell is negligible.

At intermediate frequency (10 kHz to 5 MHz), β-dispersion appears in bulk electrically heterogeneous materials due to interface polarization (Hanai, 1960; Hanai *et al.*, 1979) due to charging cell membrane interfaces within the material. In their review, Kuang & Nelson (1998) showed that β-dispersion is due to ion accumulation at cell membranes, blocking further ion movement.

At high frequency (above 100 MHz), γ-dispersion occurs as a result of permanent dipole relaxation of small molecules (of which there are a large number in biological tissue) (Pethig & Kell, 1987b).

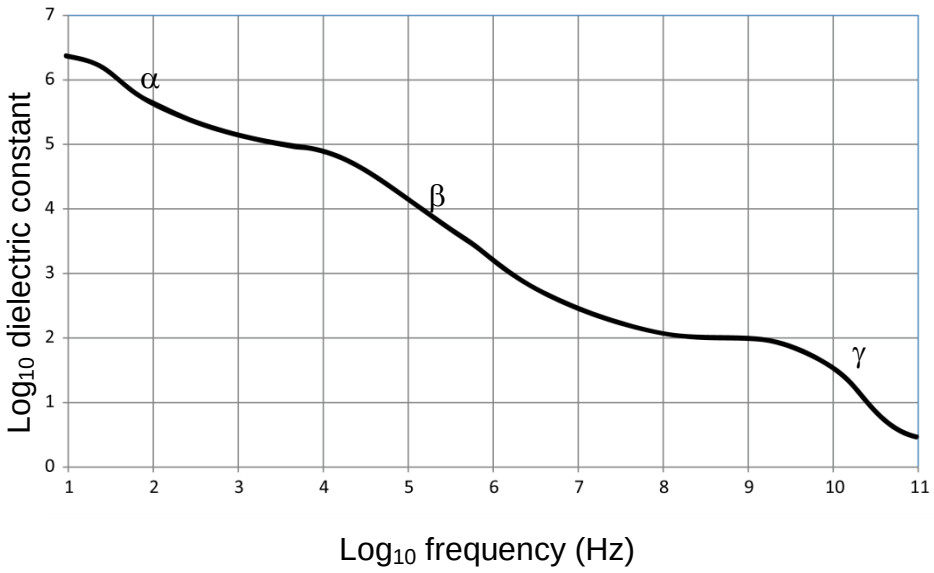

Figure 1-14: Sketch of the main dispersion regions of biological tissue (Schwan, 1963; Lazebnik, 2008)

In my fixed-frequency experiments of Chapters 4 to 7, I used 10 kHz. This lies at the boundary between α- and β-dispersion. This frequency is safely lower than 100 MHz to avoid minimizing the electrical barrier and capacitance effect of the cell membrane. Furthermore at high frequencies any anisotropy in tissue conductivity may disappear (Damez *et al.*, 2007).

1.7 States of Consciousness

Seizures are an important pathological state of brain dynamics. The healthy brain states include wake, sleep and anesthesia. These will first be discussed before returning to seizures in more detail.

1.7.1 Sleep

Sleep research started strongly in 1953, with the decade following being the most significant (Gottesmann, 2001). Sleep has many important functions. Although now disputed (Siegel, 2003), some researchers have reported that sleep deprivation leads to death (Rechtschaffen *et al.*, 1983; Everson *et al.*, 1989; Kushida *et al.*, 1989). There is ample evidence showing that sleep is important for memory consolidation (Steriade *et al.*, 1993; Buzsák, 1998; Sutherland & McNaughton, 2000; Tononi & Cirelli, 2006) and for neuronal plasticity (Sejnowski & Destexhe, 2000; Abraham, 2006; Tononi & Cirelli, 2006).

Sleep can be divided into several stages: 1, 2, 3, 4 and REM (rapid eye movement) sleep. Stage 1 is light sleep where a sleeper drifts in and out of sleep and can be awakened easily. In stage 2, eye movement stops and brain waves become slower with only an occasional burst of rapid brain waves. When a person enters stage 3, extremely slow delta waves are interspersed with smaller, faster waves. In stage 4, the brain produces delta waves almost exclusively. Stages 3 and 4 are referred to as deep sleep, and it is difficult to wake someone at this point in the sleep cycle. In the REM period, waves show similar characteristics to that experienced during wake. Neurons fire more independently, generating low voltage asynchronous EEG brain waves. Body movements are prevented during REM sleep because of reduction of muscle tone (Siegel, 2003).

1.7.2 General Anaesthesia

Anaesthesia stops signal transmission by acting on specific molecular receptors. General anaesthesia prevents consciousness and pain during surgical procedures. Sleep and anaesthesia are two states with many common properties (Tung & Mendelson, 2004; Hutt, 2011). Neuron activity changes from tonic firing to bursting. This is reflected in EEG recordings as a change in wave patterns from high frequency with low amplitude to low frequency with high amplitude.

1.7.3 Awake

Conscious perception of, and engagement with, the external world is generated during the awake state. In this state, neuronal activity is near maximum and individual neurons fire nearly independently of each other (Siegel, 2003). This independence means that EEG features high frequency (>20Hz), low amplitude activity.

1.7.4 Seizures

Seizures in the brain occur when there is a loss of balance between excitatory and inhibitory influences on neuronal activity (McCormick & Contreras, 2001), resulting in hyper-synchronized bursts of activity in cerebral cortex and hippocampus. More than 40 different types of epileptic seizures are known. Each type is thought to have its own cellular and molecular mechanism (McCormick & Contreras, 2001).

Similar activity can be activated in brain slices by lowering the Mg^{2+} in the artificial cerebrospinal fluid (ACSF) (Li Zhang *et al.*, 1995). This activity is called “seizure-like” since it is debatable whether a brain slice exhibits a seizure in a similar manner to a whole brain. For my experiments described in Chapters 5, 7 and 8, I induced seizure-like events in brain slices using the Zhang method.

2 Review of Literature and Project Motivation

The aim of this study is to find out whether seizures are related to the electrical conductivity of brain slices. This review will provide background information connected to the methodology chosen to measure the conductivity, and will highlight limitations, weaknesses and precautions taken during the experimental work. I start by revealing a gap in research and the conflict between scientific papers. The remainder will discuss the parameters that affect the measurements and the motivation for this project.

On the scale of a single neuron, the brain responds non-trivially to electrical stimulation, for example, with the formation of action potentials. However, the behaviour of the bulk system is not so clear. For instance, linear models have been used to predict behaviour of collections of nonlinear neurons (Jirsa & Haken, 1996; Robinson *et al.*, 1997; Liley *et al.*, 1999; Steyn-Ross *et al.*, 2004).

It is not immediately obvious whether cortical tissue will respond linearly or nonlinearly to stimulation. On one hand, Bédard *et al.* (2006) made a model to explain the frequency filtering properties of local field potentials (LFPs). They suggested that the frequency filtering properties of LFPs are generated from the induced electric fields in the glial or "supporting" cells which are passive cells surrounding the neurons. Bédard *et al* (2004; 2006; 2010) concluded that cortical tissue has a non-flat (i.e. nonlinear) impedance spectrum. Burdette *et al.* (1986b) and Gabriel *et al.* (1996a; 1996b) also found nonlinear results measuring the conductivity of cortical tissue from pig and dogs. However, in a study on macaque monkeys, Logothetis *et al.* (2007) found that brain tissue showed no obvious signs of nonlinear behaviour. Their results show that in grey matter, impedance is frequency independent, uniform in all orientations (homogenous), and can be modelled ideally as a resistor. This is in conflict with the nonlinear results of Bédard *et al.*, Burdette *et al.* (1986b), and Gabriel *et al.* (1996a; 1996b) and provides further motivation for studying the impedance of brain slices.

2.1 General Measurements on Conductivity

Previous measurements have shown a huge range of conductivity for biological tissue. A collection of the conductivity data of biological material reviewed by Geddes & Baker (1967) traced the published papers from 1937 to 1965. They showed that the measured *in vivo* conductivity for rabbit and cat grey matter ranged from 0.23 to 0.48 S/m depending on the type of animal and frequencies used between 5 Hz and 5 kHz. The conductivity range shown by Geddes & Baker was confirmed by Robillard & Poussart (1977) where they found that the conductivity of grey-matter, cortex and nuclei in a living adult cat brain *in vivo* ranges from 0.20 to 0.33 S/m using a sinusoidal test signal with frequencies ranging from 20 Hz and 2 kHz.

Gabriel *et al.* (1996a) reviewed the literature and found that the conductivity of grey matter for human and a variety of animals ranged from about 0.16 S/m at 100 kHz to about 20 S/m at 10 GHz. Based on that review, Gabriel *et al.* (1996c) built a model to predict the conductivity of tissue over frequencies ranging from 10 Hz to 100 GHz. They declared that their model is more accurate above 1 MHz with a better fit to experimental measurements.

Latikka *et al.* (2001) measured the conductivity of grey matter from living human brain tissue at 50 kHz and reported a value of 0.29 S/m. Sekino *et al.* (2005) estimated the conductivity of grey matter in human brain at ~0.15 S/m using magnetic resonance imaging and reported that it did not have a clear anisotropy (i.e., conductivity does not depend on direction). Logothetis *et al.* (2007) agreed with Sekino and reported that the grey matter is isotropic but disagreed in conductivity values. Logothetis *et al.* measured the conductivity at frequencies ranging from 10 Hz to 5 kHz and found the conductivity of the grey matter of monkeys ranged from 0.304 to 0.606 with average 0.404 S/m. Gabriel *et al.* (2009) in a literature survey found that the conductivity of grey matter ranges from 0.03 to 10 S/m across the frequency range 10 Hz to 10 GHz. They also reported that grey matter is more isotropic (uniform in all orientations) in conductivity than white matter. Electrical conductivity of the brain tissue was measured as an alternate

measure for tissue permeability (Liu *et al.*, 2010). They found that there is a linear relationship between drug distribution and tissue conductivity.

Overall the literature shows a wide range of conductivities and disagreement between publications.

2.2 Detecting Seizures by Measuring Conductivity

Elazar *et al.* (1966) credits Efron (1961) as the first to find an increase in resistance during induced seizures. Previously, many researchers had found that there was a qualitative change in electrical properties of brain due to different abnormal activities or events such as spreading depression, electrical activity and seizures (Freygang Jr & Landau, 1955; Van Harreveld & Ochs, 1956; Adey *et al.*, 1962; Van Harreveld & Schade, 1962).

Valentinuzzi *et al.* (1996) reported that an impedance technique could be used to monitor physiological events caused by a change in dimension (tissue size), conductivity or permittivity. In some biological activities the change in measured impedance is the only way to explain the biological event. Valentinuzzi *et al.* present all the main experiments performed on humans until 1996 to evaluate deviations in volume, location and distribution of fluids and tissue accompanying functional activity. Changes in the composition and concentrations of ions (K^+, Na^+, Cl^- and Ca^{2+}) in the brain may cause abnormal behaviour. To detect an early warning before epileptic seizures start, they said that

> *The subsurface electrochemical activity may be a more promising tool [than EEG] because the ionic activity is considered as the principal mechanism leading to development and progression of epileptic seizures (p.388)*

Glass & Miller (1988) studied the role of ionic concentration in the brain's extracellular region of cats to develop an early detection system for seizure. They reported that the cerebrospinal fluid (CSF) conductivity is halved up to 15 minutes before seizure activity.

From the above papers we conclude that it may be possible to detect the abnormal behaviour of neurons during epilepsy by measuring the conductivity of brain tissue that is seizing.

2.3 Conductivity Changes After Death

A number of experiments have been conducted to find the difference in conductivity between live and dead brain tissue. Burdette *et al.* (1986a) measured the conductivity of the brains of dogs at 2450 MHz for thirty minutes before euthanasia until ninety minutes after death. They found that the conductivity decreases at a constant rate after a lethal dose of pentobarbital was injected.

In another experiment, Burdette *et al.* (1986b) measured the conductivity of living canine brain in-situ using a monopole antenna probe. They showed that the mean conductivity of grey matter is 1.74 S/m. Their results showed that conductivity increases from about 0.7 to 2.4 S/m over the frequency range 0.1 to 4 GHz. They also studied the change in conductivity before, during and after sacrificing the animal. They did their measurements at 2450 MHz in canine brain and found that in grey matter the conductivity increases in the first eight minutes from 1.8 to about 2.1 S/m, stabilized at 2.1 S/m for five minutes then decreased gradually to 1.8 S/m within 35 minutes and stabilized at that level until the end of the experiment.

These results are in contrast to Kraszewski *et al*. (1982) who made a comparison study *in vivo* and *in vitro* in the frequency range from 100 MHz to 8 GHz. They found that, a few hours after death of cats and rats, any changes in the conductivity were within 3% which is their uncertainty. In other words, no changes could be detected.

Gamba & Delpy (1998) measured the electrical current density distribution (d.c. pulses) within piglet head tissues by magnetic resonance imaging. In their study, the electrodes were placed on the top of the head and on the roof of the mouth. The majority of the electrical current reached the brain tissue via the hole at the base of the skull where the spinal cord enters the brain

and the electrical current that reached the brain was 62% larger in a living animal than a dead animal.

Around 2003, there was considerable debate about whether the data collected from non-living tissue reflect the dielectric properties of living tissue. Therefore Schmid *et al.* (2003) used pigs to investigate this. The dielectric measurement system consisted of a dielectric probe and a network analyser. They measured the conductivity of pig cortex for about 19 hours, an hour before death to 18 hours after death. They used frequencies ranging from 800 to 1900 MHz. There was a 15% decrease in conductivity of the grey matter at 900 MHz and about 11% at 1800 MHz. So generally conductivity decreases after death.

2.4 Conductivity Changes with Temperature and Age

The rate of change of conductivity with temperature (temperature coefficient) depends on tissue type, animal, frequency and whether it is taken *in vivo* or *in vitro* (Gabriel *et al.*, 1996a). Their results are presented in Figure 2-1 using triangle (▲) symbols. Frequencies ranged from 100 kHz to 10 GHz. Baumann *et al*. (1997) measured the conductivity of human CSF over the range 10 Hz to 10 kHz, and found that at room temperature (25°C) conductivity was 1.45 S/m while at body temperature (37°C) the conductivity was 1.79 S/m. This means that conductivity is 23% higher at 37°C. Schmid *et al.* (2003) also measured the change of conductivity with temperature. Porcine brain conductivities as a function of temperature were measured about four hours after death. They found that the temperature coefficient at 1800 MHz was 0.6 %/°C and at 900 MHz is 1.2%/°C.

The age of the brain also affects conductivity. Gabriel (2005) studied the dependency of conductivity on the age of brains. Ten-, thirty- and seventy-day old Wistar strain rats were used and it was reported that the conductivity decreases with age. She used frequencies ranging from 200 kHz to 10 GHz and the conductivity changed (depending on the frequency and age) from about 0.15 to 10 S/m.

2.5 Conductivity Changes with Frequency

Gabriel *et al*. (1996a; 1996b; 1996c; 2009) and many others showed that the conductivity of cortex changes with applied frequency. Based on a model for the calculation of the dielectric properties of body tissues developed by Gabriel and others (as given in the above references), Andreuccetti *et al.* (1997) built software to calculate the relation between conductivity and frequency of brain grey matter. For example, the continuous curve of Figure 2-1 is produced using the Andreuccetti software.

Table 2-1 summarises some measured conductivities of cortex.

Table 2-1: Measured conductivities with frequency

Reference	Experimental animal	Frequency range	Conductivity (S/m)	
			from	to
Geddes & Baker, 1967	rabbit	5 Hz to 1 kHz	0.32	0.48
	cat	1 kHz	0.23	0.23
Robillard & Poussart, 1977	cat	20 Hz to 2 kHz	0.2	0.33
Burdette *et al.*, 1986 b	dogs	0.1 to 4 GHz	0.7	2.2
Gabriel *et al.*, 1996 a	Human and a variety of animals	100 kHz to 10 GHz	0.16	10.7
Gabriel *et al.*, 1996 b	Human and a variety of animals	10 Hz to 10 GHz	0.004	10
Latikka *et al.*, 2001	living human brain	50 kHz	0.29	
Sekino *et al.*, 2005	human brain	by MRI approximately d.c.	0.15	
Gabriel, 2005	Wistar strain rats	300 kHz to 10 GHz	0.15	10
Logothetis *et al.*, 2007	Macaque monkeys	10 Hz to 5 kHz	0.3	0.61
Gabriel *et al.*, 2009	Human and a variety of animals	10 Hz to 100 kHz	0.03	0.3

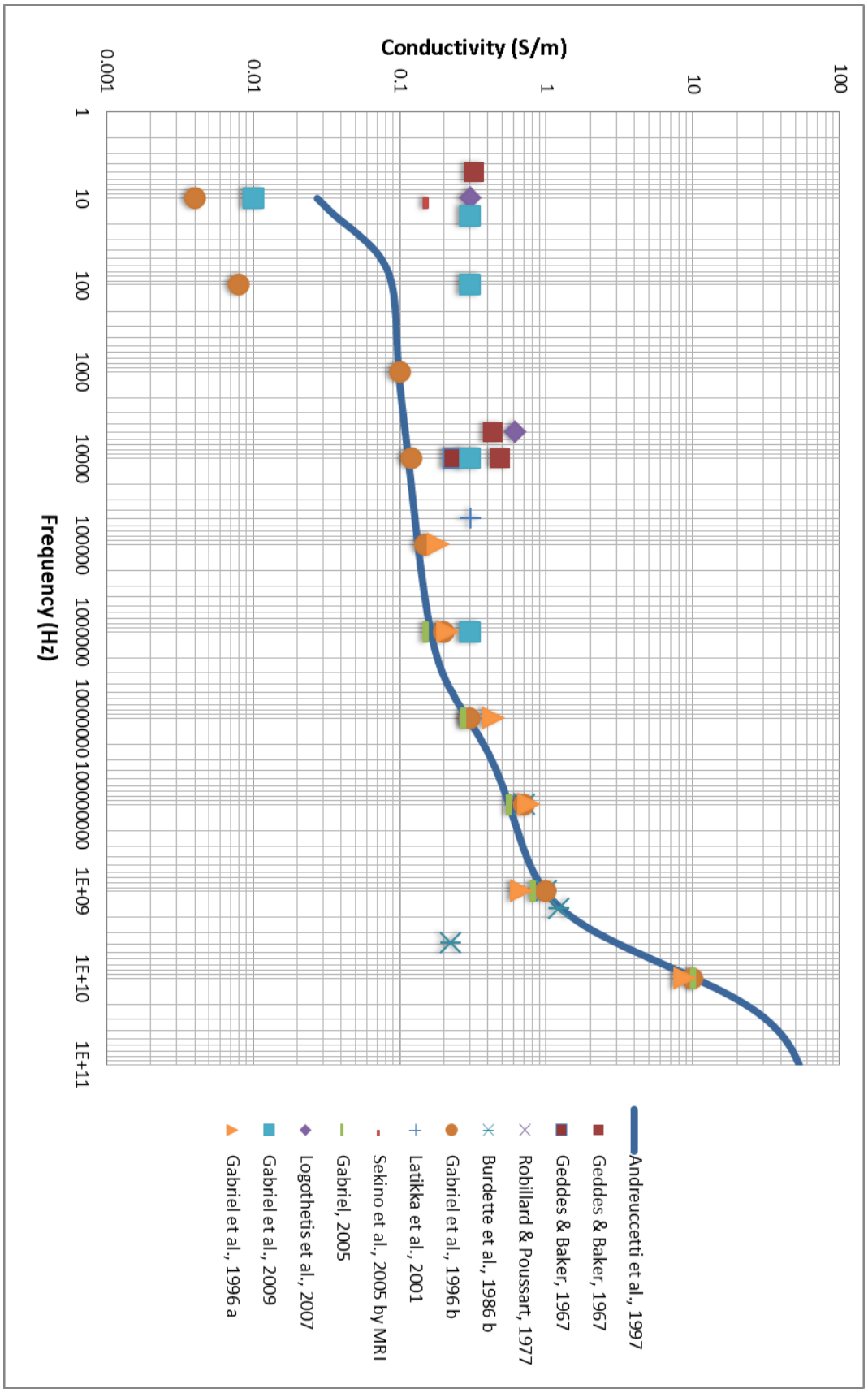

Figure 2-1: Measurements of conductivity drawn from literature. The blue line is modelling the variation of conductivity of cortex with frequency using the software of Andreuccetti et al. *(1997)*

2.6 *In Vivo* versus *in Vitro*

Experimental work is typically carried out either *in vivo* (in living tissue) or *in vitro* (in glass). The latter is easier to achieve and generally provides an excellent tool for assessing neural activities (Engel *et al.*, 2007). Other advantages of working *in vitro* rather than *in vivo* include less demanding procedures to obtain ethical approvals, less effort required to keep the brain slices alive, greater stability of slice samples due to absence of blood supply and other organs, as well as the ease of placing tissue slices under the microscope which would be difficult to achieve using the whole body of the animal. In addition, there is no need for extra complicated equipment to monitor the physiological functions of the experimental animal.

Bindman *et al.* (1988) found that the conductance in slice is half that found *in vivo*. This finding highlights a primary concern with respect to *in vitro* measurements: to what extent do they reflect the characteristics of the living animal? To answer this question I had to investigate two main points. The first is the change in dielectric properties after excision as discussed in Section 2.3. For more details see Surowiec *et al.* (1985; 1986b) and Astbury *et al.* (1988).

The second point is the change in electrical conductivity with physiological changes (see also Section 2.3). For more details see Geddes & Baker (1975), Burdette & Karow (1978), Stuchly *et al.* (1981) and Surowiec *et al.* (1986a).

2.7 Project Motivation

Since the brain is electrically active, it is reasonable to expect that it will respond non-trivially to electrical stimulation. One might expect, for example, bulk electrical activity of brain tissue to be nonlinear, anisotropic, and dependent upon the state of the brain (e.g. sleeping, awake, anaesthetized etc). However Logothetis (Logothetis *et al.*, 2007), in a study on Macaque monkeys found that brain tissue behaved in a similar manner to saline solution in regard to bulk electrical conductivity, with no obvious signs of nonlinear behaviour. This is a surprising result, and motivated us

(the Cortical Modelling Group) at the University of Waikato to study further the excitability of brain tissue.

Due to the limitations and inaccuracies of the previous studies (described in Sections 2.1 to 2.6), I found it is necessary to develop a new technique for measuring brain slices conductivity *in vitro*. Therefore, the goals of this thesis are:

1. Establishing an effective method to measure the conductivities of small (2×2 mm and 0.4 mm thickness) live brain slices.
2. Finding out whether tissue conductivity is different in normal (non-seizing) brain compared to slices of seizing brain tissue.
3. Measuring brain tissue conductivity over a frequency range from 20 Hz to 2 MHz.
4. Unlike in previous *in vitro* studies, perform *in vitro* measurements that confirm that slices are still alive after measurements.

3 Common Principles of Experimental Setup and Statistics

This chapter discusses the fundamental theories and experimental setup upon which the measurements of brain conductivity described in this thesis are based. All techniques were validated using standard KCl solutions of known concentration. Conductivity was calculated theoretically and measured experimentally by a commercial conductivity meter (RE388TX made by EDT with conductivity cell glass model E8071).

3.1 Experimental Principles

In spite of the fact that there are many methods to measure the conductivity of materials, in living tissue the methods are a few. One of the reasons is that too much current will kill the tissue. Also the measurements must be done quickly enough to minimize the disturbances to the biological system. On top of that it is challenging to measure the dimensions (height, length, thickness) of the sample under test.

In order to minimize these problems and maximize the accuracy of measurements, I used van der Pauw's method (van der Pauw, 1958a; 1958b) to measure the conductivity of mouse brain slices. This method is particularly useful as it has the advantage of being independent of the sample shape, dimensions and electrode separation (Keithley Instruments, 2004). The method and its applications are described in detail in the methodology section in Chapter 7.

I used a one-dimensional method (1D) to confirm results that I collected using the van der Pauw method. I measured conductivity of coronal and transverse slices at 10 kHz and over the frequency range from 20 to 2 MHz using the one-dimensional method in Chapters 7 and 8.

From the literature survey in Section 2.3, I concluded that tissue conductivity changes with time. Because I wanted my measurements to be

based on live tissue, my two setups were designed to do the measurements within 12 seconds after removing the ACSF that covers the slice under test. In brain slices, I drive the slice by applying alternating voltage and recording the resulting alternating current.

Because conductivity depends on age, frequency and temperature, in my study I used animals of similar age and applied a temperature coefficient to correct the measured conductivity to 25°C. At 10 kHz, temperature correction of 2%/°C was applied (Van Harreveld & Ochs, 1956). Also care was taken to minimize temperature fluctuations. A frequency of 10 kHz was chosen because of many factors: first, Cagnan *et al.* (2009) did a computational study and pointed out that a thalamocortical relay neuron responds when the input frequencies range from 2 to 25 Hz. At Chapters 5 and 7, the chosen frequency at 10 kHz is much higher than this to ensure that there is no stimulation of neurons in the cortex. Second, Gabriel *et al.* (1996b) showed that different NaCl concentrations have relatively stable conductivity as frequency ranged from 5 kHz to 1 GHz; they indicated a clear electrode polarization error in conductivity below 1 kHz and it became significant below 100 Hz.

I was not able to find any studies that verified brain slice viability after the conductivity measurements had been completed. By looking to Gamba & Delpy (1998), we know that dead tissue responds differently from live tissue. That encouraged me to do the experimental work on living slices.

I used mice as the experimental animal because the slice preparation method is well established for this animal. They are more commonly used and the facilities are available at The University of Waikato.

The set-up of this research has the following advantages:

1. Measuring the electrical conductivity of the same sample over a wide range of frequencies 20 to 2MHz.
2. Measurements can be done very quickly.
3. MATLAB gives flexibility and many ways to do the measurements.
4. There is scope for further development.

3.2 Electrodes

Recording physiological parameters from the body requires a conversion from those at the body to a form that can be carried via wires and displayed and interpreted via medical equipment or computer. Converting the body electrical signals from ion charge carriers to electron charge carriers requires an electrode interface. Electrodes may be made of metal, conductive gel and other materials. Every type of electrode has its uses and limitations.

We need to differentiate between current-carrying electrodes and pick-up electrodes. Current-carrying electrodes are used for current injection while pick-up electrodes are used to detect potential difference: a negligible current flows through these. Pick-up electrodes typically have high impedance so cannot be used to deliver current.

Electrodes can be made of different materials, for example, carbon, silver-silver chloride (Ag/AgCl), platinum, tungsten, titanium, silver, copper, gold and stainless steel. Electrodes are designed according to their application. For example, a metal plate with gel or hydrogel is usually used for skin-surface measurements. An invasive needle is used for electromyogram (EMG) and in neurology. A small transmembrane electrode (microelectrode) is used for intracellular recording.

One of the required properties of an electrode is that it be biocompatible, which means that it does not change tissue properties. Grimnes & Martinsen (2008) carried out a comparison between different electrodes types. They concluded that Ag/AgCl electrodes have low d.c. polarization but they are not biocompatible. More specifically, Moussy & Harrison (1994) found that the Ag/AgCl electrodes are not suitable for implantation over a prolonged period of time such as a week. However this is not likely to be an issue for my experiment because measurements were taken within seconds. Ag/AgCl electrodes are safe for use on skin surface for ECG and EMG recording. Grimnes & Martinsen (2008) found platinum electrodes to be non-corrosive, biocompatible but polarizable: gas bubbles are seen during d.c. measurements. Gold electrodes are non-corrosive also but less

biocompatible than platinum. Titanum is highly biocompatible. Stainless steel is mechanically durable and non-corrosive but highly d.c. polarizable and noisy. Ag/AgCl needs only one twentieth of the voltage required for platinum and carbon electrodes to permit d.c. current flow (Grimnes & Martinsen, 2008). In case of d.c. measurements, gas bubbles are seen on carbon electrodes, with erosion visible on the carbon anode. Grimnes & Martinsen (2008) reported that Cooper *et al*, (1980) injected current pulses to 0.9% saline. They measured the voltage using six different metals (chlorided silver, platinum, silver, copper, gold and stainless steel) and they reported that chlorided silver showed closest readings to the source and least wave distortion. Tungsten electrodes have high hardness and electrical conductivity. Therefore, it is used for recording from biological tissue especially if high strength and wear resistance are required.

The silver-silver chloride electrodes (Ag/AgCl) are the most common in biological application. They have the advantage of a reversible electrochemical process:

$$Ag + Cl^- \rightleftharpoons AgCl + e^- \qquad (3\text{-}1)$$

The charge carriers are chloride ions in the tissue and electrons in the silver wire. This conversion is a source of noise in electrical measurements (Brown *et al.*, 1999).

3.2.1 Polarization Potential

When a metal electrode is placed in contact with a tissue via electrolyte, charges move in and out from the metal. After a while, a potential difference builds up between the electrode and the tissue. This potential difference is maximum at d.c. and decreases with increasing current frequency. Electrode potential varies from metal to metal and it is usually much higher than typical electrophysiological potentials. Using two electrodes from the same material may reduce these effects by providing some cancellation. However, cancellation may not be complete because electrode potential varies with time, and connection between the tissue and the electrode cannot be assumed to be identical for both electrodes. Electrode potential varies with time because of chemical reactions at the contact point between electrode and

tissue. This causes a noise in measurements. It has been found that Ag/AgCl electrodes are electro-chemically stable for a period up to 200 days of continuously measured pH (Brown *et al.*, 2009).

The noise from the electrode interface is inversely proportional to the square root of the exposed area to the tissue. Electrode noise can be minimized by increasing the surface area of the electrode interface. The noise of wet-gel/metal electrodes decreases with time (Huigen *et al*., 2002). One would normally expect that noise increases with time and it may be that the electrode noise performance is dominated by the gel.

Thermal or Johnson noise is the noise which arises from the thermal effect of charge carriers. It increases with increasing temperature. Thermal noise (V_{th}) can be calculated from the Nyquist equation,

$$V_{\mathrm{th}}^2 = 4kTBR \qquad (3\text{-}2)$$

where k is the Boltzmann constant, T is absolute temperature (kelvin), B is the bandwidth (Hz) of the recording apparatus and R is the resistance (Ω) of device under test (DUT).

Huigen *et al* (2002) measured the noise arising from different electrode metals attached to conductive paste (with contact area of 3.1 cm^2). Their results between 0.5 and 500 Hz are summarized in Table 3-1. Although it is clear that the plain silver electrode has least noise, the performance of all electrodes is similar.

Table 3-1: Noise from different metals at skin temperature (Huigen et al (2002))

electrode	Noise in μVrms
Ag/AgCl	3.5
tin	3.4
stainless steel	3.4
plain silver	3.3

I used Ag/AgCl electrodes because they are suitable for current carrying and recording voltages, can be made into needle electrodes, and are naturally suited to recording from brain tissue, since brain tissue contains Cl^- ions. It gives the closest reading to the source and least wave distortion.

3.3 Impedance Measurement Instruments

Impedance (*Z*) is an important materials characterization factor. Impedance can be defined as the total opposition to current movement.

3.3.1 Agilent Impedance Meter

An Agilent E4980A (*LCR* meter) was used to measure and compare the conductivity for seizing and non-seizing slices of brain tissue. This instrument is capable of measuring inductance (*L*), capacitance (*C*) and resistance (*R*) of an electrical circuit. It is a general-purpose *LCR* meter for inspection of components, quality control and laboratory use. The Agilent E4980A can be used to measure and evaluate the *LCR* properties of materials across a frequency range of 20 Hz – 2MHz.

The Agilent E4980A was fully automated by connecting it to a system controller and data processing software (MATLAB Instrument Control Toolbox version 7.12.0.635 (R2011a)). E5810A is the GPIB/LAN gateway that used to provide remote access and control of E4980A *LCR* meter via its General-purpose Interface Bus (GPIB) connector. A Universal Serial Bus (USB) interface was also available but I have not used it (Figure 3-1).

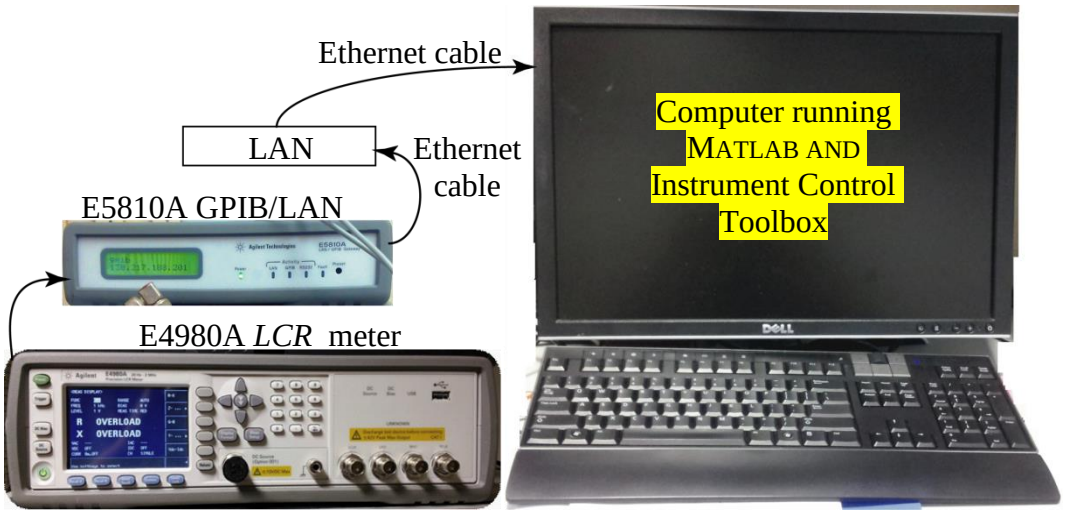

Figure 3-1: Impedance Measurement Instruments. Agilent E4980A LCR meter and E5810A GPIB/LAN gateway

3.3.2 Measurement Method

There are many approaches for impedance determination, one of them is the auto-balancing bridge method (Agilent Technology, 2009). This method can be used over a wide frequency range from 20 Hz to 110 MHz, and is accurate over a wide range of impedance values. The Agilent E4980A uses the auto-balancing bridge method.

The setup is shown in Figure 3-2. The current I_x through the device under test (DUT) is equal to the current I_r through the range resistor (R_r). The potential is zero volts at the Low point. From the measured voltages at the High terminal (V_x) and across R_r (V_r), the impedance of DUT can be calculated. From Figure 3-2 we see:

$$\frac{V_x}{Z_x} = I_X = I_r = \frac{V_r}{R_r}$$

$$\therefore Z_x = \frac{V_x}{I_x} = R_r \frac{V_x}{V_r}$$

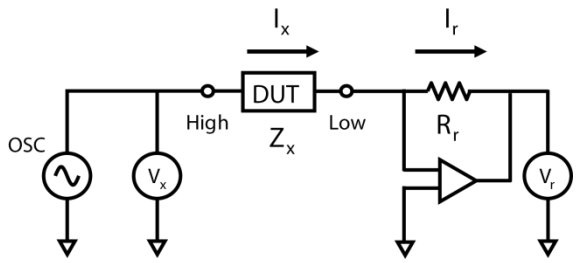

Figure 3-2: Auto-balancing bridge method. DUT denotes to Device Under Test. OSC refers to Oscillator output signal (Source: Agilent (2009))

3.4 Cabling and Terminal Configuration

As prescribed by Agilent Technology (2009), the Agilent E4980A precision *LCR* meter is equipped with four BNC connectors labelled: high current (HCUR), high potential (HPOT), low potential (LPOT) and low current (LCUR), as measurement terminals (see Figure 3-3). These terminals are named "UNKNOWN" terminals. Several connection configurations can be used to connect a DUT with the UNKNOWN terminals; the selection of the appropriate method is based on the DUT impedance and required measurement accuracy. Therefore, I present two main methods of terminal configurations, two-terminal (2T) and four-terminal (4T).

Figure 3-3: Measurement terminals of Agilent E4980A auto balancing bridge instrument

3.4.1 Two-terminal Configuration

This is the simplest method of connecting a DUT. However, it contains many sources of error. Lead inductances (L_L), lead resistances (R_L), and stray capacitance (C_o) between two leads are added to the measurement result (see Figure 3-4). To measured impedance, contact resistances (R) between the electrodes and the sample are also added. Due to these error sources, the range of the typical impedance measurement is limited to 100 Ω to 10 kΩ.

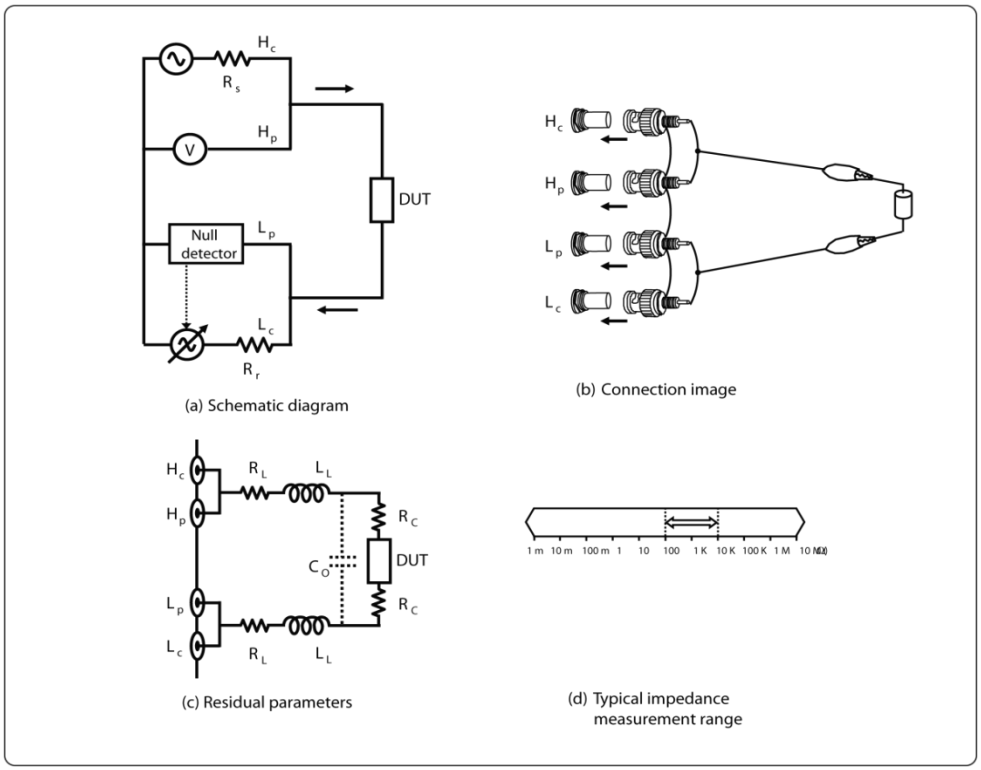

Figure 3-4: Two-terminal (2T) configuration (Source: Agilent Technology (2009))

3.4.2 Four-terminal Configuration

Following the User Manual guidance of Agilent Technology (2009), I adopted the shielded four-terminal (4T) configuration using four coaxial cables whose outer shielding conductors are connected at the two ends to the guard terminal (Figure 3-5(a) and (b)). This configuration increases the accuracy and has a wide measurement range from 10 mΩ to 10 MΩ, but the mutual coupling problem (current in one of the leads induces a small current in the other lead) remains.

The effects of lead impedances (ωL_L and R_L) and contact resistances (R_c) are reduced by the four-terminal (4T) configuration because of the independence of the signal current path and the voltage sensing leads. The voltage drop caused by the R_L, L_L, and R_c on the current leads is not sensed by the voltage leads. There is no effect of the impedances on the voltage sensing leads on the measurement because almost no signal current flows through these leads. So, measurement errors resulting from the lead impedances and contact resistances are eliminated. The 4T configuration is also called the Kelvin connection configuration.

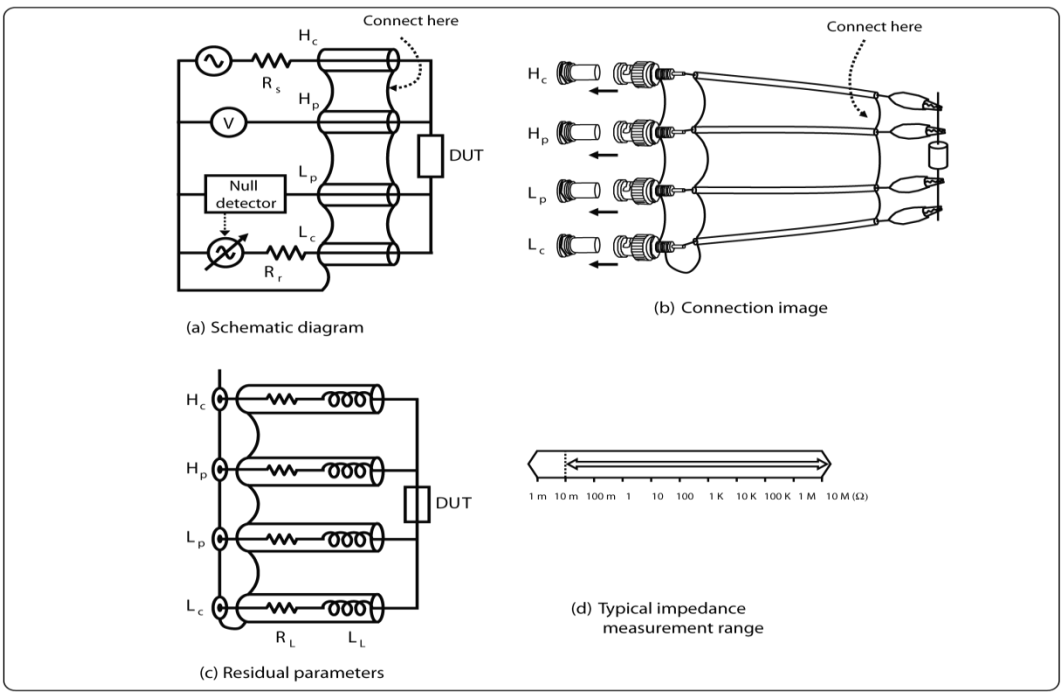

Figure 3-5: Shielded four-terminal Kelvin configuration (Source: Agilent Technology (2009))

3.5 Detect Waveform Distortion in ACSF

It is possible that ACSF is a non-linear medium and therefore it may distort the sine wave signal. My aim here was to measure the attenuation (in dB) of the first harmonic relative to fundamental at 10 kHz and about 1 V. The HP Model 3561A is a single channel Fast Fourier Transform (FFT) Signal Analyser which covers the frequency range up to 100 kHz. This equipment shows a visual representation of the spectral content of a signal (Figure 3-6).

This equipment can be used to determine the purity of the sine wave in the source generator and in the ACSF. This signal analyser was used to detect waveform distortion caused by nonlinear effect such as polarization in syringe V3 electrodes (see section 7) and two-dimensional measurements (see section 5). The circuit shown in Figure 3-7 was connected. Then, the signal analyser terminals were first connected across the source, then the 50 kΩ resistor, then the ACSF solution.

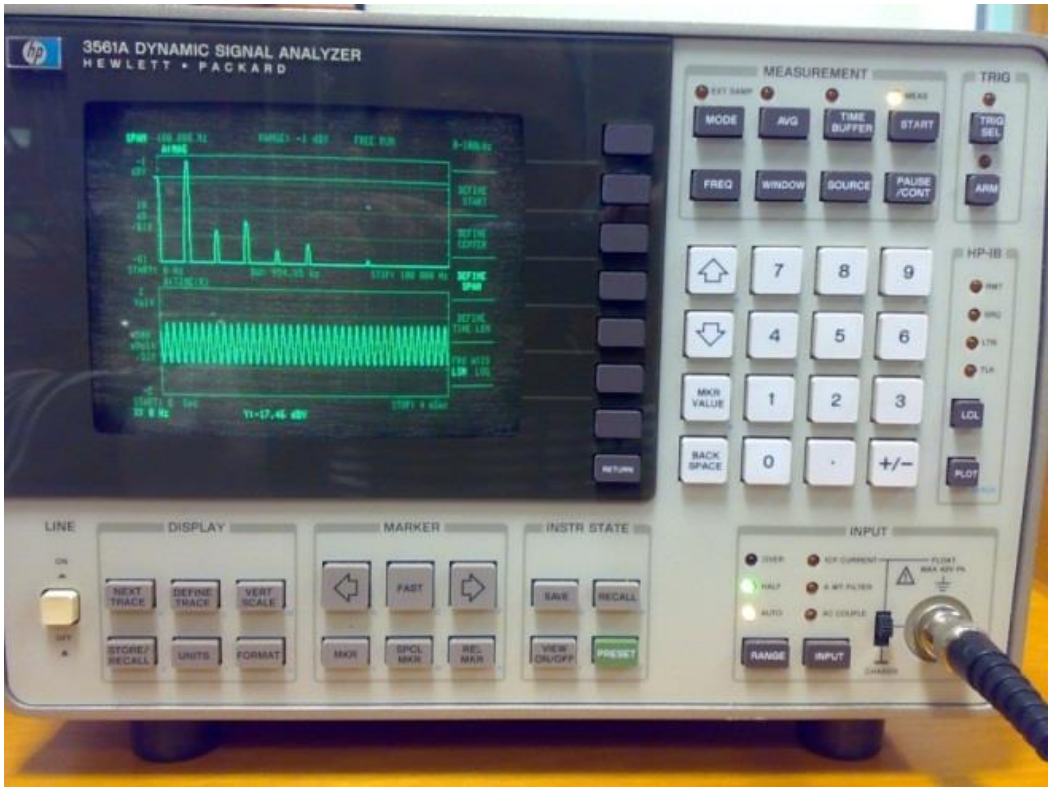

Figure 3-6: Output for ACSF from HP 3561A Dynamic Signal Analyser

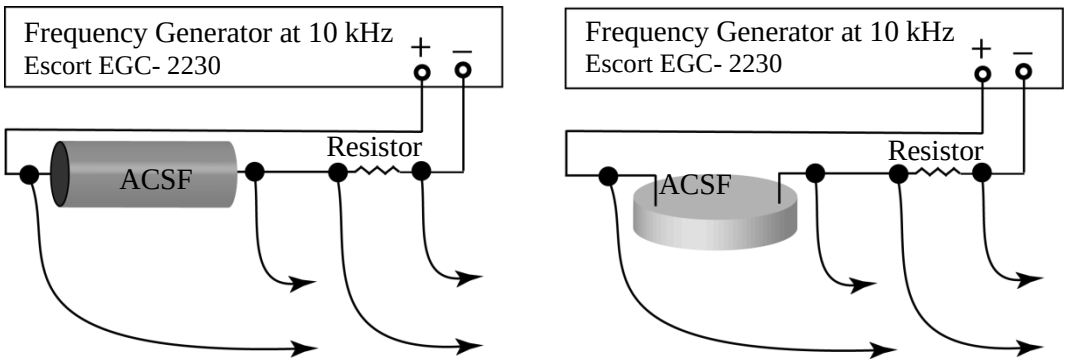

Figure 3-7: Circuit diagram for (a) one-dimensional measurements and (b) two-dimensional measurements. Arrows go to HP 3561A Signal Analyser

I measured the power in the first harmonic for the fundamental frequency (10 kHz) in ACSF solution. I found that the first harmonic is below the fundamental by 26 dB using stainless steel disk electrodes in the one-dimensional measurements (Figure 3-7 (a)) and 28 dB for stainless steel wire electrodes in the two-dimensional measurements (Figure 3-7 (b)). For the two-dimensional case the current was very low, about 5 μA, yet no appreciable distortion appeared. That means that the waves are almost pure sine wave in the ACSF. So, one-dimensional and two-dimensional measurements do not distort the sine wave in the ACSF. (The above electrodes were not used in my final measurements).

The harmonic purity tests were repeated using real tissue in a real measurement situation with the Agilent E4980A *LCR* instrument as a source of sine wave at 10 kHz. Harmonics were at least 55 dB below the level of the primary frequency in the source (Agilent E4980A). Using Ag/AgCl disk electrodes in one-dimensional method, harmonics were at least 61 dB below the level of the primary frequency. Using Ag/AgCl wire electrodes in two-dimensional method, harmonics were at least 59 dB below the level of the primary frequency.

3.6 Statistics

3.6.1 Outliers

Outliers are unusually large or small measurements (Dobbs & Miller, 2002). They can have a disproportionate influence on statistical indications, such as

the mean and the median, affecting results and their interpretations. I checked my data outliers and consider that they arise from: (a) Laboratory procedures and (b) Randomness. In order to reduce the effect of (a), I reviewed the processes to determine the cause of the outliers and then refined those procedures. To look at the effect of (b), I performed the analysis with and without the outlier to see its impact on the results.

I used the John Tukey's 'Fences' rule of thumb (Dobbs & Miller, 2002) to detect outliers. He assigned the upper fence at value 1.5 times the interquartile range (Q_3-Q_1) above the upper quartile (Q_3), according to the following equation:

$$\text{Upper fence} = Q_3 + 1.5(Q_3 - Q_1) \qquad (3\text{-}3)$$

Similarly, he assigned the lower fence at value 1.5 times the interquartile range (Q_3-Q_1) below the lower quartile (Q_1):

$$\text{Lower fence} = Q_1 - 1.5(Q_3 - Q_1) \qquad (3\text{-}4)$$

3.6.2 *P*-value

According to Moore *et al*. (2012) *P*-value is suggestive of the possibility of accepting the null hypothesis. *P*-values range from 0 to 1 (or in percentage form from 0 to 100%) and the *P*-value is the probability of having statistical results similar or more extreme than the calculated or measured value if the null hypothesis is true. The null hypothesis depends on what is being tested, but generally it states that the two samples come from the same population. I chose $P = 0.05$ as a cut-off. That is a common convention, but it is arbitrary. If *P*-value is below my cut-off level, I reject the null hypothesis, and consider that the population means are different.

3.6.3 Nonparametric and Parametric Analysis Overview

Parametric tests rely on the assumption that the population is distributed normally with parameters for the mean (μ) and standard deviation (σ) (Moore *et al*., 2012). Nonparametric tests do not make this assumption, so they are useful when data are strongly non-normal and resistant to transformation. In other words, nonparametric tests correspond to the

parametric *t*-tests (see section 3.6.5 below). Nonparametric and parametric tests are for two centre values of two populations to determine whether they are significantly different. The centre value is the mean (μ) for parametric tests and the median (η) for nonparametric tests.

I used a 2-sample median (Mann-Whitney) test for nonparametric samples. After excluding the outliers, where the conductivity distribution changed from not-normal to a normal distribution, I used the *t*-test.

3.6.4 Mann-Whitney Test

Moore *et al*. (2012) states that the Mann-Whitney test is a nonparametric hypothesis test to determine if the two populations have the same median (η). Therefore, it tests the null hypothesis that the two population medians are equal (H_0: $\eta_1 = \eta_2$) against the alternative hypothesis that they are not equal (H_1: $\eta_1 \neq \eta_2$). The Mann-Whitney test does not require the data to come from normally-distributed populations, but it does make the assumptions that the target populations have the same shape and are independent.

3.6.5 Sample *t*-test

The *t*-test is a hypothesis test for two population means (μ) to determine whether they are significantly different (Everitt, 1998). This procedure uses the null hypothesis that the difference between two population means is zero. To compare the electrical conductivities of seizing and non-seizing brain tissue, the 2-sample *t*-test analyses the difference between their two means. It aimed to determine whether the difference is statistically significant. The hypotheses of a two-tailed test would be:

- H_0: $\mu_1 - \mu_2 = 0$ (conductivities of seizing and non-seizing brain tissue are equal)
- H_1: $\mu_1 - \mu_2 \neq 0$ (conductivities of seizing and non-seizing brain tissue are different)

3.6.6 Anderson-Darling Test

The Anderson-Darling test examines testing how close the data distribution is to a normal distribution (Everitt, 1998). If the *P*-value is lower than the

chosen significance level 0.05, that is means the data do not follow the normal distribution.

3.7 Ethical Approval

Before starting this work I applied for ethical approval from The University of Waikato Faculty of Science and Engineering Animal Ethics Committee. This approval comes with restriction in number of animals, procedure of killing the animals and is time limited. Ideally I would like to use more animals, however I have successfully applied for an additional ethical approval and it is unlikely that a third will be granted.

4 Conductivity Measurements in Three Dimensions

In this study, the three-dimensional method for measuring slice conductivity does not give satisfactory results, so there are no final results. But I will demonstrate some of my attempts, errors and developments to do measurements in three dimensions. It is called three-dimensional method (3D) because I used point electrodes (i.e, only tips of wire electrodes were exposed to the slice) and current flows in three dimensions in the tissue.

I used the Agilent E4980A (*LCR* meter) to make three-dimensional conductivity measurements. A MATLAB code was written to record and analyse the slice conductivity data automatically as in Appendix B-1.

I used four electrodes: a known current is passed into the sample through the left electrode, out of the sample through the right electrode, and the potential difference between the other two (inner) electrodes is recorded (see Section 3.4). This can be done with an Agilent E4980A *LCR* meter (Figure 3-1).

4.1 Background Theory

In the following we derive an expression for the conductivity of the material in terms of the voltage and current measured by the electrodes. This expression is a special case where electrodes are arranged symmetrically. In this case vertical distance between P_1 and $+Q$ is equal to the vertical distance between P_2 and $-Q$ (i.e., the line through P_1, P_2 is parallel to line through $+Q$, $-Q$) . This was the case for all my measurements.

Consider an arrangement of electrodes as shown in Figure 4-1. Here, four point-electrodes are placed in a tissue sample in a plane: current is injected at $+Q$, removed at $-Q$, and the potential difference is recorded between P_1 and P_2.

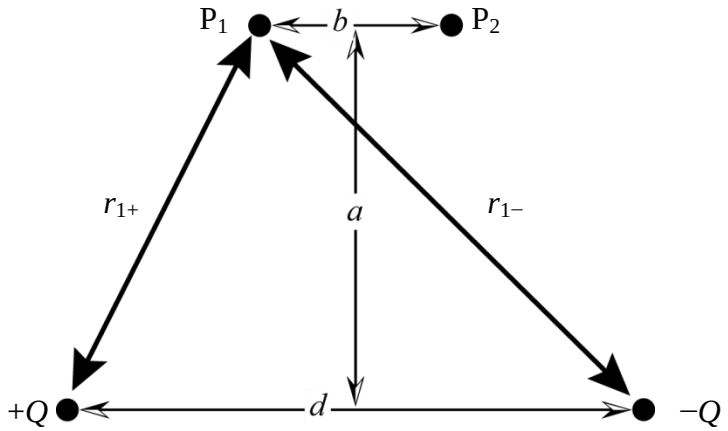

Figure 4-1: An arrangement for four point-electrodes lying in a plane

The potential V due to a single charge Q is given by

$$V = \frac{1}{4\pi\varepsilon_\circ}\frac{Q}{r} \qquad (4\text{-}1)$$

where r is the distance from the charge.

The net potential at point P_1 is therefore given by

$$V_1 = \frac{1}{4\pi\varepsilon_\circ}\left(\frac{Q}{r_{1+}} - \frac{Q}{r_{1-}}\right) = \frac{Q}{4\pi\varepsilon_\circ}\left(\frac{r_{1-} - r_{1+}}{r_{1+}\, r_{1-}}\right)$$

From the geometry of Figure 4-1:

$$r_{1+}^2 = a^2 + \frac{d^2}{4} - \frac{db}{2} + \frac{b^2}{4} = a^2 + \left(\frac{d-b}{2}\right)^2$$

$$r_{1-}^2 = a^2 + \frac{d^2}{4} + \frac{db}{2} + \frac{b^2}{4} = a^2 + \left(\frac{d+b}{2}\right)^2$$

So the net potential at P_1 is:

$$V_1 = \frac{Q}{4\pi\varepsilon_\circ}\left(\frac{\sqrt{a^2 + \left(\frac{d+b}{2}\right)^2} - \sqrt{a^2 + \left(\frac{d-b}{2}\right)^2}}{\sqrt{a^2 + \left(\frac{d-b}{2}\right)^2}\ \sqrt{a^2 + \left(\frac{d+b}{2}\right)^2}}\right)$$

Similarly the net potential at P_2 is:

$$V_2 = \frac{-Q}{4\pi\varepsilon_\circ}\left(\frac{\sqrt{a^2 + \left(\frac{d-b}{2}\right)^2} - \sqrt{a^2 + \left(\frac{d+b}{2}\right)^2}}{\sqrt{a^2 + \left(\frac{d-b}{2}\right)^2}\ \sqrt{a^2 + \left(\frac{d+b}{2}\right)^2}}\right)$$

$$= \frac{Q}{4\pi\varepsilon_\circ}\left(\frac{-\sqrt{a^2+\left(\frac{d-b}{2}\right)^2}+\sqrt{a^2+\left(\frac{d+b}{2}\right)^2}}{\sqrt{a^2+\left(\frac{d-b}{2}\right)^2}\ \sqrt{a^2+\left(\frac{d+b}{2}\right)^2}}\right)$$

So the potential difference (ΔV) between P_1 and P_2 is:

$$\Delta V = V_1 - V_2 = \frac{Q}{2\pi\varepsilon_\circ}\left(\frac{\sqrt{a^2+\left(\frac{d+b}{2}\right)^2}-\sqrt{a^2+\left(\frac{d-b}{2}\right)^2}}{\sqrt{a^2+\left(\frac{d-b}{2}\right)^2}\ \sqrt{a^2+\left(\frac{d+b}{2}\right)^2}}\right) \quad (4\text{-}2)$$

If the four electrodes are in straight line as in Figure 4-3, we have a special case where a = 0, and Equation (4-2) simplifies to:

$$\Delta V = \frac{Q}{2\pi\varepsilon_\circ}\left(\frac{\frac{d+b}{2}-\frac{d-b}{2}}{\frac{d-b}{2}\ \frac{d+b}{2}}\right)$$

$$= \frac{Q}{2\pi\varepsilon_\circ}\left(\frac{b}{\frac{d^2-b^2}{4}}\right) = \frac{2Q}{\pi\varepsilon_\circ}\left(\frac{b}{d^2-b^2}\right) \quad (4\text{-}3)$$

Gauss's law can relate the charge to output current (Figure 4-2) since

$$\int \boldsymbol{J}.d\boldsymbol{s} = I_{\text{out}} \quad (4\text{-}4)$$

where $\boldsymbol{J}=\sigma\boldsymbol{E}$ is the current density, the surface integral is taken around the electrode, σ is the conductivity and $\boldsymbol{E}$ is the electric field. Then

$$\sigma\int \boldsymbol{E}.d\boldsymbol{s} = I_{\text{out}}$$

and by Gauss' law

$$\sigma\frac{Q}{\varepsilon_\circ} = I_{\text{out}} \quad (4\text{-}5)$$

from which we identify

$$Q = I_{\text{out}}\frac{\varepsilon_\circ}{\sigma} \quad (4\text{-}6)$$

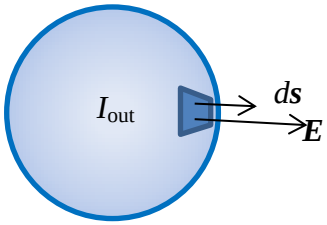

Figure 4-2: A spherical gaussian surface

Substituting in Equation (4-3) gives

$$\Delta V = \frac{2}{\pi}\frac{I_{\text{out}}}{\sigma}\left(\frac{b}{d^2 - b^2}\right) \qquad (4\text{-}7)$$

The effective impedance $Z = \frac{\Delta V}{I_{\text{out}}}$ is then given by

$$\therefore Z = \frac{\Delta V}{I_{\text{out}}} = \frac{2}{\pi\sigma}\left(\frac{b}{d^2 - b^2}\right) \qquad (4\text{-}8)$$

Re-arranging Equation (4-8) we have our final expression for conductivity:

$$\sigma = \frac{2}{\pi Z}\left(\frac{b}{d^2 - b^2}\right) \qquad (4\text{-}9)$$

where Z is the measured effective impedance of the tissue, b is the separation between the two voltmeter electrodes and d is the separation between the inward and the outward current electrodes. Note that Z is not a true impedance since the voltage and current electrodes are not co-located. This equation is designed for the co-linear four-electrode configuration as in Figure 4-3. This theory assumes a perfect coupling between electrodes and medium.

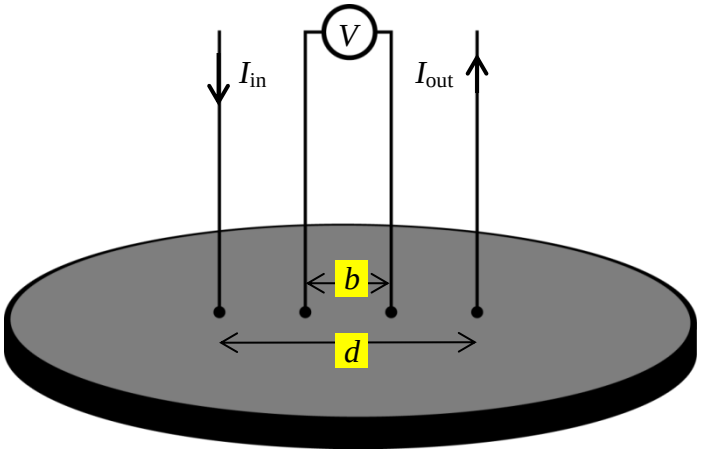

Figure 4-3: Three-dimensional four-electrodes configuration with all electrodes placed along a line

4.2 Electrodes and measurements

4.2.1 Ribbon Cable Electrodes

Ribbon (multi-wire planar) cable contains a number of parallel conducting wires embedded in a flexible insulating material. Wires are attached in a row parallel to each other to make a wide and flat ribbon shape. It is usually used to connect parts in electronic equipment. I used ribbon cables as electrodes (Figure 4-4) to measure the conductivity of the slices. Spacing between electrodes was 0.5 mm and electrode thickness was 0.5 mm as in Figure 4-5.

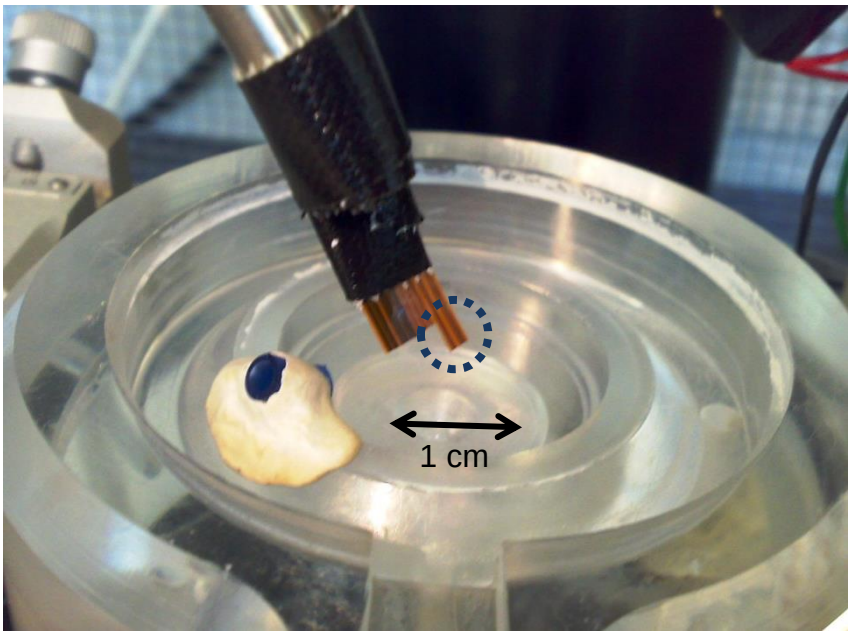

Figure 4-4: Ribbon cables electrodes. Dotted circle shows the location of the four electrodes used for impedance measurements

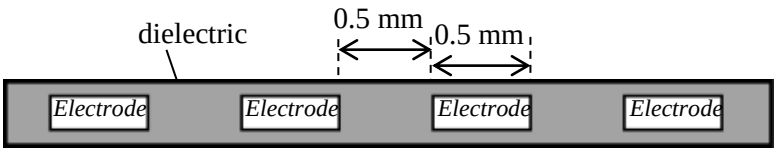

Figure 4-5: Ribbon (multi-wire planar)

I prepared Mg^{2+}-free ACSF solution as described in Section 5.3. Figure 4-6 shows recordings from Mg^{2+}-free solution were 20% below the predicted value of 1.56 S/m (Appendix A-4). Although measurements from brain slice show some promise, it was hard to reproduce. This may be because the distances between the electrodes are not large relative to the electrode width, or the slice is not infinite in extent (horizontally and vertically) compared to the electrodes as assumed by Equation (4-9). In addition to above

challenges, the slice was easily cut and damaged while inserting the electrodes. This critical issue prompted me to look for different electrodes.

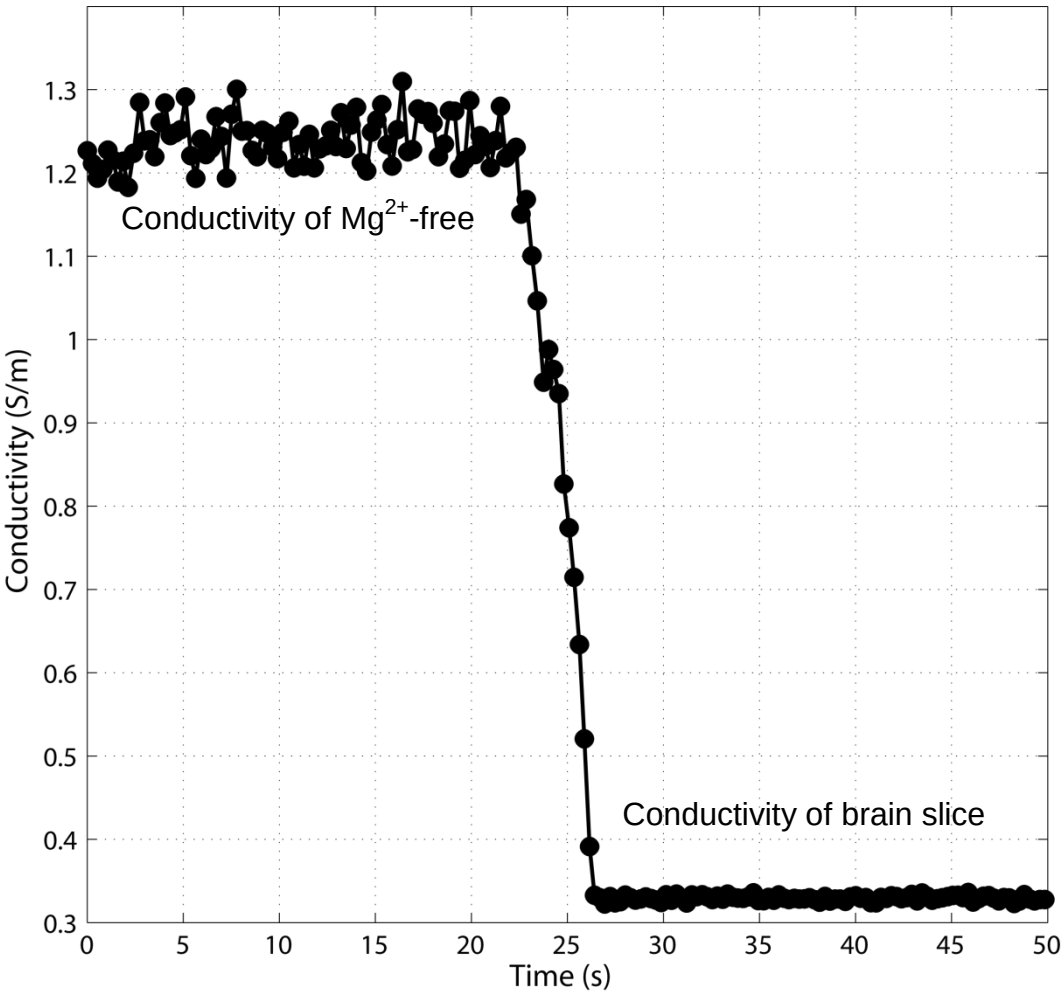

Figure 4-6: Conductivity of Mg^{2+}-free ACSF solution then brain slice using 4 ribbon-cable conductors as electrodes

4.2.2 Multielectrode Array (MEA)

Brain slices were placed on a commercially available multielectrode array (MEA) consisting of 60 pyramidal-shaped platinum square electrodes (40 µm × 40 µm) with a height from 50 µm to 70 µm, and a spacing between electrodes of 200 µm (Ayanda Systems, Lausanne, Switzerland). Figure 4-7 shows electron micrographs of the electrodes. The geometry of the electrodes improves the penetration in the tissue slice compared to the ribbon cable, thereby reducing the distance between the active cells and the electrodes.

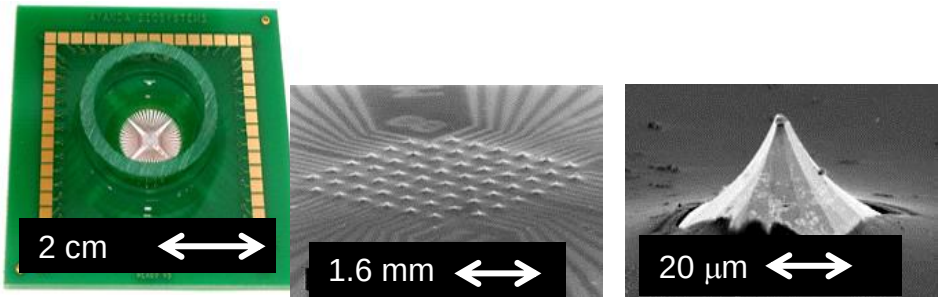

Figure 4-7: Images showing of a 3D MEA device and a close view of a single platinum electrode. Pictures from Ayanda Systems

I prepared a saline solution whose conductivity I could calculate theoretically, and then attempted to measure its conductivity using my MEA setup to make sure it was working properly. After many unsuccessful attempts, I decided to improve the system set-up by constructing a printed circuit to facilitate connection to the MEA and installing new shielding equipment for the MEA as seen in Figure 4-8. A solution of known conductivity was used in an attempt to validate the device but without success. By investigating the electrodes under an optical microscope, I found gas bubbles formed on the current electrodes, and they appeared oxidized and "burnt". That may be a result of the high impedance of the electrodes or a high current density causing excessive heating meaning that they did not easily pass current into the tissue. These electrodes are designed to measure voltage, not to pass current.

Figure 4-8: Multielectrode array (MEA) in its shield

4.2.3 Theoretical Work

Equation (4-9) is not approximate. It is an exact result valid when the assumptions are satisfied. Equation (4-9) is supported by more accurate computer modelling of the electric fields between the three-dimensional electrodes using COMSOL Multiphysics. This allows us to consider electrodes of finite width, and a tissue sample that is not infinite in extent.

For example, I used COMSOL Multiphysics to investigate the electric field between the MEA electrode elements to compare with the simple electrostatic theory for point electrodes as in Equation (4-10) (Logothetis *et al.*, 2007).

$$\Delta V = \frac{I}{2\pi\sigma}\left(\frac{1}{d} - \frac{1}{\sqrt{d^2 - 4z^2}}\right) \qquad (4\text{-}10)$$

where the distances d and z are as defined in Figure 4-10.

Figure 4-9 shows an example. I prepared a model for the equipotential surfaces in the solution in the multi-electrode array. The figure shows that the conductive electrodes and the finite geometry have a minimal effect on the electric field pattern predicted by Equation (4-10).

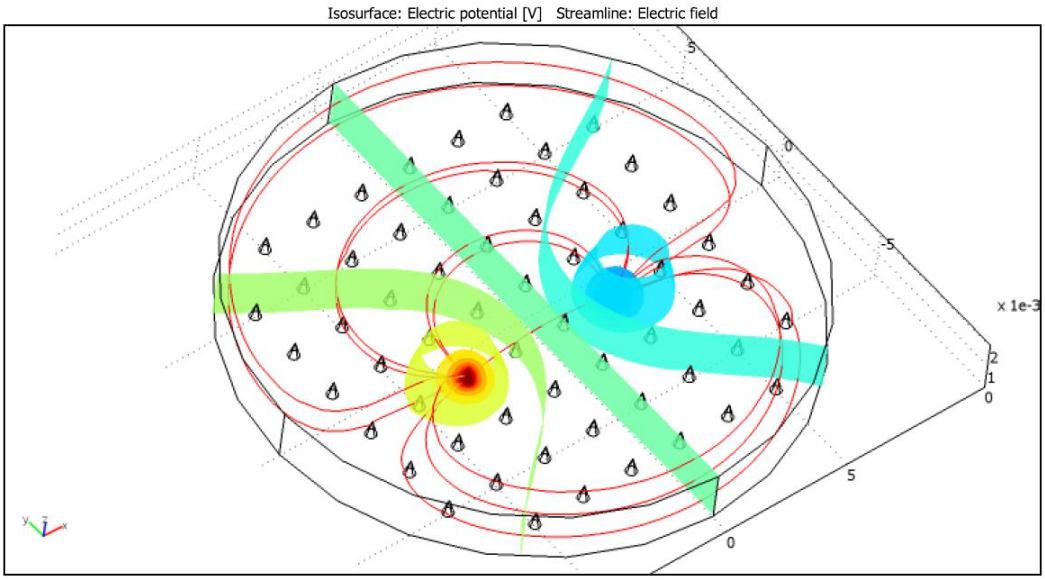

Figure 4-9: Field lines and equipotential surfaces for the MEA in ACSF. Calculations were performed using COMSOL Multiphysics

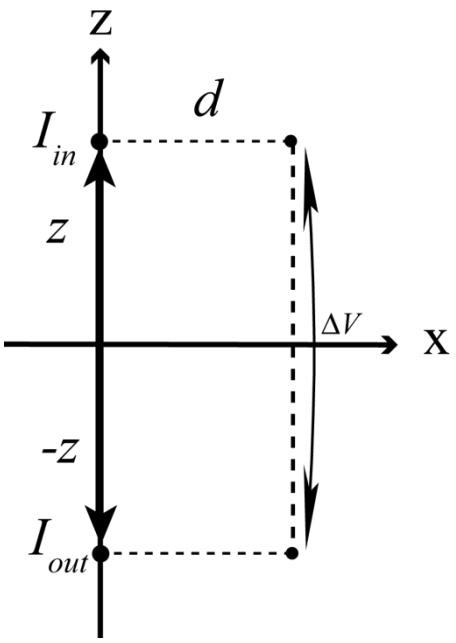

Figure 4-10: Logothetis equation (4-10) is based in this diagram where voltage electrodes are parallel to the current electrodes. This figure is a special case of Figure 4-1

The MEA electrodes have high impedance because they are very small. Therefore they are poor charge carriers. In next sections, I describe a set of stainless steel electrodes with a diameter of 125 μm. This is a large diameter relative to the platinum square electrodes (40 μm × 40 μm), giving an area ratio of stainless steel electrode area to MEA area is

$$\frac{A_{\text{stainless steel}}}{A_{\text{MEA}}} = \frac{\pi d^2/4}{w^2} = \frac{\pi d^2}{4w^2} = \frac{\pi \times (125 \times 10^{-6})^2}{4 \times (40 \times 10^{-6})^2} = 7.7 \quad (4\text{-}11)$$

So, the impedance of the stainless steel electrodes is expected to be smaller than that of the MEA electrodes by about factor of 8.

4.2.4 Free Stainless Steel Electrodes

I tried stainless steel wire electrodes of diameter 125 μm where only the tips were exposed to medium. Each electrode was held by its own manipulator. I measured the distances between the electrode tips using graph paper as in Figure 4-11. I tested my equipment by using a frequency generator and oscilloscope to measure salt solution conductivity at 1 kHz. I was not able to obtain stable or realistic measurements from a known standard solution.

That was possibly because stainless steel electrodes are noisy, the distances were not measured accurately enough, and electrodes were located at different depths in the solution. In addition, gas bubbles were seen during initial measurements as in Figure 4-12.

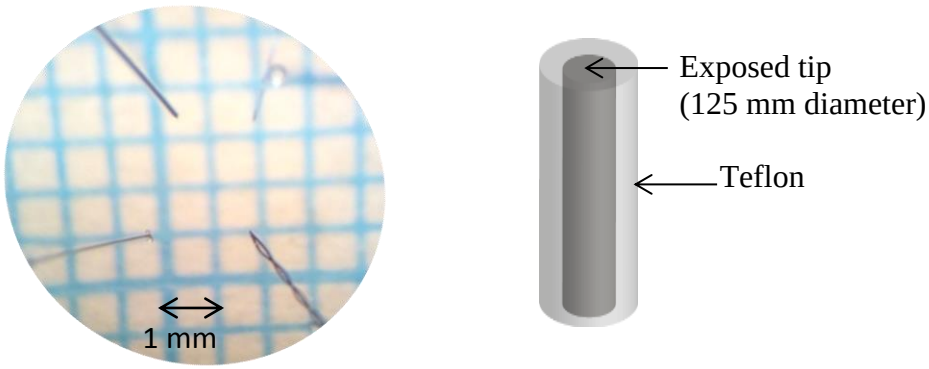

Figure 4-11: Free stainless steel electrodes viewed against a graph-paper grid for distance calibration

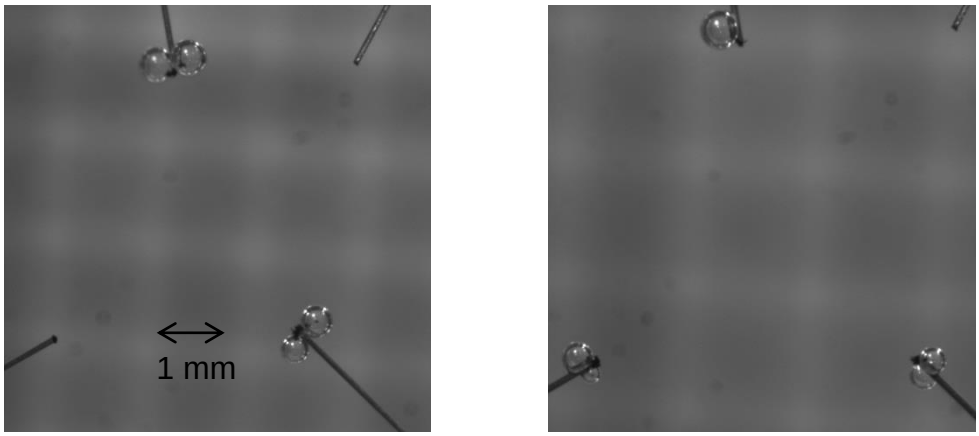

Figure 4-12: During impedance measurements for saline solution, bubbles formed at the tips of stainless steel electrodes

4.2.5 Epoxy-glued Stainless Steel Electrodes

I built another electrode configuration with fixed distances between the electrodes to increase the accuracy in distance measurements. I found this method to be stable and to give conductivity results consistent with theory. I made three different four-channel linear arrays by winding stainless steel wire around two bars (Figure 4-13a), two screws (Figure 4-13b), and a plastic plate (Figure 4-13c). I anchored the wires using epoxy glue and taped

both (wires and epoxy) with a transparent tab. Then I cut the electrodes to the required length. The electrodes were attached to gold-plated contact pins as in Figure 4-14.

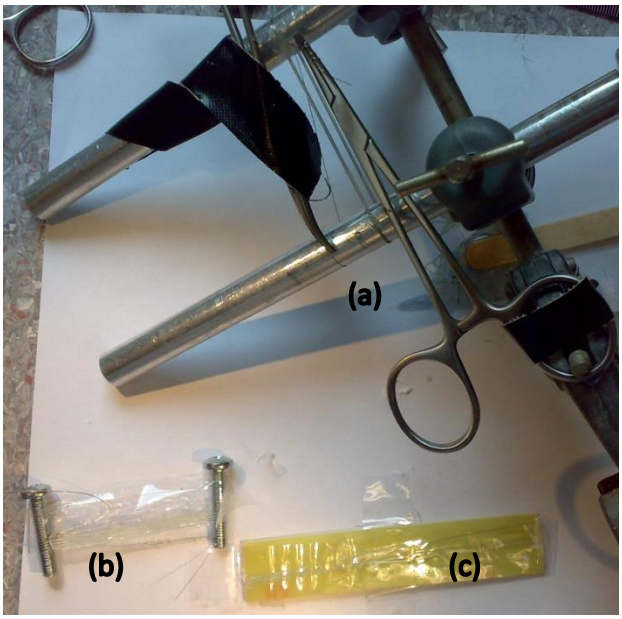

Figure 4-13: Four-channel linear arrays made by winding the stainless steel wire around two bars (a), or two screws (b) or a plastic plate (c). All three designs were glued to provide mechanical stability

However, the uncertainties in measurements of distances between electrodes were still too large. I was able to improve the accuracy in the horizontal dimension (distances between the electrodes) but failed to increase it vertically (meaning that the electrodes had different heights). Although the electrodes were mechanically stable, their tips were not. Figure 4-15a shows bending of the electrodes tips.

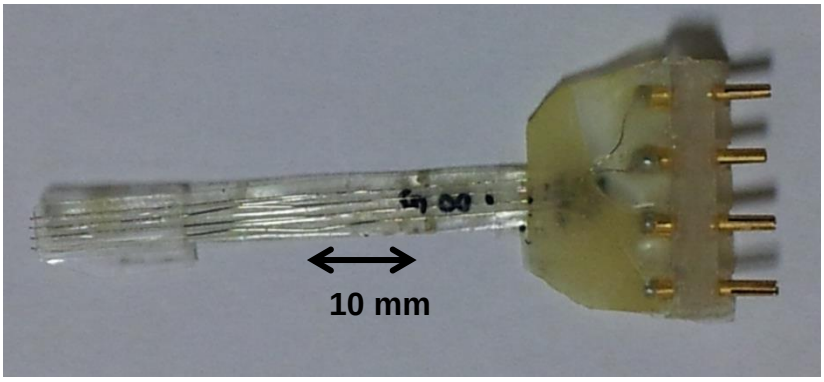

Figure 4-14: Epoxy-glued stainless steel electrodes with contact pins

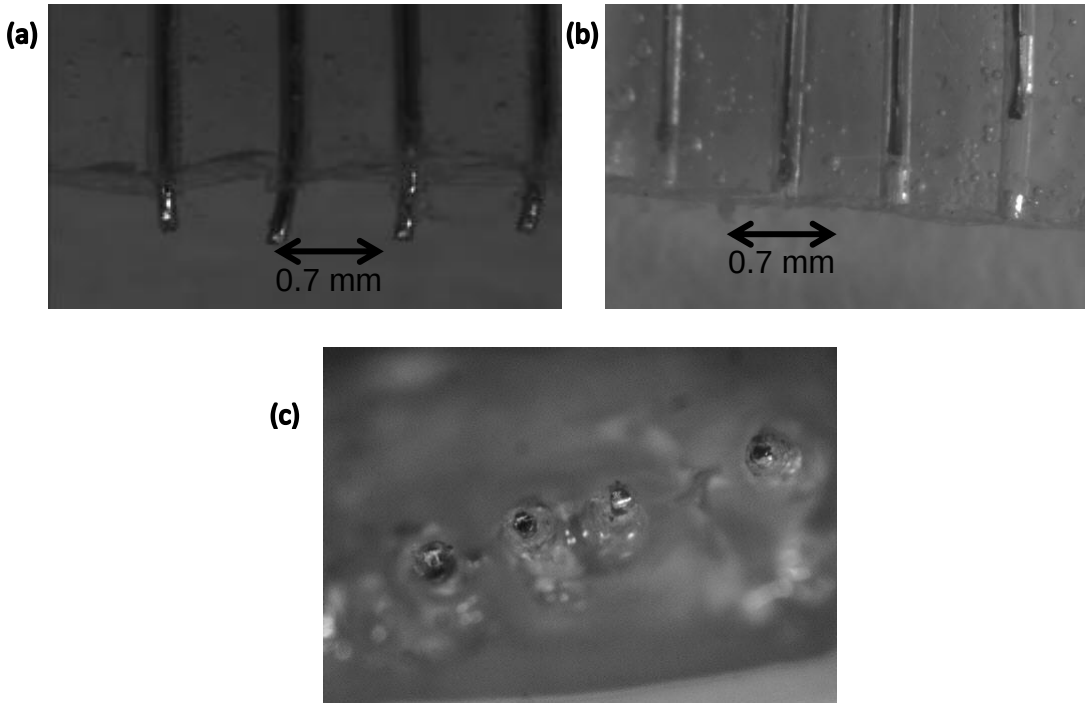

Figure 4-15: Sources of error in the electrode placement such as variable distance between electrodes are seen in parts (a) and (c). The isolating Teflon error (because of unclean cut) is seen in part (c) and the epoxy glue error in part (b)

Because of the above technical issues, I improved the electrodes to make them more mechanically stable and to minimise the distance error and another error arising from electrical isolation. The isolating error arises from two sources: Teflon or epoxy glue. Teflon uncleanly cut makes isolating spots between the electrodes (Figure 4-15c). Electrodes may also be pulled through the epoxy glue channel and as a result an electrode may not connect to the slice (Figure 4-15b).

Recordings from known concentrations of NaCl were unstable (Figure 4-16). The decrease of conductivity with time suggests that there is an interaction between electrodes and solution.

Furthermore I found another variable which is the pressure of the electrodes on the tissue. For example, when increasing the pressure on the electrodes by hand the measured conductivity decreases, and when I decrease the pressure, the conductivity increases. One possible explanation for this is that the ACSF contributes less as the electrodes better penetrate the tissue. In order to avoid this, I prepared a setup that gave a constant pressure between

the electrodes and the slice. I also tested the effect on the measurements of the uncertainty in separation between the electrodes. I used computer software (NIS-Elements BR) and a microscope digital camera to measure the distances between the electrodes shown in Figure 4-15.

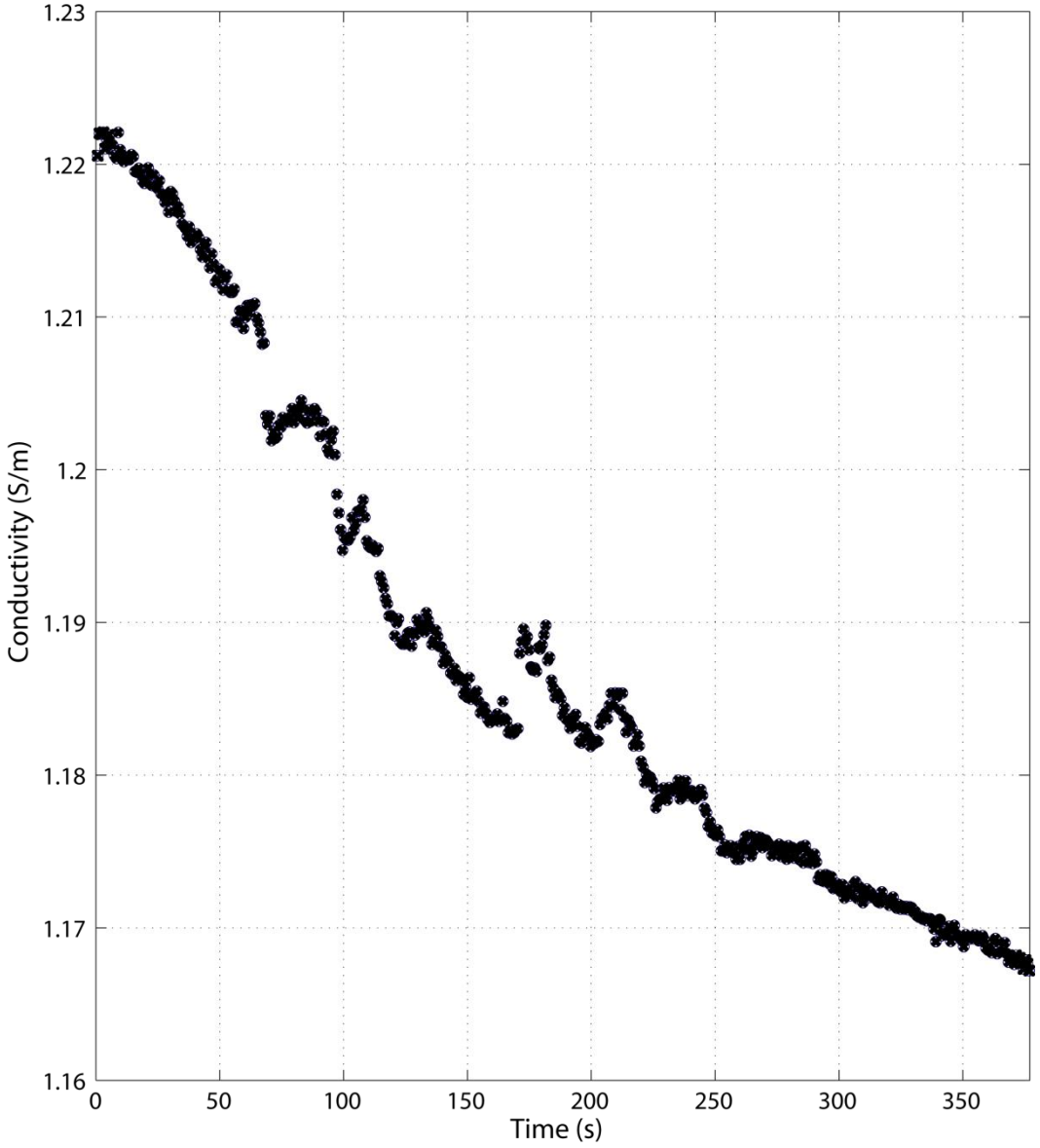

Figure 4-16: Conductivity of NaCl using epoxy-glued stainless steel electrodes. Expected conductivity = 1.3 S/m

I made a new improved set of electrodes, carefully cleaned for use in the next measurements. Recordings of conductivity from Mg^{2+}-free ACSF (ACSF compositions are in Table 5-1) using the new set of stainless steel electrodes secured with epoxy glue were typically 8-16% higher than the expected value of 1.55 S/m as shown in Figure 4-17a,b.

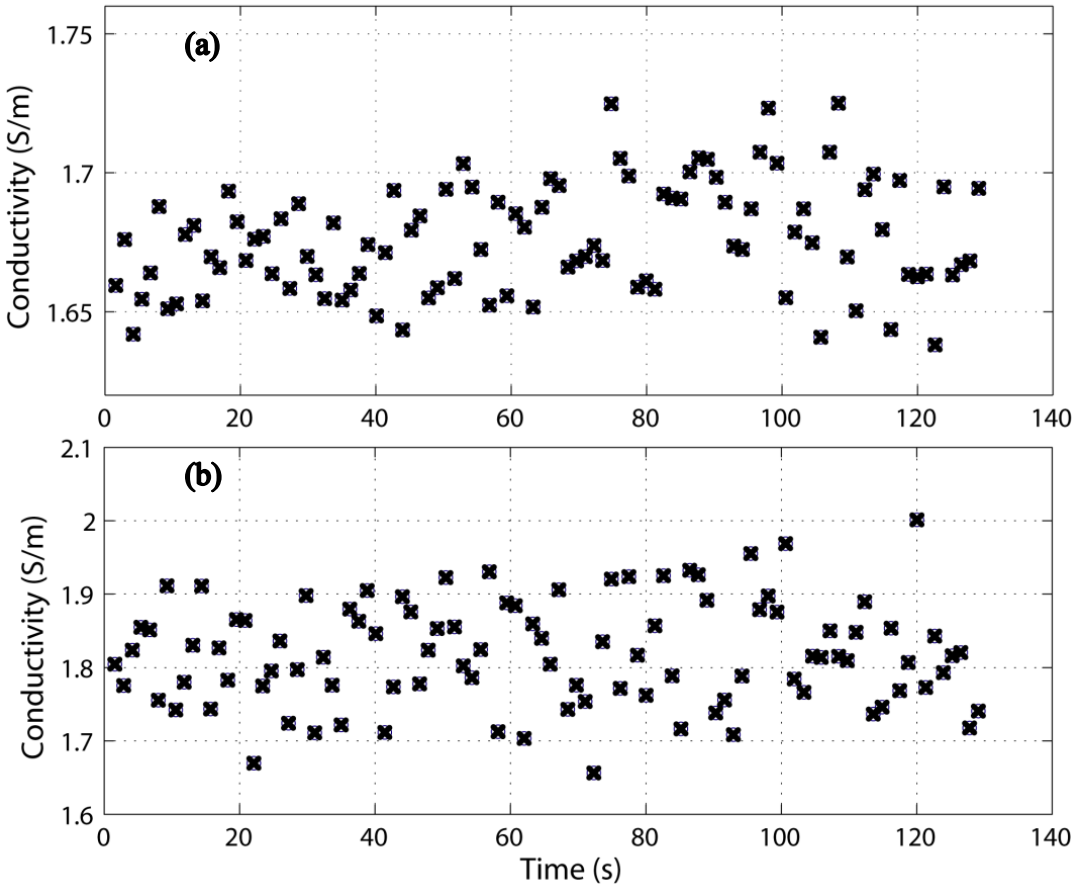

Figure 4-17: Conductivity of Mg^{2+}-free ACSF using epoxy-glued stainless steel electrodes for two separate trials

Because of the encouragingly stable measurements in Figure 4-17 compared with Figure 4-16, I calibrated the electrodes by making a set of different concentrations of KCl solution (0.01, 0.02, 0.1 and 1 M) the conductivities of which are supplied in the RE388Tx manual. I plotted the measured conductivity by my setup against the theoretical conductivity. If conductivity measured by my setup is compatible with the theoretical values, I expect a straight line of unity gradient with *y*-intercept at the origin. But I found that there are two major errors: multiplicative and subtractive. A multiplication factor is needed to normalize the gradient to one and subtraction to make the *y*-intercept equal zero. This is may arise from uncertainty of the electrode positions.

Table 4-1: Conductivity of standard solution (KCl) using different methods. Standard data in first column was supplied from user guide of conductivity meter (RE388Tx, EDT direct ion, Dover UK)

Concentration (M KCl)	Conductivity (S/m)		
	Standard at 25°C	By conductivity meter	Using *LCR* meter and epoxy-glued stainless steel electrodes
0.01	0.14	0.14	0.18
0.02	0.27	0.28	0.34
0.1	1.29	1.28	1.24
1	10.98	10.96	10.10

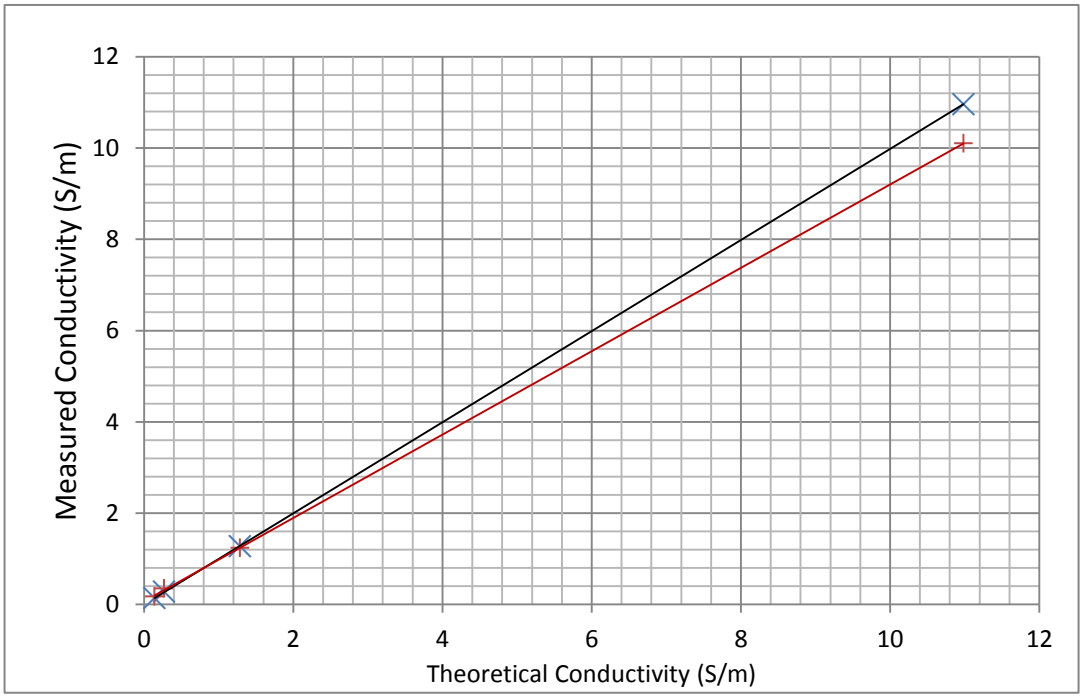

Figure 4-18: Conductivity of standard solutions using conductivity meter (×) and using-epoxy glued stainless steel electrodes (+)

From Figure 4-18, it is clear that the conductivity meter is accurate to 99.8% and the systematic error is 0.001 S/m. However the accuracy of my electrodes and *LCR* meter is 91% and the systematic error is 0.07 S/m.

Therefore more work is required to optimize my measurements. A new calibration standard solution was prepared by diluting 1 molar KCl using the

formula $M_i V_i = M_f V_f$, where M is the concentration in moles per litre, V is the volume, i refers to initial and f refers to final value. Concentrations were selected to have conductivities similar to that of ACSF. Results are shown in Table 4-2.

Table 4-2: Conductivity of standard solution (KCl) using conductivity meter and LCR meter

Concentration (M KCl)	Conductivity (S/m)		% difference
	using conductivity meter	using *LCR* meter and epoxy glued stainless steel electrodes	
0.05	0.68	0.60	−11
0.10	1.29	1.30	1
0.15	1.93	1.50	−22
0.18	2.27	1.90	−18
0.20	2.51	2.10	−16

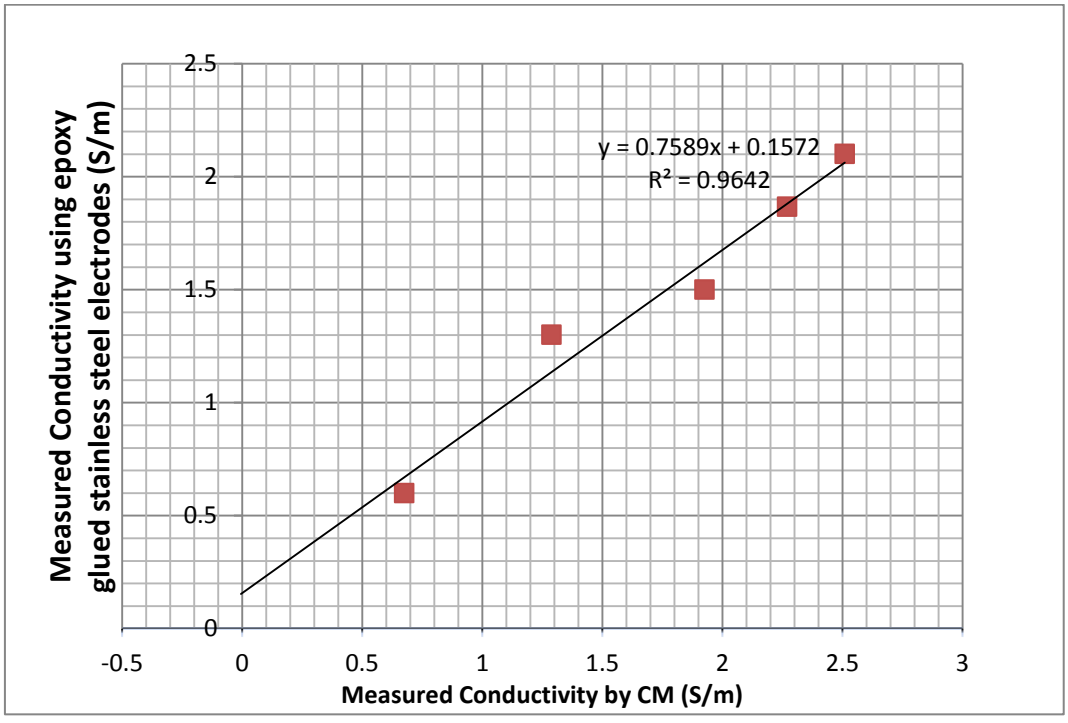

Figure 4-19: Conductivity of "Standard Solutions" using the LCR meter and epoxy glued stainless steel electrodes

Figure 4-19 shows the conductivity of KCl using the conductivity meter (CM) and the stainless steel electrodes connected to the *LCR* meter. I consider that the conductivity values obtained using the conductivity meter

provide an accurate reference. Figure 4-19 indicates that the accuracy of my stainless-steel electrode measurements is 76%. By this, I mean that their measured result is lower than the theoretical values by 24%. That could arise from many sources of errors some of which are displayed in Figure 4-15.

4.2.6 Stainless Steel Electrodes in Tubes of Glass

In an attempt to overcome those problems raised from using epoxy glued stainless steel electrodes, four electrodes were inserted inside four small tubes of glass (instead of gluing with epoxy) as in Figure 4-20. All four glass electrodes were enveloped inside a larger glass tube to make one piece with four electrodes.

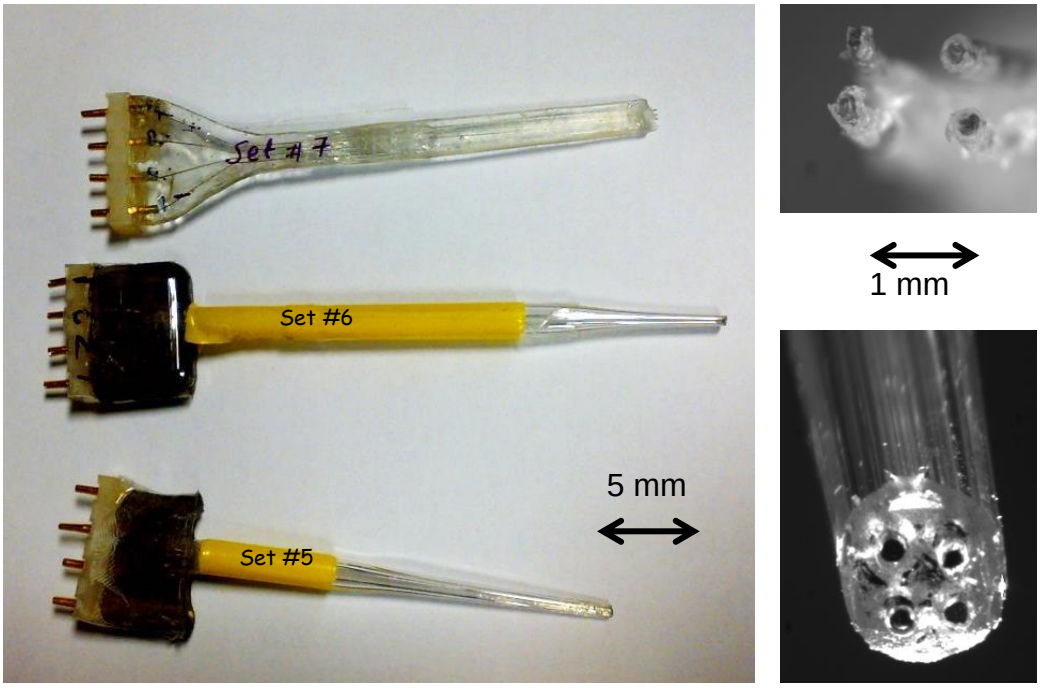

Figure 4-20: Set of electrodes made by inserting stainless steel wires of diameter 125 μm in a glass tube. Magnified heads on the right

I prepared 0.1 M KCl with an expected conductivity of 1.321 S/m. The conductivity measured using the new set up is 1.330 which is within 1% of the expected value. That was a very encouraging result for stainless steel electrodes; unfortunately the measured conductivity was unstable: the apparent conductivity increased to 1.345 S/m within 3 minutes as shown in Figure 4-21.

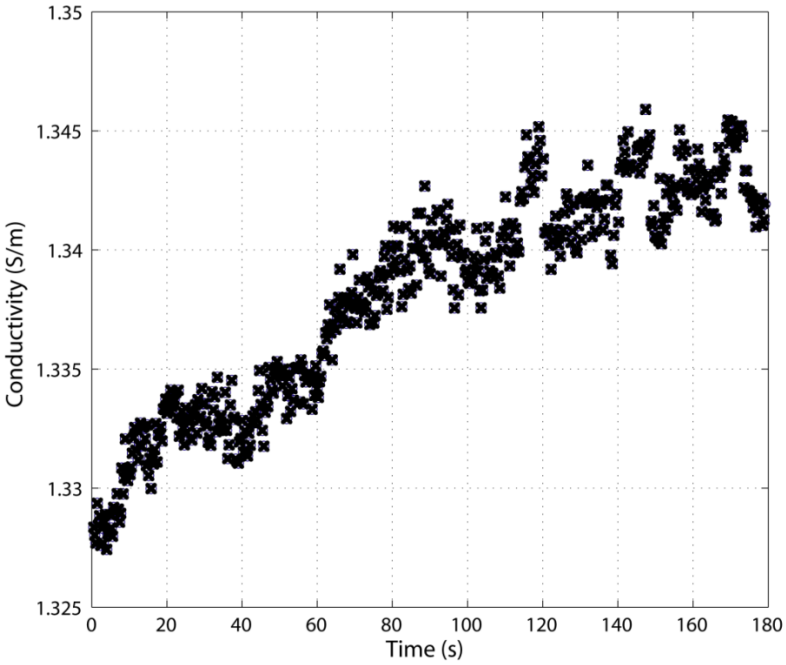

Figure 4-21: Apparent increase of salaine conductivity with time for stainless-steel-in-glass-tube electrodes

A new set of electrodes was built. Repeated measurements of saline conductivity using the new electrodes gave stable results that lay within 1% of the expected value which was 0.27 S/m (Figure 4-22).

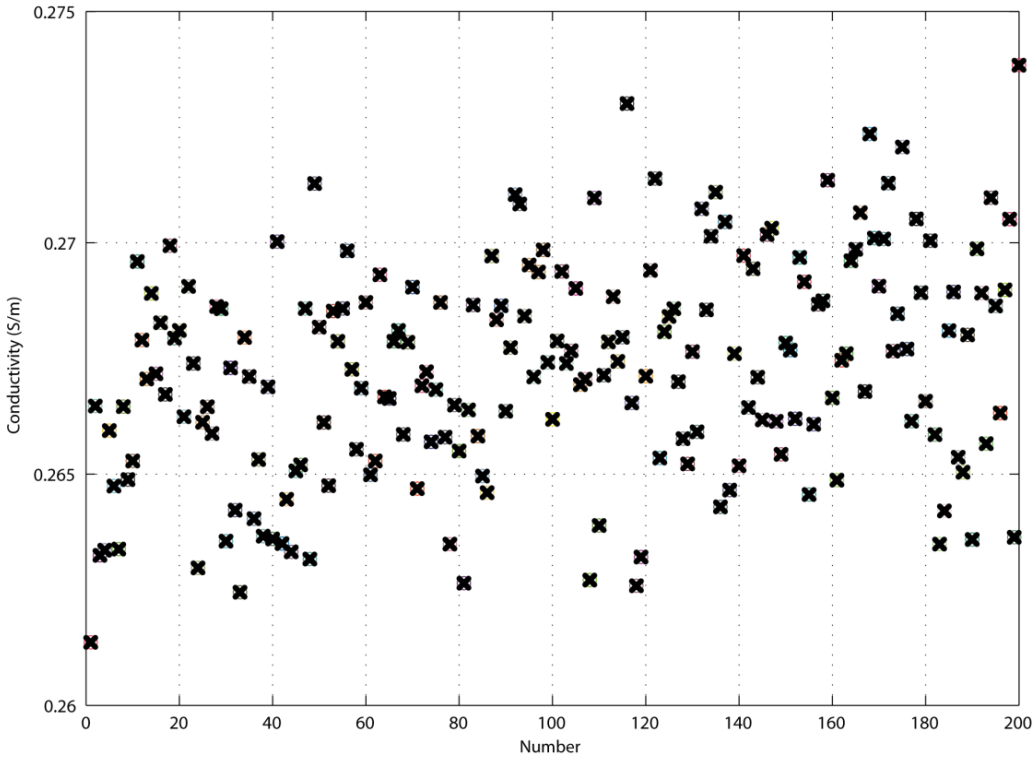

Figure 4-22: Stable conductivity measurements using stainless-steel-in-glass-tube electrodes over 200 points in 130 second

I have found that measurements done by stainless steel wire electrodes in a glass tube were not always in the expected range, nor were they reproducible. Moreover, measurements in a slice were not reliable enough to take this three-dimensional method further.

4.3 Recommendations

A possible avenue for future work is to improve measurements in three dimensions from point electrodes. Given what I have learnt from the work discussed above, I would use Ag/AgCl electrodes with a diameter between 25 to 250 μm.

Special equipment is needed to build these electrodes, so a specialized company would be needed to build a four-channel electrode set. I may take this method in a future research project. It would also be worth considering slices of thickness more than 400 μm to better match Equation (4-9) conditions.

5 Measurements in Two Dimensions

This is called a two-dimensional method (2D) because I used cylindrical electrodes (i.e., sides of electrodes were exposed to the slice); electrodes were fully inserted into the slice and symmetry arguments imply that current flows in two dimensions in the tissue. Full electrode length *d* is an effective physical quantity in 2D method. I start with discussing some unsuccessful initial attempts before moving to the successful van der Pauw method.

5.1 Development of the Method and Refinements to Calculate the Conductivity of Brain Slices at 10 kHz

In this section, I will demonstrate some of my unsuccessful attempts, errors and developments to do measurements in two dimensions. Derivation of Equation (5-1) is in Appendix A-3.

A saline concentration of one gram per litre of NaCl was used to validate the method. I used four cylindrical electrodes aligned along a line (Figure 5-1). I passed a known current into the solution through one of the electrodes, removed from the solution through a second electrode, and recorded the potential difference between the other two (middle) electrodes as in Figure 5-1. The conductivity (σ) of the NaCl could be calculated from the relationship:

$$\frac{\varphi}{I} = \left[\frac{1}{2\pi d\sigma}\right] \log_e \left(\frac{r_1 r_4}{r_2 r_3}\right) \qquad (5\text{-}1)$$

where: φ is the potential difference, I is the measured current, d is the full electrode effective length and it is also depth of the fluid, σ is the fluid conductivity, r_1 is the distance between the I_{in} and V_2 electrodes, r_2 is the distance between the I_{out} and the V_2 electrodes, r_3 is distance between the I_{in} and the V_1 electrodes, r_4 is the distance between the I_{out} and the V_1 electrodes.

5.1.1 Electrical Conductivity using Four Large Stainless Steel Cylindrical Electrodes

I recorded impedance (φ/I) for different distances r_1, r_2, r_3 and r_4, then plotted the impedance against $\log_e\left(\frac{r_1 r_4}{r_2 r_3}\right)$. A straight line fitted to data was obtained (as in Figure 5-2) and conductivity of the solution was calculated from its gradient where $\sigma = \frac{1}{2\pi d \times gradient}$.

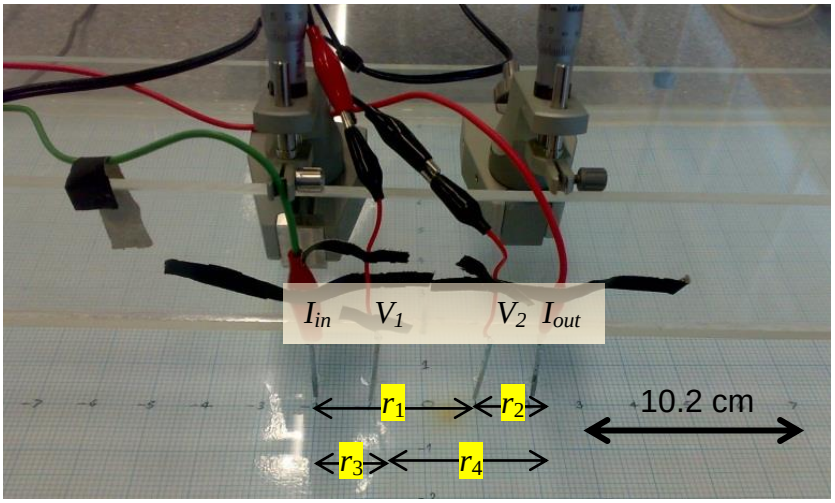

Figure 5-1: Experiment setup for conductivity measurements of liquids

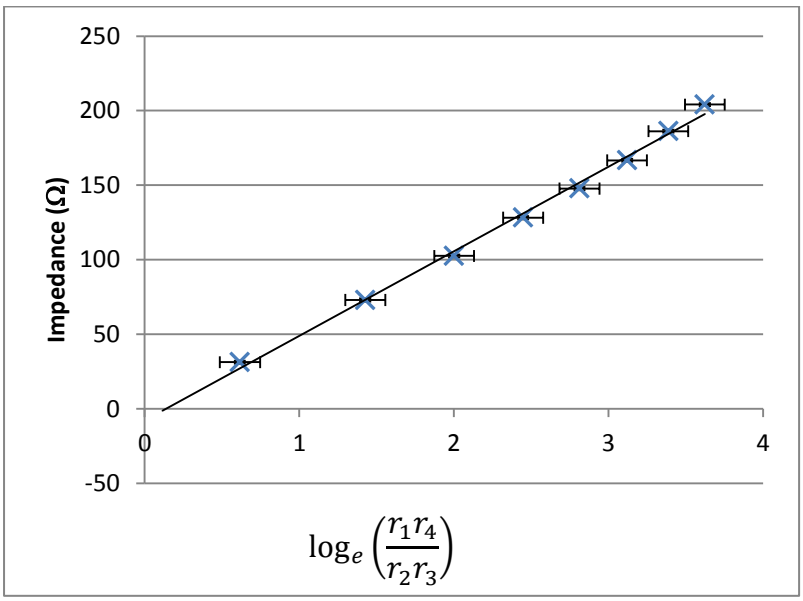

Figure 5-2: Equation (5.1) produces a straight line of zero y-intercept

Using this setup the conductivity of the NaCl was calculated as 0.18 S/m while it measured as 0.22 S/m using the conductivity meter (RE388Tx - EDT direct ion) with expected accuracy ±1μS/m. The difference between the measurements is 18%. The results showed a reasonable agreement if we considerate the uncertainty of distances which could be minimized later.

5.1.2 Electrical Conductivity using Four 0.125 mm Stainless Steel Cylindrical Electrodes

Then I tried smaller stainless steel electrodes with diameter 0.125 mm positioned with manipulators (Figure 5-3). A high percentage error was obtained. The error may be due to small contact surface area between the electrodes and the fluid. Also high uncertainty arises because of the distance measurements.

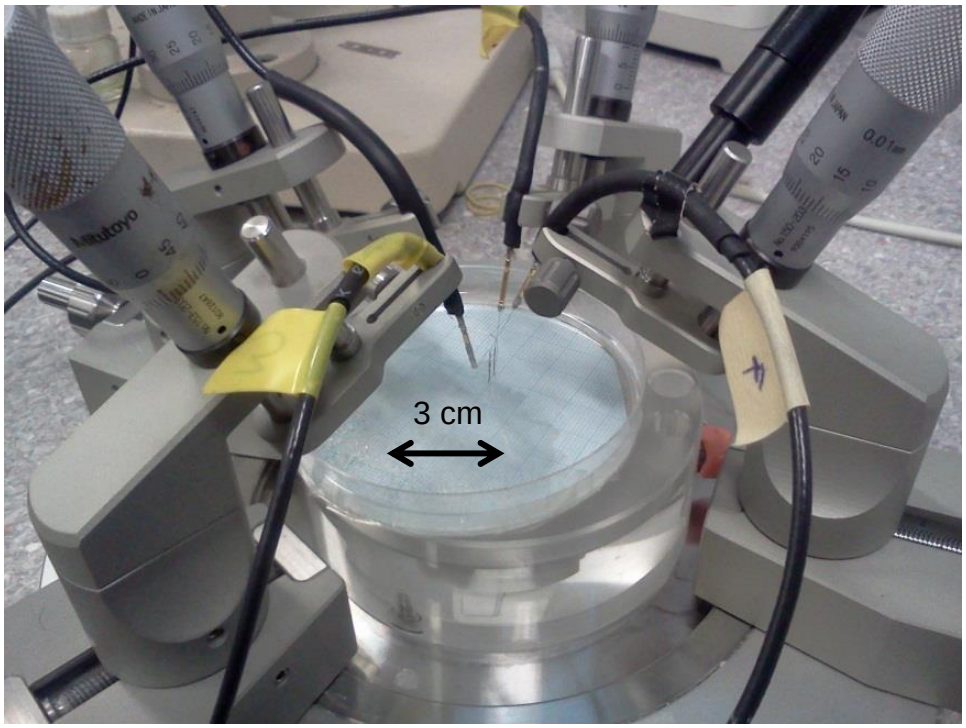

Figure 5-3: Four stainless steel electrodes positioned by electrode manipulators

5.1.3 Electrical Conductivity using Four Gold-Plated Cylindrical Electrodes

I modified the above method to use four fixed cylindrical gold-plated electrodes with diameter 1 mm as in Figure 5-4. I did conductivity measurements on saline solution. Conductivity was 44% higher than expected. The difference was mainly due to the uncertainty in distances. So building a linear array with fixed distances between the electrodes may minimize the high uncertainty in distances.

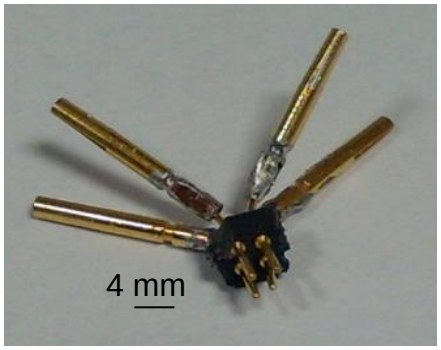

Figure 5-4: Four cylindrical gold-plated electrodes, distances between them are fixed at 2.3 mm each side

5.1.4 Small Linear Gold-Plated Electrode Array

To minimize uncertainty in the distances between the four electrodes, a linear array was built using a Galaxy CNC-1350-A milling machine. The array consists of four gold-plated copper electrodes with 0.5 mm diameter. The distance between two adjacent electrodes is 1 mm from centre to centre (Figure 5-5).

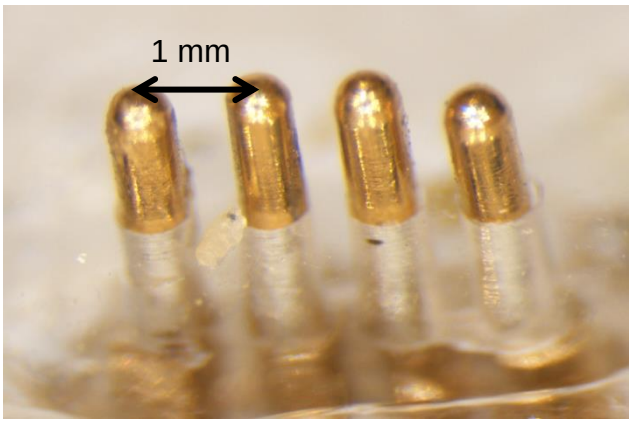

Figure 5-5: Four gold-plated copper multi-electrode array (under stereo-microscope)

After following the standard procedures (described later in Section 5-3), I inserted the electrodes so that they fully penetrated the slice. The slice is very delicate and was cut by the line of electrodes in the process. It would be ideal to sharpen the tips of the electrodes but we do not have the facilities to do this at the University of Waikato. The linear electrode array may be useful for more durable materials but is not suitable for 400-μm thin slices of brain tissue.

The linear array is the smallest size that I could build with the equipment available at the University of Waikato. However, it is not small enough to include four electrodes within a 1.5 mm length to suit the sample size.

I now describe a fresh approach to measuring 2D conductivity in a brain slice: the van der Pauw method.

5.2 Final Methodology: van der Pauw Method

Measuring the conductivity of superconductors, conductors, semiconductors and insulators is important for determining physical properties. Every category has its best form of measurement (Keithley Instruments, 2004). The resistivity of insulating materials can be measured by applying a known potential and measuring the resulting current by electrometer or picoammeter. For resistivity measurements of semiconductors, good electrical contact between sample and electrodes must be achieved as use of point electrodes causes a very high contact resistance. In 1958, van der Pauw invented a very good technique for measuring resistivity of semiconductors and small samples (1958a; 1958b). For resistivity measurements of conductive materials, a sensitive voltmeter with a current source and microohmmeter are required. For resistivity measurements of superconductors, it is essential to have a programmable current source and a nanovoltmeter. In brain slices, sample size is very small and its conductivity lies within the semiconductor region, so four-point cylindrical electrodes should be used.

5.2.1 van der Pauw Method

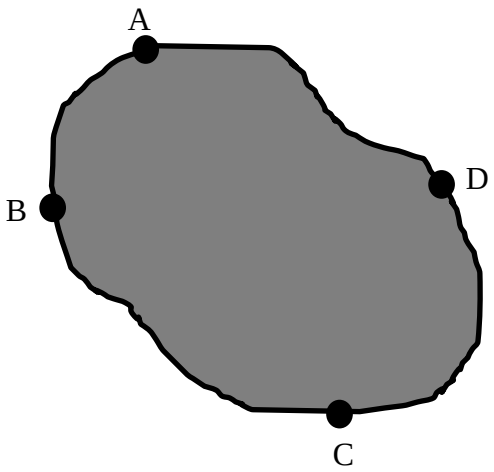

Figure 5-6: Four point-contacts on circumference of a slab of material

Consider a flat, homogenous and isotropic sample of conductive material of arbitrary shape; see Figure 5-6. Four electrical contacts are made at arbitrary positions on the perimeter, where the electrode diameter is small compared to the sample dimensions. The electrode locations are labelled A, B, C and D in a counterclockwise sense as shown in Figure 5-6. Van der Pauw defines the effective resistance $R_{\mathrm{AB,CD}}$ as the potential difference $V_{\mathrm{D}} - V_{\mathrm{C}}$ per current passed into the contact A and out of B. The resistance $R_{\mathrm{BC,DA}}$ is defined in a similar way. According to van der Pauw's theorem the conductivity σ of the material can be calculated from the following relation

$$f(\sigma) = e^{-\pi d R_{AB,CD}\sigma} + e^{-\pi d R_{BC,DA}\sigma} - 1 = 0 \qquad (5\text{-}2)$$

where d is the thickness of the sample. $R_{\mathrm{AB,CD}}$ and $R_{\mathrm{BC,DA}}$ are easily measured as illustrated later in Figure 5-13. The relationship can be derived through a conformal mapping from the shape in Figure 5-6 to a semi-infinite half-plane.

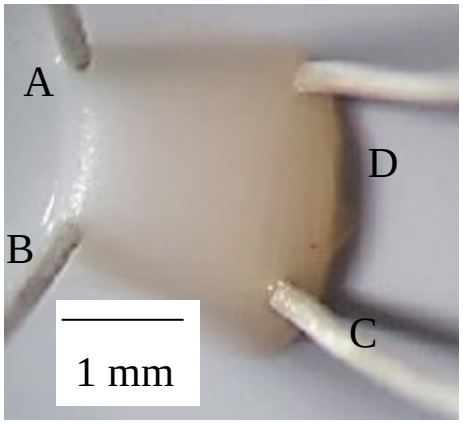

Figure 5-7: A sample of mouse brain cortex with four-point contacts at its corners on circumference

An extension of van der Pauw's theorem was made by Price (1972) for measuring specific resistivity in discs of arbitrary shape for anisotropic media. The van der Pauw method is widely used in high resistivity measurements (Keithley Instruments, 2004). Hemenger (1973) described an apparatus to do measurements on the charge carriers of semiconductors with resistance over 10^{12} Ω using the van der Pauw method. He suggested six configurations and made up a six-section six-position rotary switch to be commercially available as a purchased component. He described it as easy to operate and reliable. Using his switch he collected data up to 10^{13} Ω from high resistivity n-type ZnSe semiconductor material.

5.2.2 Estimation of errors

In his paper, van der Pauw described the error due to the position of the electrodes being not on the perimeter, or due to the fact they are not point electrodes. He estimated the error if the sample is circular with diameter *2R* and one of the electrodes is not ideal as in Figure 5-8.

- Case 1: one of the electrodes has length *l* along the perimeter.

$$\frac{\Delta\sigma}{\sigma} \approx \frac{l^2}{64\,R^2\,\ln 2}$$

- Case 2: one of the electrodes has length *l* perpendicular to the perimeter.

$$\frac{\Delta\sigma}{\sigma} \approx \frac{l^2}{16\,R^2\,\ln 2}$$

- Case 3: one of the electrodes is injected at distance *l* from the perimeter.

$$\frac{\Delta\sigma}{\sigma} \approx \frac{l^2}{8\,R^2\,\ln 2}$$

He recommended a ‘cloverleaf’ shape (Figure 5-9) for the samples if small electrodes are not available or undesirable because of their high contact resistance.

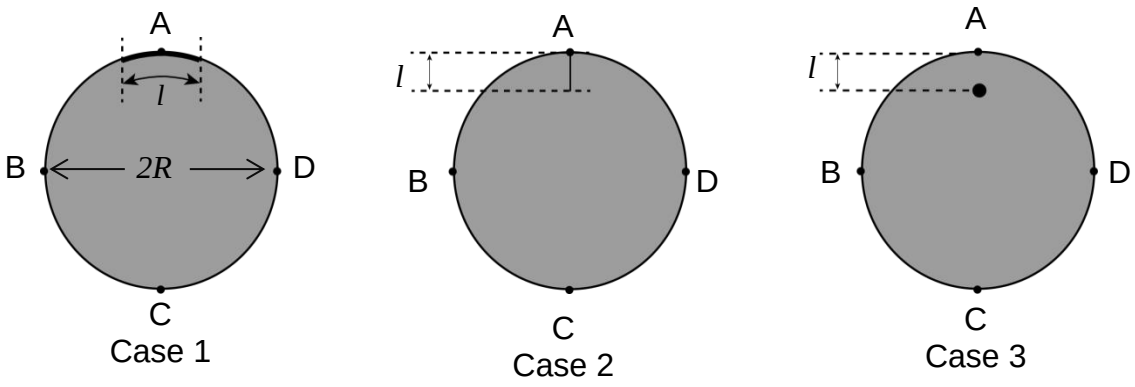

Figure 5-8: Estimation of errors in measurements in van der Pauw special cases

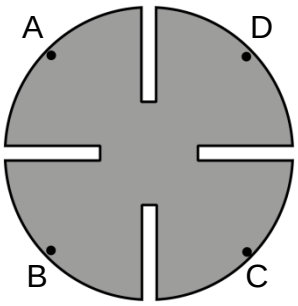

Figure 5-9: Cloverleaf shape

Applying the van der Pauw error estimates to my set up (Section 5.2.3), I found that Case 3 is the most significant. Its error is about one percent so it is ignored because it is less than the method uncertainty.

The main uncertainty in this method comes from the electrical connections between the sample and the electrodes. Ideally the electrodes should be placed on the perimeter of the sample or at the corners. Experimentally, this is impossible, and so this is another source of error. Special care must be taken to ensure good and stable contact between the electrode and the tissue. Cutting the electrode wires at an angle gives the electrode a sharp tip that

facilitates insertion into the tissue. Each electrode must be inserted into the full thickness of the slice to ensure good contact. This point is key for doing good, reliable and stable measurements using the van der Pauw method.

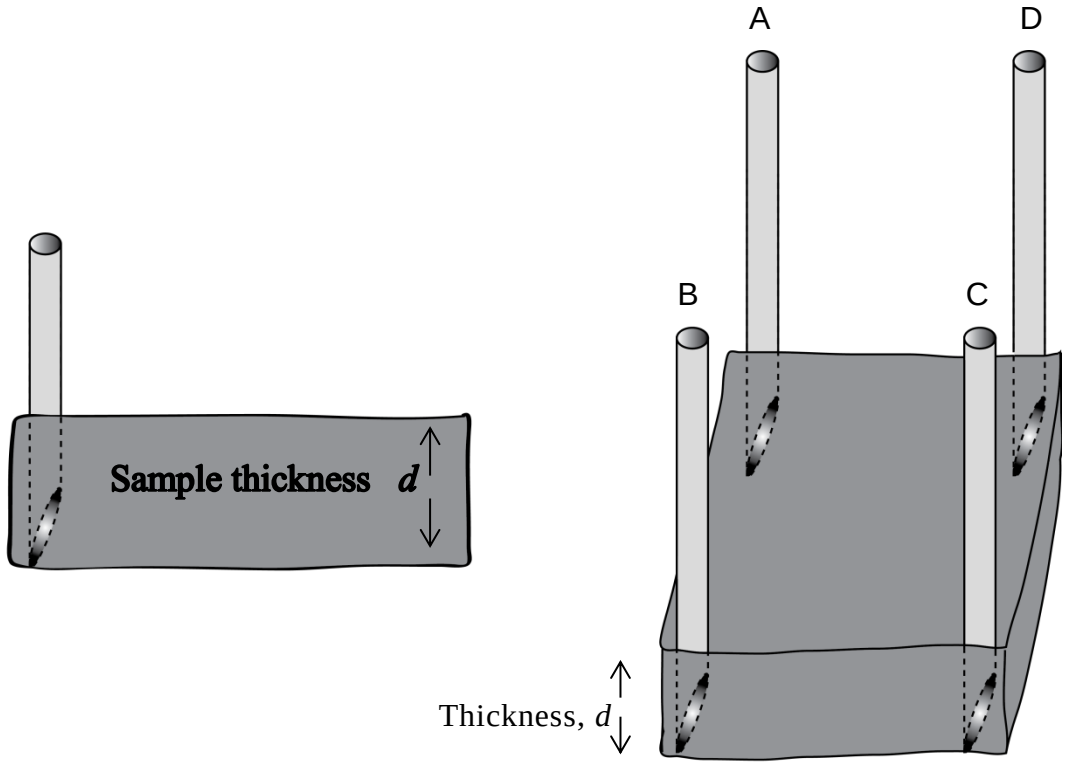

Figure 5-10: Each electrode must be inserted into the full thickness of the slice to ensure good contact

5.2.3 Sample and electrode geometry correction factor

Point electrodes cannot be used in practice. In this study a typical silver electrode has diameter 0.25 mm; therefore an approximately square sample with electrodes inserted at the each of four corners was used to optimize the measurements (Thurber, 2010) as in Figure 5-10. Koon (1989) studied the errors in measurements due to size of electrodes, positions and sample resistive inhomogeneity for the van der Pauw measurements. He used square and cloverleaf sample shapes. I used square samples rather than a cloverleaf shape because it is very difficult to cut the cloverleaf shape in a biological tissue. To minimize measurement errors he recommended sharpening the corners and putting the electrodes near the corners. The following studies considered square electrodes, however in my measurements circular electrodes were used. Weiss *et al.* (2008) showed a derivation of the van der

Pauw equation from electrostatics in a rectangular cross section with a sample of arbitrary thickness. They also studied the effect of sample thickness and the contact area of electrodes. Moreover (Weiss, 2011) generalized their work for a square sample as per the following: consider c to be the thickness of the sample, a to be the side length of the sample, δ to be thickness of the electrodes and w to be half-width between two electrodes, as in Figure 5-11.

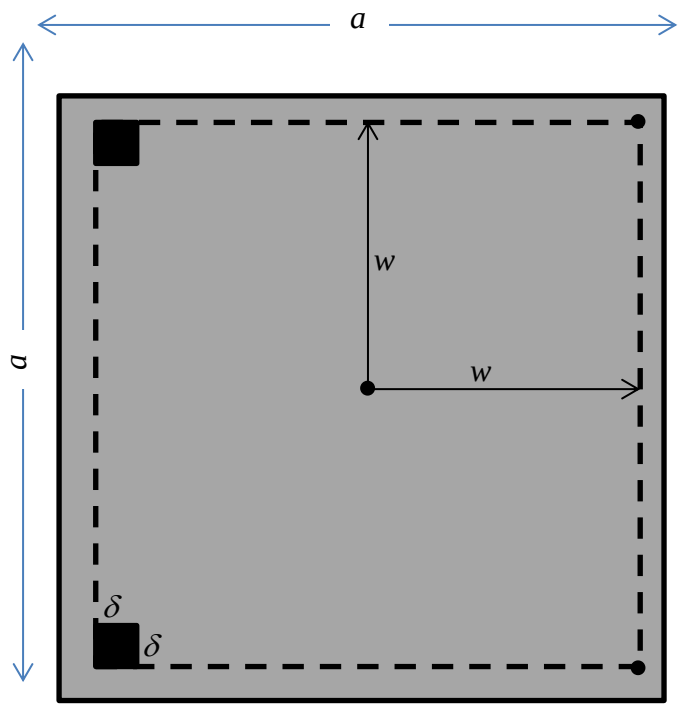

Figure 5-11: Geometry of the sample and electrodes

For my application, I identify a = 2 mm (slice width), δ = 0.25 mm (electrode width), d = 0.4 mm (slice thickness) and $w \approx 0.9$ mm, the last of these assuming that the electrode is placed of order 0.1 mm in from each corner. From these data, I calculated the following ratios: thickness to width ratio ($d/a = 0.2$) of the sample, half electrode-separation to sample width ($w/a = 0.45$) and electrode thickness to half distance between the electrode ($\delta/w = 0.28$). From Weiss (2011), these ratios leads to a correction factor of 0.96 which means calculated conductivity should be multiplied by approximately 0.96. However Chwang *et al.* (1974) have made a similar study and according to it, 1% should be added to my results. I did not apply these corrections because errors are smaller than other uncertainties in this

method. The Chwang estimate is the same value as the van der Pauw error estimation. Since these corrections are less than the uncertainty, they were ignored.

5.2.4 Four-position rotatory switch

I designed a circuit to connect the brain sample to the Agilent E4980A *LCR* meter using a four-position four-pole rotatory switch. Its circuit diagram is shown in Figure 5-12. Here, HCUR refers to current high, HPOT refers to potential high, LPOT refers to potential low and LCUR refers to current low. All four switches are mechanically linked so all four are positioned to the same terminal number. Therefore all of them start at position 1 to give the output arrangement which is seen on Figure 5-13 part 1. Then position 2 changes the electrode function as seen in part 2 in Figure 5-13 and similarly for positions 3 and 4. A photograph of the full system is in Figure 5-14.

The conductivity was calculated four times based on the four combinations $R_{AB,CD}$, $R_{BC,DA}$, $R_{CD,BA}$ and $R_{DB,CA}$ (Figure 5-13). The four pseudo resistances were measured and calculated by the Agilent E4980A. MATLAB was used to solve equation (5-2) for conductivity σ by the Newton-Raphson method (Figure 5-15). MATLAB CODE is reported in Section B-2. The averages of conductivities for the same sample were taken to increase the accuracy of conductivity determination.

Assuming the slice is isotropic, one would expect that the measured conductivity of the slices should be the same regardless of how the electrodes are arranged. So I made four measurements on each slice and rejected the measurements if the average absolute difference between them exceeded 20%. It is possible that large differences may arise from lack of contact between electrodes and tissue, or they are not exactly on the perimeter, or may be due to the fact that they are not ideal point electrodes.

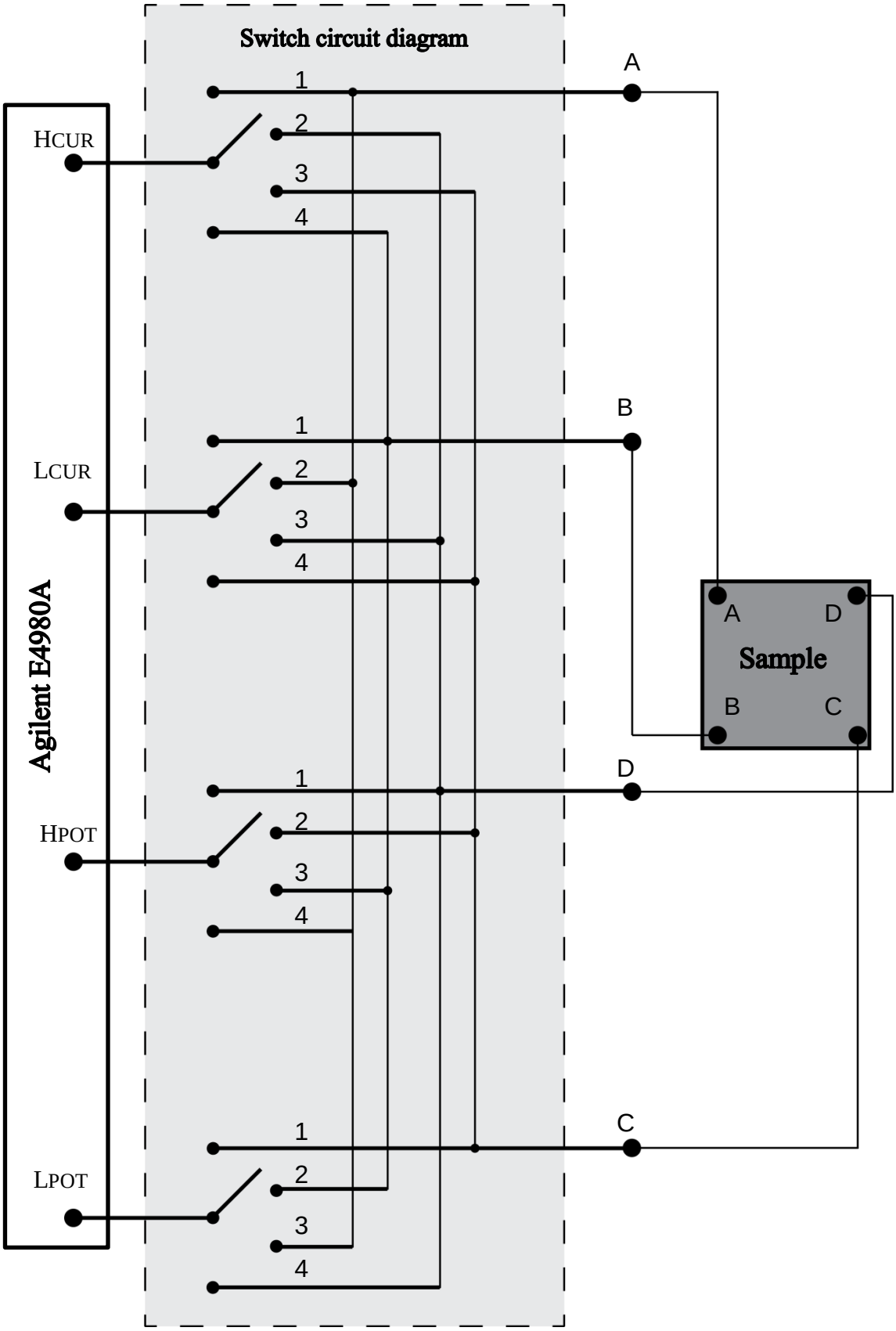

Figure 5-12: Four-position four-pole rotatory switch circuit diagram

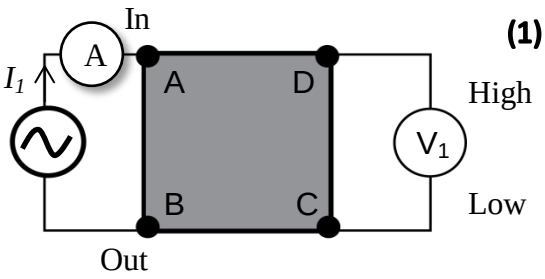

(1)

$R_{AB,CD}$ is calculated by dividing the voltage difference (V_1) between D and C by the current flowing between A and B:

$$R_{\mathrm{AB,CD}} = \frac{V_1}{I_1}$$

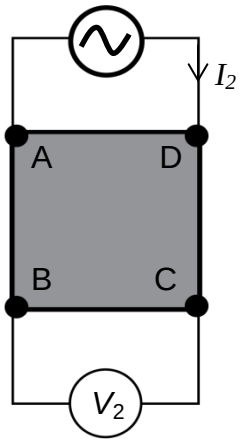

(2)

$R_{DA,BC}$ is calculated by dividing the voltage difference (V_2) between C and B by the current flowing between D and A:

$$R_{\mathrm{DA,BC}} = \frac{V_2}{I_2}$$

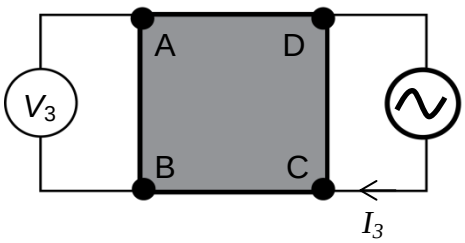

(3)

$R_{CD,AB}$ is calculated by dividing the voltage difference (V_3) between B and A by the current flowing between C and D:

$$R_{\mathrm{CD,AB}} = \frac{V_3}{I_3}$$

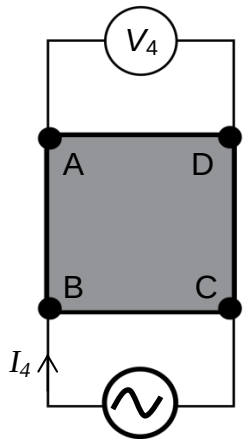

(4)

$R_{BC,\ DA}$ is calculated by dividing the voltage difference (V_4) between A and D by the current flows between B and C:

$$R_{\mathrm{BC,DA}} = \frac{V_4}{I_4}$$

Figure 5-13: Four circuit configurations to determine $R_{AB,CD}$, $R_{DA,BC}$, $R_{CD,AB}$ and $R_{BC,\ DA}$

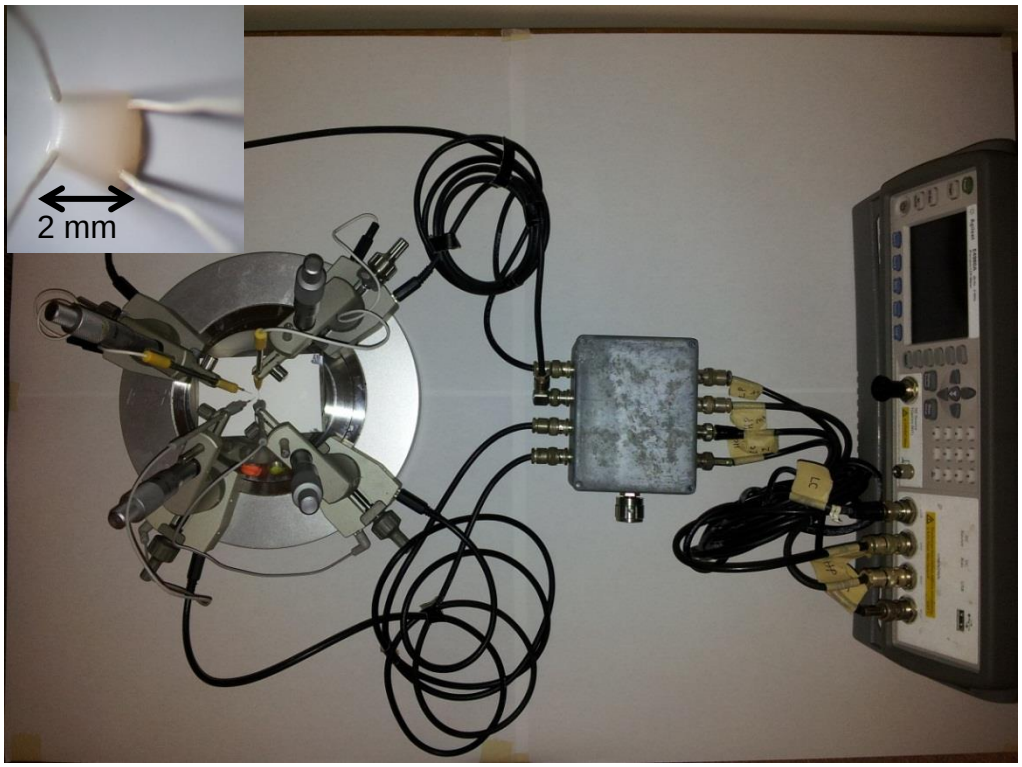

Figure 5-14: Agilent E4980A, 4-way, 4-pole switch and manipulators that hold the four electrodes

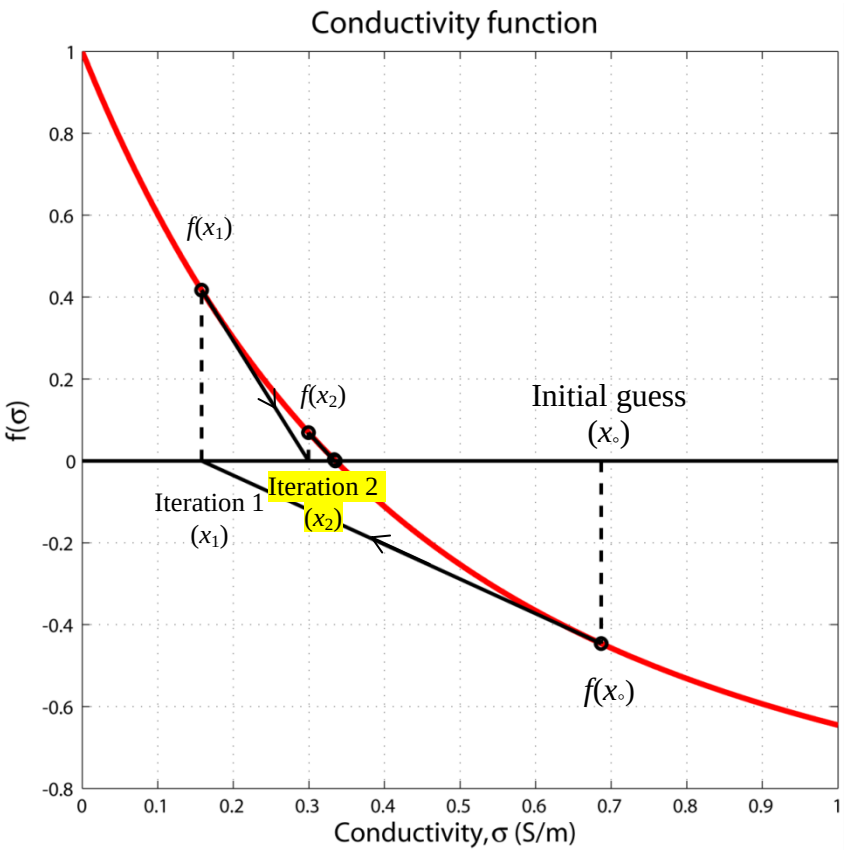

Figure 5-15: Demonstration of the Newton-Raphson method for solving van der Pauw Equation (5-2) for conductivity. Tangent extrapolation from the curve to x-axis indicates the value of next iteration

5.3 Cortical Slice Preparation

All samples used in this research were provided from wild type mice (i.e. not modified genetically) strain C57/Bl6/129SV. Brain slices were prepared from-10-week old female animals according to standard procedures (Voss *et al.*, 2010). Animals were anaesthetized by carbon dioxide then decapitated in accordance with local animal ethics guidelines. The brain was removed then placed in ice-cold artificial cerebrospinal fluid (ACSF). ACSF is a solution designed to minimize neural cell death after the brain is removed and sliced. A modified neuronal protection ACSF was used (Nowak & Bullier, 1996). Using a vibratome (Campden Instruments, UK), coronal slices of thickness 400 µm were produced by cutting between bregma[1] −2 mm to −5 mm as shown in Figure 5-16c. Slices were then transferred to a holding chamber containing carbogenated ACSF. These ACSF compositions were either "magnesium-free" or "normal". All three solutions (neuronal protection, magnesium-free and normal; compositions shown in Table 5-1) were bubbled with carbogen (95% O_2, 5% CO_2).

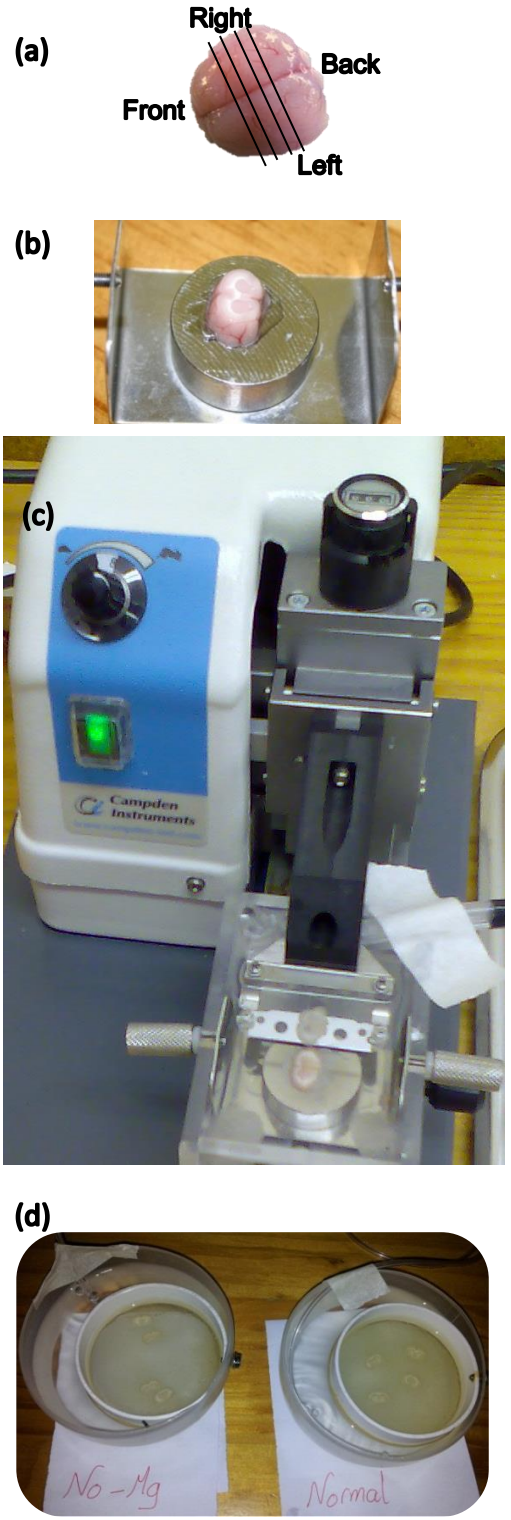

Figure 5-16: (a) Mouse brain showing the coronal slicing direction (b) Brain cut into a block and prepared for slicing (c) Vibratome for cutting the slices (d) Half of the cut slices placed in magnesium-free ACSF, while the other half were placed in normal ACSF solution for later experimental procedures

[1] Bregma is the point on top of the skull where the three main sections of the skull meet.

Table 5-1: Solution compositions

	ACSF composition in (mM)		
	"Neuro protected"	"Magnesium-free"	"Normal"
NaCl	92.7	124	125
$NaHCO_3$	24	26	26
NaH_2PO_4	1.2	1.25	1.25
KCl	3	5	2.5
$MgCl_2$	19	-	1
$CaCl_2$	-	2	2
D-glucose	25	10	10

Seizure-like state was activated by magnesium-free ACSF (Li Zhang *et al.*, 1995), while the normal ACSF maintains slice viability (health) but prevents seizure-like activity. Magnesium blocks NMDA receptors which minimizes excitatory activity. Thus, removing Mg^{2+} from the solution unblocks NMDA channels and leads to heightened excitatory activity. All slices were allowed to recover for at least one hour before continuing with the experimental protocol. The ratio of normal to magnesium-free ACSF solutions conductivities is 1.0005 which indicates that their conductivities are effectively identical therefore any changes in the measured conductivity of slices are not caused by the conductivity of the solutions.

Seizure-like event activity was confirmed in slices that were held in magnesium-free ACSF before continuing with the conductivity measurements. This was done by positioning a 50-µm teflon-coated tungsten electrode into the cortical tissue (Figure 5-17) and recording local field potential activity, referenced to a silver/silver chloride electrode in the ACSF solution. Local field potential activities were amplified by AC/DC differential amplifier (A-M Systems, Inc-Model 3000). The settings of the bioamplifier were 1000 Hz for the low pass filter and 1 Hz for the high pass filter. Local field potential activities were then converted to digital signals

through a digital converter (AD Instrumentation power lab 8/30) at a sampling rate of 1 kHz. An example of the type of activity recorded is shown in Figure 4-11. Cortical slices held in normal ACSF are quiescent and do not normally exhibit any local field potential activity. For this reason, tissue viability was assumed for slices held in normal ACSF on the basis that a single slice cut from the same brain generated seizure-like activity when exposed to magnesium-free ACSF.

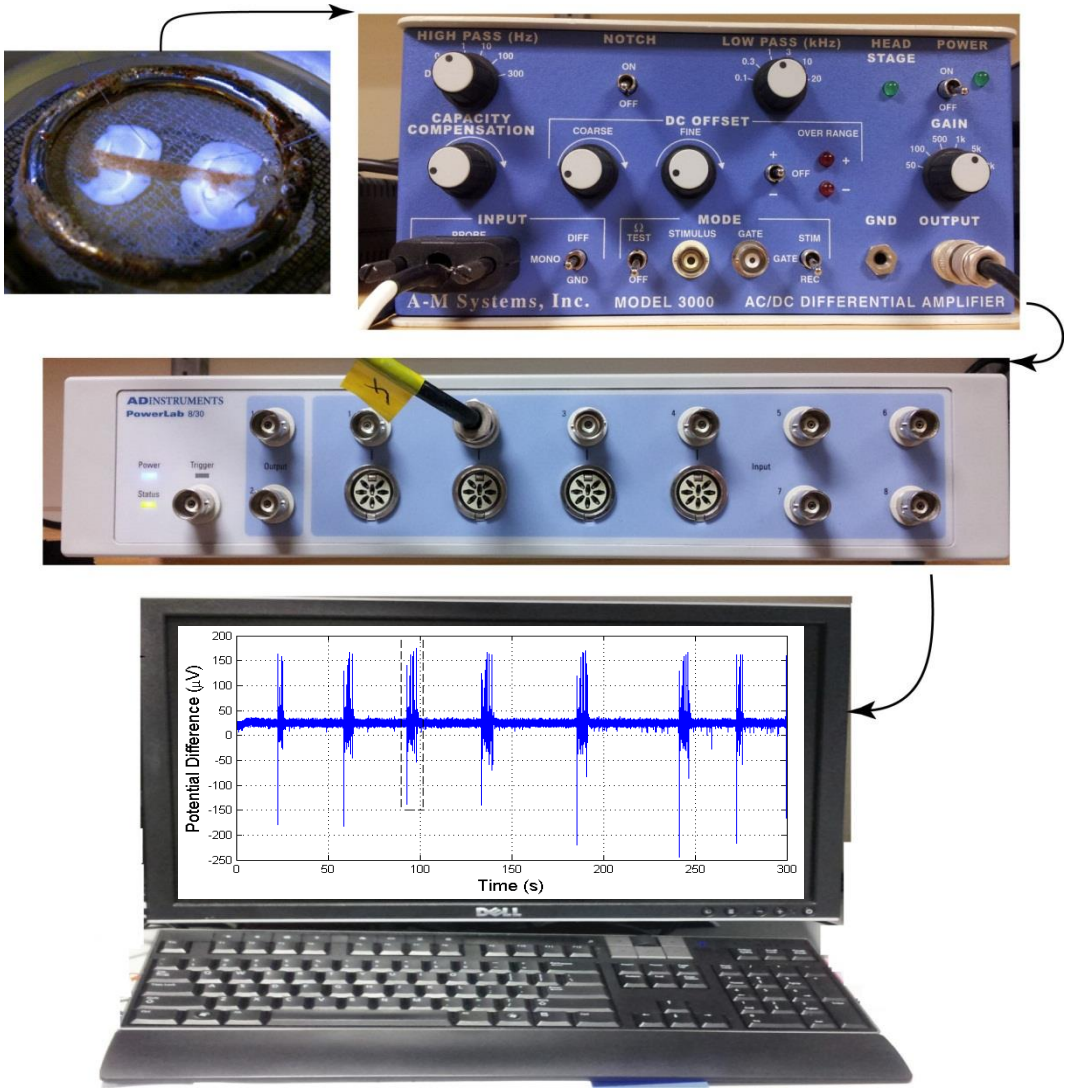

Figure 5-17: Recording local field potential activity by a 50-μm teflon-coated tungsten electrode positioned in the cortical tissue. The slice sits on a mesh in order to allow ACSF to bathe the slice. Reference electrode is hidden in this photo. Local field potentials are amplified then converted to a digital signal and viewed on a PC screen

One slice at a time was prepared for conductivity measurement. The slice was placed on a stage and a small (about 2×2 mm) piece of cortical tissue

was sectioned and removed. Excess ACSF solution was removed by filter paper from around the tissue section and the four silver-wire electrodes positioned as in Figure 5-7.

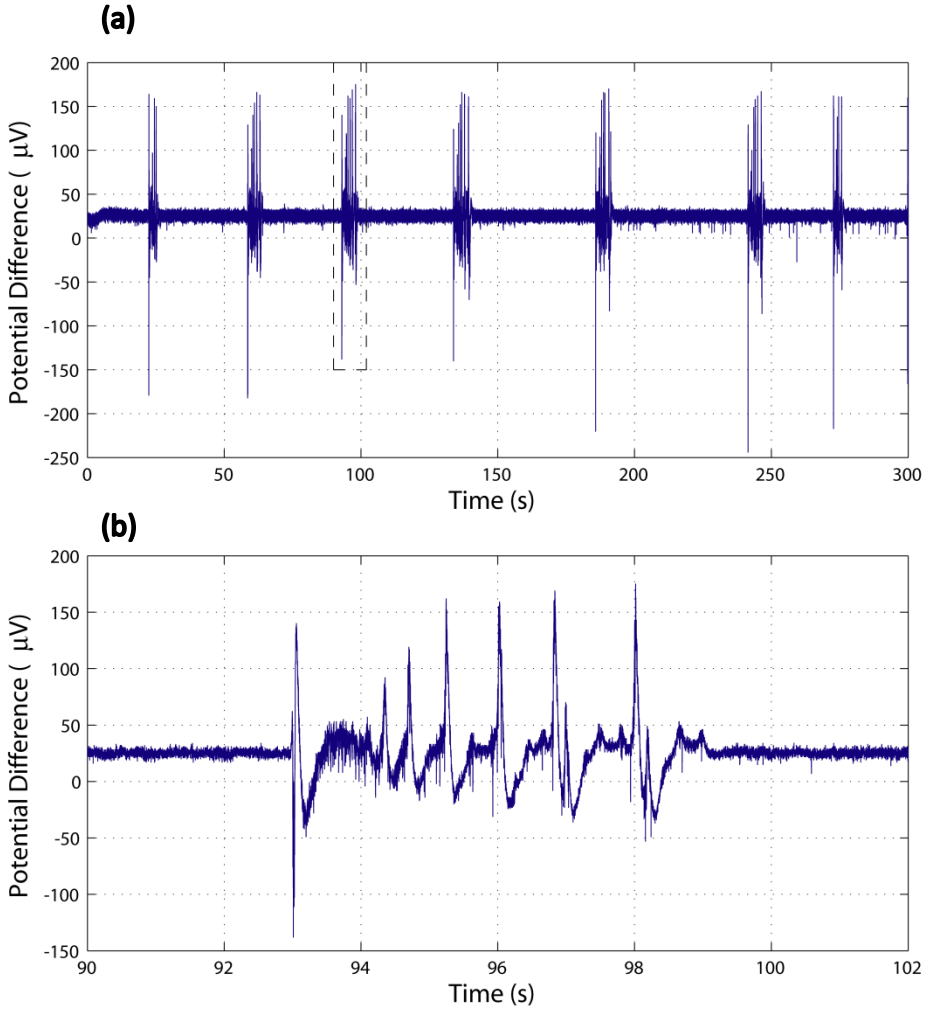

Figure 5-18: Seizure-like event activity (a) with compressed time showing multiple seizure-like events and (b) enlarged view of one seizure-like event

5.4 Results of Measured Conductivity with Aging

In one slice, we measured the effect of tissue aging on conductivity at five minute intervals over a thirty-minute period. We found that conductivity tended to increase with time (Figure 5-19), probably as a result of tissue degradation and/or drying out. Conductivity increase might be caused by rupture of cell membranes; this will increase ionic concentration in the extracellular space thus increasing tissue conductivity (Haemmerich *et al.*, 2002; Damez *et al.*, 2007). For this reason, I ensured that the recordings

were made within 2-3 minutes after the slice was removed from the bath, and within 12 seconds of removal of ACSF. (Conductivity changes after cell death was discussed in Section 2.3).

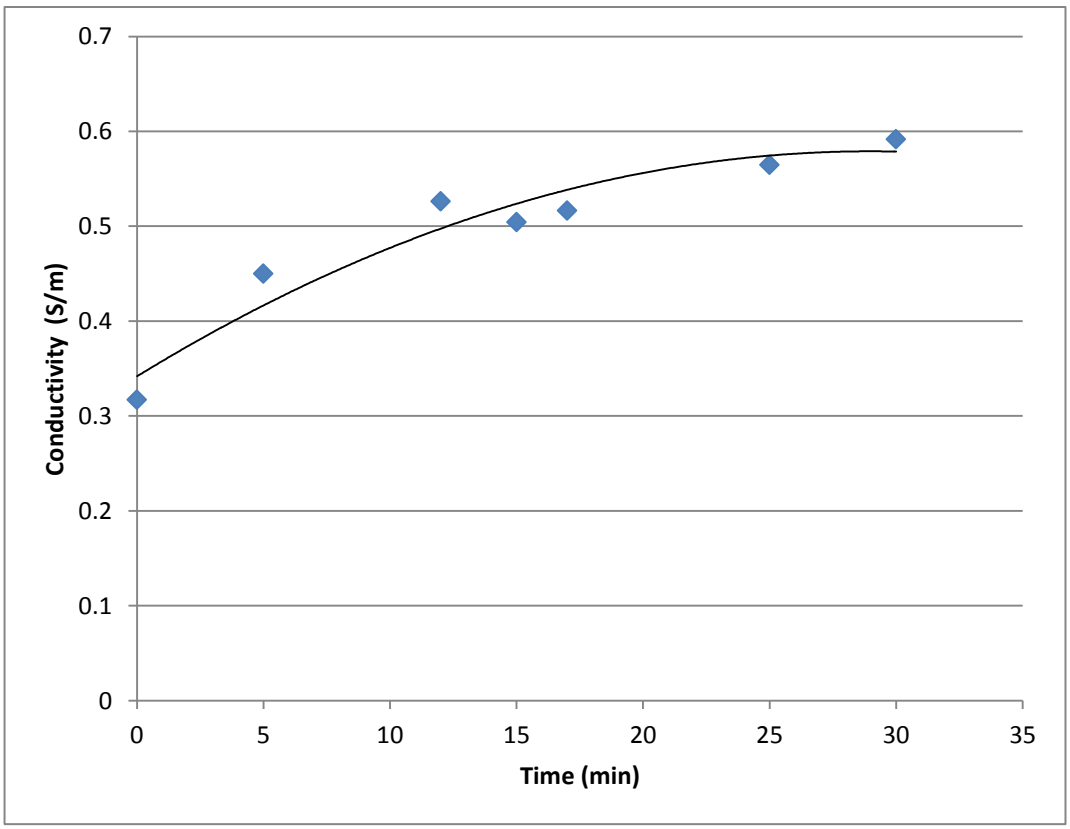

Figure 5-19: Conductivity increases with aging, line is for eye guide only

5.5 Results of Measured Conductivity

I carried out this experiment over three days on the brain extracted from three animals, one brain each day. Half of the slices from each animal were placed in magnesium-free ACSF, while the other half were placed in normal ACSF. My results show that there is no significant difference (p = 33%) between the measured conductivities from different animals while there is a significant difference (p = 2%) between the conductivities from seizing and non-seizing slices without outliers. A 'five-point summary' is shown by a boxplot: Figure 5-20 shows the minimum, lower quartile, median, upper quartile and maximum values, including outliers in Figure 5-20 and excluding them in Figure 5-21.

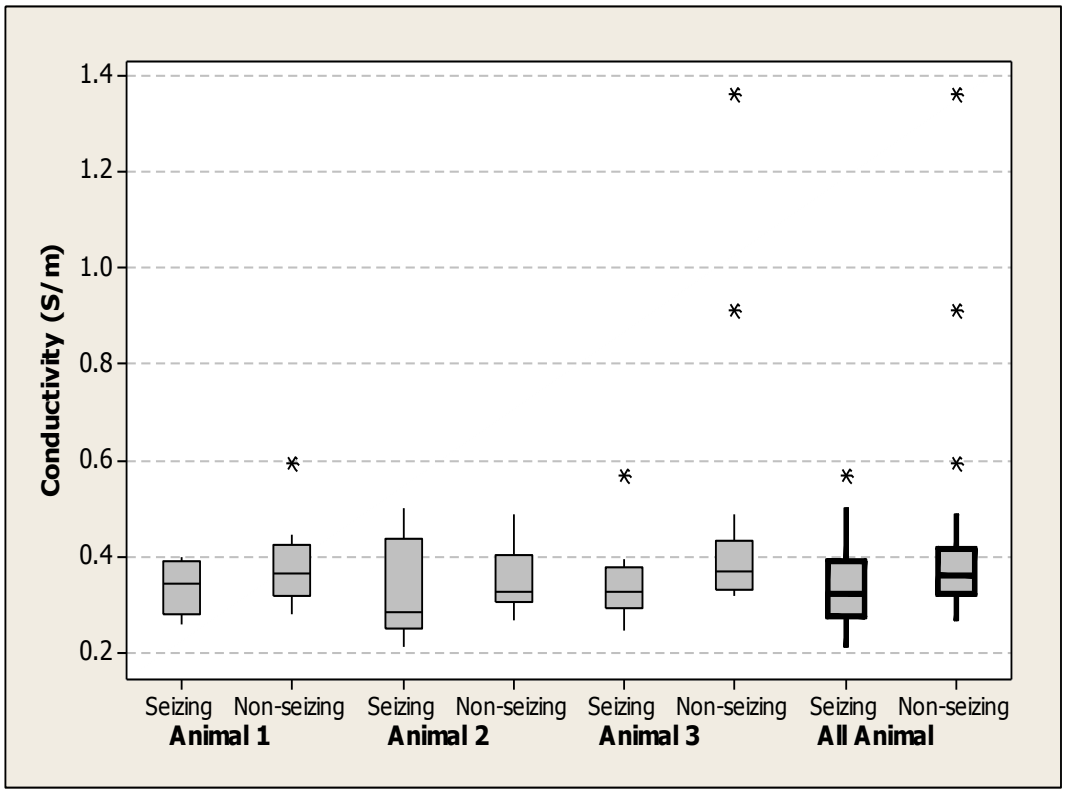

*Figure 5-20: Comparison of conductivity of seizing and non-seizing slices (outliers signified by *)*

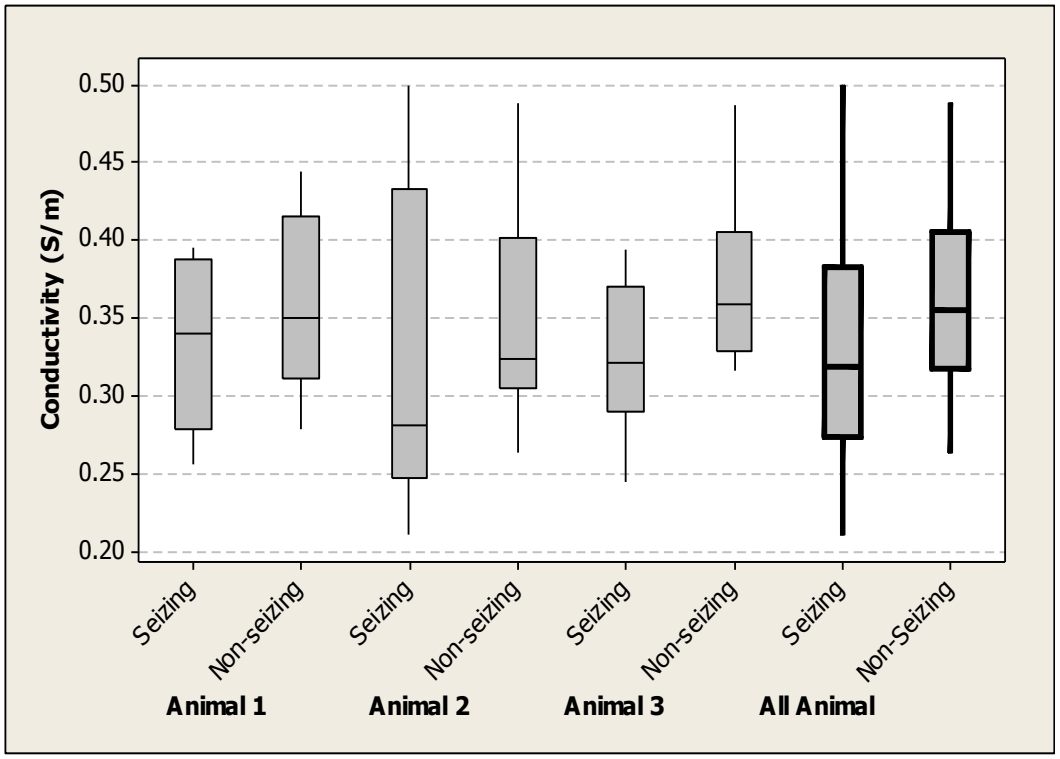

Figure 5-21: Comparison of conductivity of seizing and non-seizing slices after excluding the outliers

With outliers included, my results still show that there is no significant difference (p = 94%) between the measured conductivities from different animals, while there is a significant difference (p = 1%) between the conductivities of seizing and non-seizing slices. Figures 5-22 to 5-24 show the frequency of conductivities with outliers. Table 5-2 summarizes the results.

Although values were selected when the difference between the four measurements (see Figure 5-13) was no more than 20%, to confirm the robustness of my findings, I tried accepting data when the four measurements were within 10%, and within 5%, but found no change in the significance of the difference in conductivities between seizing and non-seizing slices.

Table 5-2: Mean and median conductivities and significance of difference between seizing and non-seizing slices using Mann-Whitney Test (MW-test) including outliers data and two-sample t-test when excluding outliers. Standard uncertainty included for the mean

	Seizing (S/m)	Non-seizing (S/m)	Significance (*P*-value)
Allow ±20% within-slice variability			
Mean (excluding outliers)	0.3284±0.012	0.3618±0.0088	0.025 (*t*-test)
Median (including outliers)	0.32117	0.35991	0.013 (*MW*-test)
Allow ±10% within-slice variability			
Mean (excluding outliers)	0.3276±0.013	0.3620±0.0088	0.032 (*t*-test)
Median (including outliers)	0.31868	0.36098	0.0071 (*MW*-test)
Allow ±5% within-slice variability			
Mean (excluding outliers)	0.3256±0.012	0.3631±0.0090	0.017 (*t*-test)
Median (including outliers)	0.32117	0.36531	0.0072 (*MW*-test)

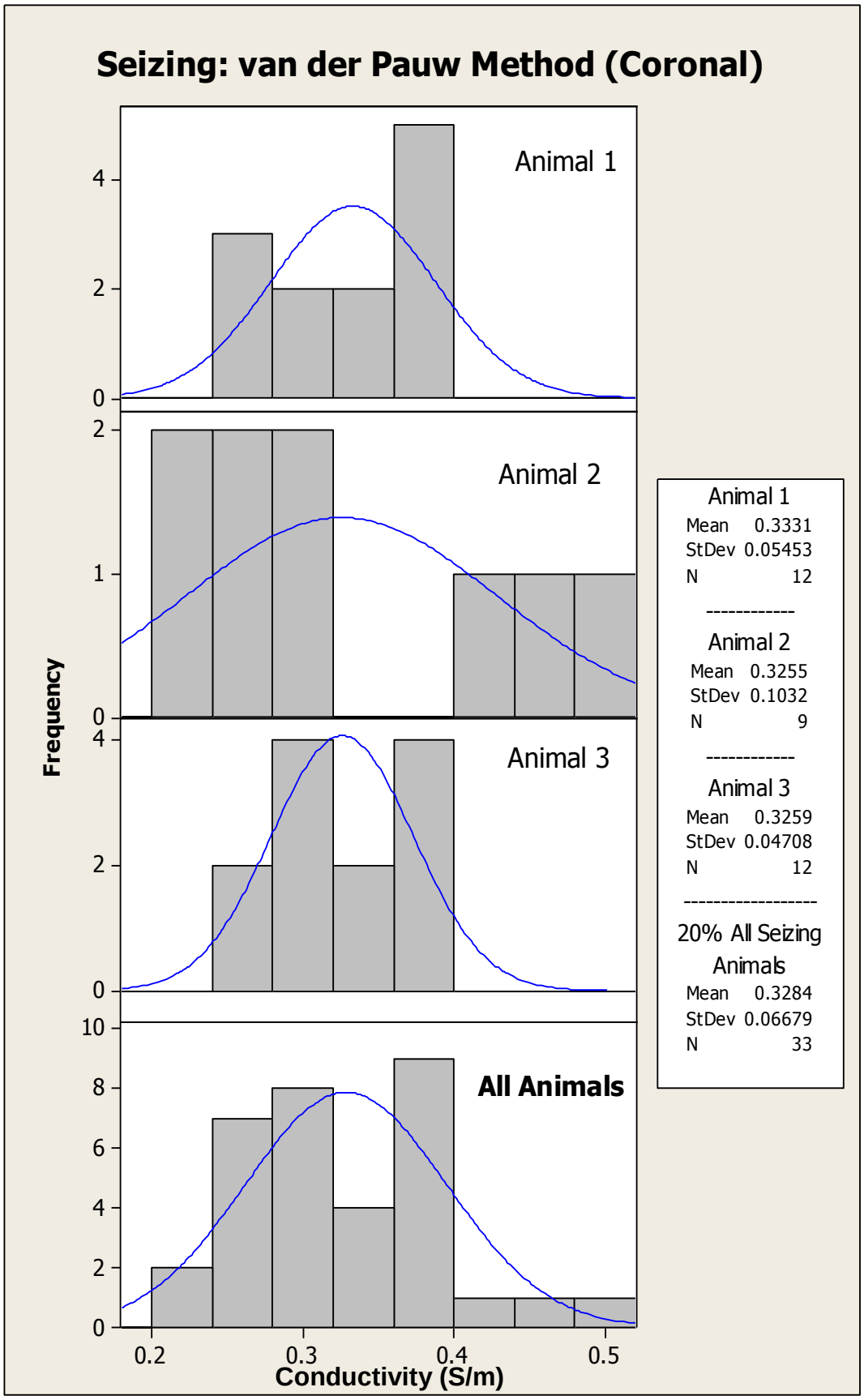

Figure 5-22: Comparison between conductivities of three seizing brains.

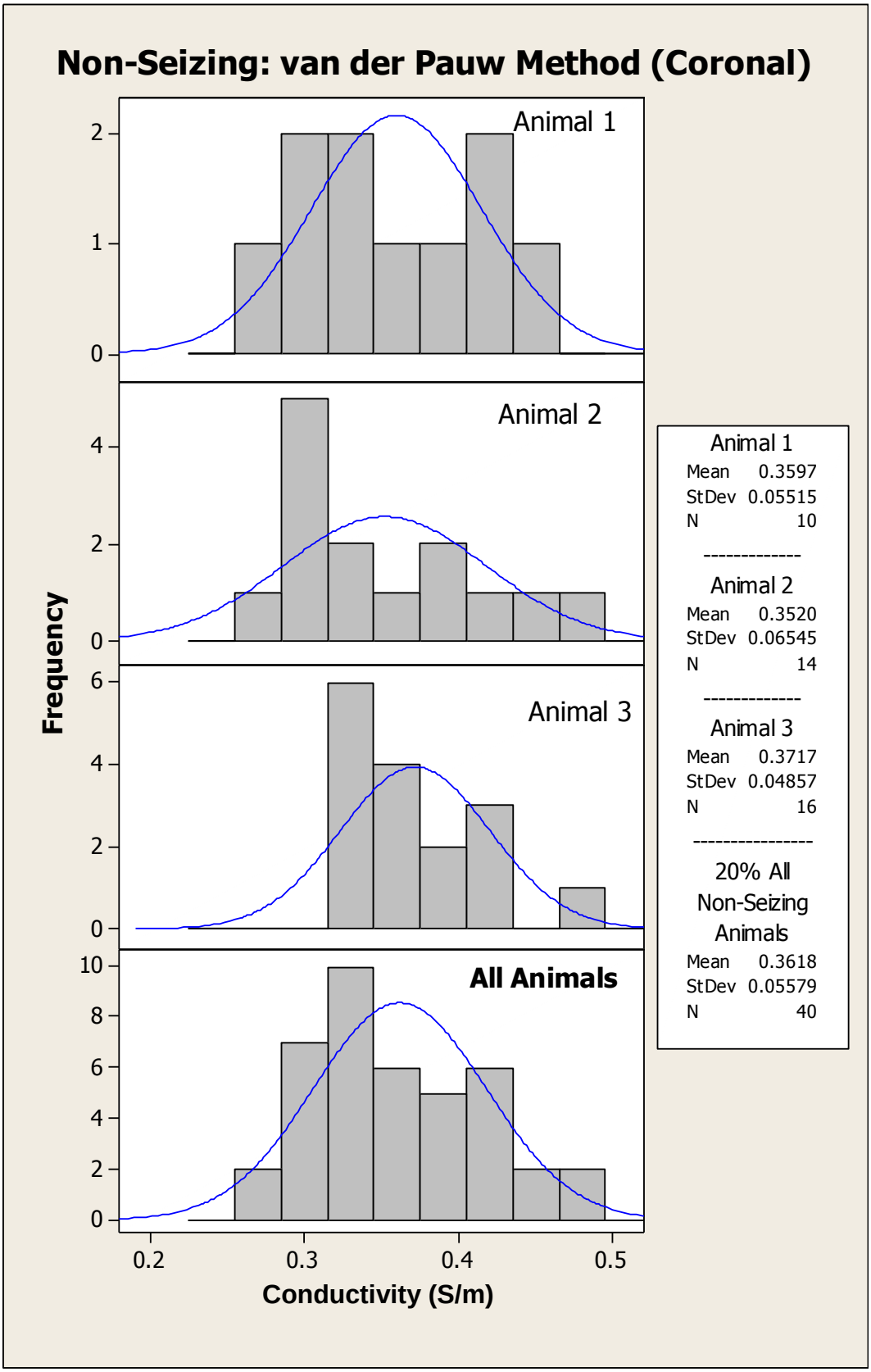

Figure 5-23: Comparison between conductivities of three non-seizing brains

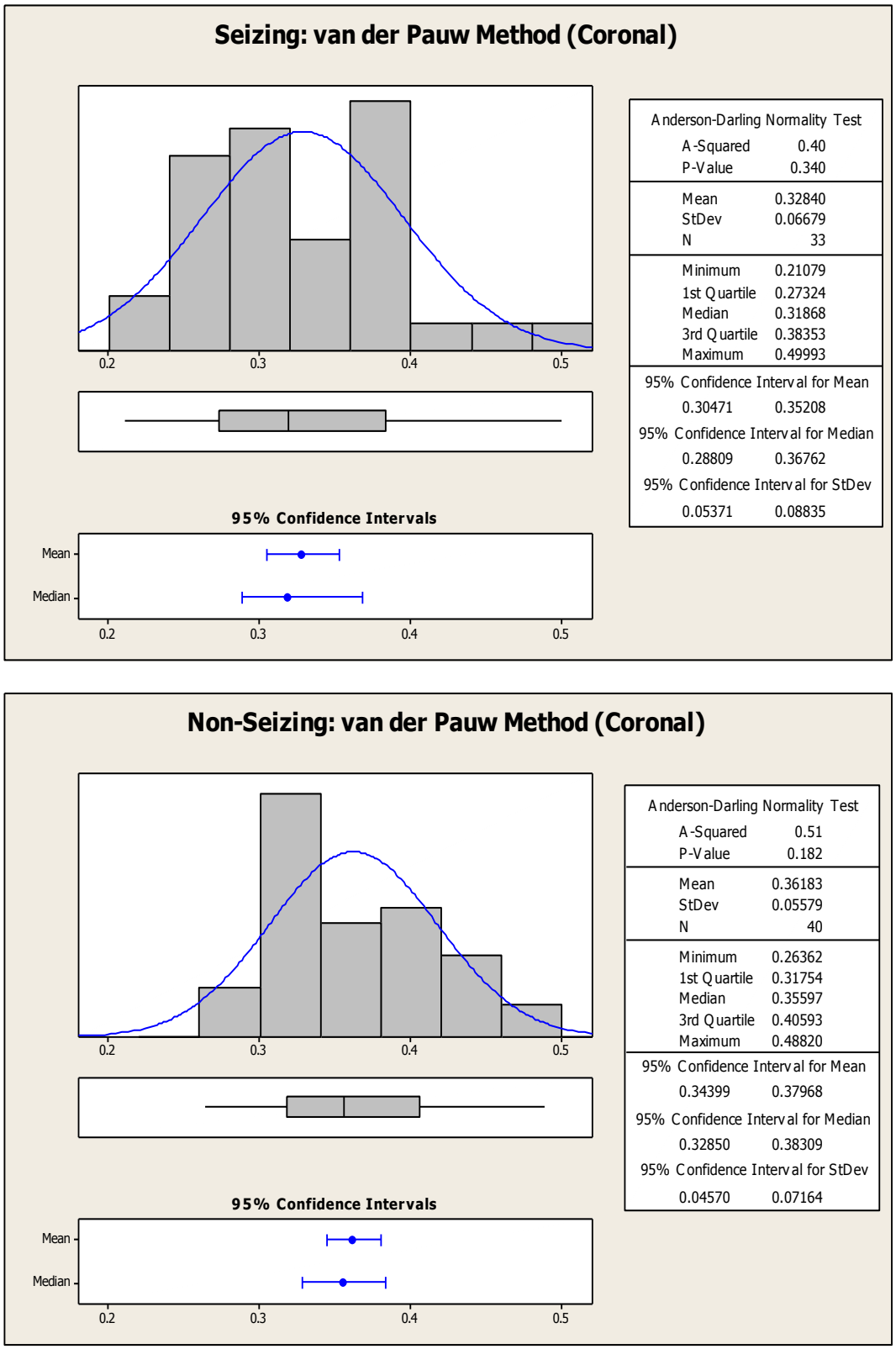

Figure 5-24: Comparison between conductivities of seizing and non-seizing slices

5.6 Conclusion for van der Pauw Experiment

The *P*-value shows that there is a significant difference between the means of seizing and non-seizing slices, with the non-seizing slices having a 13% higher conductivity. This result is broadly consistent with Van Harreveld & Schade (1962): they found a 10% conductivity decrease in rabbit cortex, and 5% decrease in cat cortex *in vivo* during seizure induced by metrazol injection. They assumed that the decrease in conductivity during seizures originates from ion migration from the extracellular space to the cell interior.

Conductivity may decrease not only due to migration of electrolytic solution to the inside of the neurons as Van Harreveld & Schade (1962) suggested, but may also occur because of closure of gap junctions. We can estimate the gap junction contribution to the conductivity as described in Appendix A, and the result is ~0.03 S/m, which corresponds to a 10% decrease in conductivity if all gap junctions are closed.

Elazar *et al.* (1966) assumed the changes in conductivity were due to two mechanisms. First, increasing blood pressure would increase conductivity. However, the more powerful contribution is depression of the excitability of the tissue, so overall the conductivity decreases. In my study, blood flow cannot influence my readings because there is no blood flowing in the slice.

From the above we may say the conductivity may decrease because of electrolyte immigration, or neuron depression of tissue excitability, or gap junction closure. More work is needed to find out which parameter determines conductivity of neural tissue. The gap junction effect could be investigated by comparing the brain conductivity of wild type and Cx36 gene knockout mice. Cx36 gap junctions are the most common gap junction subtype in the adult cerebral cortex. Also the role of gap junctions could be investigated by studying the effect of gap junction-blocking drugs on brain conductivity.

5.7 Chapter Summary

After several attempts to perform electrical conductivity measurements in two dimensions, I successfully measured the conductivity of seizing and non-seizing mouse brain slices at 10 kHz using van der Pauw method. I found that the conductivity of seizing is statistically significantly lower than non-seizing slices.

6 Initial Attempts for Conductivity Measurements in One Dimension

In this chapter, I will demonstrate two of four of my initial attempts and developments to do conductivity measurements in one dimension. The aim is to measure the electrical conductivity of a slice of brain tissue while it is in ACSF. The first two trials, versions one and two, are very similar to version 3 but the results were not strong enough to present. So I will start with version 3. None of the initial attempts for One-dimensional method gave satisfactory results, so there are no conclusive results reported in this chapter. All good results obtained by One-dimensional method are reported in Chapter 7.

This is called a one-dimensional method (1D) because I used planar electrodes. This implies that current flows in one dimension in the tissue.

6.1 Measurements Using Syringe Version 3 (V3)

Syringe V3 is a 10 ml syringe which has been modified by inserting a pair of circular flat stainless steel electrodes at its internal cylinder top and its piston top as shown in Figure 6-1. Syringe V3 was used to measure the electrical conductivity of brain slices by connecting it to the Agilent *LCR* meter (E4980A).

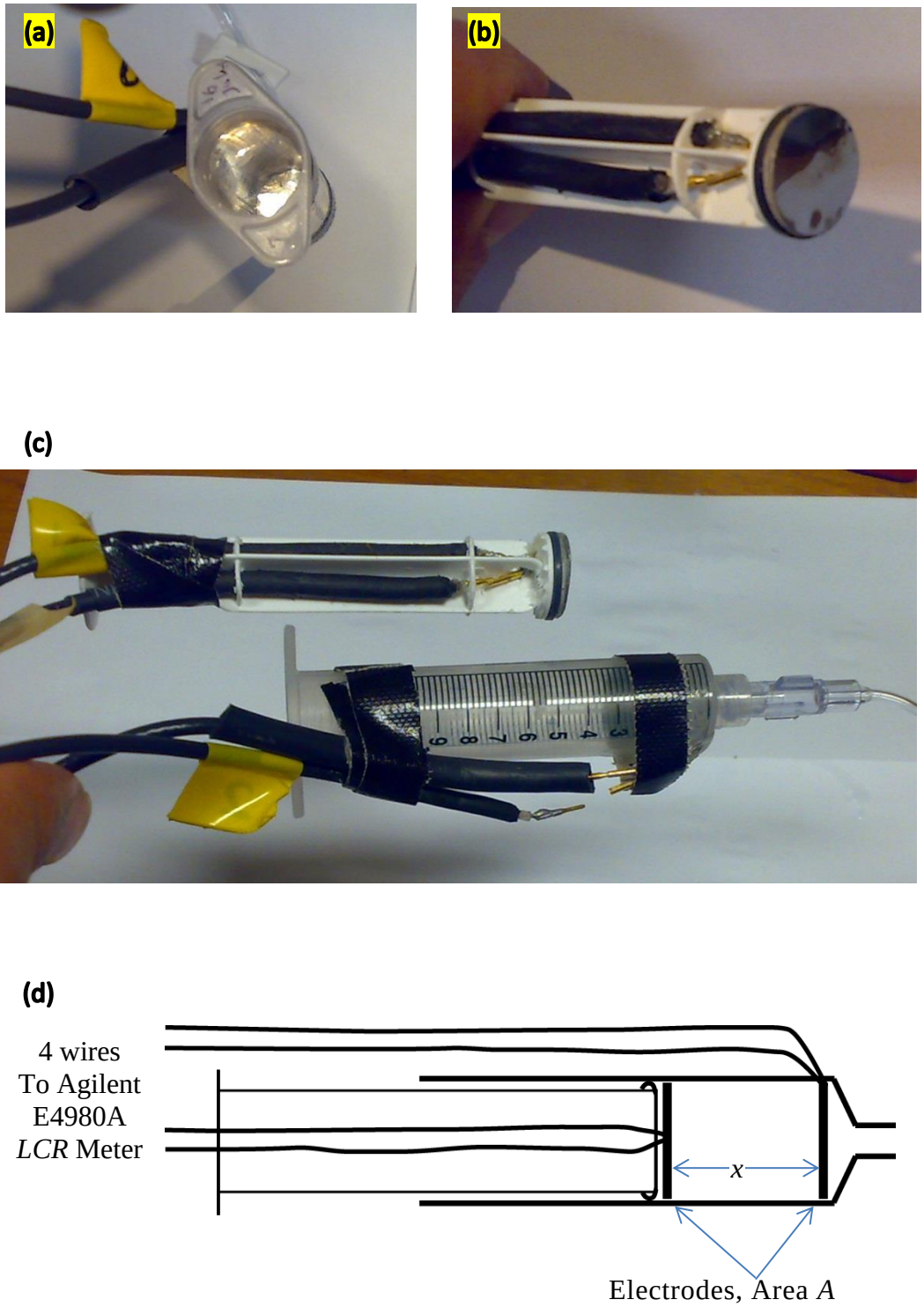

Figure 6-1: Syringe V3: (a) stainless steel electrodes at internal top of the cylinder. (b) stainless steel electrodes at internal top of the piston (c) side view of V3. (d) schematic diagram for Syringe V3

6.2 Theory and Methodology to Calculate the Conductivity of Brain Slice in One-dimension

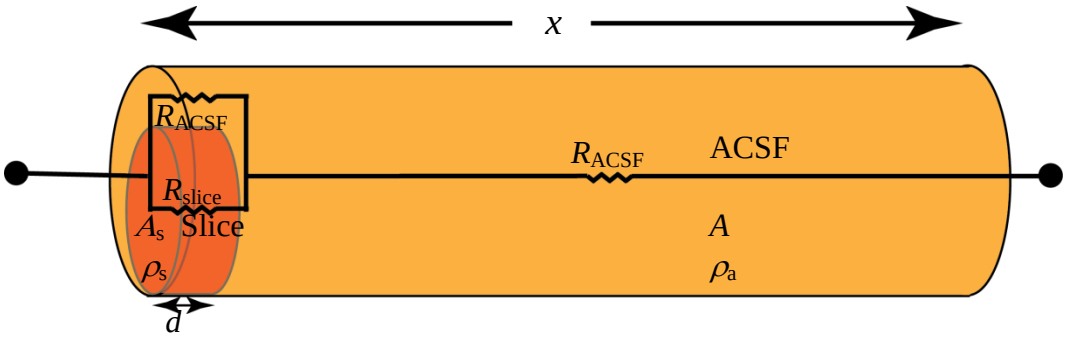

Figure 6-2: A Syringe V3 of cross-sectional area A, length x containing ACSF and brain slice of thickness d and cross-sectional surface area A_s

An equation was derived to calculate the conductivity of brain slice by considering ACSF and brain slice as resistors connected in series and parallel (Figure 6-2). If we know electrode area A, the brain slice area A_s, the ACSF resistivity ρ_a, electrode separation x and slice thickness d, we can calculate the resistance between electrodes as a combination of parallel resistances of ACSF and slice connected in series with resistance of ACSF as shown in :

$$R = R_{\text{slice and ACSF}} + R_{\text{ACSF}} \tag{6-1}$$

$$= \frac{1}{\frac{1}{\left(\frac{d\rho_s}{A_s}\right)} + \frac{1}{\left(\frac{d\rho_a}{A - A_s}\right)}} + \frac{\rho_a(x-d)}{A} \tag{6-2}$$

$$= \frac{1}{\frac{A_s}{d\rho_s} + \frac{A - A_s}{d\rho_a}} + \frac{\rho_a(x-d)}{A} \tag{6-3}$$

I will apply Equation (6-3) first to ACSF only (i.e., no brain tissue present). In this case, d = 0 and Equation (6-3) simplifies to

$$R = \frac{\rho_a\, x}{A} \tag{6-4}$$

With a slice of tissue present, Equation (6-3) can be rearranged as:

$$\frac{RA}{\rho_a} = d\left(\frac{1}{\frac{A_s}{A}\left(\frac{\rho_a}{\rho_s} - 1\right) + 1} - 1\right) + x \tag{6-5}$$

Alternatively, in terms of conductance $G = \frac{1}{R}$, conductivity of ACSF $\sigma_a = \frac{1}{\rho_a}$ and conductivity of slice $\sigma_s = \frac{1}{\rho_s}$, Equation (6-5) becomes:

$$\frac{\sigma_a A}{G} = d\left(\frac{1}{\frac{A_s}{A}\left(\frac{\sigma_s}{\sigma_a}-1\right)+1}-1\right)+x \qquad (6\text{-}6)$$

Equation (6-5) indicates that a plot of $\frac{RA}{\rho_a}$ against x should have gradient one and y-intercept of $\left(\frac{1}{\frac{A_S}{A}\left(\frac{\rho_a}{\rho_S}-1\right)+1}-1\right)$. This means that the y-intercept can be used to find σ_s.

6.3 Validation of Syringe V3 by Measuring the Conductivity of ACSF

Measurement of electric conductivity of ACSF only (i.e., no tissue present) was repeated using different electrode separations four times. I did this experiment to demonstrate that the Syringe system works. The distance between the electrodes (x) was measured using a digital calliper (Digmatic-Mitutoyo Corporation, Model CD-6"); resistance was measured using the *LCR* meter (Agilent E4980A) at frequency of 10 kHz (Figure 6-3); and the ACSF conductivity σ_a calculated from $\sigma_a = \frac{x}{RA}$ where x is the electrode separation, R is the measured ACSF resistance and A is the electrode area. The resistance was measured at different electrode separations, and the average with standard uncertainty bars are shown in Figure 6-4.

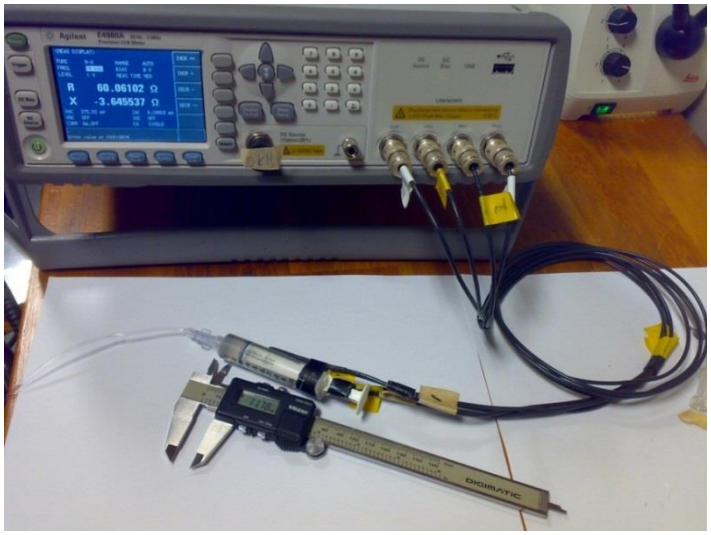

Figure 6-3: The Syringe (V3), digital calliper (Digmatic-Mitutoyo Corporation, Model CD-6") and LCR meter (Agilent E4980A)

Figure 6-4 suggests that the calculated conductivity at distances 13 to 40 mm is stable while it is unstable from 0 to 13 mm. There is likely to be a systematic uncertainty or error present at zero to 13 mm because each of the four measurements that contribute to Figure 6-4 behaves similarly. The behaviour could possibly be calibrated but random fluctuations add to the sources of uncertainty.

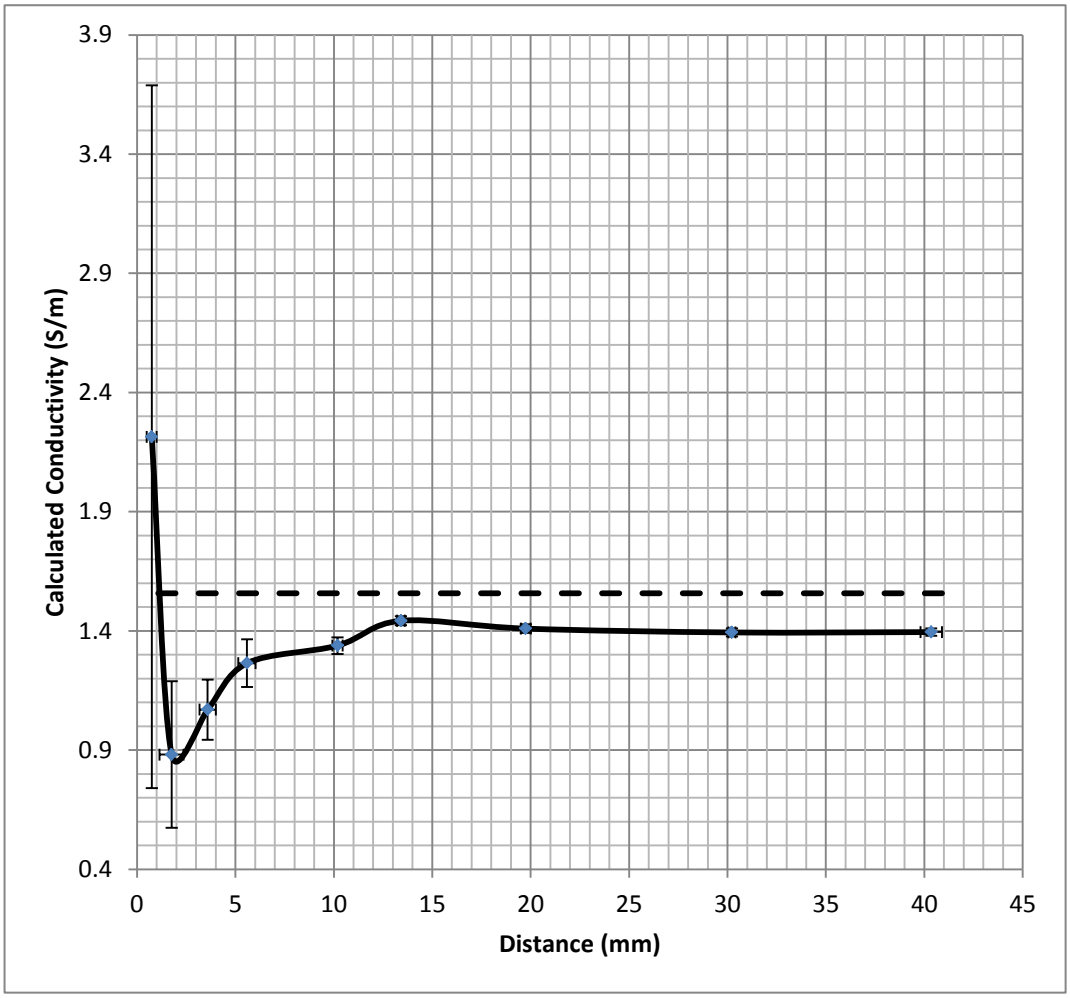

Figure 6-4: Using Syringe (V3), Solid line shows the average of the measured conductivity with electrode separation. Standard uncertainties are shown for each individual point by error bars. Dashed line shows the expected value as measured by conductivity meter (RE388Tx, EDT direct ion, Dover UK)

The conductivity measurement fluctuates by no more than 1% (1.410 ± 0.011 S/m) when the separation is between 13 to 40 mm. However, the measured conductivity fluctuates between 0.9 and 2.2 S/m over separations from 1 to 13 mm. That error may arise from the electrodes, where they may not be 100% flat and parallel. To minimize that error, the

minimum usable separation between the electrodes should be 13 mm. At separations more than 13 mm, the difference between the expected value (1.558± 0.008 S/m) and average measured value (1.410 ± 0.011 S/m) is 9%. So this method may be reformed (next section) to measure the brain electrical conductivity.

6.4 Measuring the Conductivity of Brain Slice

Resistivity of ACSF only was measured with the conductivity meter (RE388Tx, EDT direct ion, Dover UK). Then the resistance *R* of ACSF was measured against the distance (*x*) between the electrodes. The distance between the electrodes was measured using a digital calliper and the resistance was measured using the *LCR* meter (Agilent E4980A) at 10 kHz as shown in Figure 6-3.

A brain slice was then inserted into the Syringe V3 as in Figure 6-2, and the procedures for ACSF repeated. A graph of $\frac{RA}{\rho_a}$ against electrode separation *x* was generated. Equation (6-5) predicts that the *y*-intercept should equal $d\left[\frac{1}{\frac{A_s}{A}\left(\frac{\rho_a}{\rho_s}-1\right)+1}-1\right]$, but because the *y*-intercept in the reference (ACSF only) was not equal to zero, the difference between the two intercepts is considered. By knowing *A*, A_s, *d*, ρ_a, and the *y*-intercept, ρ_s could be calculated.

6.5 Results

The resistance (*R*) of ACSF was measured at different electrode separations (*x*). The quantity $\frac{RA}{\rho_a}$ was plotted on the *y*-axis as in Figure 6-5.

The graph for ACSF only should be a straight line of unity slope passing through the origin with gradient equal to one. Linear regression gives a gradient of 0.9921±0.0004, which is small difference from the theory. However, statistically it is highly different. In addition to the graph shows a systematic offset error, as the *y*-intercept equals (0.4 ± 0.1) mm.

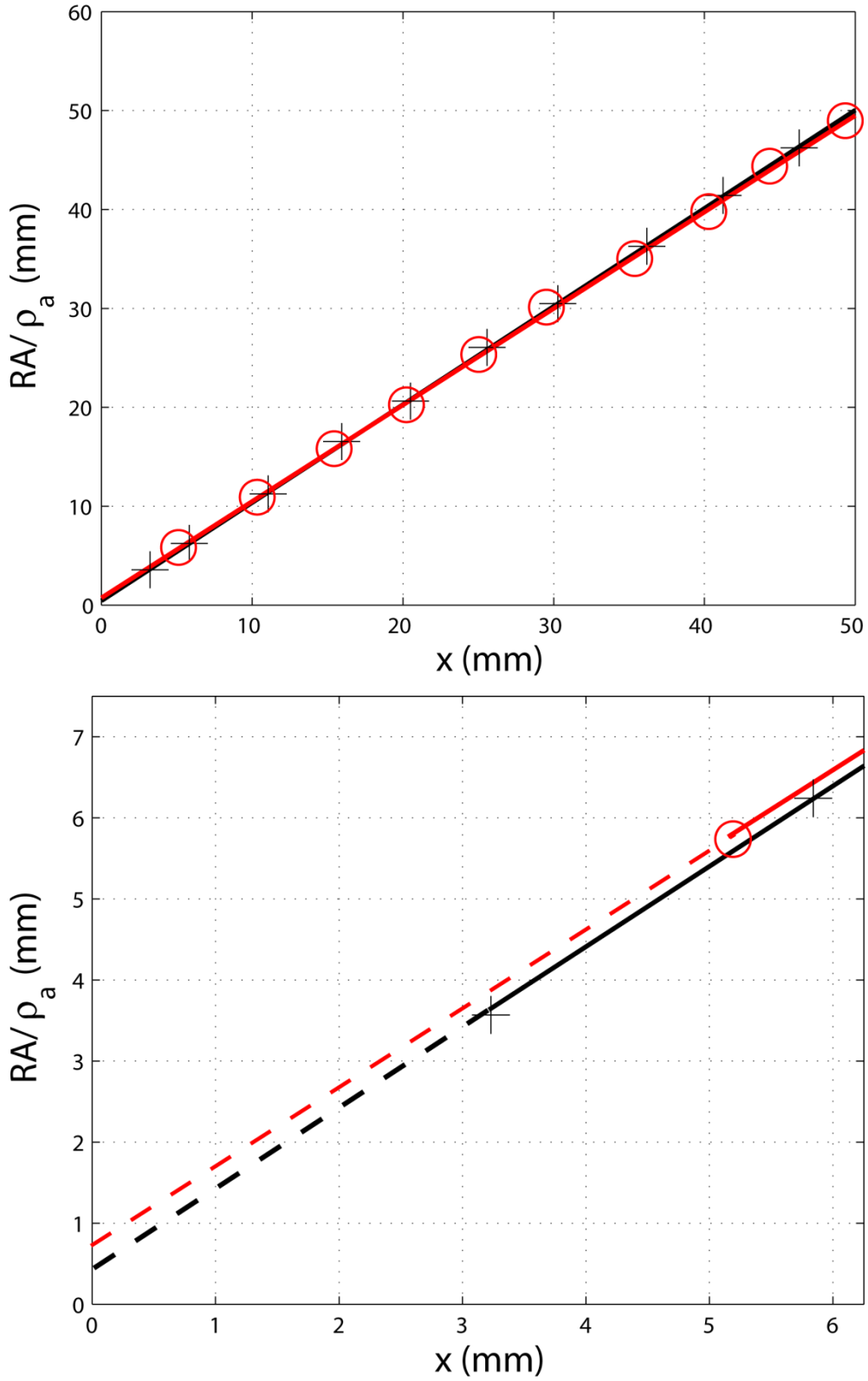

Figure 6-5: Syringe measurement of resistance versus different electrode separation for ACSF only (+) and ACSF with a slice (○). (a) The two lines look identical visually. (b) Zoom in to show the y-axis intercept.

The plot for a brain slice with ACSF gives a *y*-intercept of (0.74 ± 0.26) mm. Subtracting the *y*-intercept for ACSF only, we get (0.34 ± 0.28) mm. This difference in intercepts is now mapped to a conductivity value. MATLAB was used and Equation (6-5) to generate a graph (Figure 6-6) to show the conductivity of the brain slice ρ_s against *y*-intercept.

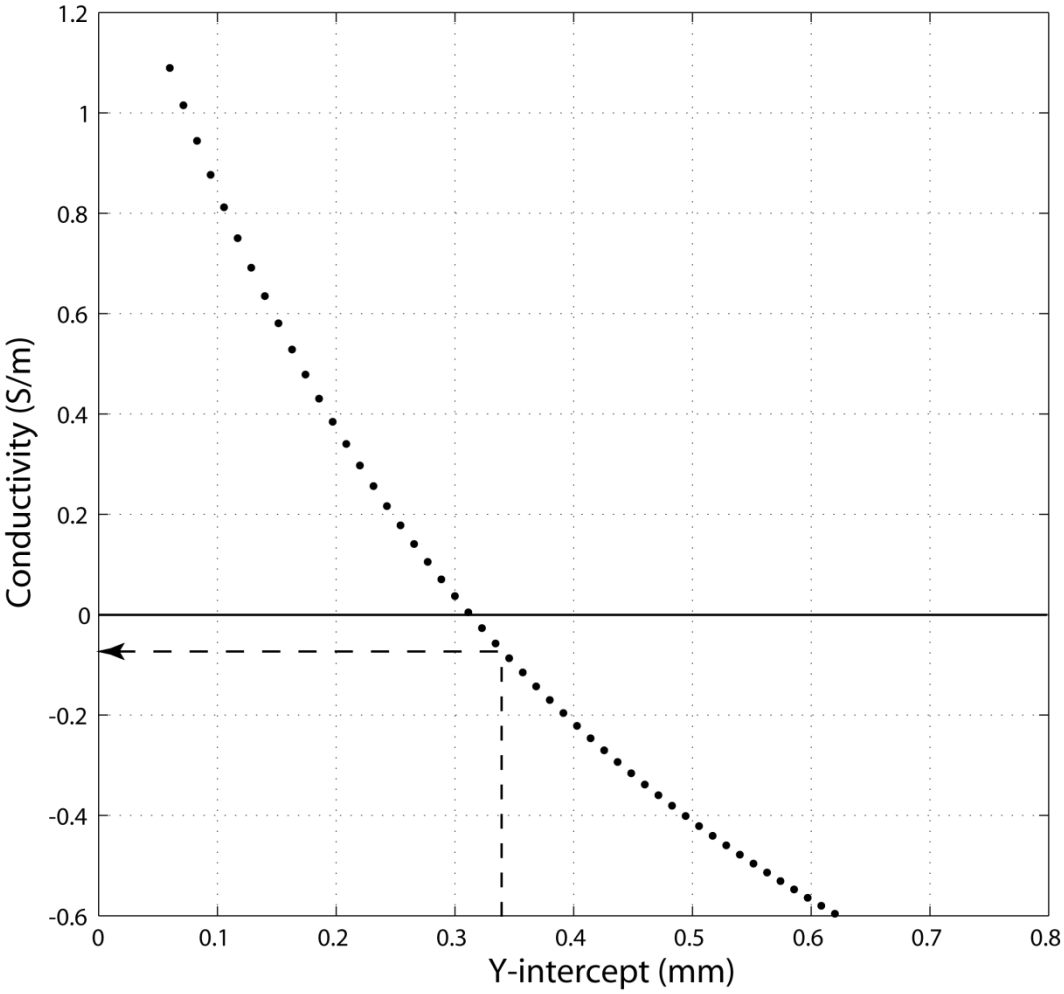

Figure 6-6: MATLAB graph to show the conductivity of the brain slice against y-intercept uncertainty range. Negative conductivity value produced at y*-intercept 0.34 mm is unphysical*

Figure 6-6 shows that the conductivity is extremely sensitive to small changes in *y*-intercept. This solution is ill-conditioned: a small uncertainty in the *y*-intercept causes a much larger uncertainty in the results. This method can produce negative conductivity values which are unphysical and unacceptable and provides another reason to reject this method.

One of the challenges with the one-dimensional measurements by a V3 Syringe is the uncertainty in the distance between the electrodes. As noted

from Figure 6-6, this has a large influence on calculated conductivity. Another difficulty arises from the air bubbles that form inside the syringe. It is important to remove these, as their effect increases as the separation between the electrodes decreases because of the relative volume of bubble to fluid increases. These are removed by adding more air and rotating the syringe 360 degrees in the three dimensions. This forms a large air bubble which is made by trapping all the small ones together; the large air bubble is then released.

From the above results I could summarize that the conductivity measurement fluctuates within uncertainty from −0.6 S/m to 1.1 S/m, which means many parameters need to be optimized to reduce its uncertainty range. These parameters are: electrode area A, brain slice area A_s and electrode separation x.

From Figure 6-6, it is clear that within experimental uncertainty the maximum value of brain slice conductivity is 1.1 S/m and the minimum value is −0.6 S/m. I am not accepting −0.6 S/m as it is impossible. That huge range led me to think about optimizing the syringe V3 method. Therefore the effect of the capacitance at the interface between the electrodes and the ACSF was studied in the next section.

6.6 Capacitance Effect of the Electrodes

The electrode-ACSF interface has capacitance and thus a reactance effect on the measurements. This effect depends on the frequency at which the measurements are taken. So frequencies from 100 Hz to 12 kHz were applied at 6 mm electrode separation to find the best frequency at which to measure the conductivity.

The test signal comes from a sinewave generator (Protek B8012) via a power amplifier II (Pasco scientific CI-6552) then to the electrode-ACSF syringe interface placed in series with a resistor. The output was monitored using Scientific Workshop 750 software. The circuit in Figure 6-7 was connected, the syringe V3 was used and the voltages across a resistor and ACSF were

recorded simultaneously, then the phase difference φ between the voltage waveforms across the resistor and the ACSF was calculated (Figure 6-8).

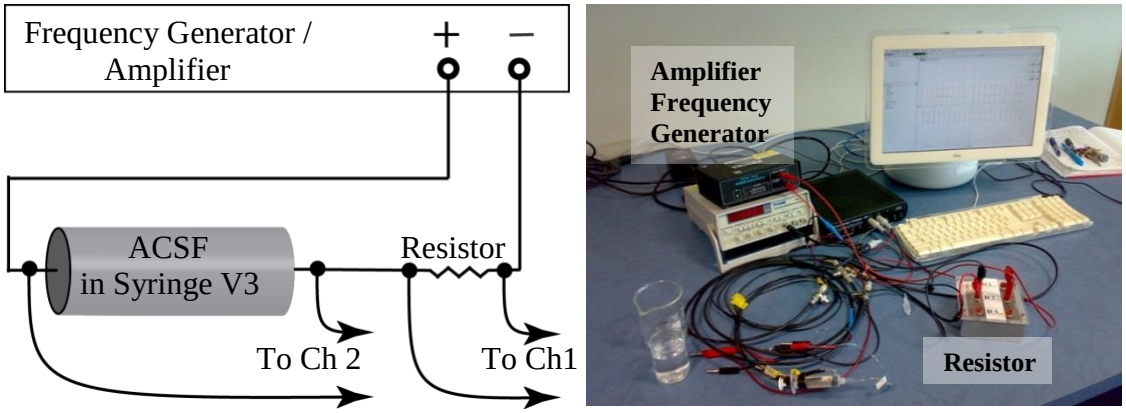

Figure 6-7: A function generator (Protek B8012), power amplifier II (Pasco scientific CI-6552), the syringe V3, ACSF and computer

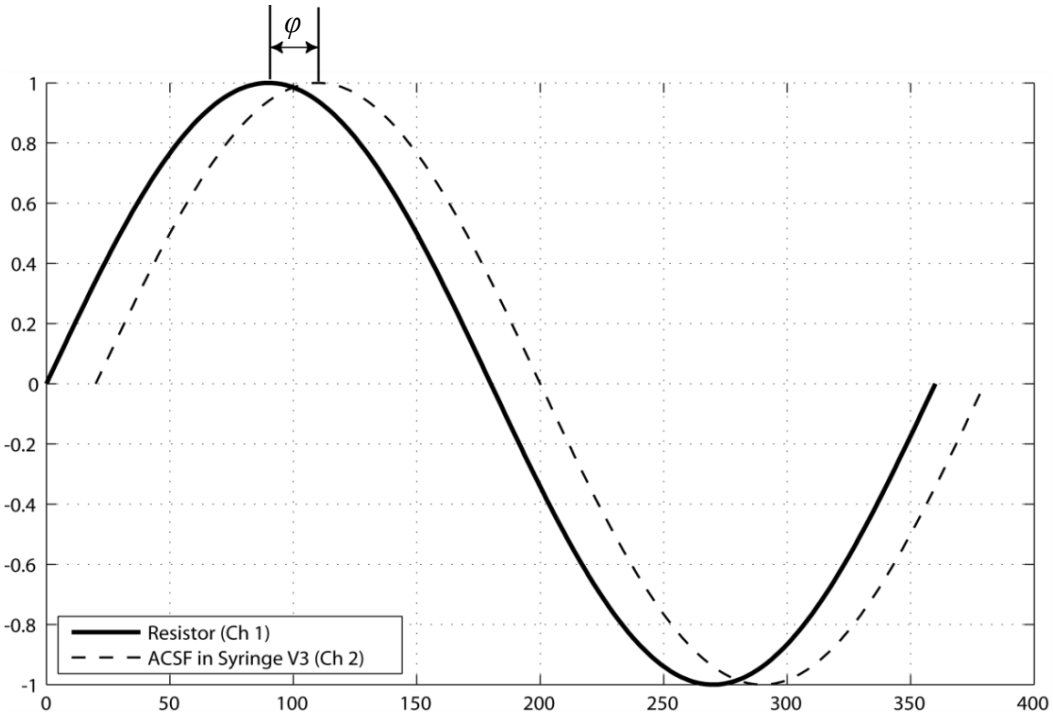

Figure 6-8: Phase difference φ between the voltage waveforms across the resistor and the ACSF was calculated

The results shows that the phase difference decreases as the frequency increases and it is zero from about 8 kHz upward which means the resistance of the solution becomes dominant. This suggests that at 10 kHz, capacitance effects are not a major problem with the setup.

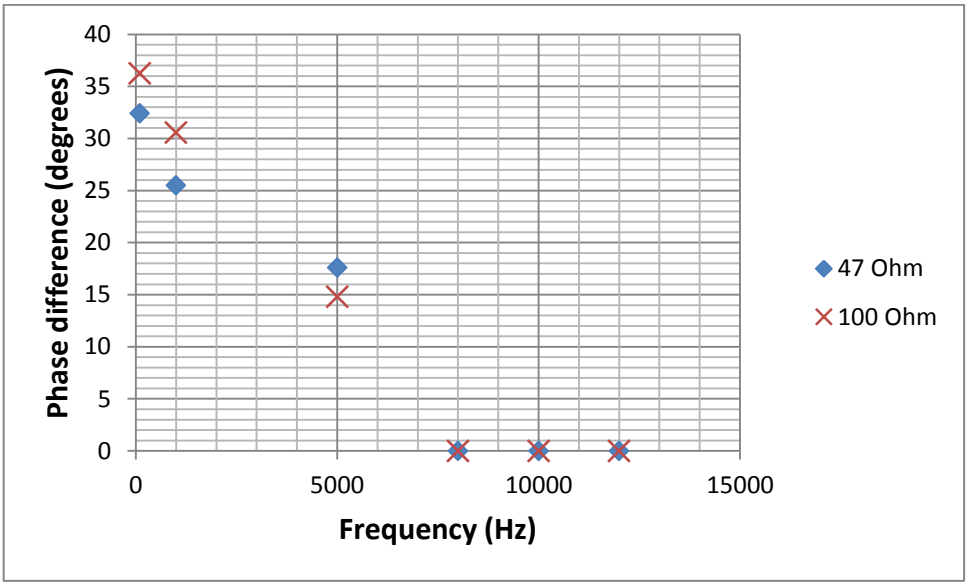

Figure 6-9: The relation between the phase difference and the frequency (Hz) in ACSF solution for two resistors using the Syringe V3

6.7 Optimizing the One-Dimensional Method Using Two-piston Tube V4

I designed and built V4 to avoid the high measurement uncertainties of the V3 design. Figure 6-10 shows the two-piston tube V4. The key feature of the tube is that the electrodes are designed to cut a circular segment of slice tissue in a manner similar to that of a hole punch.

6.7.1 The Advantages of the V4 System

1. The brain slice area will be exactly that of the surface area of the electrodes because the electrode is used as a cutter.
2. Silver paste electrodes may be more reliable than stainless steel electrodes for measurements in solutions as explained in Section 3.2.
3. Measurement of electrode surface area will be much more accurate because it matches the cross section area of the inner glass tube.
4. The random and systematic error in the electrode separation will be minimized. I used the tube as in Figure 6-10. I made the two electrodes touch each other and reset the digital calliper to read zero at this point.

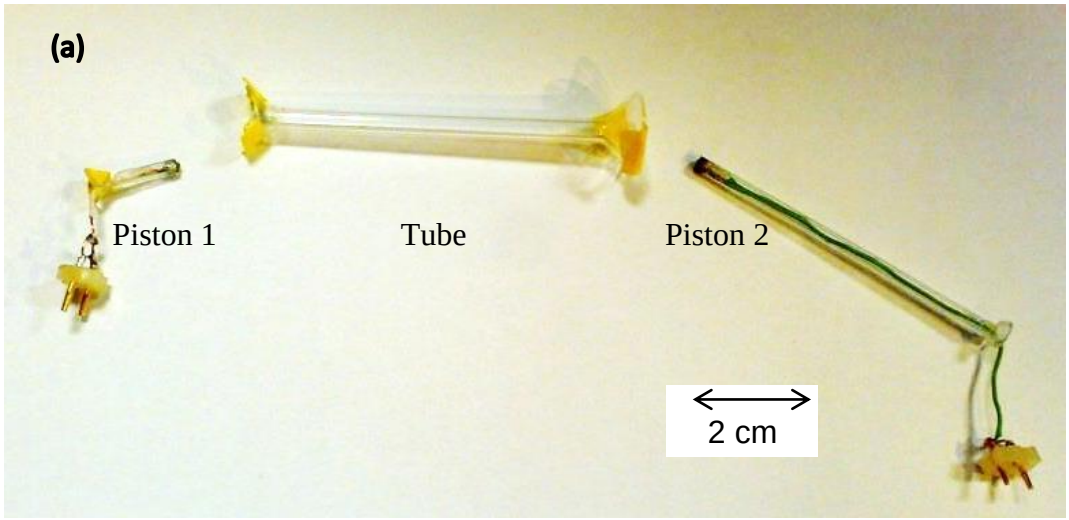

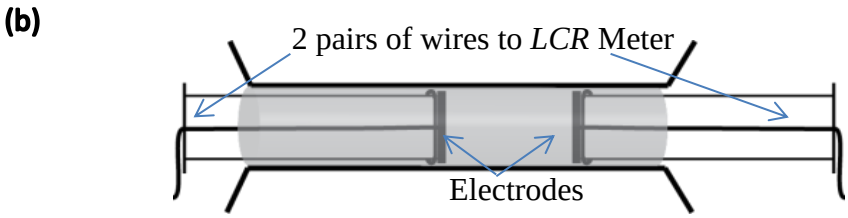

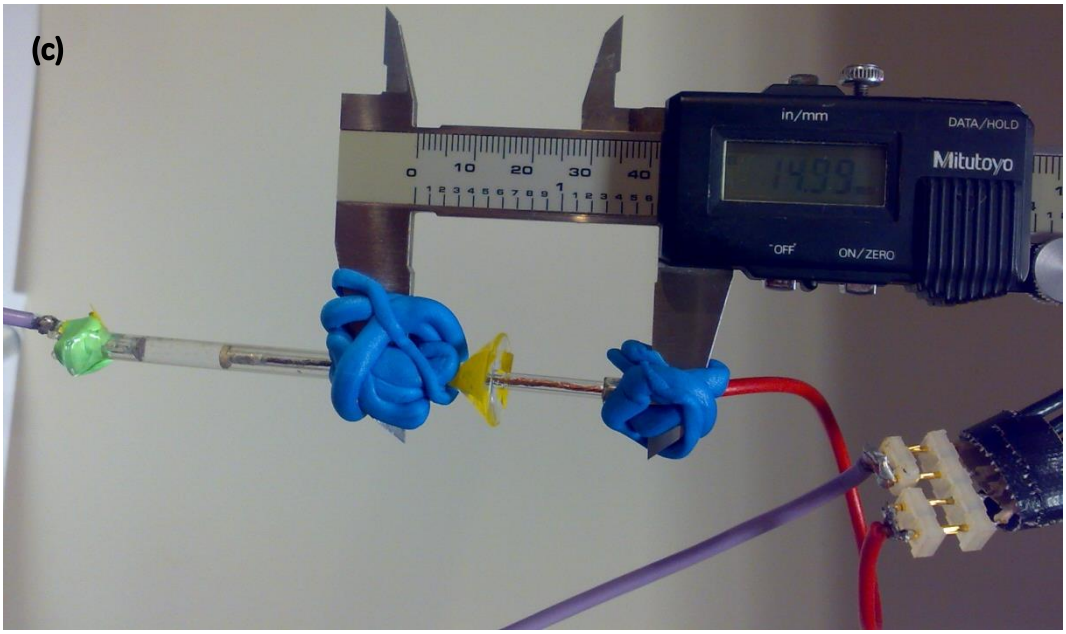

Figure 6-10: Two-piston tube V4. (a) made of three glass pieces, two pistons and tube. (b) schematic diagram. (c) Calliper used to measure the distance. The bond between the calliper and the tube V4 (Blu-Tack) is more secure than it looks

6.7.2 Design

The outer diameter of the inner glass tube was 3 mm, which was equal to the inner diameter of the outer tube. The effective length of the glass piston was about 5 cm. The inner glass tube was wired from end to tip (the green wire in the right tube in Figure 6-10a). The tip was coated with about one millimetre layer of conducting material which consists of silver, acrylic resin, solvents including acetone and 4-chlorobenzinotrifluoride. This layer was applied using a commercially available Circuit Writer pen. The conducting surface was then sanded by a polishing film of thickness 15 µm (AFW Technologies) to ensure a smooth and flat electrode surface.

6.7.3 Method

After preparing the slices as described in Section 5.3, circular pieces of tissue equal in diameter to that of the electrode were punched out using the electrode itself in an action similar to that of a hole puncher. Then measurements were done using Equation (6-5). The same steps as in Section 6.1 were followed, but there were many complications and limitations, such as the brain slice folding inside the tube, and leakage of ACSF from the tube. This method therefore did not give the results that had been hoped for. So, I moved to the final methodology described in the next chapter.

6.8 Chapter Summary

Two unsuccessful one-dimensional attempts to perform conductivity measurements of a live brain slice while it is bathed in ACSF were illustrated. The main reasons for failing are uncertainties in electrode separation measurements and surface area of the slice. Also presence of ACSF was a challenge because a special set up is needed to prevent leakage but to allow ACSF to enter and leave the Syringe when distance changes. Also ACSF has higher conductivity than that of the tissue.

7 Successful Methodology for Conductivity Measurements in One Dimension

I started this one-dimensional work with Syringe V3 as described in Chapter 6. In this chapter I describe the design, construction and implementation of a "slice holder" device for measuring slice conductivity. This device holds the electrodes at a fixed separation distance of 400 µm which is equal to the normal thickness of the brain slices. Construction steps for the slice holder are shown in Figure 7-1. The device consisted of two pieces of acrylic with holes of 10-mm diameter equal to the electrode diameter drilled into them using a Baron-Max milling machine. The electrodes were Ag/AgCl electrodes commercially available for ECG recording, manufactured by Kendall-Ltd (see Figure 7-1 (a,b)). I flattened the active surface of the electrodes by heating them using hot air and pushing them against a non-stick flat metal surface as in Figure 7-1 (d). Then I glued them in position in a prepared acrylic holder as in Figure 7-1(e). The flattened electrode surface area roughly is 8×10^{-5} m^2. Figure 7-2 shows the two electrodes with 400-µm thick material between them.

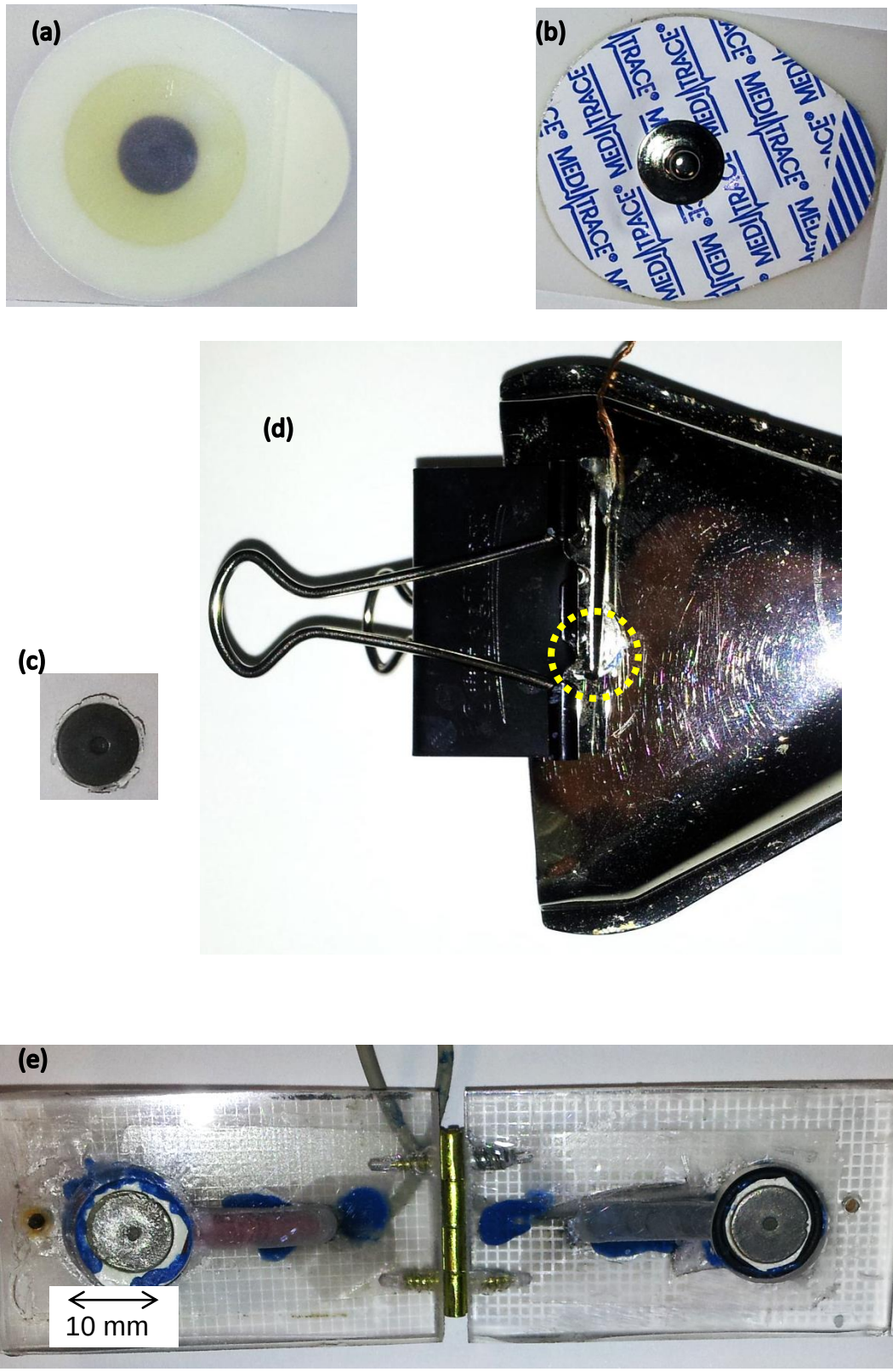

Figure 7-1: Slice holder construction. (a,b) Ag/AgCl electrodes. (c) Electrodes after removing gel and stickers. (d) Flattening the electrode by pressing it on hot surface. Dotted circle shows the location of the electrode (e) Completed slice holder

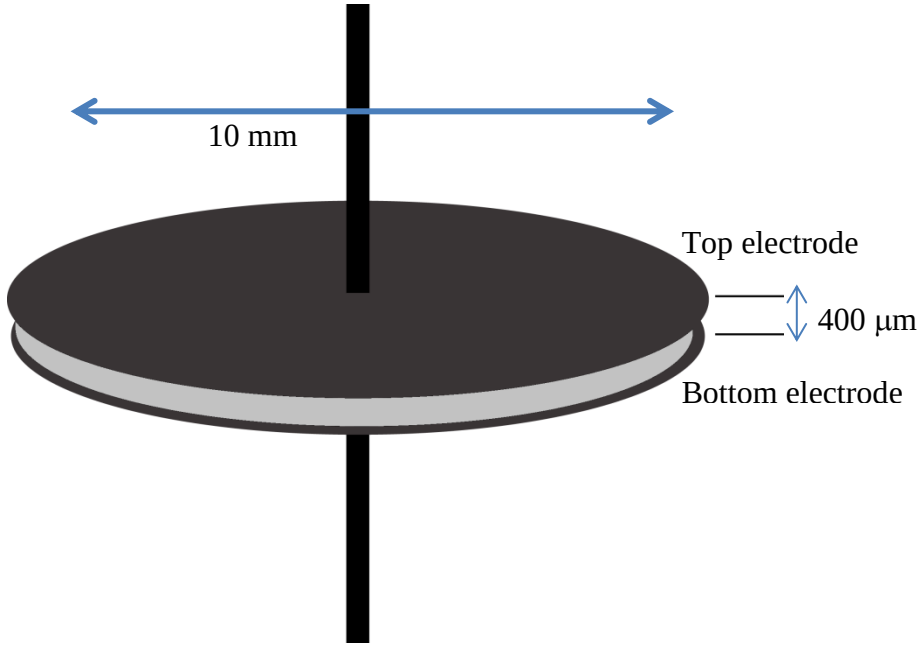

Figure 7-2: Schematic digram illistrates the two electrodes sperated by 400 µm gap to house the tissue slice

7.1 Comparison of One-Dimensional method with van der Pauw Method

Advantages:

1. The slice is placed between the electrodes, so less surface area of slice is exposed to air; this minimizes evaporation from and drying of the slice.
2. Measurements can be repeated many times.
3. Conductivity changes with time can be studied continuously.
4. Measurements can be made over a range of frequencies. This advantage is used in Chapter 8.
5. Current density is much smaller for one-dimensional electrodes, because the electrodes have a bigger surface area than the wire electrodes of the two-dimensional method. This means that less heat is transferred to the sample and therefore less damage is done. Brown *et al*. (1999) reported that the main biological effects of the current on tissue are electrolysis, neural stimulation and heating. The relative effect of these damages does not change with the current but it changes with the current density.

Disadvantage: The major disadvantage is that I cannot see the slice under examination, and the slice is destroyed after measurements because the tissue often sticks to the electrodes causing tearing as the slice holder is opened.

7.2 Cortical Slice Preparation

Mouse brain slices of thickness 400 μm were sliced in the coronal plane. Half of the slices were bathed in normal ACSF and the other half in magnesium-free ACSF. Full details of cortical slice preparation were given in Section 5.3.

7.3 Method

The equipment was connected as seen in Figure 7-3. Each slice was cut into segments as in Figure 7-4. A photo was taken, under the microscope, and imported into NIS-Elements BR which is a standard research application software for analysis of microscope photos. It was used to measure the segment area automatically. After measuring the segment area, the segment was removed from its ACSF solution and placed on one of the slice holder electrodes. I removed the ACSF by blotting with filter paper just before closing the slice holder. Then I opened it again and removed any residual solution. Then I closed the slice holder and applied the same pressure for all samples by using a bulldog clip. Finally I ran the MATLAB code (Appendix B-3) which calculates the conductivity from $\sigma = \frac{d}{RA}$ where d is the thickness, R is its resistance at 10 kHz and A is the segment area. The MATLAB code records the conductivity directly to an Excel file.

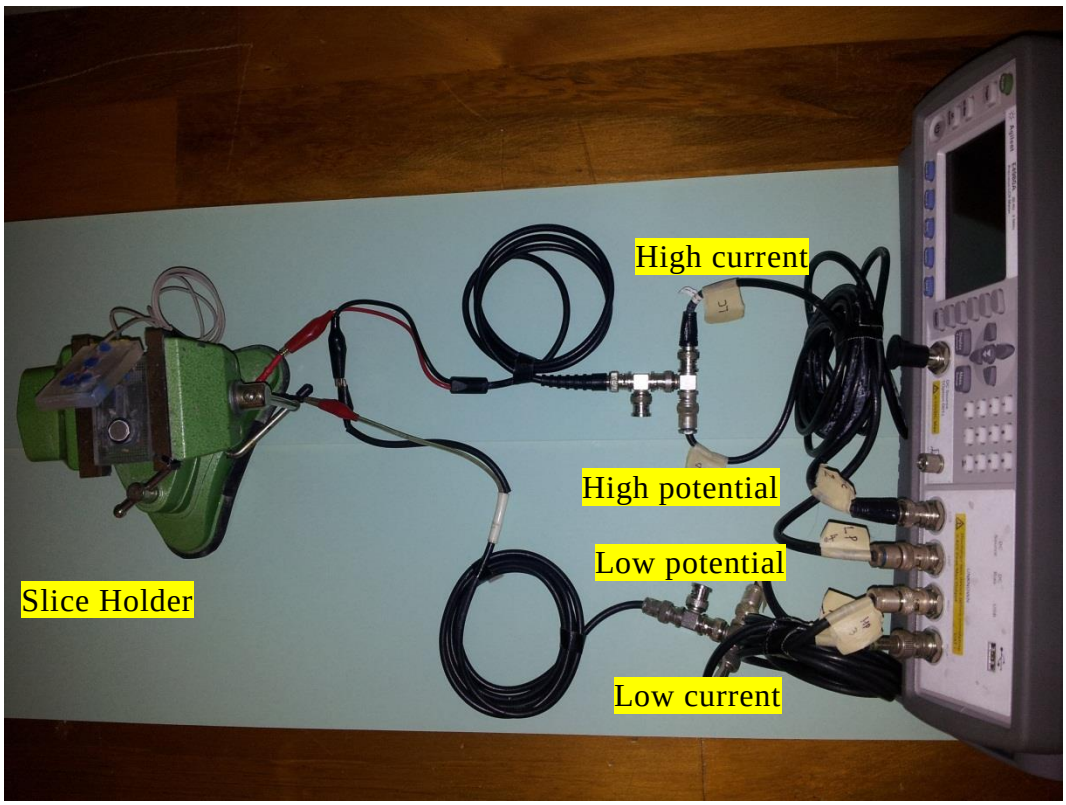

Figure 7-3: One-dimensional setup using slice holder

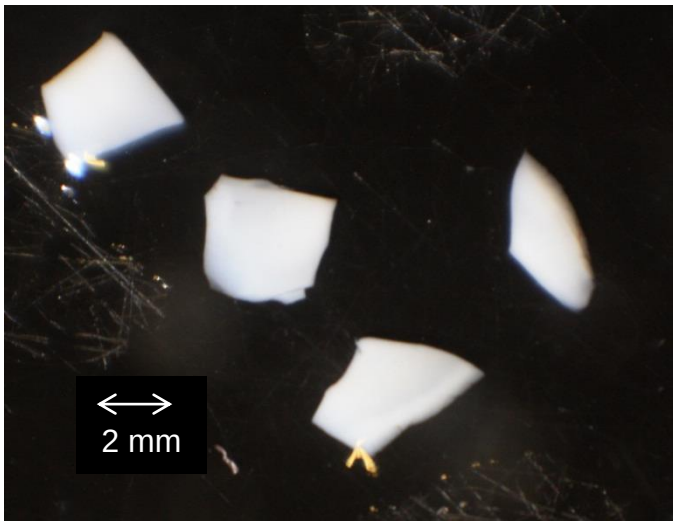

Figure 7-4: Slice segments

7.4 Effect of Source Voltage Level on Measured Impedance

Impedance of samples of air, tissue, and ACSF were measured at different voltage levels with the 1D method. From Figure 7-5 it is clear that the impedance is independent on the source voltage level over the range 1 mV to 2 V. The tissue impedance was about 0.02% of air impedance. This

experiment was done to investigate the effect of current on sample properties. My results show that brain tissue conductivity is not affected by current movement due to potential difference up to 2 V. Figure 7-5 shows stability of impedance; this provide evidence that in 1D measurements the sample impedance was dominant not the interface between the electrode and the sample.

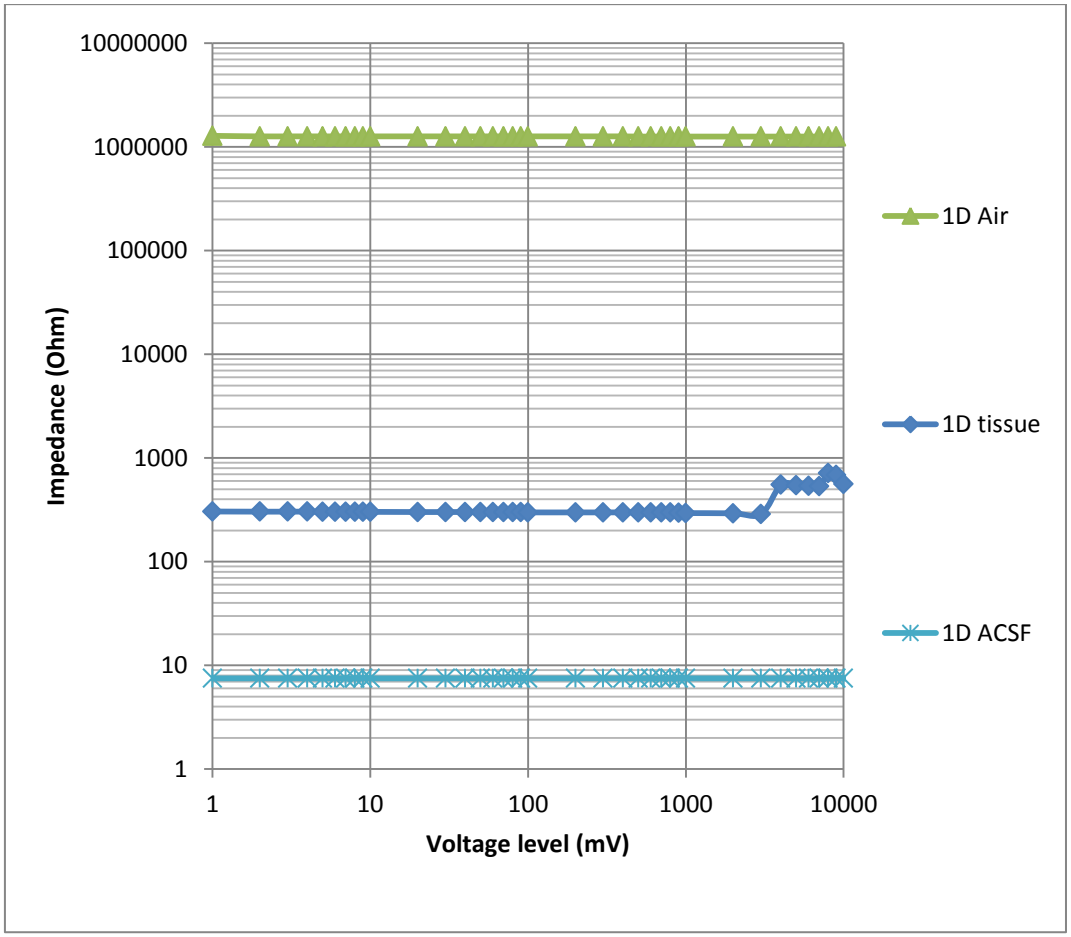

Figure 7-5: Impedance of samples were measured at different source voltage levels in 1D method at 10 kHz

Measured impedance of air is 1.3×10^6 Ω. In contrast, according to dimensions of the 'slice holder', the predicted impedance using the formula $Z_{10kHz} = 1/\omega C$ (with C = 1.7 pF) is 9×10^6 Ω. This discrepancy is probably due to imperfect flattening of electrode surface. This imperfection does not affect the conductivity measurements as I put the slice segments only onto well-flattened parts of the electrode surface.

7.5 Results and Discussion for Coronal Slices

I carried out the experiment over three days on the brains extracted from three animals, one brain each day. Slices were cut in the coronal direction. Half of the slices from each animal were placed in no-Mg ACSF, while the other half were placed in normal ACSF. The study results show that the difference in conductivities of the seizing and non-seizing slices is highly significant ($p = 1\times10^{-11}$). A five-point summary boxplot (Figure 7-6), shows the minimum, lower quartile, median, upper quartile and maximum values (stars indicate outliers).

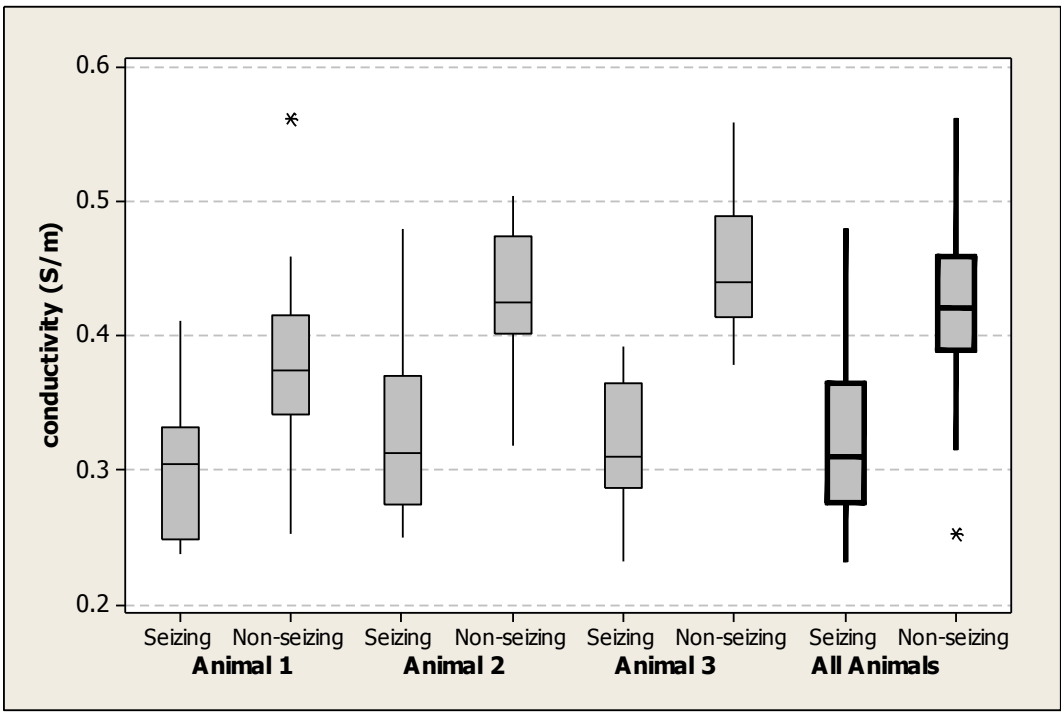

*Figure 7-6: Comparison of conductivity of seizing and non-seizing slices using the one-dimensional method with slicing in the coronal direction. Outliers signified by **

Mean, median and more details are shown in Table 7-1.

Table 7-1: Mean and median conductivities and significance of difference between seizing and non-seizing slices using a Mann-Whitney test (MW-test) including outliers data and a two-sample t-test excluding outliers. Minitab was not able to return the very small P-values of t- and MW-tests. Animals 2 and 3 had no outliers. Standard uncertainty included for the mean

	Seizing σ (S/m)	Non-seizing σ (S/m)	Significance (*p*-value)
Slices from animal 1			
Mean (excluding outliers)	0.303±0.013	0.369±0.014	0.002 (*t*-test)
Median (including outliers)	0.305	0.370	0.0008 (MW-test)
Slices from animal 2			
Mean	0.328±0.014	0.432±0.011	<0.0005 (*t*-test)
Median	0.312	0.425	<0.00005 (MW-test)
Slices from animal 3			
Mean	0.317±0.010	0.449±0.011	<0.0005 (*t*-test)
Median	0.310	0.440	<0.00005 (MW-test)
All animals			
Mean (excluding outliers)	0.317±0.007	0.427±0.008	<0.0005 (t-test)
Median (including outliers)	0.310	0.420	<0.00005 (MW-test)

Figure 7-7, Figure 7-8 and Figure 7-9 show a histogram of conductivities including outliers. In particular, Figure 7-9 shows a comparison between the seizing and non-seizing cases.

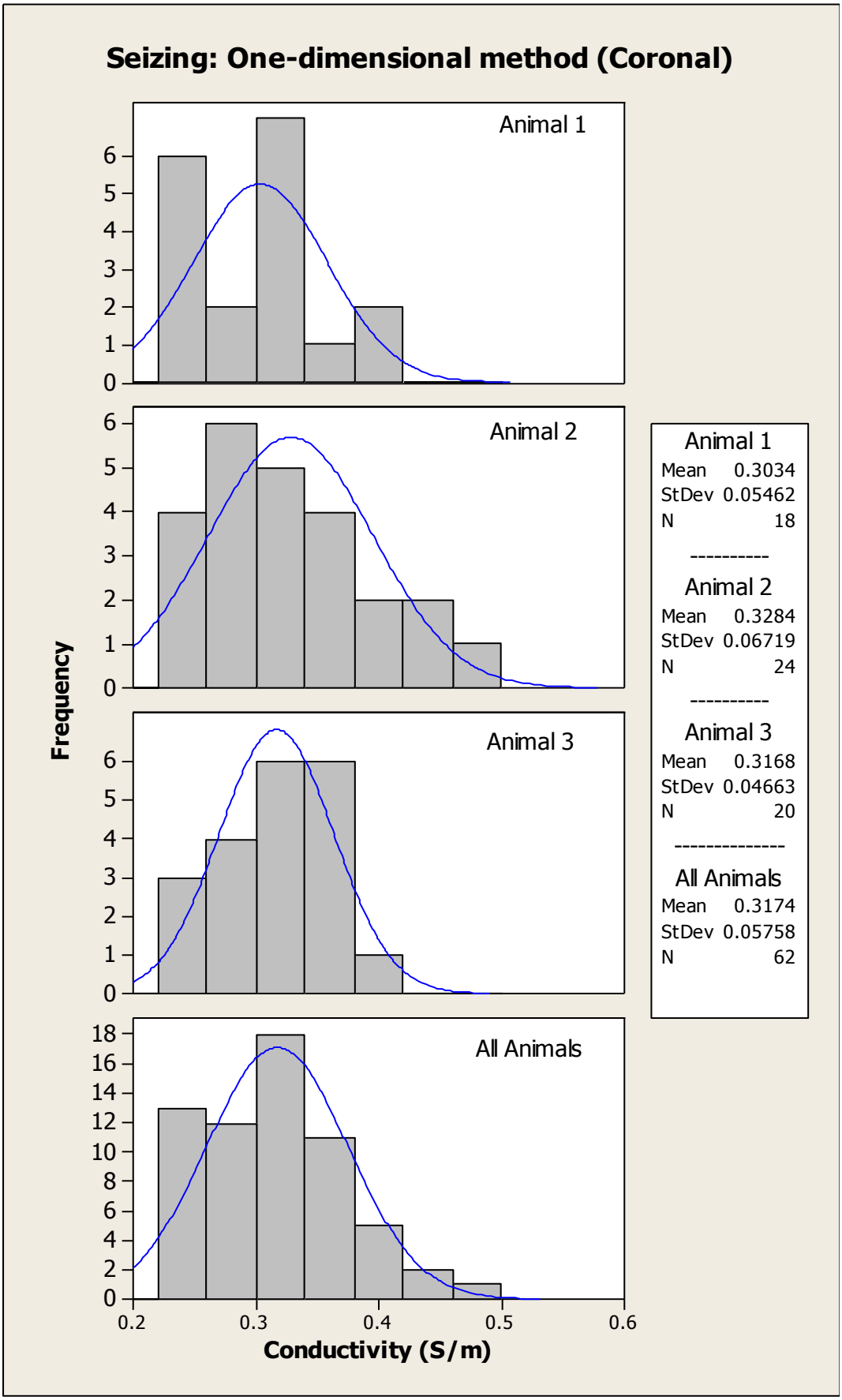

Figure 7-7: Comparison between conductivities of three seizing brains using one-dimensional method in coronal direction. A fitted distribution line shows a normal distribution

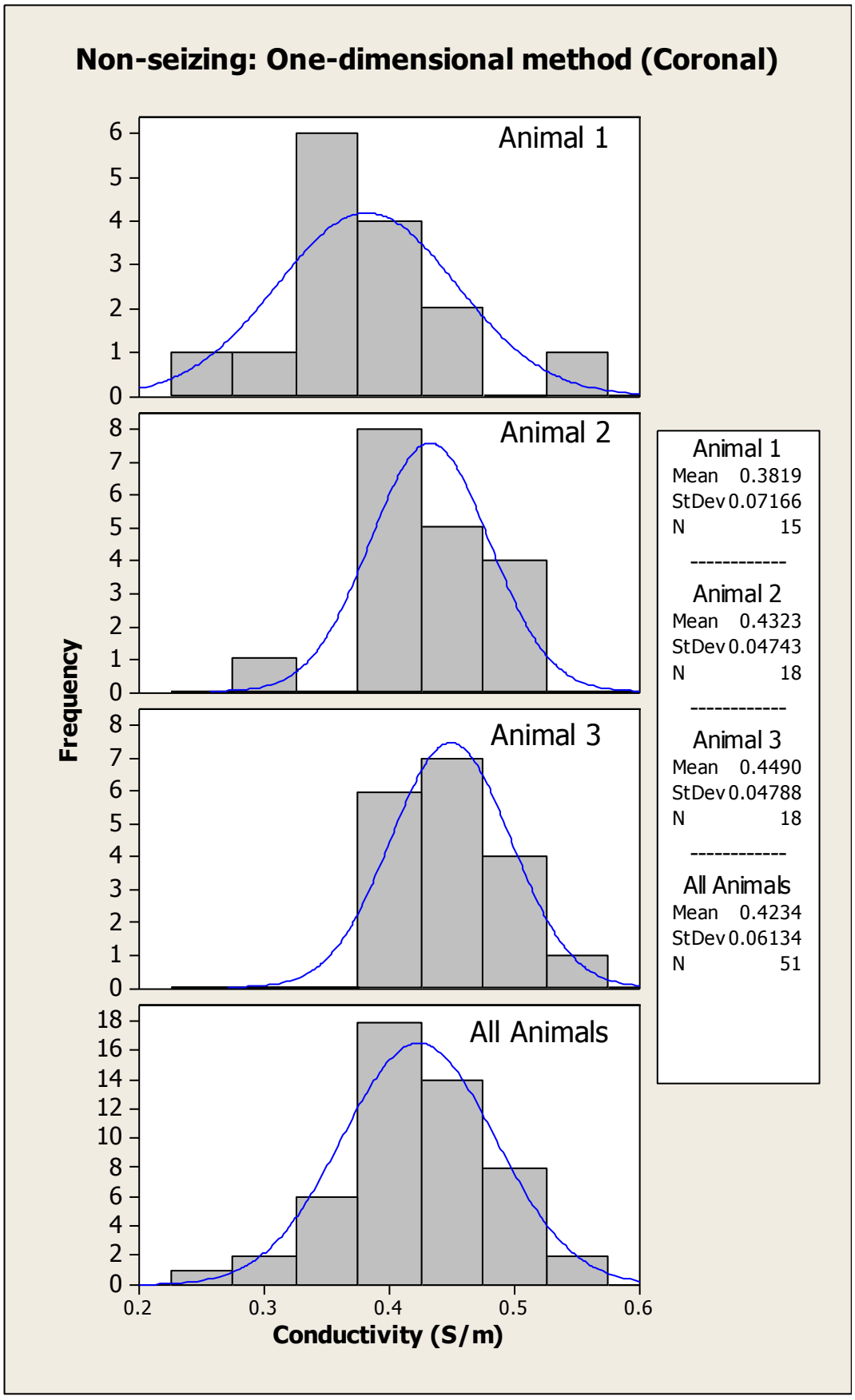

Figure 7-8: Comparison between conductivities of three non-seizing brains using one-dimensional method in coronal direction. A fitted distribution line shows a normal distribution

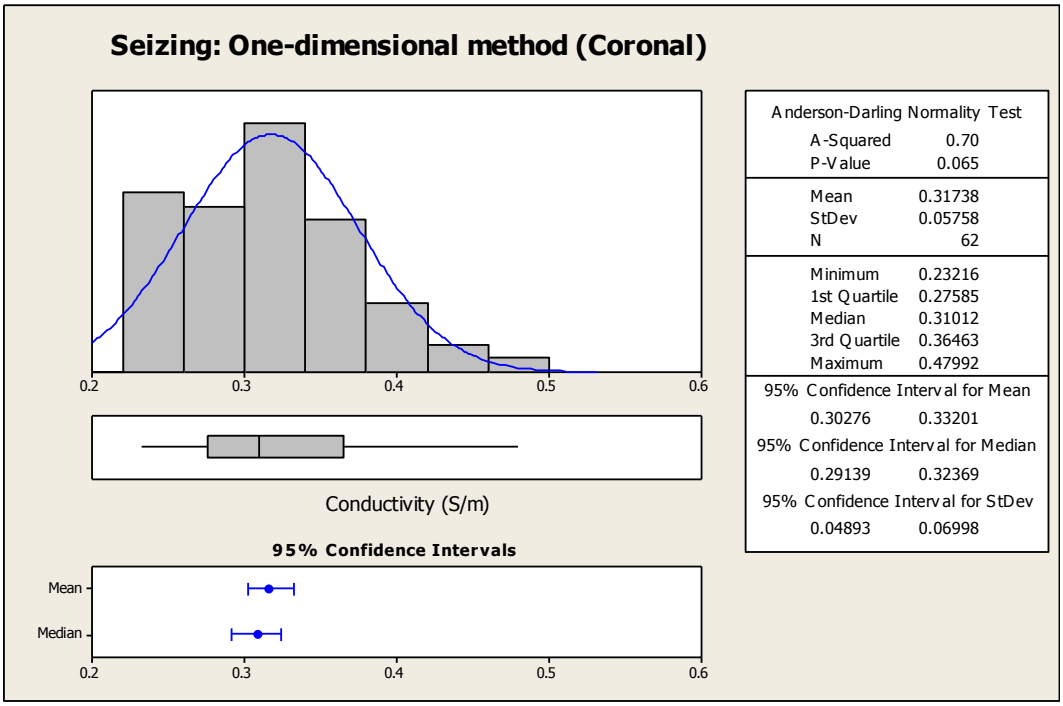

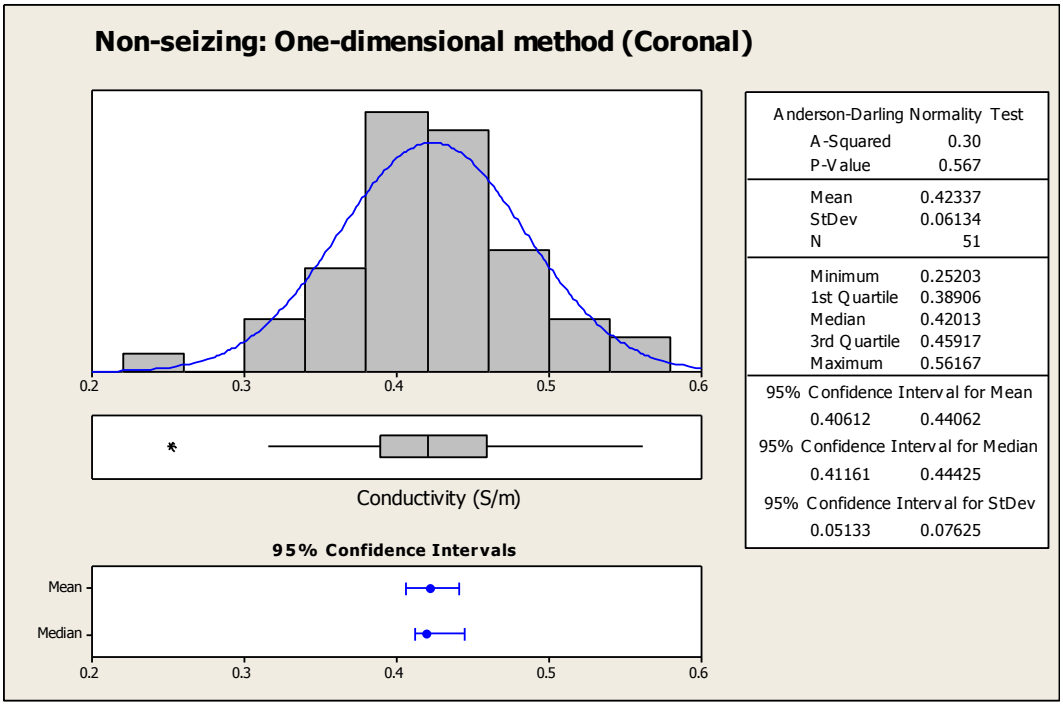

*Figure 7-9: Comparison between conductivities of seizing and non-seizing slices using one-dimensional method in coronal direction. * denotes an outlier. A fitted curve line shows normal distribution*

7.6 Results and Discussion for Transverse Slices

I carried out the transverse-slice experiment over two days on the brains extracted from two animals, one brain each day. Cortical slices were

prepared as described in Section 5.3, but, slices were cut in the transverse (horizontal) rather than coronal plane. I found that it is harder to slice in the transverse direction rather than the coronal direction because the transverse direction is less mechanically stable.

Half of the slices from each animal were placed in magnesium-free ACSF, while the other half were placed in normal ACSF. The results show that there is a highly significant difference ($p = 8\times10^{-7}$) between the conductivities from seizing and non-seizing slices including two outliers. The five-point summary boxplot of Figure 7-10 shows the minimum, lower quartile, median, upper quartile and maximum values (stars are outliers).

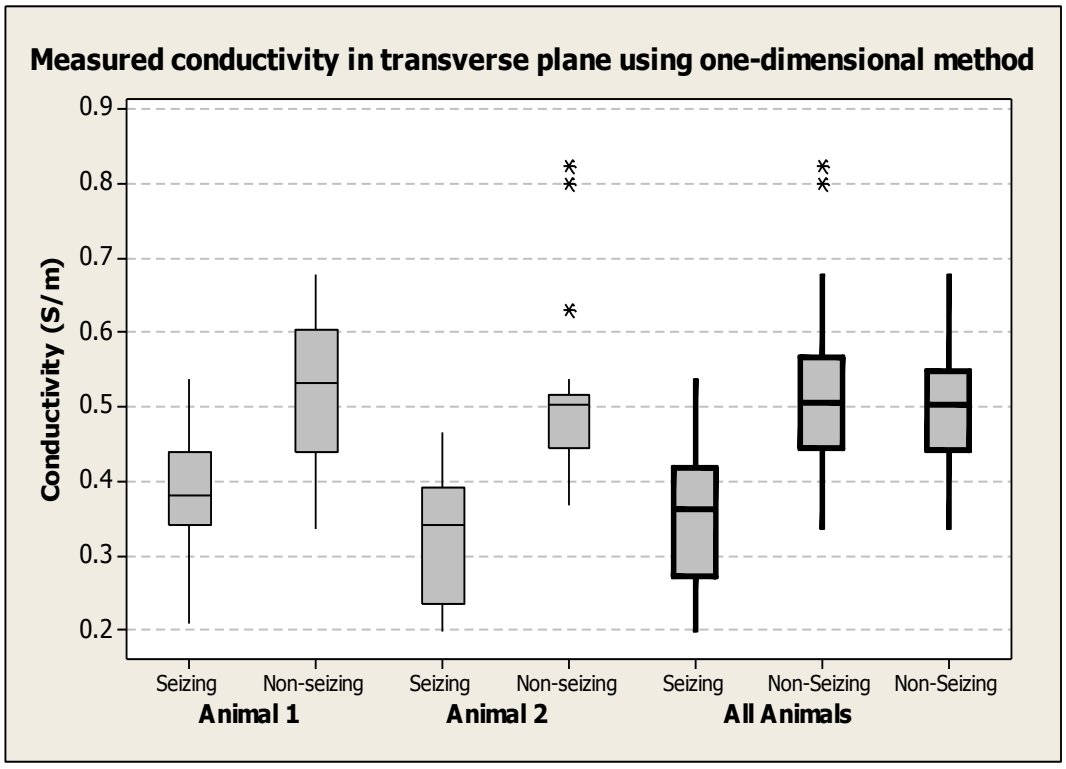

*Figure 7-10: Comparison of conductivity of seizing and normal slices using one-dimensional method in transverse direction. * is outlier. Outliers are excluded in the last boxplot for all animals*

Further details are shown in Table 7-2.

Table 7-2: Mean conductivities and significance of difference between seizing and non-seizing transverse slices using a Mann-Whitney test (MW-test) including outliers and a two-sample t-test excluding outliers. Minitab was not able to return the very small values of P-value for the t- and MW-tests. Standard uncertainty included for the mean

	Seizing σ (S/m)	Non-seizing σ (S/m)	Significance (*P*-value)
Slices from animal 1			
Mean	0.378±0.020	0.521±0.020	<0.0005 (t-test)
Median	0.381	0.532	0.0001 (MW-test)
Slices from animal 2			
Mean (excluding outliers)	0.324±0.021	0.469±0.012	<0.0005 (t-test)
Median (including outliers)	0.341	0.503	<0.00005 (MW-test)
All animals			
Mean (excluding outliers)	0.353±0.015	0.503±0.013	<0.0005 (t-test)
Median (including outliers)	0.362	0.506	<0.00005 (MW-test)

Figures 7-11, 7-12 and 7-13 show the conductivity histograms.

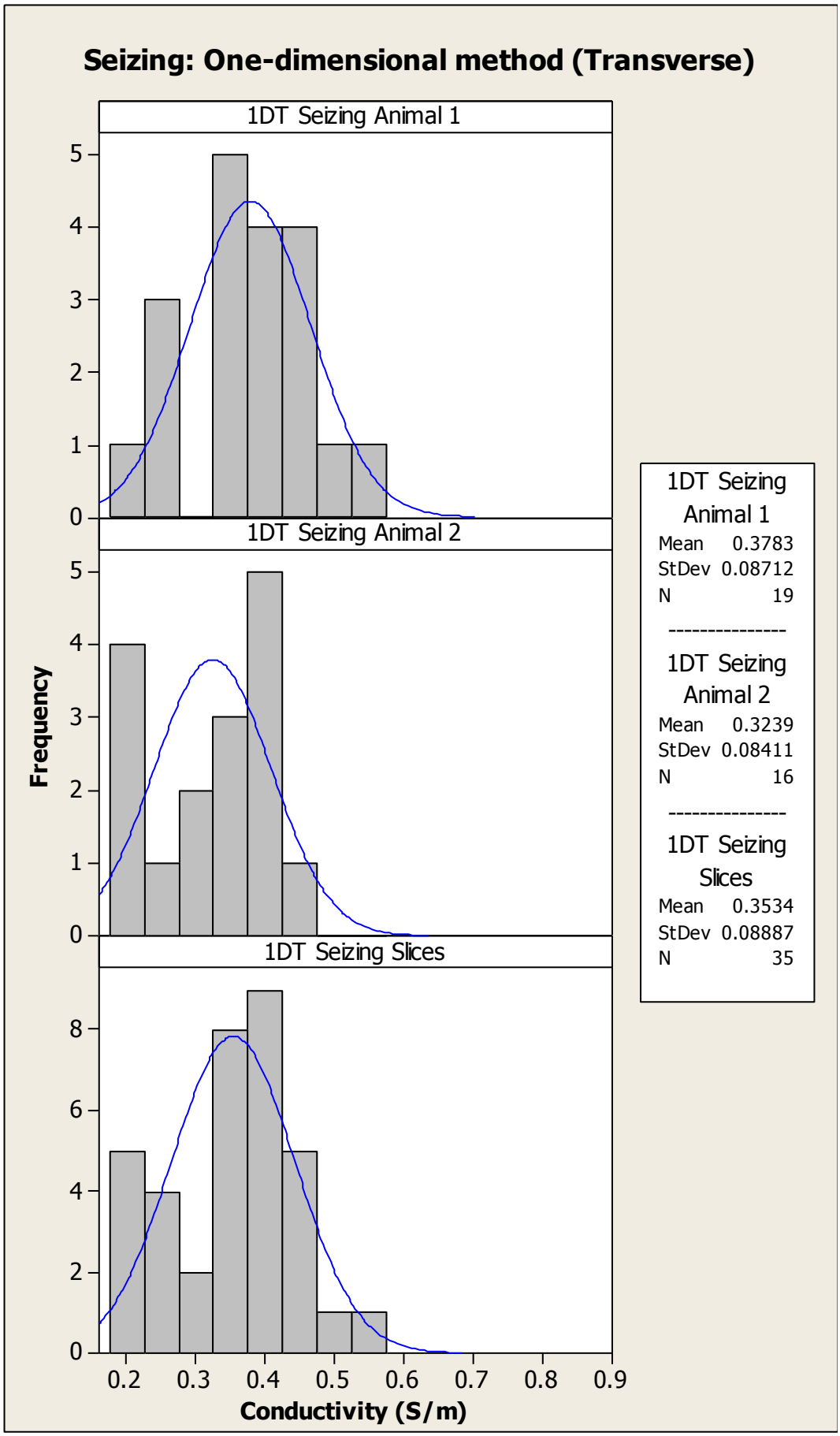

Figure 7-11: Comparison between conductivities of seizing slices from two animals, measured using one-dimensional method in transverse direction (1DT)

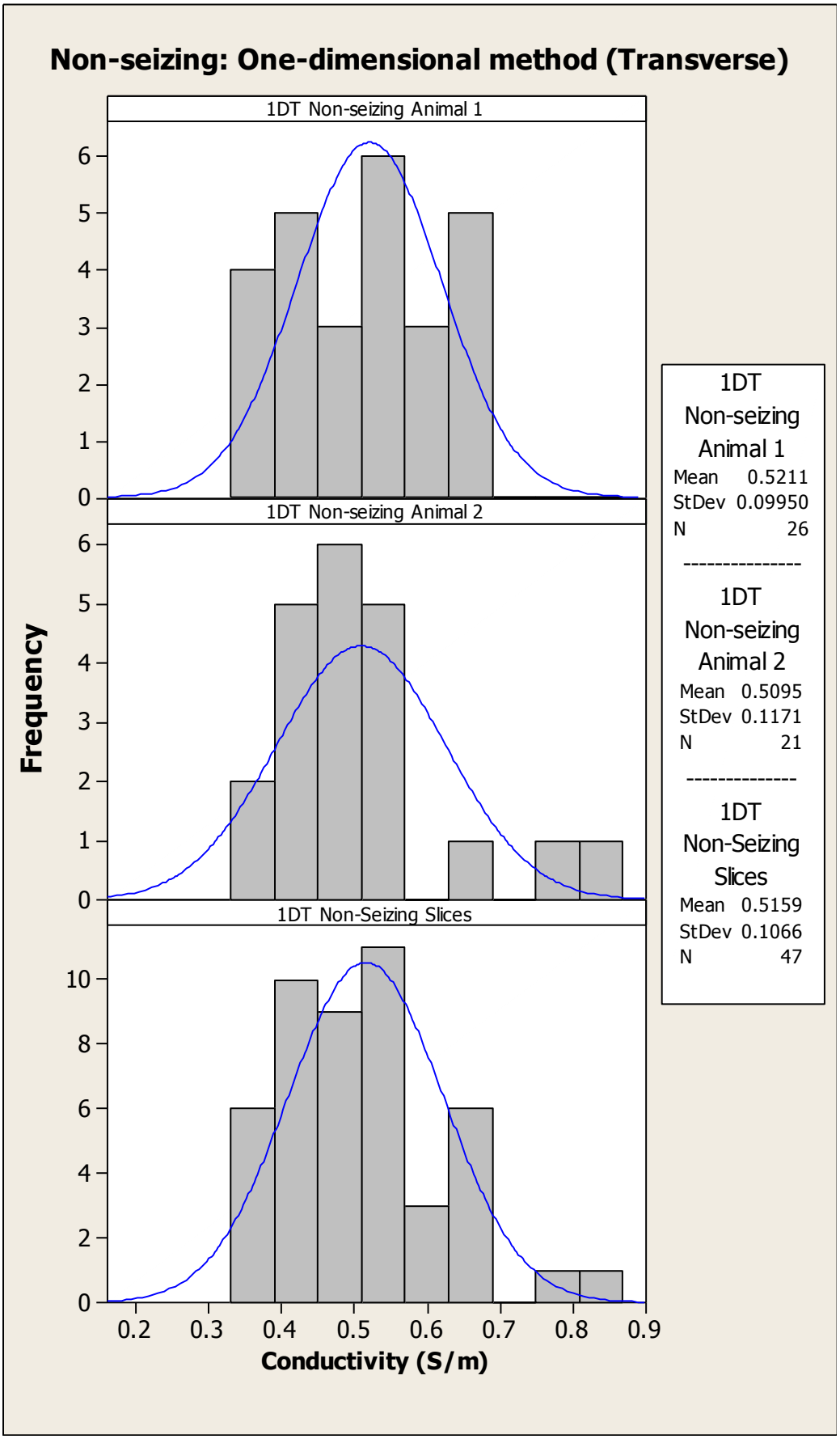

Figure 7-12: Comparison between conductivities of seizing slices from two animals, measured using one-dimensional method in transverse direction (1DT)

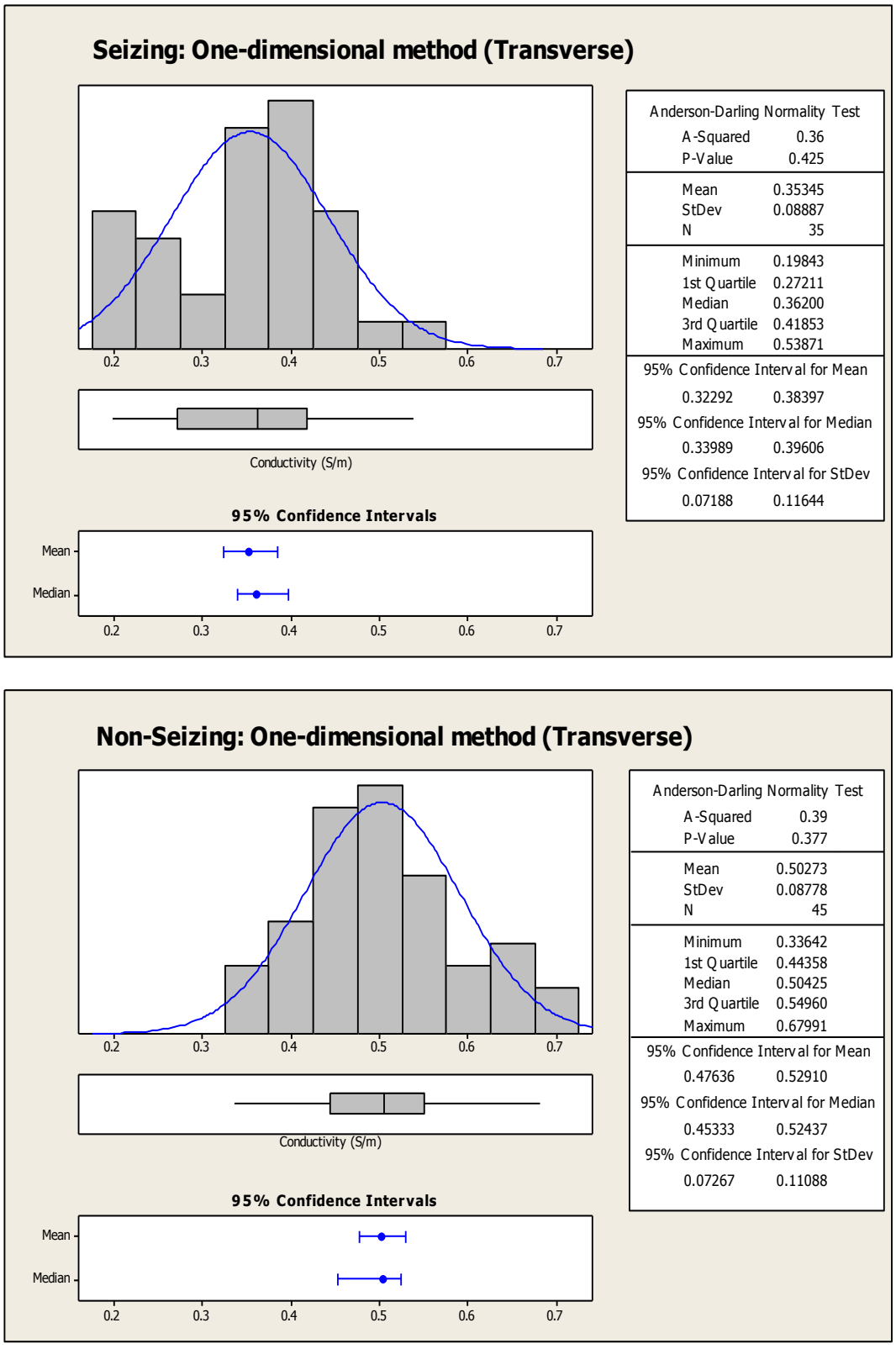

Figure 7-13: Comparison between conductivities of seizing and non-seizing slices using one-dimensional method in transverse direction

7.7 Conclusion and Discussion

Two flattened Ag/AgCl electrodes have been used to measure the 10-kHz electrical conductivities of seizing and non-seizing mouse cortex segments. I used brain segments that had been sliced in either the coronal or transverse direction. My results show that the conductivity of seizing segments is significantly lower than that of non-seizing segments for both slice orientations. Also I found that the conductivity changes with slice direction.

Gabriel *et al*. (2009) reported that in cerebellum white matter the conductivity anisotropy ratio is 10 while in grey matter the anisotropy ratio is between 2 and 5. Findings of Gabriel *et al*. (2009) and Yedlin *et al*. (1974) appear consistent with the higher non-seizing conductivities in the transverse direction. My measurements are different because of the gradual change of the orientation of the neurons with respect to the slices as shown in Figure 7-14.

The orientation of the pyramidal cell dendrites is perpendicular to the surface in the transverse cuts for the first two or three slices only (Hagan *et al.*, 2012). That orientation may increase the conductivity in this direction. For slice 1 the axis of the pyramidal neuron is perpendicular to the plane, in the same direction as the current. For slices 4 and 5 it is roughly within the plane perpendicular to the current, so consecutive transverse samples may not be equivalent. More data for this specific orientation is required to prove that. This is an avenue for future work.

In the one-dimensional coronal slices (1DC) method, the current travels parallel to the anterioposterior axis as shown in Figure 7-14. However, in the one-dimensional transverse slices (1DT) method, the current alternates between superior (higher) and inferior (lower) sides in a direction perpendicular to the current movement in the coronal slices. Therefore a direct comparison between the results for transverse and coronal is difficult.

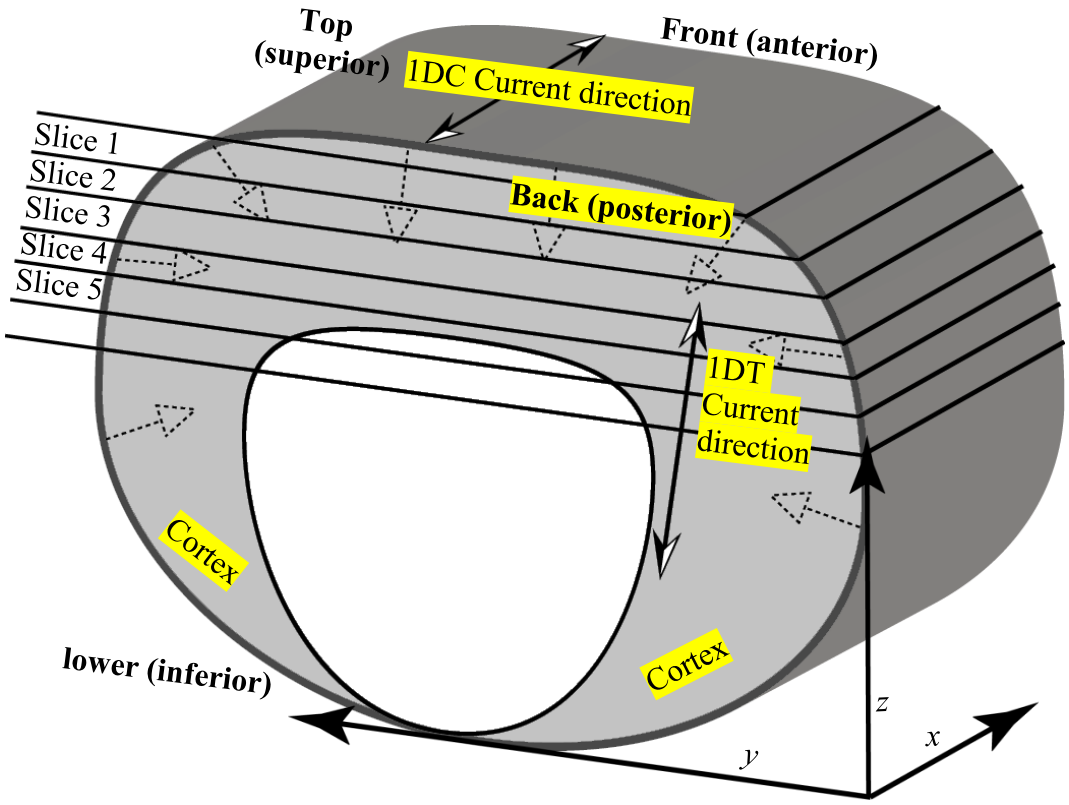

Figure 7-14: A schematic diagram of coronal section of mouse brain. Grey region represents the mouse brain cortex. Slices 1 to 5 are transverse slices. The current direction in one-dimensional coronal slices (1DC) is parallel to anterioposterior axis while in one-dimensional transverse slices (1DT) is parallel to vertical axis (dorsoventral axis) or alternate between higher (superior) and lower (inferior) sides. Dotted arrows indicates orientaion of pyramidal cells

The values of conductivity of slices using slice holder Figure 7-1 (e) are generally higher than values gained by using van der Pauw method. This may be expected because of a layer of the presence of dead cells on the slice surface. These are the cells that are destroyed during the slicing procedure (Heuschkel *et al*., 2002).

Another explanation for increasing conductivity in 1DT may be related to the time taken to do the measurements. Slices held in normal solution sometimes start seizing spontaneously (Voss, L. J. 2012, pers. comm.). The last group (1D transverse as described in Section 7.6) of slices was processed much faster than the first group because I had become more skilled in the procedure. This means that the transverse group would have

less possibility of spontaneous seizure activity. This may explain why the conductivity in the last group is higher than the others. An obvious improvement for further work would be to randomize the order in which measurements are made.

8 Frequency-dependence of Resistivity of Seizing and Non-Seizing Brain Slices

The dependence of electrical properties of tissue on stimulus frequency is of great interest for researchers. Frequency-dependence of the electrical behaviour is a consequence of the mechanism of current flow through the tissue and, thus, is very important in understanding various biological mechanisms such as seizures. The electrical properties of brain tissue are frequency dependent (Gabriel *et al*. (1996a; 1996b; 1996c; 2009) and Andreuccetti *et al*.(1997), as described in Section 2.5). All work that I found in the literature was done *in vivo* or *in vitro* on dead tissue. The present work is unique in using live tissue *in vitro*. The measured conductivities reported in this chapter can be compared with Chapter 7 results at 10 kHz only.

8.1 Method

Cortical slices were prepared as described in Section 5.3. Coronal slices were used in the One-Dimensional Method described in Chapter 7. Frequency was swept from 20 Hz to 2 MHz. These are the limits of the Agilent E4980 *LCR* meter. I carried out the experiment over three days on the brains extracted from three animals, one brain each day. Half of the slices from each animal were placed in magnesium-free ACSF, while the other half were placed in normal ACSF. I faced technical difficulties with MATLAB which led to a time delay for processing the second half of the slices from animal one. Therefore, I discarded all results from the first animal due to this unexpected experimental error. For the other two animals 35 non-seizing segments and 28 seizing segments were measured. The final MATLAB code is reported in Appendix B-4.

8.2 Results and Discussion for Conductivity and Frequency

The effect of frequency between 20 Hz to 2 MHz on conductivity is shown in Figure 8-1 for the second and third animals. Results from animal 2 are

lower than any other animal that I had analysed earlier at 10 kHz. A doubling of conductivity with frequency is observed over the range from 20 Hz to 2 MHz for both animals. Figure 8-2 superimposes measured conductivities of animal 3 (Figures 8-1) on calculated conductivities using the Andreuccetti *et al.*(1997) software and values reported in the literature. While my results are higher than predicted by the Andreuccetti *et al.*(1997) software, they are within the range of other values published in the literature.

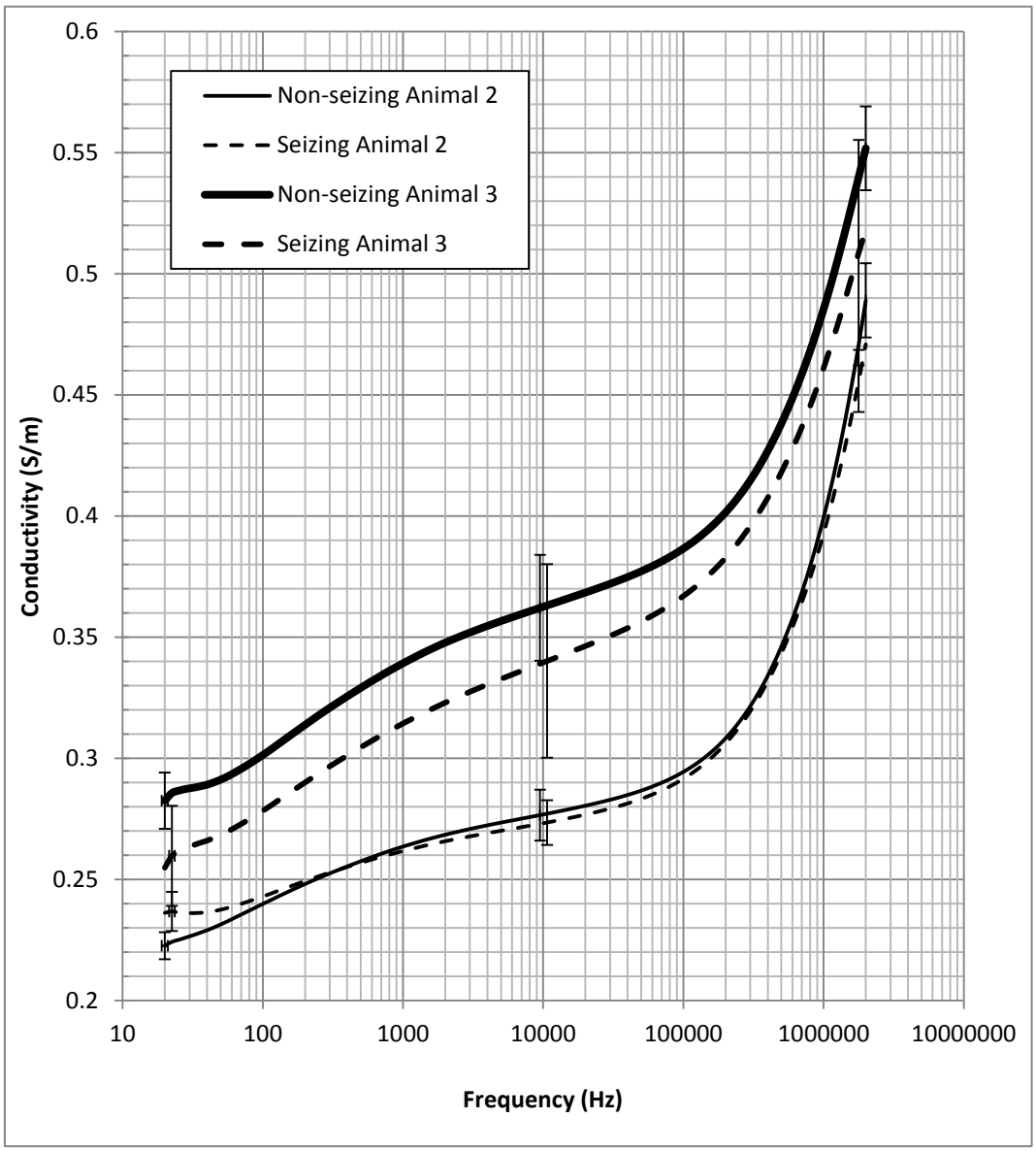

Figure 8-1: Comparison of conductivities for seizing and non-seizing slices for animal 2 using one-dimensional method in coronal direction. Error bars show the standard uncertanties in the mean at selected points

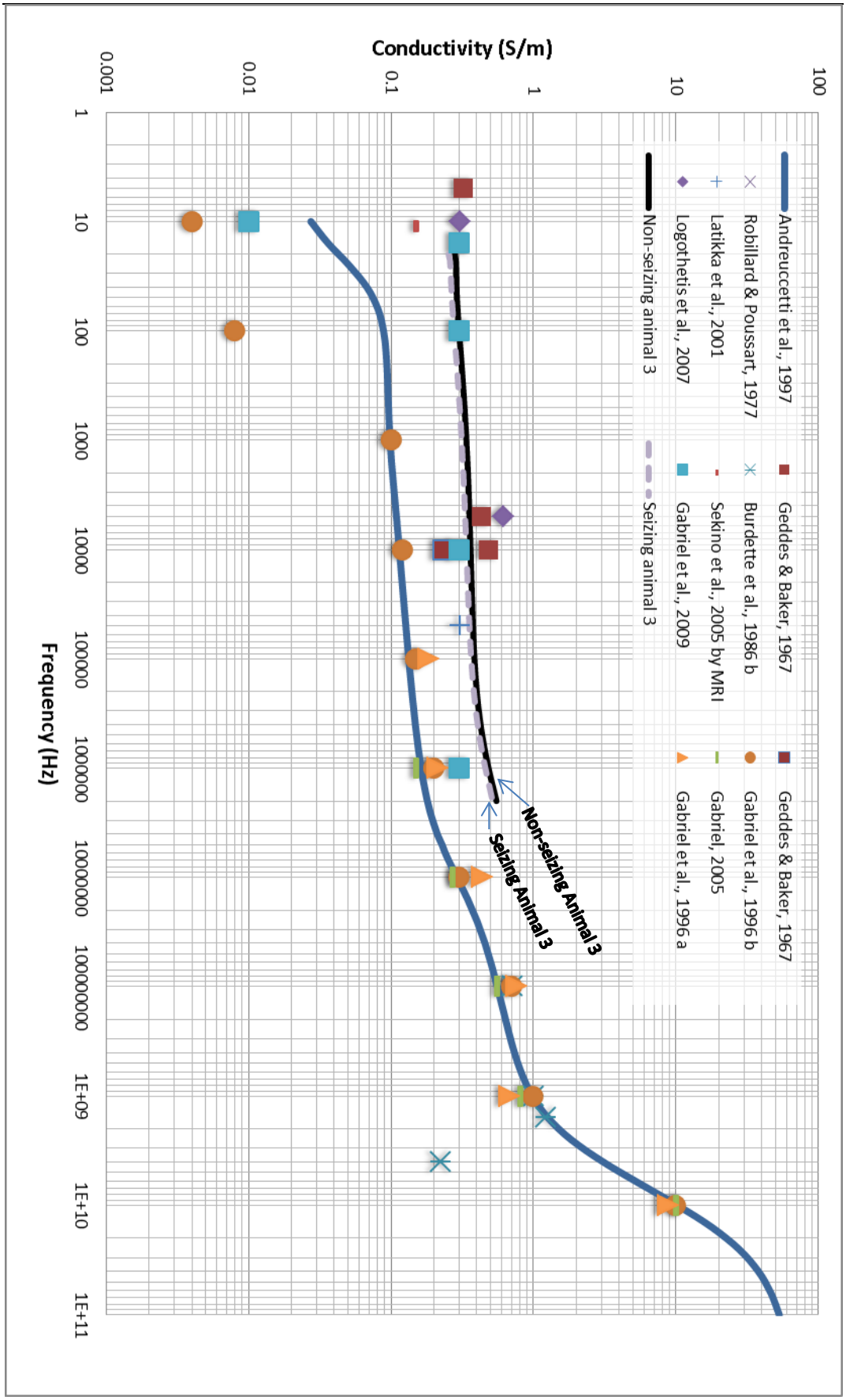

Figure 8-2: Superimposing of measured conductivities of animal 3 on calculated conductivities using Andreuccetti et al.(1997) software and values found in the literature

The study results show that the difference in conductivities of the seizing and non-seizing slices is highly significant using a 2-sample *t*-test ($p = 3\times10^{-3}$ and $p < 1\times10^{-3}$ for second and third animals respectively). However, values of conductivity of slices at 10 kHz for animal two and three are different from those obtained in Section 7.5 (Results and Discussion for Coronal Slices) as shown in Table 8-1. The difference in conductivities values may be a result of re-calibrating the distance between two electrodes before the frequency-dependent measurements. The difference for the second animal is well outside the range of the previous one-dimensional measurements.

Table 8-1: Comparison of conductivities difference between seizing and non-seizing slices at 10 kHz. Standard uncertainty included for the mean

	Seizing σ (S/m)	Non-seizing σ (S/m)
All animals at 10 kHz from Table 7-1		
Mean (Excluding outliers)	0.303±0.013	0.369±0.014
Median (Including outliers)	0.305	0.370
Slices from animal 2 at 10 kHz		
Mean	0.273±0.009	0.277±0.010
Median	0.278	0.270
Slices from animal 3 at 10 kHz		
Mean	0.339±0.040	0.362±0.022
Median	0.320	0.345

8.3 Results and Discussion for Real and Imaginary parts of Impedance and Frequency

For the present work I will plot resistivity (rather than conductivity) because this is the convention in modelling electrical properties. The method for electrical impedance measurements of brain slices has been established in Chapter 7. I have taken advantage of this to study the behaviour of seizing and non-seizing brain slices between 20 Hz and 2 MHz. This frequency covers α and β dispersions as shown in Figures 8-3 and 8-4. These figures show plots of imaginary part and real part of resistivity for individual slice segments. On Figure 8-5 the mean resistivity is compared between the two animals for seizing and non-seizing conditions. The slice segments have different areas, so I multiplied the impedance of the individual slice segment's imaginary and real parts by its area and divided by its thickness in order to have a measure of resistivity. The solid lines in Figures 8-3 and 8-4 represent the averages over the segments. The conductivity calculated using $\sigma = \frac{L}{RA}$ where L is the thickness of the segment (400 μm), R is its resistance and A is the segment area. The MATLAB code (Appendix B-4) records the conductivity directly to an Excel file.

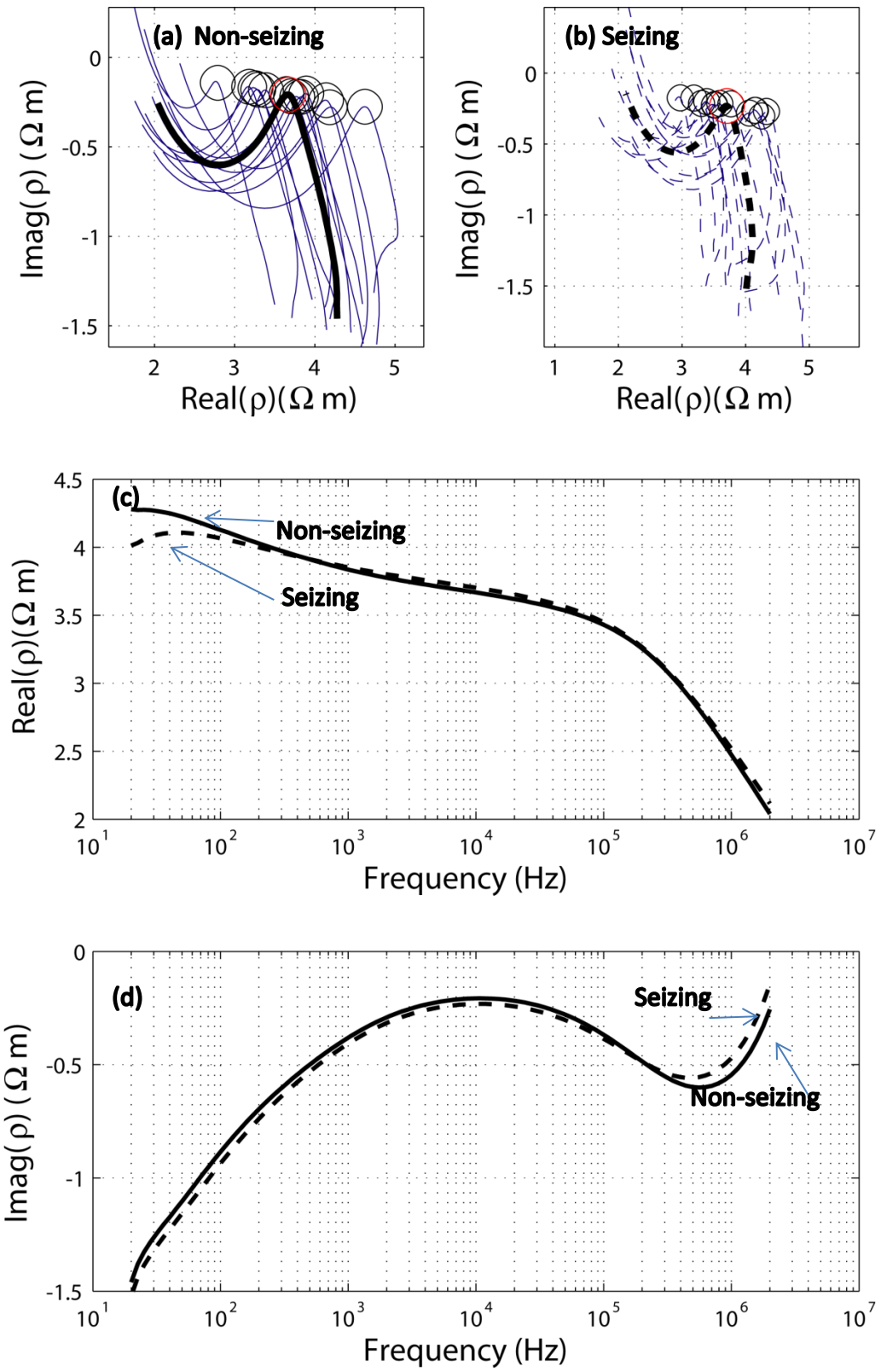

Figure 8-3: Plots of imaginary and real parts of resistivity for individual coronal slice segments from animal 2. Circles show values of resistivity components at 10 kHz. (a) Thick solid line shows average of all non-seizing segments. (b) Thick dashed line shows average of all seizing segments. (c) and (d) show variation of mean real and imaginary parts with frequency

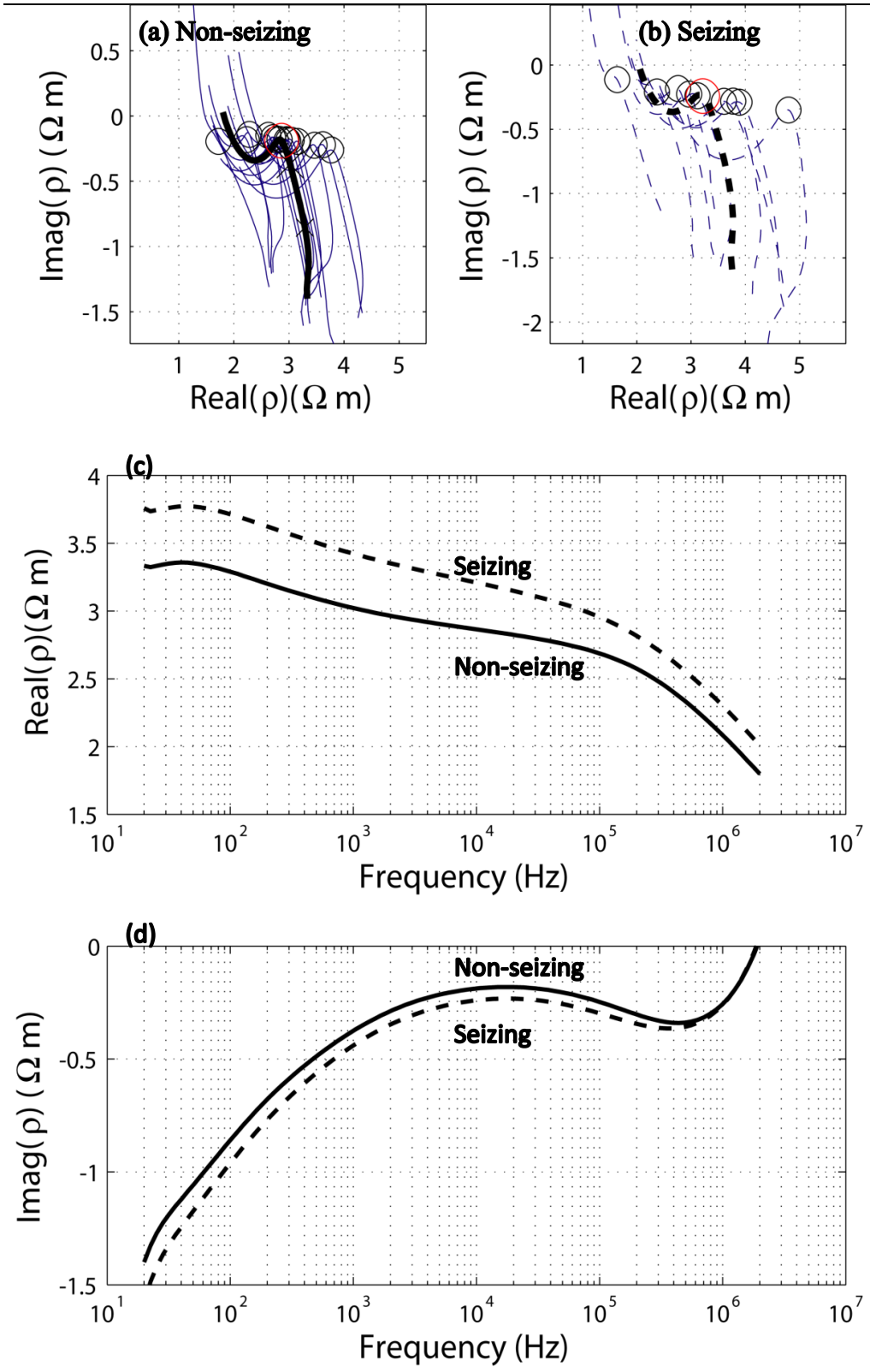

Figure 8-4: Plots of imaginary and real parts of resistivity for individual coronal slice segments from animal 3. Circles show values of resistivity components at 10 kHz. (a) Thick solid line shows average of all non-seizing segments. (b) Thick dashed line shows average of all seizing segments. (c) and (d) show variation of mean real and imaginary parts with frequency

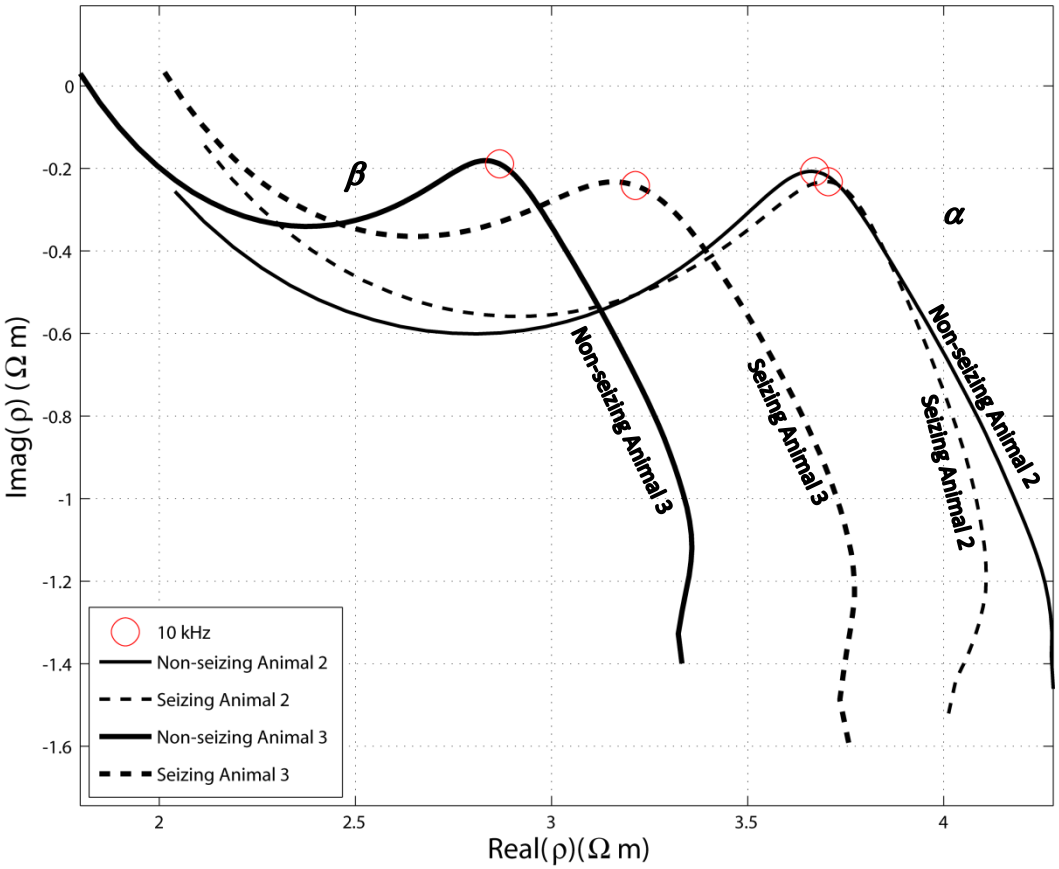

Figure 8-5: Plots of imaginary and real parts of resistivity for non-seizing and seizing coronal slice averaged from animals 2 and 3. Circles show values of resistivity components at 10 kHz

The α- and β-dispersions are clear in Figure 8-5. The α-dispersion is shown at frequencies below 10 kHz (10 kHz is the peak marked by a circle in Figure 8-5). The α-dispersion is caused by counterion polarization around the cell membrane at the cell membrane surface. The β-dispersion is shown at frequencies above 10 kHz. It comes from interfacial polarization of cell membrane which forms an insulating layer separating intracellular and extracellular fluids. For this reason the cell membrane is modelled as a capacitor connected in parallel with a resistor in Section 8.4. (Miklavčič *et al.*, 2006).

8.4 Modelling Real and Imaginary parts of Impedance

The object of this section is to find reasonable values for components in the Fricke Model to simulate the measured tissue impedance (or resistivity)

shown in Section 8.3. Shown in Table 8-1, the measurements from animal 3 are consistent with the data reported earlier in Chapter 7. However, the measured conductivity from animal 2 is lower. Therefore, for the purposes of modelling, only data from animal 3 are considered.

A reasonable model has a resistance R_1 representing intracellular fluid in series with capacitance C_1 representing the cell membranes, both in parallel with R_2 which represents extracellular fluid (Figure 8-6). In Section 1.4.2, I described the Fricke model for tissue, here I am including the electrode tissue interface with a similar model to simulate my experimental results. The electrode tissue interface is modelled by a capacitor C_3 connected in parallel with resistor R_3. In bulk tissue, the relevant parameters are resistivity (rather than resistance), with units Ωm, and permittivity (rather than capacitance), with units F/m.

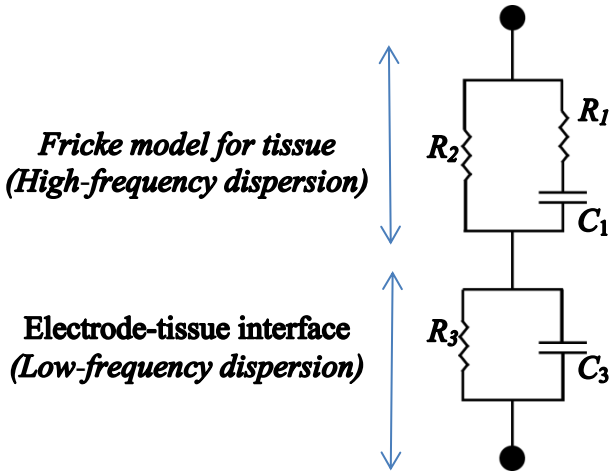

Figure 8-6: Fricke model for tissue including electrode tissue interface

A MATLAB code was written to model α- and β-dispersions (code details are in Appendix B-5) for non-seizing slice segments (Figure 8-7a) and seizing slice segments (Figure 8-7b). Values were selected by trial and error (Table 8-2) to provide a best fit from the model to the experimental results. The best fit was justified using a sum of squares of the differences between the results of the model and experiment. Figure 8-7 (a) and (b) show the model superimposed on experimental results. The quality of the fit is not spectacular but it does minimize the sum of squares over the full α- and β-dispersions frequency range,

$$S = \sum_{i=1}^{N} |x_i - \rho(f_i)|^2 \qquad (8\text{-}1)$$

where x_i is the measured resistivity at frequency f_i and ρ is the calculated resistivity of the model of Figure 8-6 and the sum is taken over all measured frequencies. These were spaced logarithmically between 20 Hz and 2 MHz. The frequencies f_α and f_β were calculated from equations $f_\alpha = \frac{1}{2\pi R_3 C_3}$ and $f_\beta = \frac{1}{2\pi(R_1+R_2)C_1}$ respectively. These are the centres of α- and β- distortions.

Table 8-2: Chosen resistivities (R_1, R_2 and R_3) and permittivities (C_1 and C_3)

	R_1 (Ωm)	R_2 (Ωm)	C_1 (F/m)	f_β (Hz)	R_3 (Ωm)	C_3 (F/m)	f_α (Hz)
Non-seizing	6.9	2.93	7.5×10^{-8}	216×10^{3}	3.4	3.2×10^{-3}	14.6
Seizing	7.36	3.4	47×10^{-8}	31×10^{3}	3.8	3.0×10^{-3}	14.0

It is clear that all resistivity values are larger for the seizing segments than non-seizing segments agreeing with previous results. Lower conductance and better charge storage for seizing cases are consistent with closure of gap junction leakage paths.

The imperfect fit of the model shows that there are other electrical elements controlling the experimental data, not just the three resistors and the two capacitors as in Figure 8-6. Samples tend to behave inconsistently below 100 Hz as in Figure 8-4(a) and (b). This is explained by Miklavčič *et al.* (2006) and Gabriel *et al.* (1996b) where they reported that electrode polarization errors can affect impedance measurements below 1 kHz, becoming significant below 100 Hz.

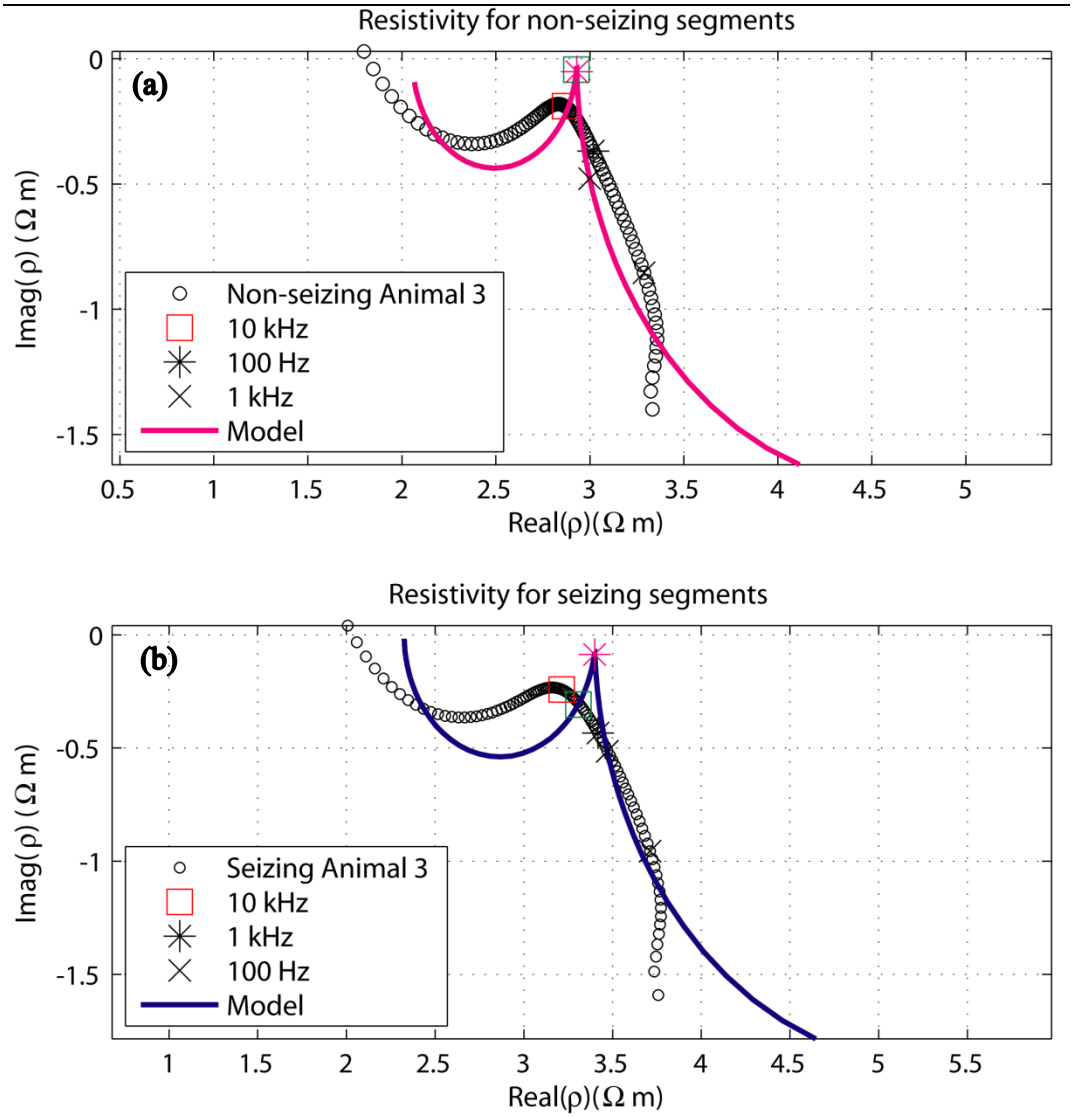

Figure 8-7: Modelling resistivity of brain segments superimposed on the actual experimental results for animal 3. (a) non-seizing, (b) seizing

In order to improve the fit between model and data I focused only on β-dispersion as shown in Figures 8-8 (a) and (b), and obtained the revised values listed in Table 8-3.

Table 8-3: Chosen resistivities (R_1, R_2 and R_3) and permittivities (C_1 and C_3)

	R_1 (Ωm)	R_2 (Ωm)	C_1 (F/m)	f_β (Hz)	R_3 (Ωm)	C_3 (F/m)	f_α (Hz)
Non-seizing	4.9±0.1	2.87±0.01	$(5.1\pm0.1)\times10^{-8}$	400×10^{3}	6.4±0.1	$(2.5\pm0.5)\times10^{-3}$	10
Seizing	7.5±0.1	3.15±0.01	$(6.0\pm0.1)\times10^{-8}$	400×10^{3}	6.4±0.1	$(2.5\pm0.5)\times10^{-3}$	10

It is clear that both β-dispersion resistivity values are larger for the seizing segments than non-seizing segments, agreeing with previous results.

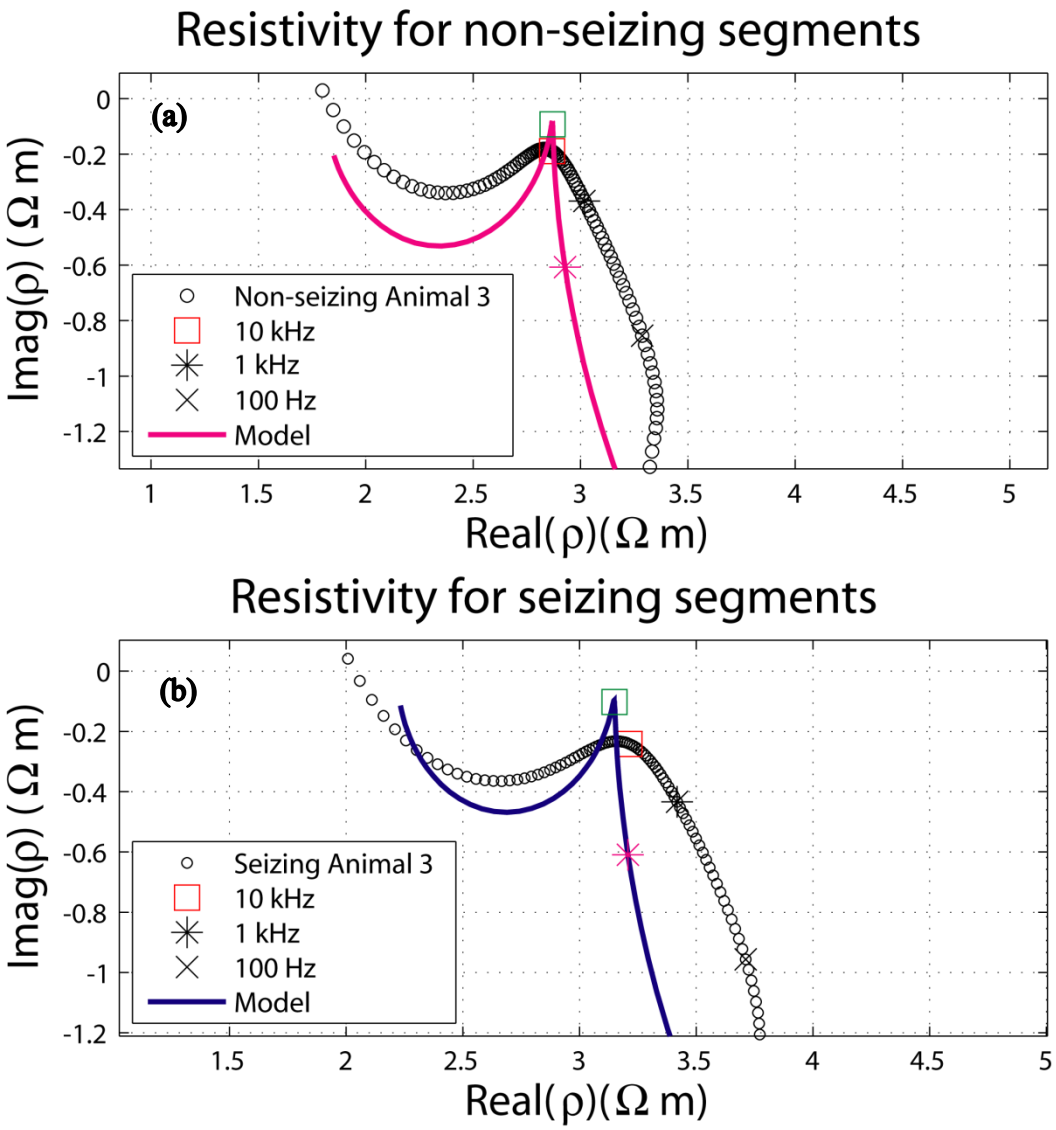

Figure 8-8: Revised model fit for β-dispersion of brain segments superimposed on the actual experimental results for animal 3. (a) non-seizing (b) seizing

8.5 Conclusion and Discussion

One of the main results of this chapter is finding that 10 kHz lies at the boundary separating the regions of dispersion. This makes 10 kHz a good choice to use for experiments where only a single frequency is possible, as in case of the van der Pauw method (Section 5.2). It has been proposed that the dependence of brain tissue impedance on frequency is due to changes in cell membrane conductivity and movement of ions and charged particles (Damez *et al.*, 2007). My results agree with this proposal. Also the

resistivity of seizing slices is higher than the resistivity of non-seizing slices segments over the frequency range 10 kHz to 2 MHz. This is consistent with earlier finding that seizing slices have lower conductivity than non-seizing slices at 10 kHz.

Cole and Debye models are generally used to describe biological tissue (Miklavčič *et al.*, 2006). I did not use any of these because Cole produces only β-dispersion and it is known that Debye model does not fit the measured data well over a wide range of frequencies (Brown *et al.*, 1999).

The modelling results shown in Figures 8-7 and 8-8 indicate that the simple circuit of Figure 8-6 does not provide an accurate description of my experimental results. Accordingly there are other elements playing a role. On the other hand, the β-dispersion resistivities are higher in seizing slices model than the non-seizing model. This agrees with my previous finding that the conductivity of seizing slices is lower than that for non-seizing slices.

9 Conclusion, Discussion and Future Work

Two successful methods for performing conductivity measurements in live brain sections were demonstrated: 2D van der Pauw and 1D slice-holder methods.

In the van der Pauw method, the conductivity was measured in two dimensions in coronal slices, where the current moves in the coronal plane as shown by arrows in Figure 9-1. With the 1D slice-holder method, coronal and transverse directions were considered separately. The methods (vdP, 1DC and 1DT) are not directly comparable unless one assumes isotropy in conductivity within the tissue. This assumption is probably false (Section 7.7). One of the main advantages of one-dimensional method is the decreased current density in the interface between the electrodes and the tissue because the electrodes have a substantially larger surface area.

The mean brain conductivities measured by the above methods are summarised in Table 9-1. The seizing results are very similar for all the measurements. If the seizing case has closed gap junctions, this suggests that the conductivity due to sources other than gap junctions is isotropic. However, the conductivity of the non-seizing cortex suggests that when gap junctions are open there is anisotropy.

Table 9-1: The mean brain cortex measured conductivities

	Conductivity (S/m)		
	van der Pauw	1D coronal	1D transverse
Non-seizing	0.362±0.009	0.427±0.008	0.503±0.013
Seizing	0.328±0.012	0.317±0.007	0.353±0.015

Figure 9-1 shows the conductivities measured by all three methods in non-seizing and seizing states.

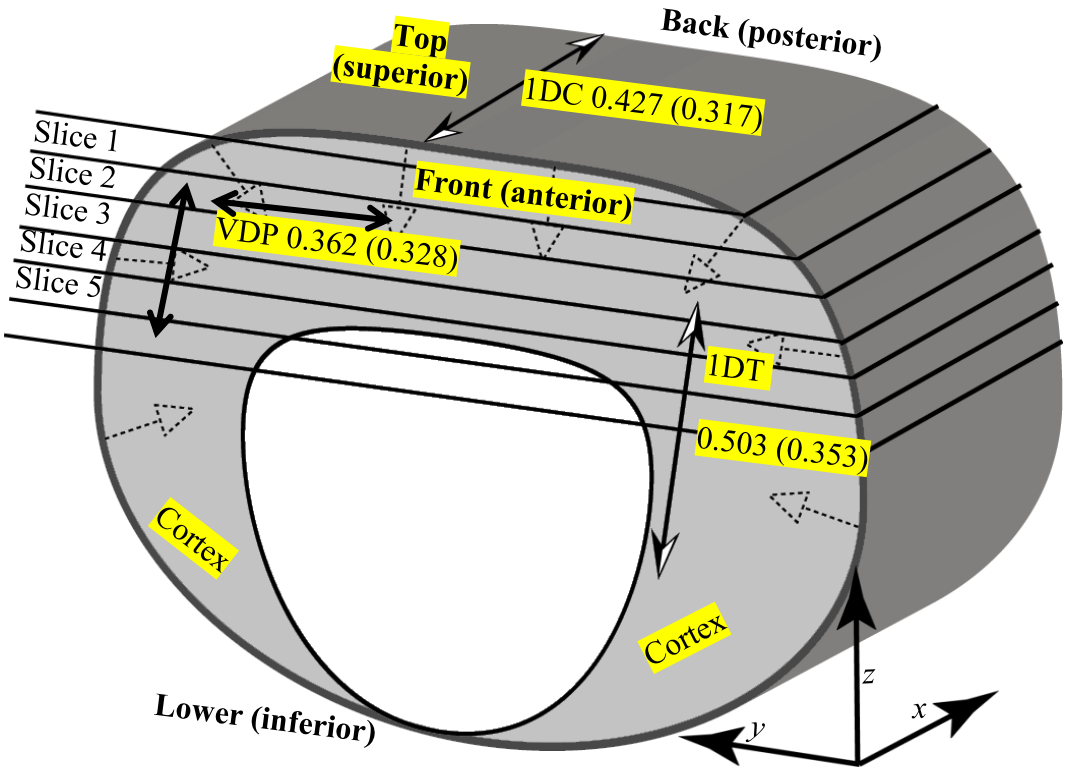

Figure 9-1: A schematic diagram of coronal section of mouse brain. Conductivity measurements are indicated for the van der Pauw (VDP), one-dimensional coronal (1DC) and one-dimensional transverse (1DT) slices. The non-seizing and (seizing) values in S/m are shown with no brackets and (brackets) respectively. Arrows show the direction of the current

In addition to measuring conductivity at 10 kHz using 1D and 2D methods, I successfully measured the conductivity of seizing and non-seizing slices over range of frequency from 20 Hz to 2 MHz. This advantage was used in Chapter 8. The measured resistivity of seizing slices segments is higher than the resistivity of non-seizing slices segments over the frequency range 20 Hz to 2 MHz. This consistent with earlier finding that seizing slices have lower conductivity than non-seizing slices at 10 kHz.

Modelling produces higher resistivities in seizing slices than non-seizing model. This agrees with all other reported results in this thesis leading to the overall conclusion that the conductivity of seizing slices is lower than that of non-seizing slices.

The ratio of normal to magnesium-free ACSF solutions conductivities is 1.0005 which indicates that their conductivities are effectively identical. Wilson (Wilson, M. T. 2012, pers. comm.) estimated the conductivity of the two solutions from conductivity data recorded in (Weast, 2003) (Appendix A-4): his estimated conductivities are 1.614 S/m and 1.613 S/m for the normal and magnesium-free ACSF solutions at 25°C respectively. In addition, I measured samples of the two solutions with an RE388TX Conductivity Meter (EDT Instruments Ltd, UK). The normal and magnesium-free solutions have mean conductivities at 25°C of 1.578±0.012 S/m and 1.558±0.008 S/m respectively. Calculated and measured data confirm that any difference between the conductivities of the two solutions is small. Therefore the difference in conductivity between the seizing and non-seizing slices is due to tissue properties not due to the difference in ACSF composition. However, quantitative values obtained should be used with caution as the measured conductivity may be influenced by ACSF.

The way to do these measurements was full of challenges and difficulties. Some of these related to obtaining ethical approvals to do the research and limits on the number of animals. Some of them were technical difficulties (establishing the methodology) like using very small samples, delivering current through tiny electrodes and doing the measurements quickly enough to ensure viability of the slices. Furthermore, availability of lab and equipment and ensuring animals are correct age were another worry.

Some of the points mentioned in this study were discussed previously (Freygang Jr & Landau, 1955; Van Harreveld & Ochs, 1956; Adey *et al.*, 1962; Van Harreveld & Schade, 1962). However, these earlier investigations lacked details in conductivity of brain slices, they used whole brain as homogenized brain preparation, and all of their measurements were indirect. In contrast, the present study utilized direct measurements. These papers came to my attention late in my work. This is possibly because they are old and there has been little recent work in this topic. However my methodology would not have changed if I had found these papers earlier.

In a future study, the effect of gap junctions on brain conductivity could be studied by three different methods. In the first method slices would be prepared as described in Sections 5.3 and 7.3. One-third of slices go to normal ACSF, one-third to ACSF containing mefloquine and one-third to ACSF containing carbenoxolone. Mefloquine, specifically blocks Cx36 gap junction only (Cruikshank et al., 2004) while carbenoxolone blocks all gap junctions (Juszczak & Swiergiel, 2009). The second method would compare the conductivity of wild type with genetically modified mice lacking the gene that codes for the Cx36 protein. The third method would control the rate of gene expression associated with the connexin proteins (Stoppini *et al.*, 1991; Yoon *et al.*, 2010).

Another study could investigate the gradual orientation-dependent of the conductivity in transverse slices, in other words to study the effect of orientation as we move from slice 1 to slice 5 (see Figure 9-1). This may help quantify the degree of anisotropy in the conductivity.

The answer to the research question: is there is a link between seizure activity and electrical conductivity of brain tissue is YES. That is proved by four different ways: van der Pauw (Ch. 5), one-dimensional coronal direction (Ch. 7), one-dimensional transverse direction (Ch. 7) at 10 kHz and one-dimensional coronal direction over frequency range 20 Hz to 2 MHz (Ch. 8).

Moreover, in Section 2.7 four goals were set out for this research;

1. Establishing an effective method to measure the conductivities of small live brain slices,
2. Finding out whether tissue conductivity is different in seizing and non-seizing states,
3. Measuring brain tissue conductivity over a frequency range from 20 Hz to 2 MHz,
4. Confirming that slices are still alive after measurements.

All these goals were successfully met. Many challenges and limitations were faced; these required a huge amount of effort and time, but success was achieved in the end as documented and discussed in this thesis.

Appendix A Extension of Others Work

A-1 Estimate of Tissue Conductivity Due to Gap Junctions

In this appendix I will show how Wilson (Wilson, M. T. 2012, pers. comm.) derived an estimate of the conductivity due to open gap junctions in the cortex. Gap junctions were explained in detail in Section 1.2.

Consider a gap junction acting as a resistor R_{gap} connected between two cells (neurons) as in Figure A-1. A "Fukuda cell" is an expression to describe a square zone of side 0.4 mm that circumscribes a circular region of radius of about 200 μm that covers the region of influence of neuron's gap junctions (Fukuda *et al.*, 2006). We could model all gap junction resistances by a single resistor of resistance R_g between two Fukuda cells as in Figure A-2.

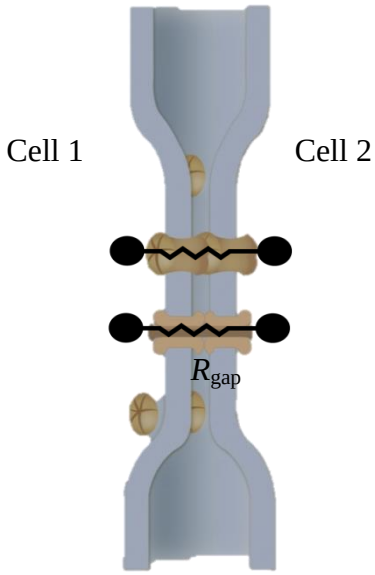

Figure A-1: Schematic diagram for gap junction between two neurons

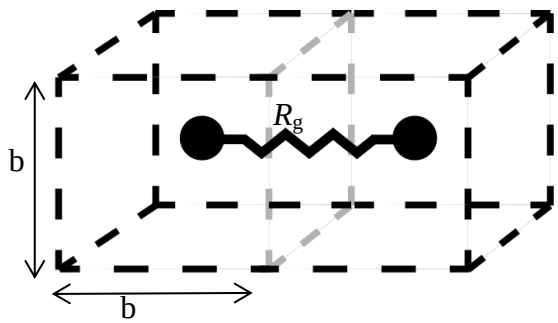

Figure A-2: Fukuda cell

Proceeding along the line of Steyn-Ross *et al.* (2007), neurons reach a distance "b" with their gap junctions. The equivalent resistance between the two Fukuda cells can be explained as follows. If the volume density of the inhibitory neurons is N, and each neuron has N^{γ} gap junctions then the number of connections between the two Fukuda cells is $\frac{b^3 N N^{\gamma}}{6}$, six in the denominator because each cell borders six others in three dimensions. If each gap junction has a resistance R_{gap}, then the equivalent resistance R_{g} of the inter-cell resistance due to gap junctions is:

$$R_g = \frac{R_{\text{gap}}}{\text{Number of connections}} = \frac{6\,R_{gap}}{b^3\,N\,N^{\gamma}} \qquad \text{(A-1)}$$

According to Mears *et al.*, (1995) Fukuda *et al.*, (2006) Steyn-Ross *et al.*, (2007) a middle range value for R_{gap} is 300 MΩ, with a neuron density of $N \approx 10^{13}$ neuron/m^3 (Beaulieu & Colonnier, 1989; Cooper & Robertson, 1997) gap junctions per neuron, $N^{\gamma} \approx 60$ and distance between Fukuda cells $b = 3\times10^{-4}$ m.

Consider tissue as made up of a three-dimensional grid of resistors between two Fukuda cells, as shown in Figure A-3.

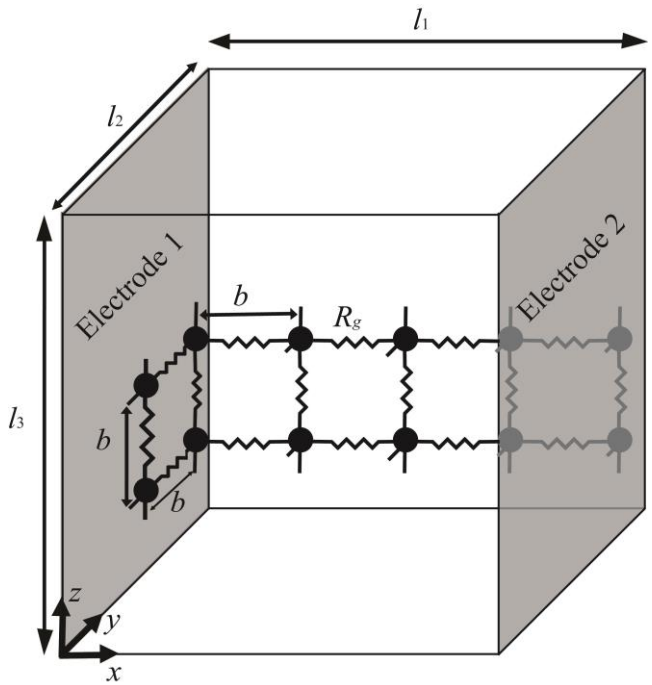

Figure A-3: A three-dimensional network of resistors modelling the electrical connections between Fukuda cells

Each line of resistors left to right has resistance $R_g \frac{l_1}{b}$ since there are $\frac{l_1}{b}$ of them. But, from the left electrode to the right electrode, there are $\frac{l_2 l_3}{b^2}$ lines, so total resistance between electrodes along dimension l_1 is

$$R = \frac{R_g \left(\frac{l_1}{b}\right)}{\frac{l_2 l_3}{b^2}} = \frac{R_g \; l_1 \; b}{l_2 l_3} \qquad \text{(A-2)}$$

Conductivity is defined from

$$R = \frac{l_1}{\sigma l_2 l_3} \qquad \text{(A-3)}$$

Comparing equations (A-2) and (A-3) gives us

$$\sigma = \frac{1}{R_g \; b} \qquad \text{(A-4)}$$

Substituting for R_g from equation (A-1) into equation (A-4), and we get

$$\sigma = \frac{N \; N^{\gamma} b^2}{6 \; R_{gap}} \approx \frac{10^{13} \text{ m}^{-3} \times 60 \times (3 \times 10^{-4} \text{ m})^2}{6 \times 300 \times 10^6 \Omega} \approx 0.03 \text{ Sm}^{-1}$$

This is close to the observed difference between seizing and non-seizing states.

A-2 Converting Conductance to Conductivity

Van Harreveld & Schade (1962) measured the impedance of brain tissue at 1 kHz. They used a bridge circuit to measure impedance as in Figure A-4. Our aim is to convert their measured impedance between electrodes to conductivity, σ.

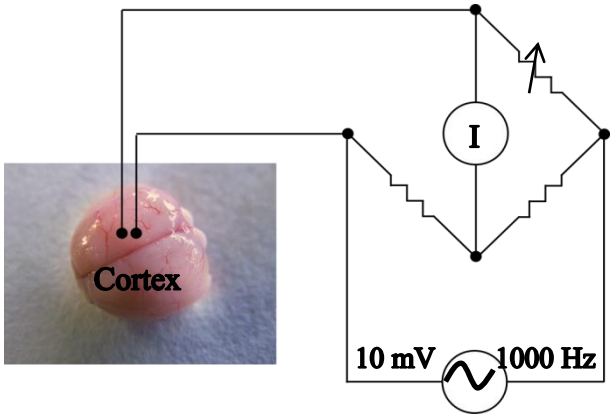

Figure A-4: My interpretation of van Harreveld & Schade set up

In the three dimensional case; consider a to be the wire electrode radius, R to be the distance between the two electrodes (centre to centre), X to be an arbitrary point of distance r_1 from A and r_2 from electrode B. The two electrodes carry charges $+q$ and $-q$ *as in* Figure A-5.

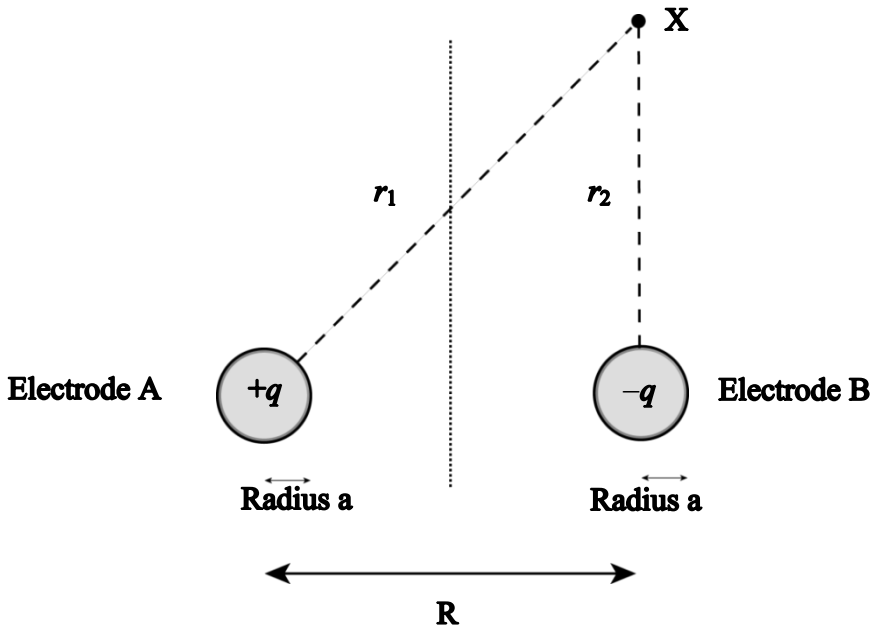

Figure A-5: Two spherical electrodes of radius a and distance R between the two electrodes (centre to centre)

The potential V at point X, referenced to infinity is $V = \frac{q}{4\pi\varepsilon_\circ}\left(\frac{1}{r_1} - \frac{1}{r_2}\right)$. Therefore, the potentials at the electrodes A and B are $V_A = \frac{q}{4\pi\varepsilon_\circ}\left(\frac{1}{a} - \frac{1}{R-a}\right)$ and $V_B = \frac{q}{4\pi\varepsilon_\circ}\left(\frac{1}{R-a} - \frac{1}{a}\right)$ and so the potential difference between electrodes is

$$V_A - V_B = \frac{q}{4\pi\varepsilon_\circ}\left(\frac{1}{a} - \frac{1}{R-a} - \frac{1}{R-a} + \frac{1}{a}\right) = \frac{2q}{4\pi\varepsilon_\circ}\left(\frac{1}{a} - \frac{1}{R-a}\right)$$

If $R \gg a$ then $\frac{1}{a} + \frac{1}{R-a} \approx \frac{1}{a}$ So, the potential difference between electrodes is

$$V_A - V_B = \frac{q}{2\pi\varepsilon_\circ a} \qquad \text{(A-5)}$$

The current density $\boldsymbol{J}$ is given by $\boldsymbol{J} = \sigma\boldsymbol{E}$. From Gauss' Law: $\int \boldsymbol{J}.d\boldsymbol{s} = \sigma \int \boldsymbol{E}.d\boldsymbol{s} = \sigma\frac{q_{\text{enclosed}}}{\varepsilon_\circ}$

If we consider our surface integral to be around the electrode, then $\int \underline{J}.d\underline{s} = I_{\text{out}}$. Therefore $\frac{q_{\text{enclosed}}}{\varepsilon_\circ} = \frac{I_{\text{out}}}{\sigma}$. Substitute this into equation (A-5) we find the potential difference $V_A - V_B = \frac{I_{\text{out}}}{2\pi\sigma a}$. The measured impedance Z is then = $\frac{V_A - V_B}{I_{\text{out}}} = \frac{1}{2\pi\sigma a}$. We therefore have a relationship between the impedance Z and the conductivity σ.

In reality the electrodes were on the tissue surface, not implanted in tissue. Therefore we have only half the volume of the cortex expected to a given voltage, so only half the current flows and the impedance is doubled.

So, the tissue impedance $Z = 2 \times \frac{1}{2\pi\sigma a} = \frac{1}{\pi\sigma a}$ corresponding to a tissue conductivity of $\sigma = \frac{1}{\pi a Z}$ .This assumes spherical electrodes. Van Harreveld & Schade used electrodes of diameter 1 or 2 mm (the reference is unclear as to which) so 0.5 mm $\leq a \leq$ 1 mm, for an impedance ranging over $48 \times 10^{-5} \leq Z \leq 43 \times 10^{-5}$ Ω. So, if a = 0.5 mm, $0.27 \leq \sigma \leq 0.31$ S/m. Or, if a = 1 mm, $0.14 \leq \sigma \leq 0.16$ S/m. This is approximately the same order of my results.

A-3 Deriving an Expression for the Conductivity in 2D

In the following we derive an expression for the conductivity of the material in terms of the voltage and current measured by cylindrical electrodes. Consider an arrangement of electrodes as shown in Figure A-6. Here, cylindrical electrodes are placed in a sample in a plane, current is injected at I_{in}, removed at I_{out}, and the potential difference is recorded between q and p.

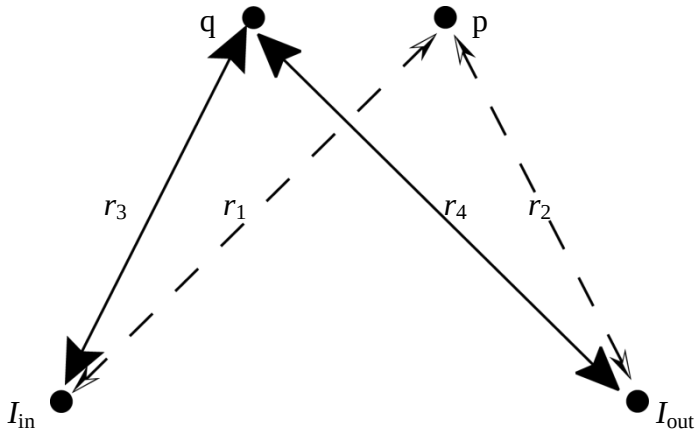

Figure A-6: An arrangement for infinitesimally thin cylindrical electrodes in 2 dimensions

From Gauss' law, the magnitude of the electric field at distance r due to a cylindrical charge distribution of length d is

$$E = \frac{1}{2\pi\varepsilon_\circ d}\frac{Q}{r} \qquad \text{(A-6)}$$

The electric potential V at a position $\boldsymbol{r}$ referenced to a point r_0 a long way from the electrodes is

$$V = \int \boldsymbol{E}.d\boldsymbol{r} = \frac{1}{2\pi\varepsilon_\circ}\frac{Q}{d}\log_e\left(\frac{r}{r_0}\right) \qquad \text{(A-7)}$$

But from Equation (4-6)

$$Q = I_{out}\frac{\varepsilon_\circ}{\sigma} \qquad \text{(A-8)}$$

Substituting in Equation (A-7) gives

$$V = \frac{1}{2\pi d}\frac{I}{\sigma}\log_e\left(\frac{r}{r_0}\right) \qquad \text{(A-9)}$$

Potential at point p due to current I_{in} and I_{out} is therefore

$$V_p = \frac{1}{2\pi d}\frac{I}{\sigma}\log_e\left(\frac{r_1}{r_2}\right) \qquad \text{(A-10)}$$

Similarly, potential at point q due to current I_{in} and I_{out}

$$V_q = \frac{1}{2\pi d}\frac{I}{\sigma}\log_e\left(\frac{r_3}{r_4}\right) \tag{A-11}$$

Then, the potential difference $\varphi = V_p - V_q$ is

$$\varphi = \left[\frac{I}{2\pi d\sigma}\right]\log_e\left(\frac{r_1 r_4}{r_2 r_3}\right) \tag{A-12}$$

The effective impedance $Z = \frac{\varphi}{I}$ is then given by

$$Z = \frac{\varphi}{I} = \left[\frac{1}{2\pi d\sigma}\right]\log_e\left(\frac{r_1 r_4}{r_2 r_3}\right) \tag{A-13}$$

A-4 Molarity (Theoretical) Conductivity Calculation of Solutions

I will show how Wilson (Wilson, M. T. 2012, pers. comm.) calculated the theoretical conductivity of normal and magnesium-free ACSF at 25°C. He used available data in the CRC Handbook of chemistry and physics (Weast, 2003). He assumed the conductivities were due to a linear combination of effects due to individual ions. Their contribution at infinite dilution in both normal and magnesium-free ACSF is shown in Table A-1.

Conversion of conductivity contribution from infinite dilution to high concentration solution is essential to calculate the effective conductivity. This conversion was done based on data for NaCl given in the CRC Handbook. From equation on Figure A-7:

$$y = -0.0439x^3 - 0.5877\,x^2 - 2.6318x + 8.579 \qquad \text{(A-14)}$$

where x is the logarithm (base 10) of the concentration in moles per litre, and y is the conductivity per unit concentration in (S/m)/M. The predicted conductivity per unit concentration of NaCl at 0.17 M (which is the total molarity of ACSF solutions) (x=0.17) is 10.28 ((S/m)/M). So the overall correction for non-infinite dilution is 10.28/12.44 = 0.8258, where 12.44 (S/m)/M is the conductivity per concentration at infinite dilution. For magnesium-free ACSF, multiplying the overall correction (0.8258) by the total contribution of ions (1.9536) gave the theoretical conductivity (1.6133 S/m) and for the normal ACSF it is 1.6141 S/m.

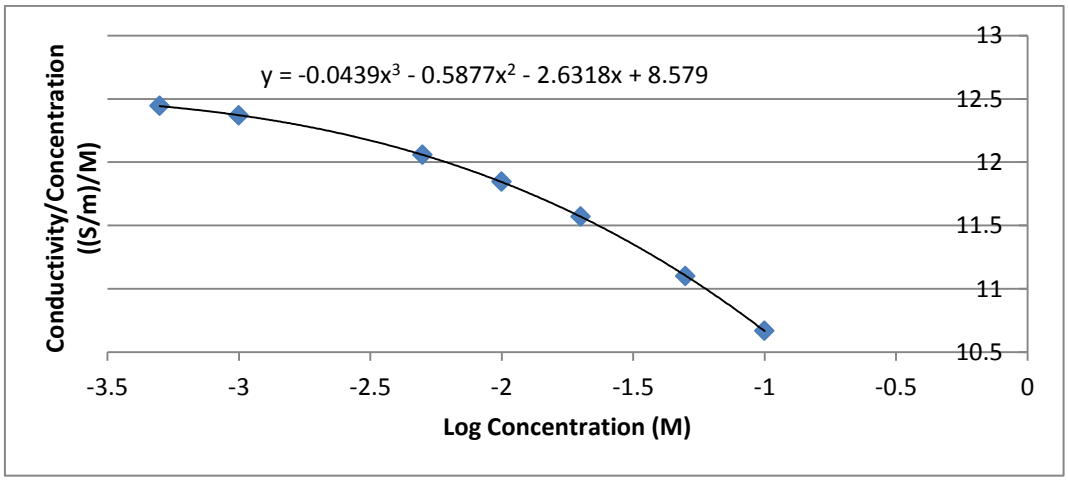

Figure A-7: Conductivity per unit concentration of NaCl (S m^{-1} /M). Data are from the CRC Handbook. The line is a cubic fit to the data

Table A-1: Conductivities due to ions

Ion	Molar Conductivities at infinite dilution ($S\ m^{-1}\ /M$)	Magnesium-free ACSF		Normal ACSF	
		Concentration (mM)	Contribution (S/m)	Concentration (mM)	Contribution (S/m)
Na^+	5.011	151.25	0.7579	152.25	0.7629
K^+	7.348	5.00	0.0367	2.50	0.0184
Mg^{2+}	10.60	0.00	0.00	1.00	0.0106
Ca^{2+}	11.894	2.00	0.0238	2.00	0.0238
D-glucose[2]	0.00	10.0	0.00	10.00	0.00
Cl^-	7.631	133	1.0149	133.50	1.0187
HCO_3^-	4.45	26.0	0.1157	26.00	0.1157
$H_2PO_4^-$	3.60	1.25	0.0045	1.25	0.0045
Total			1.9536		1.9546
Convert conductivity contribution from infinite dilution to high concentration solution			**1.6133**		**1.6141**

It is clear that theoretically the ratio of normal and magnesium-free ACSF conductivities is 1.0005. In another words they are essentially identical.

[2] A value for glucose is not in the CRC Handbook but conductivity is assumed to be close to zero based on its high value of its logarithmic acid dissociation constant (pKa) for dissociation in water.

Appendix B **Computer Codes**

Most of MATLAB codes consist of four parts: First; open the device (Agilent E4980); second, do the measurements; third perform the analysis; and finally fourth, close the device.

```
% Test access to Agilent E4980 LCR meter via TCP/IP using
Instrument
% Control Toolbox.

% To find the VISA resource name for the Agilent device, issue the
% following command:
%
%    info = instrhwinfo('visa', 'agilent')
% then examine the field called ObjectConstructorName
%
%     info.ObjectConstructorName
% ans =
%     'visa('agilent', 'TCPIP0::130.217.188.201::inst0::INSTR');'
%     'visa('agilent',
'TCPIP0::gpib.phys.waikato.ac.nz::gpib0,17::INSTR');'
%     'visa('agilent', 'GPIB14::17::INSTR');'
%     'visa('agilent', 'GPIB12::17::INSTR');'
%     'visa('agilent', 'GPIB3::17::INSTR');'
%
%   LAN_Gateway = '130.217.188.201'
%
% ASR 1-Jul-2009,
% v3: 8-Sep-2009
% v4: 17-Sep-2009
% v5: Maher 22 Feb 2010 to measure the conductivity using Maher's
Equation
% v6: Maher 30 Nov 2010 to measure the conductivity using Maher's
Equation
% and graph it with time in Linear scale.
% v7: Maher 2 Dec 2010 to measure the conductivity using Maher's
Equation
% and graph it with time in Linear scale. Over 24 hrs.
% v8: Maher and Ehsan 13 Dec 2010 to plot graphs directly
```

To open the device for all codes from Section B-1 to B-4

```
clear all
% close all
format short g
format compact

%--------------------------------------------------------------
% Check to see if there are any 'stray' VISA objects-- if there
are, then delete them!
old_VISA = instrfind('type', 'visa-tcpip');
if ~isempty(old_VISA)
    disp('WARNING!! Detected one or more stale VISA objects.
Deleting...');
    delete(old_VISA);
end
%--------------------------------------------------------------

BUFF_SIZE = 1000;
```

```
% create VISA object
vt = visa('agilent', 'TCPIP::130.217.188.201::gpib0,17::INSTR');
set(vt, 'InputBufferSize', BUFF_SIZE);
set(vt, 'Timeout', 2);      % (1 sec seems to be too short!)

fopen(vt);
vt;

instrfind
% ask Agilent box to identify itself; delete CR sequence at EOS
[idn, cnt, msg] = query(vt, '*IDN?');
fprintf('Hello from <%s>\n\n', idn(1:cnt-1));

% display string on Agilent screen and play welcome sound
fprintf(vt, ':display:line "Hello, Maher Elbohouty"');

for i = [1 2 3 2 1 ]
    fprintf(vt, ':syst:beep:tone %d', i);
    fprintf(vt, ':syst:beep');
    pause(0.2);
end
```

B-1 Three-Dimensional-Method Code in MATLAB

The Matlab code (v8) that I used to measure the effective conductivity in chapter 5 is:

To do the measurements:

```
% Set the measurement integration time
fprintf(vt, ':aper long');

% Attempt to set impedance mode to real/imag
fprintf(vt, ':function:imp rx');

% Now attempt a frequency sweep
freq = linspace(5e3, 5e3,100)';  % requested frequencies 8640
time =0;
freq_set = zeros(size(freq));               % returned frequencies
Z = complex(zeros(size(freq)));             % returned impedances
(complex)
[Zsd_real Zsd_imag] = deal(zeros(size(freq)));     % uncertainties
in impedance
clf
for i = 1: length(freq)
    tic;  %pause (1.578722)   %(0.646371)
    fprintf(vt, sprintf(':freq %d', freq(i)));  % requested freq
    [str, cnt, msg] = query(vt, ':freq?');      % actual freq

    % perform sanity check on frequency!
    freq_set(i) = str2num(str);
    freq_err = (abs(freq(i) - freq_set(i)))/freq(i);
    if freq_err > 0.01          % 0.01 ==> 1 percent mismatch
        msg = sprintf('[f_req, f_actual] = [%g, %g] Hz', freq(i),
freq_set(i))
        msg = sprintf('Frequency mismatch: %s (Should never
happen!)', msg);
```

```
        error(msg)
    end

    freq_set(i)

    % read the impedance
    for j = 1: 1
        [str, cnt, msg] = query(vt, ':fetch?');
        % another sanity check-- Time out?
        if length(str) == 0
            fprintf('msg = [%s]\n\n', msg);
        end
        fprintf('Result = [%s]\n\n', str(1:length(str)-1));
        r = sscanf(str, '%f,%f', 2);
        Zraw(j) = complex(r(1), r(2));

    end

    Zraw.'
    Z(i) = mean(Zraw);
    Zsd_real(i) = std(real(Zraw));
    Zsd_imag(i) = std(imag(Zraw));
    %     compute magnitude and phase
    Z_abs(i) = abs(Z(i)); Z_phase(i) = angle(Z(i))*180/pi;
```

To do analysis and output

```
    % compute series resistance and capacitance
    R = real(Z(i));
    C = 1 ./ (2*pi*freq_set.*abs(imag(Z(i))));
    sigma_C = Zsd_imag ./ (2*pi*freq_set.*(imag(Z(i))).^2);

    figure(1)
    subplot(521)
    plot(i, real(Z(i)), '-bo'); zoom on; grid on; hold on
    title('real(Z)');

    subplot(522)
    plot (i, imag(Z(i)), '-ro'); zoom on; grid on;hold on
    title('imag(Z)');

    subplot(523)
    plot(real(Z(i)), imag(Z(i)), '-ok'); zoom on; grid on;hold on
    title('Imag(Z) vs Real(Z)', 'interp', 'none');
    subplot(524)
    errorbar(C*1e6, sigma_C*1e12, '-'); zoom on; grid on;hold on
    title('Capacitance (microF) vs freq');
    % To calculate the conductivity of the solution by knowing it
Impedance
    % using Maher's Equation:

    %     Conductivity = (zeros(size(Z_abs)))';
    a = 0.000; % (m) the distance between the I and V electrodes
    b = 0.85e-3 %0.75e-3 %0.0007; % the distance between the two V
electrodes (m)
    d = 2.5e-3 %2.15e-3%0.0014; % the distance between the two I
electrodes (m)

    r1s = a^2 +(d^2/4)-(d*b/2)+(b^2/4);
    r11s=a^2 +(d^2/4)+(d*b/2)+(b^2/4);

    c = (sqrt (r11s)-sqrt (r1s))/(sqrt (r1s)* sqrt (r11s));
```

```
    Conductivity(i) = c/(2 *pi*Z_abs(i))

    subplot(5,2, [5 6])
    plot(i, Conductivity(i), '-o', 'color', [rand rand rand]);
zoom on; grid on;hold on
    %     plot(freq_set, Conductivity, '-o'); zoom on; grid on;
    xlabel ('frequency (Hz)'); ylabel ('Conductivity (S/m)')
    %     errorbar(freq_set, Conductivity, Conductivity, '-o');
zoom on; grid on;
    title('Conductivity of NaCl using 4 ribbon cable connector as
electrods', 'interp', 'none');
    t_intervals = toc;
    time = time + t_intervals;
    subplot(5,2, [7 8])
    plot(time, Conductivity(i), '-o'); zoom on; grid on; hold on
    %     plot(freq_set, Conductivity, '-o'); zoom on; grid on;
    xlabel ('time (Sec)'); ylabel ('Conductivity (S/m)')
    %     errorbar(freq_set, Conductivity, Conductivity, '-o');
zoom on; grid on;
    title('Conductivity of NaCl using 4 ribbon cable connector as
electrods', 'interp', 'none');
    % AXIS([XMIN XMAX YMIN YMAX ZMIN ZMAX])
    subplot(5,2, [9 10])
    plot(time, freq_set(i), '-o'); zoom on; grid on; hold on
    xlabel('time (Sec)'); ylabel('Frequency (Hz)')
    [freq_set  Z];


end
save Conductivity_7.25g_NaCl_24hrs3.mat    % Use with literal
filename
```

Closing:

```
fclose(vt);
delete(vt);
return
```

B-2 Two-Dimensional-Method Code in MATLAB

The Matlab code (v11) that I used to measure the effective conductivity in chapter 5 is

```
% v9: Maher 6 April 2011 to plot graphs directly using the new
Equation
% v10: Maher 23 May 2011 to plot graphs directly using the Phys204
Equation
% v11: Maher 7 July 2011 to plot graphs directly using modified
Phys204 Equation to apply it in rectangle shape.
% v11: Maher 17 July 2011 to plot graphs directly by measuring the
% conductance and then calculate the conductivity.
```

To do the measurements:

```
for x = 1:6
    x
    input ('Repleace the slice, please')

    %-------------------------------------------------------------
    % Set the measurement integration time
    fprintf(vt, ':aper long');
```

```
    % Attempt to set conductance mode to real/imag
    fprintf(vt, ':function:imp rx');

    % Now attempt a frequency sweep
    freq = linspace(10e3, 10e3,4)';  % requested frequencies 8640
    time =0;
    freq_set = zeros(size(freq)); % returned frequencies
    Z = complex(zeros(size(freq)));% returned impedances (complex)
    [Zsd_real Zsd_imag] = deal(zeros(size(freq)));     %
uncertainties in impedance

    % to recored the Conductivity in an Excel file
    d = [0 0 0 0];
    for i = 1: length(freq)
        tic;  pause (3)
        fprintf(vt, sprintf(':freq %d', freq(i)));  % requested
freq
        [str, cnt, msg] = query(vt, ':freq?');      % actual freq

        % perform sanity check on frequency!
        freq_set(i) = str2num(str);
        freq_err = (abs(freq(i) - freq_set(i)))/freq(i);
        if freq_err > 0.01          % 0.01 ==> 1 percent mismatch
            msg = sprintf('[f_req, f_actual] = [%g, %g] Hz',
freq(i), freq_set(i));
            msg = sprintf('Frequency mismatch: %s (Should never
happen!)', msg);
            error(msg)
        end

        freq_set(i);

        % read the impedance
        for j = 1: 1
            [str, cnt, msg] = query(vt, ':fetch?');
            % another sanity check-- Time out?
            if length(str) == 0;
                fprintf('msg = [%s]\n\n', msg);
            end
            fprintf('Result = [%s]\n\n', str(1:length(str)-1));
            r = sscanf(str, '%f,%f', 2);
            Zraw(j) = complex(r(1), r(2));

        end
```

```
        Zraw.'
        Z(i) = mean(Zraw);
        Zsd_real(i) = std(real(Zraw));
        Zsd_imag(i) = std(imag(Zraw));
        %     % compute magnitude and phase
        Z_abs(i) = abs(Z(i)); Z_phase(i) = angle(Z(i))*180/pi;
```

To do analysis and output

```
    % compute series resistance and capacitance
        R = real(Z(i));
        C1 = 1 ./ (2*pi*freq_set.*abs(imag(Z(i))));
        sigma_C = Zsd_imag ./ (2*pi*freq_set.*(imag(Z(i))).^2);
```

```
        for h = [3 4 5 4 3 ]
            fprintf(vt, ':syst:beep:tone %d', h);
            fprintf(vt, ':syst:beep');
            pause(0.1);
        end
    end

        conductivity = (zeros(size(Z_abs)))';

    for j = 1:4;

        %22 November 2011. Solver for Van der Pauw equation Uses
Newton Raphson method done by Marcus

        R_ABCD = Z_abs(j);   %first reading in ohms
        if (j == 4)
            R_BCDA=Z_abs(1)
        else
            R_BCDA = Z_abs(j+1);   %second reading in ohms
        end
        depth = 400e-6;   %thickness of slice in metres

        initial_guess = 1/((R_ABCD + R_BCDA)*depth);  %first guess
at the answer based on dimensions

        n=0;
        discrepancy = 1;
        while (abs(discrepancy) > 1e-4)

            next_guess = initial_guess + (1/(pi*depth))*( exp(-
pi*initial_guess*R_ABCD*depth) + exp(-
pi*initial_guess*R_BCDA*depth) -1)/...
                ( R_ABCD*exp(-pi*initial_guess*R_ABCD*depth) +
R_BCDA*exp(-pi*initial_guess*R_BCDA*depth) );
            discrepancy = next_guess - initial_guess;   %the
difference between the two values

            initial_guess=next_guess;   %print out to see how its
going

            n=n+1;

            if (n == 100)
                'Error: too many iterations'
                break
            end
        end

        n

        ['conductivity is ' num2str(initial_guess) ' S m^-1']
%Assign final value in S m-1

        conductivity(j)=initial_guess;   %assign a numerical value
        d(j) = d(j)+ conductivity(j);
        %Check calculation. Answer should be 1.
        ['vdp function is ' num2str( ( exp(-
pi*initial_guess*R_ABCD*depth) + exp(-
pi*initial_guess*R_BCDA*depth)) ) ]
```

```
    end
    name = sprintf('B%d', x);
    xlswrite('Conductivity.xls', d, 'sheet1', name);


    figure(1)
    plot(conductivity, '-o'); zoom on; grid on;hold on
        xlabel ('Number'); ylabel ('Conductivity (S/m)')
        title('Conductivity of Brain Slices', 'interp', 'none');


    [freq_set  Z];

    ['Average conductivity ' num2str(mean(conductivity))]

    file_name = strcat('120208Conductivity_of_slices_in_NoMg
_ACSF_using_4_Ag_electrods', name );
    save file_name.mat    % Use with literal filename
```

Closing:

```
  fclose(vt);
    delete(vt);

end

return
```

B-3 One-Dimensional-Method Code in MATLAB

The MATLAB code (v14) that I used to measure the effective conductivity in chapter 7 is

```
%  v10: Maher 23 May 2011 to plot graphs directly using the
Phys204 Equation
%  v14:Maher 7 Dec  2011 conductivity using Ag/AgCl plate
electrode, 1D method
```

To do the measurements:

```
for x=1:20
     %-----------------------------------------------------------------
    % Set the measurement integration time
    fprintf(vt, ':aper long');

    % Attempt to set impedance mode to re4al/imag
    fprintf(vt, ':function:imp rx');

    % Now attempt a frequency sweep
    freq = linspace(20,2e6,100)';  % requested frequencies
    %     freq = linspace(10e3,10e3,100)';  % requested
frequencies
    freq_set = zeros(size(freq));               % returned
frequencies
    Z = complex(zeros(size(freq)));             % returned
impedances (complex)
    [Zsd_real Zsd_imag] = deal(zeros(size(freq)));     %
uncertainties in impedance
```

```
    x
    %     a = input ('Area of brain slice = ');
    %     A = a*1e-7; %  (m^2) the Slice area
    A = pi*(0.005)^2;
    % to recored the Conductivity in an Excel file
    d = zeros(length(freq),2);

    for i = 1: length(freq)
        tic;% pause(60);
        fprintf(vt, sprintf(':freq %d', freq(i)));  % requested
freq
        [str, cnt, msg] = query(vt, ':freq?');      % actual freq

        % perform sanity check on frequency!
        freq_set(i) = str2num(str);
        freq_err = (abs(freq(i) - freq_set(i)))/freq(i);
        if freq_err > 0.01          % 0.01 ==> 1 percent mismatch
            msg = sprintf('[f_req, f_actual] = [%g, %g] Hz',
freq(i), freq_set(i));
            msg = sprintf('Frequency mismatch: %s (Should never
happen!)', msg);
            error(msg)
        end
        freq_set(i);
        % read the impedance
        for j = 1: 1
            [str, cnt, msg] = query(vt, ':fetch?');
            % another sanity check-- Time out?
            if length(str) == 0;
                fprintf('msg = [%s]\n\n', msg);
            end
            fprintf('Result = [%s]\n\n', str(1:length(str)-1));
            r = sscanf(str, '%f,%f', 2);
            Zraw(j) = complex(r(1), r(2));
        end

        Zraw.';
        Z(i) = mean(Zraw);
        Zsd_real(i) = std(real(Zraw));
        Zsd_imag(i) = std(imag(Zraw));
        % compute magnitude and phase
        Z_abs(i) = abs(Z(i)); Z_phase(i) = angle(Z(i))*180/pi;
```

To do analysis and output

```
        %    figure(1)
        Conductivity = (zeros(size(Z_abs)))';
        %    Ag/AgCl Electrods
        L = (400e-6); % (m) the distance between the electrodes
        Conductivity(i) = (L /( A *Z_abs(i)))
        d(i,1) = d(i,1)+ freq(i);
        d(i,2) = d(i,2)+ Conductivity(i);

        t_intervals = toc;
        time = time + t_intervals;
        plot(time/60, Conductivity(i), '-o', 'color', [rand rand
rand]); zoom on; grid on;hold on
        xlabel ('time(min)'); ylabel ('Conductivity (S/m)')
        %         plot(freq(i), Conductivity(i), '-o', 'color',
[rand rand rand]);
```

```
        %         zoom on; grid on;hold on xlabel
('Frequency(Hz)'); ylabel
        %         ('Conductivity (S/m)')

        title('Conductivity of Seizing Slice ', 'interp', 'none');
    end
    name = sprintf('A%d', x);
    if x == 1
        %         col_letter = sprintf('%s',x+64);
        range = sprintf('A%d:B%d',2,2+length(freq)-1);
        xlswrite('Conductivity.xls', d, range);
    else
        col_letter = sprintf('%s',x+65);
        range =
sprintf('%s%d:%s%d',col_letter,2,col_letter,2+length(freq)-1);
        xlswrite('Conductivity.xls', d(:,2), range);
    end
    save 120604to25Conductivity_of_NaCl_using_1D_Transverse.mat
% Use with literal ilename
```

Closing:

```
    fclose(vt);
    delete(vt);
end
return
```

B-4 Study of Complex Conductivity and Resistivity using One-Dimensional-Method Code in MATLAB

```
% v14:Maher 7 Dec 2011 conductivity using Ag/AgCl plate electrode,
1D methode
% v15: From v14 directly Real imiag 1D.
% v16: adding dynamic updating of file name by ASR
```

To do the measurements:

```
%-----------------------------------------------------------------
--
% Set the measurement integration time
fprintf(vt, ':aper long');

% Attempt to set impedance mode to real/imag
fprintf(vt, ':function:imp rx');

% Now attempt a frequency sweep
freq = logspace(log10(20),log10(2*10^6),100)';  % requested
frequencies
%     freq = linspace(10e3,10e3,100)';  % requested frequencies
freq_set = zeros(size(freq));               % returned frequencies
Z = complex(zeros(size(freq)));             % returned impedances
(complex)
[Zsd_real Zsd_imag] = deal(zeros(size(freq)));     % uncertainties
in impedance
%-----------------------------------------------------------------
--

for m = 1:20
    % play welcome sound by Agilent
time =0;
```

```
for ii = [111 ]
    fprintf(vt, ':syst:beep:tone %d', ii);
    fprintf(vt, ':syst:beep');
    pause(0.3);
end


    m
     a = input ('Area of brain slice = ');
     A = a*1e-7; %  (m^2) the Slice area

clf  %to clear the pravouse figure
     % build a date- & time-string
T = clock;
date_str = sprintf('%4d', T(1));
for i = 2: 3
    date_str = sprintf('%s%02d', date_str, T(i));
end
date_str = sprintf('%s-', date_str);
for i = 4: 5
    date_str = sprintf('%s%02d', date_str, T(i));
end

% define our updating variable
x_set = 1: 10;  % slice number

fignum = 2;

     % to record the Conductivity in an Excel file
    d = zeros(length(freq),2);

    for i = 1: length(freq)
        tic;% pause(60);
        fprintf(vt, sprintf(':freq %d', freq(i)));  % requested
freq
        [str, cnt, msg] = query(vt, ':freq?');      % actual freq

        % perform sanity check on frequency!
        freq_set(i) = str2num(str);
        freq_err = (abs(freq(i) - freq_set(i)))/freq(i);
        if freq_err > 0.01          % 0.01 ==> 1 percent mismatch
            msg = sprintf('[f_req, f_actual] = [%g, %g] Hz',
freq(i), freq_set(i));
            msg = sprintf('Frequency mismatch: %s (Should never
happen!)', msg);
            error(msg)
        end

        freq_set(i);
        % read the impedance
        for j = 1: 3
            [str, cnt, msg] = query(vt, ':fetch?');
            % another sanity check-- Time out?
            if length(str) == 0;
                fprintf('msg = [%s]\n\n', msg);
            end
            fprintf('Result = [%s]\n\n', str(1:length(str)-1));
            r = sscanf(str, '%f,%f', 2);
            Zraw(j) = complex(r(1), r(2));
        end
```

```
        Zraw.';
        Z(i) = mean(Zraw);
        Zsd_real(i) = std(real(Zraw));
        Zsd_imag(i) = std(imag(Zraw));
        % compute magnitude and phase
        Z_abs(i) = abs(Z(i)); Z_phase(i) = angle(Z(i))*180/pi;
```

To do analysis and output

```
    figure(fignum)
    subplot(321)
    plot(freq(i), real(Z(i)), '-bo'); zoom on; grid on; hold on
    title('real(Z)'); xlabel ('Frequency(Hz)'); ylabel ('real(Z)
(\Omega)')

    subplot(322)
    plot (freq(i), imag(Z(i)), '-ro'); zoom on; grid on; hold on
    title('imag(Z)'); xlabel ('Frequency(Hz)'); ylabel ('imag(Z)
(\Omega)')

    subplot(3,2, [3])
    plot(real(Z(i)), imag(Z(i)), '-ok'); zoom on; grid on; hold on
    title('Imag(Z) vs Real(Z)', 'interp', 'none');
    xlabel ('real(Z)(\Omega)'); ylabel ('imag(Z) (\Omega)')

    subplot(3,2, [4])
    plot(real(Z(i)*A), imag(Z(i)*A), '-ok'); zoom on; grid on;
hold on
    title('Imag(Z) vs Real(Z) per unit area', 'interp', 'none');
    xlabel ('real(Z)(\Omega)'); ylabel ('imag(Z) (\Omega)')

        %    Ag/AgCl flat Electrodes
        L = (400e-6); % (m) the distance between the electrodes
           Conductivity(i) = (L /( A *Z_abs(i)))

        d(i,1) = freq(i);
        d(i,2) = Conductivity(i);
d
        t_intervals = toc;
        time = time + t_intervals;

      subplot(3,2, [5 6])
%         plot(time/60, Conductivity(i), '-o', 'color', [rand rand
rand]); zoom on; grid on; hold on
%         xlabel ('time(min)'); ylabel ('Conductivity (S/m)')
              plot(freq(i), Conductivity(i), '-o', 'color',
[rand rand rand]);
              zoom on; grid on; hold on;
              xlabel ('Frequency(Hz)'); ylabel ('Conductivity
(S/m)')

        title('Conductivity of Seizing Slice ', 'interp', 'none');
    end

    name = sprintf('A%d', m);
    if m == 1
        %     col_letter = sprintf('%s',m+64);
        range = sprintf('A%d:B%d',2,2+length(freq)-1);
        xlswrite('ConductivityS.xlsx', d, range);
    else
        col_letter = sprintf('%s',m+65);
```

```
        range =
sprintf('%s%d:%s%d',col_letter,2,col_letter,2+length(freq)-1);
        xlswrite('ConductivityS.xlsx', d(:,2), range);
    end

    fig_name = sprintf('%s-figure_%d.fig', date_str, m);
    mat_name = sprintf('%s-matlab_%d.mat', date_str, m);

    % save selected data to .mat file
    disp(sprintf('Saving data to "%s"', mat_name));
    save(mat_name)

    % save figure also
    saveas(fignum, fig_name, 'fig');
end
```

Closing:

```
fclose(vt);
delete(vt);

return
```

B-5 Fitting Fricke Model to Experimental Resistivity Spectrum Code in MATLAB

```
% Maher: 18 Oct 2012
% Maher V2: 24 Nov 2012
% Maher V3: 26 Dec 2012
% This file should run with:
Maher_Beta_Fricke_cortex_modle_S_10kHz_2MHz.m
clear; % clc; clf;
```

To load experimental results

```
% Loading experimental data
load('Z_measured_NS3')


figure(1);
plot(real(Z_measured_NS3), imag(Z_measured_NS3), 'color',
'k','linewidth',3); zoom on; grid on;hold on
plot(real (Z_measured_NS3(54)), imag (Z_measured_NS3(54)), 'ro',
'markersize', 12); % indicate 10 kHz
plot(real (Z_measured_NS3(35)), imag (Z_measured_NS3(35)), 'k*',
'markersize', 12); % indicate 1 kHz
plot(real (Z_measured_NS3(15)), imag (Z_measured_NS3(15)), 'kx',
'markersize', 12); % indicate 100 Hz
```

Modelling parameters:

```
% Modelling Non-seizing for beta dispersion:
R1= 4.9; % Ohm
R2 = 2.87; % Ohm
R3 = 6.4; % Ohm
C1 = 5.1e-8; % Farad
C3 = 2.5e-4; % Farad
```

Calculation and output

```
freq = logspace(log10(20),log10(2*10^6),100)';  % requested
frequencies
w = 2*pi*freq;

% First Circuit:
Xc1 = 1./(j*w*C1);
Z1 = (R1+Xc1).*R2./(R1+R2+Xc1);

% Second Circuit:
Xc3 = 1./(j*w*C3);
Z2 = Xc3.*R3./(Xc3+R3);
Z_Model_N3=Z1+Z2;

% subplot(3,1,1)
plot(real(Z_Model_N3), imag(Z_Model_N3),'m','linewidth',2)
plot(real (Z_Model_N3(54)), imag (Z_Model_N3(54)), 'gs',
'markersize', 12); % indicate 10 kHz
plot(real (Z_Model_N3(35)), imag (Z_Model_N3(35)), 'm*',
'markersize', 12); % indicate 1 kHz
plot(real (Z_Model_N3(15)), imag (Z_Model_N3(15)), 'kx',
'markersize', 12); % indicate 100 Hz
legend('Non-seizing Animal 3','10 kHz','1 kHz','100 Hz','Model',3)
title('Resistivity for non-seizing segments', 'fontsize', 18);
xlabel ('Real(\rho)(\Omega m)','fontsize',16); ylabel ('Imag(\rho)
(\Omega m)','fontsize',16)
axis equal;
% subplot(3,1,2)
% semilogx(freq, real(Z), 'g','linewidth',2); zoom on; grid on;
hold on
% title('Modelling of real part against frequency of non-seizing
mouse brain cortex ', 'fontsize', 18);
% xlabel ('Frequency (Hz)', 'fontsize', 14); ylabel ('Real(Z)
(\Omega)', 'fontsize', 14)
%
% subplot(3,1,3)
%
% semilogx(freq, imag(Z_Model_N3), 'g','linewidth',2); zoom on;
grid on; hold on
% title('Modelling of imaginary part against frequency of non-
seizing mouse brain cortex ', 'fontsize', 18);
% Sum of squares; beta dispersion starts from point 54
S= sum((abs(Z_measured_NS3(54:100)-Z_Model_N3(54:100))).^2)
```

References

Abraham, W. C. (2006), *Memory maintenance the changing nature of neural mechanisms*, Current Directions in Psychological Science, 15 (1), 5-8.

Adey, W., Kado, R. and Didio, J. (1962), *Impedance measurements in brain tissue of animals using microvolt signals*, Experimental Neurology, 5 (1), 47-66.

Agilent Technology (2009), *Agilent impedance measurement handbook: A Guide to Measurement Technology and Techniques*, 4th ed., Author, USA.

Andreuccetti, D., Fossi, R. and Petrucci, C. (1997), *Calculation of the dielectric properties of body tissues in the frequency range 10 Hz - 100 GHz*, viewed 08 March 2012 http://niremf.ifac.cnr.it

Astbury, J., Goldschmidt, M., Evans, S., Niebauer, G. and Foster, K. (1988), *The dielectric properties of canine and normal and neoplastic splenic tissues*, in "Proceedings of the Fourteenth Annual Northeast Bioengineering Conference", IEEE, New York, pp. 107-108.

Baumann, S., Wozny, D., Kelly, S. and Meno, F. (1997), *The electrical conductivity of human cerebrospinal fluid at body temperature*, IEEE Transactions on Biomedical Engineering, 44 (3), 220-223.

Beaulieu, C. and Colonnier, M. (1989), *Number and size of neurons and synapses in the motor cortex of cats raised in different environmental complexities*, The Journal of Comparative Neurology, 289 (1), 178-187.

Bédard, C., Kröger, H. and Destexhe, A. (2004), *Modeling extracellular field potentials and the frequency-filtering properties of extracellular space*, Biophysical Journal, 86 (3), 1829-1842.

Bédard, C., Kröger, H. and Destexhe, A. (2006), *Model of low-pass filtering of local field potentials in brain tissue*, Physical Review E, 73 (5), 1-24.

Bédard, C., Rodrigues, S., Roy, N., Contreras, D. and Destexhe, A. (2010), *Evidence for frequency-dependent extracellular impedance from the transfer function between extracellular and intracellular potentials*, Journal of Computational Neuroscience, 29 (3), 389-403.

Bindman, L. J., Meyer, T. and Prince, C. A. (1988), *Comparison of the electrical properties of neocortical neurones in slices in vitro and in the anaesthetized rat*, Experimental Brain Research, 69 (3), 489-496.

Brown, B. H., Smallwood, R. H. and Barber, D. C. (1999), *Medical Physics and Biomedical Engineering*, Institude of Physics Publishing, London, UK.

Brown, R., Brewer, P. and Brett, D. (2009), *Long-term equilibrium potential and electrochemical impedance study of Ag/AgCl electrodes used in Harned Cell measurements of pH*, Accreditation and Quality Assurance: Journal

for Quality, Comparability and Reliability in Chemical Measurement, 14 (3), 139-145.

Burdette, E., Friederich, P., Seaman, R. and Larsen, L. (1986a), *In situ permittivity of canine brain: Regional variations and postmortem changes*, IEEE Transactions on Microwave Theory and Techniques, 34 (1), 38-50.

Burdette, E. and Karow, A. (1978), *Kidney model for study of electromagnetic thawing*, Cryobiology, 15 (2), 142-151.

Burdette, E. C., Cain, F. L. and Seals, J. (1986b), *In situ tissue permittivity at microwave frequencies: Perspective, techniques, results*, in Larsen, L. E. and Jacobi, J. H. (Eds.), "Medical Applications of Microwave Imaging", IEEE, New York, pp. 13-40.

Buzsák, G. (1998), *Memory consolidation during sleep: A neurophysiological perspective*, Journal of Sleep Research, 7 (S1), 17-23.

Cagnan, H., Meijer, H. G. E., Van Gils, S. A., Krupa, M., Heida, T., Rudolph, M., Wadman, W. J. and Martens, H. C. F. (2009), *Frequency-selectivity of a thalamocortical relay neuron during Parkinson's disease and deep brain stimulation: A computational study*, European Journal of Neuroscience, 30 (7), 1306-1317.

Chwang, R., Smith, B. and Crowell, C. (1974), *Contact size effects on the van der Pauw method for resistivity and Hall coefficient measurement*, Solid-State Electronics, 17 (12), 1217-1227.

Cole, K. S. (1940), *Permeability and impermeability of cell membranes for ions*, Cold Spring Harbor Symposia on Quantitative Biology, 8, 110-122.

Cooper, C. L. and Robertson, I. T. (1997), *International Review of Industrial and Organizational Psychology, Vol. 11, 1996*, Wiley, Chichester, UK.

Cooper, R., Osselton, J. W. and Shaw, J. C. (1980), *EEG Technology*, 3rd ed., Butterworth, London, UK.

Cruikshank, S. J., Hopperstad, M., Younger, M., Connors, B. W., Spray, D. C. and Srinivas, M. (2004), *Potent block of Cx36 and Cx50 gap junction channels by mefloquine*, Proceedings of the National Academy of Sciences of the United States of America, 101 (33), 12364-12369.

Damez, J. L., Clerjon, S., Abouelkaram, S. and Lepetit, J. (2007), *Dielectric behavior of beef meat in the 1-1500 kHz range: Simulation with the Fricke/Cole-Cole model*, Meat Science, 77 (4), 512-519.

Debye, P. J. W. (1929), *Polar Molecules*, Dover Publications, New York.

Dobbs, S. and Miller, J. (2002), *Statistics 1*, 10th ed., Cambridge University Press, Cambridge, UK.

Efron, R. (1961), *The alteration of electrical impedance of the brain during induced seizures (cat)*, in "Transactions of the Research Conference on Cooperative Chemotherapy Studies in Psychiatry and Broad Research

Approaches to Mental Illness", Veterans Administration, Washington, pp. 11-11A/176.

Elazar, Z., Kado, R. and Adey, W. (1966), *Impedance changes during epileptic seizures*, Epilepsia, 7 (4), 291-307.

Engel, J., Pedley, T. A., Engel, J., Pedley, T. A., Aicardi, J., Dichter, M. A., Moshé, S., Perucca, E. and Trimble, M. (2007), *Epilepsy, A Comprehensive Textbook*, 2nd ed., Lippincott Williams & Wilkins, Philadelphia.

Everitt, B. (1998), *The Cambridge Dictionary of Statistics*, Cambridge University Press, Cambridge, UK.

Everson, C., Bergmann, B. and Rechtschaffen, A. (1989), *Sleep deprivation in the rat: III. Total sleep deprivation*, Sleep, 12 (1), 13-21.

Fabrizi, L., Sparkes, M., Horesh, L., Abascal, J. F. P.-J., McEwan, A., Bayford, R. H., Elwes, R., Binnie, C. D. and Holder, D. S. (2006), *Factors limiting the application of electrical impedance tomography for identification of regional conductivity changes using scalp electrodes during epileptic seizures in humans*, Physiological Measurement, 27 (5), S163-S174.

Foster, K. R. and Schwan, H. P. (1989), *Dielectric-properties of tissues and biological-materials - A critical-review*, Critical Reviews in Biomedical Engineering, 17 (1), 25-104.

Freygang Jr, W. and Landau, W. (1955), *Some relations between resistivity and electrical activity in the cerebral cortex of the cat*, Journal of Cellular and Comparative Physiology, 45 (3), 377-392.

Fricke, H. (1925), *The electric capacity of suspensions with special reference to blood*, The Journal of General Physiology, 9 (2), 137-152.

Fricke, H. (1932), *XXXIII. The theory of electrolytic polarization*, The London, Edinburgh, and Dublin Philosophical Magazine and Journal of Science, 14 (90), 310-318.

Fukuda, T., Kosaka, T., Singer, W. and Galuske, R. A. W. (2006), *Gap junctions among dendrites of cortical GABAergic neurons establish a dense and widespread intercolumnar network*, The Journal of Neuroscience, 26 (13), 3434-3443.

Gabriel, C. (2005), *Dielectric properties of biological tissue: Variation with age*, Bioelectromagnetics, 26 (S7), S12-S18.

Gabriel, C., Gabriel, S. and Corthout, E. (1996a), *The dielectric properties of biological tissues: I. Literature survey*, Physics in Medicine and Biology, 41 (11), 2231-2249.

Gabriel, C., Peyman, A. and Grant, E. (2009), *Electrical conductivity of tissue at frequencies below 1 MHz*, Physics in Medicine and Biology, 54, 4863-4878.

Gabriel, S., Lau, R. W. and Gabriel, C. (1996b), *The dielectric properties of biological tissues: II. Measurements in the frequency range 10 Hz to 20 GHz*, Physics in Medicine and Biology, 41, 2251-2269.

Gabriel, S., Lau, R. W. and Gabriel, C. (1996c), *The dielectric properties of biological tissues: III. Parametric models for the dielectric spectrum of tissues*, Physics in Medicine and Biology, 41, 2271–2293.

Gamba, H. and Delpy, D. (1998), *Measurement of electrical current density distribution within the tissues of the head by magnetic resonance imaging*, Medical and Biological Engineering and Computing, 36 (2), 165-170.

Geddes, L. and Baker, L. (1967), *The specific resistance of biological material—A compendium of data for the biomedical engineer and physiologist*, Medical and Biological Engineering and Computing, 5 (3), 271-293.

Geddes, L. A. and Baker, L. E. (1975), *Principles of Applied Biomedical Instrumentation*, Wiley, New York.

Glass, M. and Miller, G. E. (1988), *Cerebrospinal impedance measurement for early detection of epileptic seizures*, in "Proceedings of the Annual International Conference of the IEEE Engineering in Medicine and Biology Society, Pts 1-4, New Orleans, Nov. 4 - 7 1988", pp. 759-760.

Gottesmann, C. (2001), *The golden age of rapid eye movement sleep discoveries. 1. Lucretius--1964*, Progress in Neurobiology, 65 (3), 211-287.

Grimnes, S. and Martinsen, Ø. G. (2008), *Bioimpedance and Bioelectricity Basics*, Academic Press, London, UK.

Haemmerich, D., Ozkan, O. R., Tsai, J. Z., Staelin, S. T., Tungjitkusolmun, S., Mahvi, D. M. and Webster, J. G. (2002), *Changes in electrical resistivity of swine liver after occlusion and postmortem*, Medical and Biological Engineering and Computing, 40 (1), 29-33.

Hagan, C. E., Bolon, B. and Keene, D. (2012), *Nervous system*, in Treuting, P. M., Dintzis, S. M., Frevert, C. W., Liggitt, D. and Montine, K. S. (Eds.), "Comparative Anatomy and Histology: A Mouse and Human Atlas", Elsevier, London, UK, pp. 339-394.

Hanai, T. (1960), *Theory of the dielectric dispersion due to the interfacial polarization and its application to emulsions*, Colloid & Polymer Science, 171 (1), 23-31.

Hanai, T., Asami, K. and Koizumi, N. (1979), *Dielectric theory of concentrated suspensions of shell-spheres in particular reference to the analysis of biological cell suspensions*, Bulletin of the Institute for Chemical Research, Kyoto University, 57, 297-305.

Hemenger, P. M. (1973), *Measurement of high resistivity semiconductors using the van der Pauw method*, Review of Scientific Instruments, 44 (6), 698-700.

Heuschkel, M. O., Fejtl, M., Raggenbass, M., Bertrand, D. and Renaud, P. (2002), *A three-dimensional multi-electrode array for multi-site stimulation and recording in acute brain slices*, Journal of Neuroscience Methods, 114 (2), 135-148.

Holder, D. S., Rao, A. and Hanquan, Y. (1996), *Imaging of physiologically evoked responses by electrical impedance tomography with cortical electrodes in the anaesthetized rabbit*, Physiological Measurement, 17 (4A), A179-A186.

Huigen, E., Peper, A. and Grimbergen, C. (2002), *Investigation into the origin of the noise of surface electrodes*, Medical and Biological Engineering and Computing, 40 (3), 332-338.

Hutt, A. (Ed.) (2011), *Sleep and Anesthesia: Neural Correlates in Theory and Experiment*, Springer, New York.

Jirsa, V. K. and Haken, H. (1996), *Field theory of electromagnetic brain activity*, Physical Review Letters, 77 (5), 960-963.

Juszczak, G. R. and Swiergiel, A. H. (2009), *Properties of gap junction blockers and their behavioural, cognitive and electrophysiological effects: Animal and human studies*, Progress in Neuro-Psychopharmacology and Biological Psychiatry, 33 (2), 181-198.

Keithley Instruments (2004), *Low Level Measurements Handbook: Precision DC Current, Voltage and Resistance Measurements*, 6th ed., Keithley, Cleveland, OH.

Koon, D. W. (1989), *Effect of contact size and placement, and of resistive inhomogeneities on van der Pauw measurements*, Review of Scientific Instruments, 60 (2), 271-274.

Kraszewski, A., Stuchly, M. A., Stuchly, S. S. and Smith, A. M. (1982), *In vivo and in vitro dielectric properties of animal tissues at radio frequencies*, Bioelectromagnetics, 3 (4), 421-432.

Kuang, W. and Nelson, S. (1998), *Low-frequency dielectric properties of biological tissues: a review with some new insights*, Transactions of the American Society of Agricultural Engineers 41 (1), 173-184.

Kushida, C., Bergmann, B. and Rechtschaffen, A. (1989), *Sleep deprivation in the rat: IV. Paradoxical sleep deprivation*, Sleep, 12 (1), 22-30.

Latikka, J., Kuurne, T. and Eskola, H. (2001), *Conductivity of living intracranial tissues*, Physics in Medicine and Biology, 46 (6), 1611–1616.

Lazebnik, M. (2008), *Ultra Wideband Spectroscopy and Dielectric-Properties Contrast Enhancement for Microwave Breast Cancer Detection and Treatment*, ProQuest, Ann Arbor.

Lee, R. and Astumian, R. (1996), *The physicochemical basis for thermal and non-thermal 'burn' injuries*, Burns, 22 (7), 509-519.

Lee, R. C. (2005), *Cell injury by electric forces*, Annals of the New York Academy of Sciences, 1066 (1), 85-91.

Li Zhang, C., Dreier, J. P. and Heinemann, U. (1995), *Paroxysmal epileptiform discharges in temporal lobe slices after prolonged exposure to low magnesium are resistant to clinically used anticonvulsants*, Epilepsy Research, 20 (2), 105-111.

Liley, D. T. J., Cadusch, P. J. and Wright, J. J. (1999), *A continuum theory of electro-cortical activity*, Neurocomputing, 26, 795-800.

Liu, Y., Paliwal, S., Bankiewicz, K. S., Bringas, J. R., Heart, G., Mitragotri, S. and Prausnitz, M. R. (2010), *Ultrasound-enhanced drug transport and distribution in the brain*, AAPS PharmSciTech, 11 (3), 1005-1017.

Lodish, H., Berk, A., Matsudaira, P., Kaiser, C. A., Krieger, M., Scott, M. P., Zipursky, S. L. and Darnell, J. (2003), *Molecular Cell Biology*, 5th ed., W. H. Freeman, New York.

Logothetis, N. K., Kayser, C. and Oeltermann, A. (2007), *In vivo measurement of cortical impedance spectrum in monkeys: Implications for signal propagation*, Neuron, 55 (5), 809-823.

Matthews, P. and Jezzard, P. (2004), *Functional magnetic resonance imaging*, Journal of Neurology, Neurosurgery & Psychiatry, 75 (1), 6-12.

McCormick, D. A. and Contreras, D. (2001), *On the cellular and network bases of epileptic seizures*, Annual Review of Physiology, 63 (1), 815-846.

Mears, D., Sheppard, N. F., Atwater, I. and Rojas, E. (1995), *Magnitude and modulation of pancreatic β-cell gap junction electrical conductance in situ*, Journal of Membrane Biology, 146 (2), 163-176.

Miklavčič, D., Pavšelj, N. and Hart, F. X. (2006), *Electric properties of tissues*, in "Wiley Encyclopedia of Biomedical Engineering", Wiley, New York, pp. 1-12.

Moore, D. S., McCabe, G. P. and Craig, B. A. (2012), *Introduction to the Practice of Statistics*, 7th ed., W.H. Freeman, New York.

Moussy, F. and Harrison, D. J. (1994), *Prevention of the rapid degradation of subcutaneously implanted Ag/AgCl reference electrodes using polymer coatings*, Analytical Chemistry, 66 (5), 674-679.

Nowak, L. G. and Bullier, J. (1996), *Spread of stimulating current in the cortical grey matter of rat visual cortex studied on a new in vitro slice preparation*, Journal of Neuroscience Methods, 67 (2), 237-248.

Oh, T., Gilad, O., Ghosh, A., Schuettler, M. and Holder, D. S. (2011), *A novel method for recording neuronal depolarization with recording at 125–825 Hz: implications for imaging fast neural activity in the brain with electrical impedance tomography*, Medical and Biological Engineering and Computing, 49 (5), 593-604.

Pethig, R. and Kell, D. B. (1987b), *The passive electrical properties of biological systems: Their significance in physiology, biophysics and biotechnology*, Physics in Medicine and Biology, 32, 933-970.

Price, W. L. V. (1972), *Extension of van der Pauw's theorem for measuring specific resistivity in discs of arbitrary shape to anisotropic media*, Journal of Physics D: Applied Physics, 5 (6), 1127-1132.

Rechtschaffen, A., Gilliland, M. A., Bergmann, B. M. and Winter, J. B. (1983), *Physiological correlates of prolonged sleep deprivation in rats*, Science, 221 (4606), 182-184.

Robillard, P. N. and Poussart, Y. (1977), *Specific-impedance measurements of brain tissues*, Medical and Biological Engineering and Computing, 15 (4), 438-445.

Robinson, P. A., Rennie, C. J. and Wright, J. J. (1997), *Propagation and stability of waves of electrical activity in the cerebral cortex*, Physical Review E, 56 (1), 826-840

Ryerse, J. S. (1989), *Isolation and characterization of gap-junctions from Drosophila-melanogaster*, Cell and Tissue Research, 256 (1), 7-16.

Schmid, G., Neubauer, G., Illievich, U. M. and Alesch, F. (2003), *Dielectric properties of porcine brain tissue in the transition from life to death at frequencies from 800 to 1900 MHz*, Bioelectromagnetics, 24 (6), 413-422.

Schwan, H. P. (1957), *Electrical properties of tissue and cell suspensions*, Advances in Biological and Medical Physics, 5, 147-209.

Schwan, H. P. (1963), *Electric characteristics of tissues*, Radiation and Environmental Biophysics, 1 (3), 198-208.

Sejnowski, T. J. and Destexhe, A. (2000), *Why do we sleep?*, Brain Research, 886 (1–2), 208-223.

Sekino, M., Inoue, Y. and Ueno, S. (2005), *Magnetic resonance imaging of electrical conductivity in the human brain*, IEEE Transactions on Magnetics, 41 (10), 4203-4205.

Shah, L. M., Anderson, J. S., Lee, J. N. and Wiggins, R. (2010), *Functional magnetic resonance imaging*, Seminars in Roentgenology, 45 (2), 147-156.

Sheeler, P. and Bianchi, D. E. (1983), *Cell Biology*, 2nd ed., John Wiley, New York.

Siegel, J. M. (2003), *Why we sleep*, Scientific American, 289 (5), 92-97.

Steriade, M., McCormick, D. A. and Sejnowski, T. J. (1993), *Thalamocortical oscillations in the sleeping and aroused brain*, Science, 262 (5134), 679-685.

Steyn-Ross, M. L., Steyn-Ross, D. A. and Sleigh, J. W. (2004), *Modelling general anaesthesia as a first-order phase transition in the cortex*, Progress in Biophysics & Molecular Biology, 85 (2-3), 369-385.

Steyn-Ross, M. L., Steyn-Ross, D. A., Wilson, M. T. and Sleigh, J. W. (2007), *Gap junctions mediate large-scale Turing structures in a mean-field cortex driven by subcortical noise*, Physical Review E, 76 (1), 011916-1 - 011916-16.

Stoppini, L., Buchs, P.-A. and Muller, D. (1991), *A simple method for organotypic cultures of nervous tissue*, Journal of Neuroscience Methods, 37 (2), 173-182.

Stuchly, M. A., Athey, T. W., Stuchly, S. S., Samaras, G. M. and Taylor, G. (1981), *Dielectric properties of animal tissues in vivo at frequencies 10 MHz–1 GHz*, Bioelectromagnetics, 2 (2), 93-103.

Surowiec, A., Stuchly, S., Keaney, M. and Swarup, A. (1986a), *In vivo and in vitro dielectric properties of feline tissues at low radiofrequencies*, Physics in Medicine and Biology, 31, 901-909.

Surowiec, A., Stuchly, S. and Swarup, A. (1985), *Radiofrequency dielectric properties of animal tissues as a function of time following death*, Physics in Medicine and Biology, 30, 1131-1141.

Surowiec, A., Stuchly, S. S. and Swarup, A. (1986b), *Postmortem changes of the dielectric properties of bovine brain tissues at low radiofrequencies*, Bioelectromagnetics, 7 (1), 31-43.

Sutherland, G. R. and McNaughton, B. (2000), *Memory trace reactivation in hippocampal and neocortical neuronal ensembles*, Current Opinion in Neurobiology, 10 (2), 180-186.

Thurber, W. R. (2010), *Resistivity and hall measurements*, viewed 2012, http://www.nist.gov/pml/div683/hall_resistivity.cfm

Tononi, G. and Cirelli, C. (2006), *Sleep function and synaptic homeostasis*, Sleep Medicine Reviews, 10 (1), 49-62.

Tung, A. and Mendelson, W. B. (2004), *Anesthesia and sleep*, Sleep Medicine Reviews, 8 (3), 213-225.

Valentinuzzi, M. E., Morucci, J.-P. and Felice, C. J. (1996), *Biomedical impedance techniques in medicine, part II: Monitoring of physiological events by impedance*, Critical Reviews in Biomedical Engineering, 24 (4 - 6), 353-466.

van der Pauw, L. J. (1958a), *A method of measuring specific resistivity and Hall effect of discs of arbitrary shape*, Philips Research Report, 13 (1), 1-9.

van der Pauw, L. J. (1958b), *A method of measuring the resistivity and Hall coefficient on lamellae of arbitrary shape*, Philips Technical Review, 20 (8), 220-224.

Van Harreveld, A. and Ochs, S. (1956), *Cerebral impedance changes after circulatory arrest*, American Journal of Physiology--Legacy Content, 187 (1), 180-192.

Van Harreveld, A. and Schade, J. (1962), *Changes in the electrical conductivity of cerebral cortex during seizure activity*, Experimental Neurology, 5 (5), 383-400.

Voss, L. J., Melin, S., Jacobson, G. and Sleigh, J. W. (2010), *Role of Cx36 gap junction modulation in general anaesthetic anticonvulsant action*, European Journal of Pharmacology, 643 (1), 58-62.

Wang, M., Orwar, O., Olofsson, J. and Weber, S. G. (2010), *Single-cell electroporation*, Analytical and Bioanalytical Chemistry, 397 (8), 3235-3248.

Weast, R. C. (2003), *CRC Handbook of Chemistry and Physics*, 84th ed., CRC Press, Boca Raton, FL.

Weiss, J. D. (2011), *Generalization of the van der Pauw relationship derived from electrostatics*, Solid-State Electronics, 123-127.

Weiss, J. D., Kaplar, R. J. and Kambour, K. E. (2008), *A derivation of the van der Pauw formula from electrostatics*, Solid-State Electronics, 52 (1), 91-98.

Yedlin, M., Kwan, H., Murphy, J., Nguyen-Huu, H. and Wong, Y. (1974), *Electrical conductivity in cat cerebellar cortex*, Experimental Neurology, 43 (3), 555-569.

Yerworth, R. J., Bayford, R. H., Cusick, G., Conway, M. and Holder, D. S. (2002), *Design and performance of the UCLH Mark 1b 64 channel electrical impedance tomography (EIT) system, optimized for imaging brain function*, Physiological Measurement, 23 (1), 149-158.

Yoon, J. J., Nicholson, L. F. B., Feng, S. X., Vis, J. C. and Green, C. R. (2010), *A novel method of organotypic brain slice culture using connexin-specific antisense oligodeoxynucleotides to improve neuronal survival*, Brain Research, 1353, 194-203.